University of Nottingham

Nottingham, United Kingdom

Studies on the Cell Autonomous Role for Notch in Definitive Haematopoiesis and Tet Genes' Requirements in Early Organogenesis

by

Mohammad Hussein Al Khamees

This thesis is submitted for the degree of

Doctor of Philosophy

September 2015

DECLARATION

I, Mohammad Al Khamees, confirm that the work presented in this thesis is my own, and none of it has been submitted in support of an application for any degree or qualification other than that for which I am now a candidate.

ABSTRACT

In vertebrates, haematopoiesis is maintained by self-renewing multipotent haematopoietic stem cells (HSCs) in the adult bone marrow. HSCs are specified and generated during early embryonic development from arterial endothelial cells in the ventral wall of the dorsal aorta (vDA) that become haemogenic. Examination of *mib* mutants and *rbpja/b* morphants zebrafish embryos, that have defects in Notch signalling show that both arterial specification and HSCs development require an intact Notch signalling pathway. Utilizing in-house generated zebrafish Notch reporter lines, we show that Notch signalling initiates in the migrating hEC progenitors before their arrival to the midline to form the DA. Following arterial specification, Notch activity rapidly increases in the DA cells and persists at high levels until the time point of HSC emergence from the vDA, then sharply falls to hardly detectable levels. Embryos treated with the γ-secretase inhibitor DAPT or DAPM lose HSC development but retain arterial specification. Quantification of the residual Notch activity in our reporter lines by RT-PCR, revealed that low levels of Notch signalling retained in treated embryos are sufficient for arterial gene expression, while high levels of Notch signalling are required for hECs induction. Additional to these loss of function experiments, our endothelial specific gain of function studies suggested that continuous expression of *nicd* in the ECs in stable transgenic lines prevent cells from differentiation into mature HSCs that can leave the vDA to seed

the CHT. By contrast, transient expression of *nicd* in ECs appeared to expand HSC fate and allow cells to seed the CHT, suggesting that down-regulation of Notch signalling is essential to enable cells committed to the blood lineage to leave the vDA and seed the CHT. These data represent the first demonstration, to our knowledge, that cell autonomous Notch induction in ECs in vivo is sufficient to expand HSC formation in vertebrates.

Ten-Eleven-Translocation (Tet) proteins are a family of enzymes known to be actively involved in DNA de-methylation by 5-mC oxidation. This process is essential for proper development and cell lineage specification. Here, we used zebrafish *tet1/2/3* morpholinos to study the role of Tet enzymes in zebrafish development and organogenesis. Our results showed that individual depletion of Tet1 or Tet3 enzymes is sufficient to arrest zebrafish development at the onset of somitogenesis, whereas *tet2* morphants appear normal. Moreover, analysis of mildly affected morphants shows that Tet1 knockdown leads to atypical neurogenesis in zebrafish embryos. Global 5hmC levels are dramatically reduced in both *tet1* and *tet3* morphants, indicating the importance of Tet proteins in vertebrate organogenesis.

DEDICATION

This work is dedicated to my brother and greatest teacher:

Ali

Your words of wisdom, joy and hope are still fresh in my ears, guiding me through my life.

TABLE OF CONTENTS

DECLARATION 2
ABSTRACT 3
DEDICATION 5
TABLE OF CONTENTS 6
LIST OF FIGURES 11
LIST OF TABLES 14
ACKNOWLEDGEMENTS 15
CHAPTER 1 18
1 Introduction 18
1.1 Haematopoiesis 18
1.2 Embryonic Haematopoiesis in Vertebrates 21
1.2.1 Embryonic Haematopoiesis 22
1.2.2 Definitive Haematopoiesis 23
1.3 HSCs are derived from a sub population of endothelial cells (haemogenic endothelium) in the AGM region 26
1.4 Zebrafish as a model to study haematopoiesis 28
1.5 Haematopoietic Development in Zebrafish 29
1.6 Notch signalling distinguishes Erythroid/myeloid progenitors (EMPs) from true HSCs 32
1.7 Notch signalling in definitive HSC 33
1.8 is the requirement for Notch in definitive HSCs formation cell autonomous? 42
1.9 Recently reported non-cell autonomous requirements for Notch in definitive haematopoiesis 43
1.10 Reporting Notch activity in zebrafish 48
1.10.1 Notch reporter transgenic lines as tools to monitor and lineage trace cells with Notch activity 51
1.11 *flk1* promoter drives endothelial specific gene expression during early zebrafish development 52
1.12 Tet proteins and oxidative demethylation of 5mC in vertebrate development 66
1.13 Project aims 71
CHAPTER 2 72
2 Materials and Methods 72
2.1. Zebrafish maintenance 72
2.2 General manipulation of zebrafish 72
2.2.1 Microinjection 72
2.2.2 Microinjection needle preparation 73
2.2.3 Microinjection 73
2.2.3.1 Co-injection of *tol2* vectors and *transposase* mRNA for transient and stable transgenesis 74

2.2.3.2 Co-injection of *attB* donor vector and *PhiC31 integrase* mRNA for site specific transgenesis 75

2.2.3.3 Co-injection of CRISPR donor plasmid and DNA-Cas9 & guide mRNA for site specific transgenesis 77

2.2.3.4 cre mRNA in vitro synthesis and microinjection for whole embryo *cre* mediated recombination 77

2.2.3.5 Morpholino injections 78

2.2.4 Treatment with the γ-secretase Inhibitor XVI (DAPM) 79

2.2.5 Heat shock experiments with the quadruple transgenic embryos *Tg(hsp:loxp-mCherry-loxp-gal4-vp16/flk1:cre/uas:nicd/csl:venuslow)* 79

2.3 General DNA and RNA work 80

2.3.1 DNA Phenol-Chloroform Extraction 80

2.3.2 PCR amplification 81

2.3.3 Restriction enzyme digestion 82

2.3.4 Agarose gel electrophoresis 83

2.3.5 Extraction of DNA from agarose gels 84

2.3.6 DNA ligation and transformation 84

2.3.7 Plasmid DNA Isolation 85

2.3.8 Measurement of nucleic acid concentrations 86

2.3.9 DNA Sequencing 86

2.3.10 Gibson assembly 86

2.3.10.1 Primer design, PCR amplification and backbone plasmid preparation 88

2.3.10.2 Calculating needed fragment concentration 89

2.3.10.3 Assembly mix incubation 89

2.3.11 Zebrafish embryo sampling for quantifying remaining Notch activity in DAPM treated and mib mutant embryos by quantitative PCR 90

2.3.12 Total RNA extraction 92

2.3.13 Reverse transcription and cDNA synthesis 93

2.3.14 Relative quantitative PCR (qPCR) 94

2.3.14.1 TaqMan 94

2.3.14.2 SYBR Green 95

2.4 Histology 96

2.4.1 Whole mount in situ RNA Hybridization (WISH) 96

2.4.1.1 Embryo collection and fixation 96

2.4.1.2 Whole-mount RNA in situ hybridization (WISH) 97

2.4.1.3 post hybridization 98

2.5 Image acquisition and data analysis 100

CHAPTER 3 102

3 Result I Notch reporter gene expression pattern during zebrafish early development . 102

3.1 Introduction 102

3.2 The three in-house generated Notch reporter lines have identical expression patterns 103

3.3 Notch signalling activity is detectable at the 5 somite stage (11.5 hpf) with fluorescent reporter proteins 106

3.4 Notch reporter protein is detectable in the position of the DA by 18hpf by fluorescence microscopy..... 109

3.5 Double in situ hybridization shows co-localization of Notch and the endogenous endothelial gene (*flk1*) mRNA at 18hpf..... 111

3.6 Notch activity increases in the developing DA from the time point of DA formation to the time point of HSC development..... 114

3.7 In situ hybridization of Notch reporter mRNA expression strongly suggests initiation of Notch activity in the migrating hEC progenitors before their arrival to the mid-line 115

3.8 Discussion of results..... 118

CHAPTER 4..... 121

4 Result II Low level of Notch is sufficient for arterial specification whereas high level is required for HSCs formation..... 121

4.1 Introduction..... 121

4.2 Notch activity is up-regulated in the DA after arterial specification to the time point of HSCs development..... 123

4.3 High level of Notch coincides with loss of Flt4 in the DA at the time point of HSC development 126

4.4 Blocking Notch pathway with different approaches leads to absence of HSCs markers in the vDA but with differential effects on arterial specification. 128

4.5 Blocking Notch pathway with different approaches differentially affect Notch reporter expression in the DA..... 129

4.6 Quantification of the residual Notch activity revealed that low level of Notch is sufficient for arterial gene expression while high levels are required for hEC induction 133

4.7 Discussion of results..... 135

CHAPTER 5..... 137

5 Result III Developing a molecular tool to over-activate/ block Notch pathway in the endothelium 137

5.1 Identification of *ef1α nicd* and *Ef1α dnrbpj* transgenic founders. 138

5.2 Injecting the transgenic *Tg(ef1α-loxP-cer-loxP-nicd)* and *Tg(ef1α-loxP-cer-loxP-dnRbpj)* F1 embryos with *cre* mRNA..... 142

5.2.1 *cre* mRNA efficiently recombines the *loxP* sites in the Cre reporter line *Tg(ef1α:loxP-gfp-loxP-dsRed2)* and activates expression of downstream gene 143

5.2.2 Injecting the generated *Tg(ef1α-loxP-cer-loxP-nicd)*^{qmc122} with *cre* mRNA does not produce specific phenotypes 145

5.2.3 Injecting the generated *Tg(ef1α-loxP-cer-loxP- dnRbpj)*^{qmc131} with *cre* mRNA does not block Notch signalling..... 146

5.2.4 Embryos generated from crossing the *Tg(ef1α-loxP-cer-loxP-nicd)*^{qmc122} to Tg(*flk1:cre)*^{qmc101} appeared normal..... 150

5.2.5 Embryos generated from crossing the *Tg(ef1α-loxP-cer-loxP- dnRbpj)*^{qmc131} to Tg(*flk1:cre)*^{qmc101} appeared normal..... 151

5.2.6 Using the zebrasish *ubi* promoter instead of the *ef1α* promoter 153

5.2.7 Injecting the P323 and P325 constructs and establishment of the *Tg(ubi-loxP-cer-loxP-nicd)* and *Tg(ubi-loxP-cer-loxP-dnRbpj)* lines 153

5.2.8 Screening the P323 and P325 injected fish for *Tg(ubi-loxP-cer-loxP-nicd)* and *Tg(ubi-loxP-cer-loxP-dnRbpj)* founders. 154

5.2.9 Injecting the *Tg(ubi-loxP-cer-loxP-nicd)*^{qmc125} embryos with *cre* mRNA 156

5.2.10 Generation of the *tol2-ubi-loxP-mCherry-s.stop-loxP-nicd* (P351) and *tol2-ubi-loxP-mCherry-s.stop-loxP-dnRbpj* (P352) Constructs 159

5.2.11 Injecting the P351 and P352 constructs and establishment of *Tg(ubi-loxP-mCherry-s.stop-loxP-nicd)* and *Tg(ubi-loxP-mCherry-s.stop-loxP-dnRbpj)* lines 159

5.3 Discussion of results 162

Chapter 6 165

6 Result IV Endothelial Notch induction is sufficient to expand HSCs 165

6.1 Introduction 165

6.2 Haemogenic endothelial Notch over-activation by combining the GAL4-UAS and Cre-loxP systems 165

6.2.1 Generating the *Tol2-ubi-loxP-mCherry-s.stop-loxP-gal4-vp16* construct 165

6.2.2 Injecting the P356 and Establishment of the *Tg(ubi-loxP-mCherry-s.stop-loxP-gal4-vp16)* transgenic lines 166

6.2.3 Identification of the *Tg(ubi-loxP-mCherry-s.stop-loxP-gal4-vp16)* founders *qmc130, qmc133, qmc134, qmc135* 166

6.2.4 Generation of the triple transgenic fish *Tg*(*f.flk1:cre;uas:nicd;csl:venus)* 168

6.2.5 Endothelial Notch induction up-regulates expression of the Notch reporter gene specifically in the endothelium 168

6.3 Single embryo PCR results confirmed that endothelial Notch reporter up-regulation was due to endothelial Notch induction while lack of circulation might be caused by Gal4-vp16 protein accumulation 173

6.4 PCR results showed strong correlation between endothelial Notch induction and ISV defects and loss of tip cells: 178

6.5 Generating the *hsp-loxP-mCherry-pA-loxP-tgal4-vp16* construct P385 181

6.6 Injecting the P385 construct and establishment of *Tg(hsp-loxP-mCherry-pA-loxP-tgal4-vp16)* lines 182

6.7 Endothelial Notch induction after heat shock leads to prominently high Notch activity in the endothelium 184

6.8 Notch endothelial induction moderately expands HSC markers but most cells do not leave the DA to seed the CHT. 185

6.9 Generation and injection of the *tol2-m.flk1:nicd-gfp* construct P405. 192

6.10 Generation and injection of the *tol2-fli1:nicd-gfp* construct P409. 198

6.11 Discussion of results 203

CHAPTER 7 206

7 Results V Both Tet1 and Tet3 enzymes are essential for organogenesis in zebrafish .. 206

7.1 Zebrafish *tet* genes morpholinos design and injection 206

7.2 Observed *tet1* and *tet3* morphants phenotypes are specific to depletion of *tet1* and *tet3* transcripts and not due to binding to un-intended targets 213

7.3 Injecting *tet1* or *tet3* leads to deletion of targeted exons, frame shifts and premature termination of *tet1* and *tet3* genes 219

7.4 Quantitative RT-PCR shows significant reduction in *tet1* transcript in *tet1* morphants and significant reduction in both *tet1* and *tet3* transcripts in *tet3* morphants 224

7.5 Notch signalling is altered in *tet1* and *tet3* morphants 225

7.6 *tet1* knockdown alter neurologic program in zebrafish embryos 232

7.7 5hmC levels decrease in the *elavl3* promoter in both *tet1* and *tet3* morphants 235
7.8 Global 5hmC level dramatically decrease in *tet1* morphants 237
7.9 Discussion of results 239
CHAPTER 8 242
8 Discussion 242
8.1 Analysing Notch activity during zebrafish early development 242
8.2 High level of Notch is required for *flt4* suppression and HSCs formation in the DA whereas low level is sufficient for arterial specification 246
8.3 Studying the cell autonomous requirements for Notch in zebrafish definitive haematopoiesis 249
8.4 *tet1* and *tet3* deletion abolishes organogenesis and leads to decrease in global 5-hydroxymethylcytosine content in zebrafish 257
8.5 Future perspectives 264
APPENDICES 266
REFERENCES 283

LIST OF FIGURES

Figure 1.1: Lineage Hierarchy of blood cell progenitors. 20

Figure 1.2: Comparison of the spatiotemporal haematopoietic ontogeny in different vertebrates. 31

Figure 1.3: Representation of the Notch signalling pathway. 34

Figure 1.4: Approaches used to block Notch pathway. 39

Figure 1.5: blocking Notch pathway with different approaches block HSCs formation. 40

Figure 1.6: Diagram showing the heat shock over-activation of Notch pathway with the Gal4-Uas system. 41

Figure 1.7: The effects of Notch over-activation on arterial and HSCs specification. 42

Figure 1.8: Diagram showing signalling pathways involved in HSC formation. 45

Figure 1.9 EBV components and their cellular counterparts 50

Figure 1.10: *flk1* expression pattern during zebrafish early development. 57

Figure 1.11: Minimal and *flk1* promoter drive *cre* expression in the endothelium. 60

Figure 1.12: Cre-mediated endothelial specific deletion of the floxed *gfp* and expression of *dsRed* in recombined cells. 63

Figure 1.13: Notch endothelial mis-expression constructs. 65

Figure 1.14: Tet enzymes mediate active DNA demethylation that affect promoters accessibility to transcription factors. 68

Diagram showing the chemical structures of cytosine bases at their methylated and demethylated states, the role of Tet enzymes in active cytosine demethylation and how could this process affect promoter accessibility to transcription factors and gene expression. 68

Figure 2.1: One-step assembly of fragments with overlapping sequences with the Gibson assembly approach. 87

Figure 2.2: Sampling method for quantifying the remaining Notch reporter gene mRNA in DAPM treated, *mib* mutants compared to control embryos. 91

Figure 3.1: Generated in-house Notch reporter lines drive identical expression pattern. 105

Figure 3.2: Notch activity is detectable in Notch reporter line at 5 somites stage (11.5hpf). 108

Figure 3.3: Notch signalling is detectable in the position of arterial and haematopoietic progenitors in the DA by 18hpf. 110

Figure 3.4: double in situ hybridization shows co-localization of the Notch reporter RNA and the endogenous endothelial marker flk1 RNA. 113

Figure 3.5: Notch activity in the DA increases after arterial specification. 115

Figure 3.6: Notch reporter mRNA become detectable at 8hpf. 117

Figure 4.1: Notch reporter fluorescent protein expression is up-regulated after arterial specification of the DA to the time point of HSC development. 125

Figure 4.2: High level of Notch activity correlates with Flt4 downregulation in the DA at the time point of HSC development. 127

Figure 4.3 Blocking Notch pathway with different approaches differentially affects Notch reporter expression. 131

Figure 4.4 Blocking Notch pathway with different approaches differentially affect arterial and haematopoietic specification. 132

Figure 4.5 Notch reporter remaining levels in DAPM treated and *mib* mutants compared to un-treated control. 134

Figure 5.1 identified *Tg(ef1α-loxP-cer-loxP-nicd)* and *Tg(ef1α-loxP-cer-loxP-dnRbpj)* transgenics. 141

Figure 5.2 *cre* mRNA injection to the Cre reporter line. 145

Figure 5.3 *cre* mRNA injection to *Tg(ef1α-loxP-cer-loxP- dnRbpj)^{qmc131}* embryos. 149

Figure 5.4 *ubi* promoter drive ubiquitous *cerulean* expression in *Tg(ubi-loxP-cer-loxP-nicd)^{qmc125}* F1. 155

Figure 5.5 Injecting *cre* mRNA to the *Tg(ubi-loxP-cer-loxP-nicd)^{qmc125}* embryos produce neurological and somatic phenotypes. 157

Figure 5.6 Establishment of the *Tg(ubi-loxP-mCherry-s.stop-loxP-nicd)^{qmc127}* and *Tg(ubi-loxP-mCherry-s.stop-loxP-dnRbpj)^{qmc129}* lines 161

Figure 6.1 identification of embryos with strong ubiquitous expression of *mCherry* from outcrossing injected fish to WT and establishment of the transgenic lines *Tg(ubi-loxP-mCherry-s.stop-loxP-gal4-vp16)^{qmc130}*, and *qmc135*. 167

Figure 6.2 Endothelial Notch induction up-regulates expression of the Notch reporter gene. 170

Figure 6.3 Quantification of the difference in Notch reporter fluorescent protein level between un-induced and endothelial Notch-induced embryos. 171

Figure 6.4 Single embryos PCR genotyping shows a strong correlation between endothelial Notch induction and Notch reporter fluorescent protein up-regulation. 174

Figure 6.5 Endothelial Notch induction perturbs normal tip cell migration in response to VEGF signal and leads to defective ISV sprouting. 177

Figure 6.6 Single embryos PCR genotyping shows a strong correlation between endothelial Notch induction and defected ISV sprouting and absence of tip cells. 179

Figure 6.7 Endothelial Notch induction partially recue the loss of HSC formation caused by accumulation of Gal4-vp16 protein in the endothelium. 180

Figure 6.8 Establishment of the transgenic lines 183

Figure 6.9 Endothelial Notch induction up-regulates expression of the Notch reporter gene specifically in the endothelium. 184

Figure 6.10 HSC specification is altered with endothelial Notch induction. 186

Figure 6.11: HSC expansion persists until day 2 with Notch endothelial induction. 188

Figure 6.12 Late endothelial induction does not expand HSC. 190

Figure 6.13 Early endothelial Notch induction with *m.flk1:cre* promotes HSCs self-renewal while late induction does not. 192

Figure 6.14 Transient endothelial Notch induction after injecting the *tol2-m.flk1:nicd-gfp* construct P405 up-regulates Notch reporter fluorescent protein in Notch reporter embryos. 195

Figure 6.15 Transient endothelial Notch induction after injecting the *tol2-m.flk1:nicd-gfp* plasmid P405 expand Notch reporter expression in CHT. 197

Figure 6.16 Transient endothelial Notch induction in *tol2-m.flk1:nicd-gfp* injected embryos expand expression of the haematopoietic markers *runx1* and *c-myb*. 198

Figure 6.17 Transient endothelial Notch induction in *tol2-fli1:nicd-gfp* injected embryos up-regulates Notch reporter fluorescent protein. 201

Figure 6.18 Transient endothelial Notch induction by injecting the *tol2-fli1:nicd-gfp* plasmid P409 expand HSCs in the DA and CHT. 202

Figure 7.1 *tet* morpholinos designed to delete the dioxygenase domains sequences in the *tet* genes. 207

Figure 7.2 Tet1 and Tet3 but not Tet2 are essential for zebrafish organogenesis. 210

Figure 7.3 *tet1* and *tet3* morphants develop severe abnormality in organogenesis. 211

Figure 7.4 Confirmatory *tet1* and *tet3* morpholinos with different targets and similar predicted outcome. 215

Figure 7.5 Targeting different sequence in *tet1* gene produce identical phenotypes. 217

Figure 7.6 Targeting different sequence in *tet3* gene produce identical phenotypes. 218

Figure 7.7: *tet2* morpholino injection with high amount does not affect embryonic development, and addition of *p53* Mo does not rescue *tet1* or *tet3* morphants. 219

Figure 7.8 *tet1* exon 7 splice acceptor morpholino leads to deletion of exon 7, frame-shift and premature termination of Tet1 protein translation. 222

Figure 7.9 *tet3* exon 4 splice acceptor morpholino leads deletion of exon 4, frame-shift and premature termination of Tet3 protein translation. 223

Figure 7.10 *tet1* mRNA significantly reduced in both *tet1* and *tet3* morphants whereas *tet3* transcript only reduced in *tet3* morphants. 225

Figure 7.11 Notch activity severely reduced in *tet3* morphants and not affected in *tet2* morphants. 227

Figure 7.12 Notch activity is altered in *tet1* morphants. 228

Figure 7.13 Notch signalling persists in *tet1* morphants despite alteration in its expression pattern in late somitogenesis. 231

Figure 7.14 *tet1* knockdown leads to atypical neurogenesis in zebrafish embryos. 234

Figure 7.15 Real time PCR quantification results of 5hmC DNA immunoprecipitation (DIP) of indicated genomic regions in *tet1*, *tet3* morphants compared to their uninjected controls, all examined at 24 hpf. 236

Appendix 1: Tol2 plasmids generated and injected to generate the Notch reporter lines..... 266

Appendix 2: GFP expression driven by the *flk1* promoter in *Tg(flk1:EGFP)s843* line recapitulates endogenous *flk1* expression. 267

Appendix3: Cre expression driven by the *flk1* promoter in *Tg(flk1:cre) s898* line recapitulates endogenous *flk1* expression. 268

Appendix 4: Identification of the minimal *flk1* promoter. 269

Appendix 5: Minimal and full *flk1* promoters drives identical expression pattern in stable reporter transgenic lines. 270

Appendix 6: Cloning steps followed to replace ***ef1α*** promoter with the *ubi* promoter in the constructs P311 and P312. 272

Appendix 7: Cloning steps followed to replace the *cerulean pA* fragment in P323 and P325 with the *mCherry-s.stop* cassette fragment. 274

Appendix 8: Cloning steps followed to generate the *Tol2-ubi-loxP-mCherry-s.stop-loxP-gal4-vp16* construct P356. 275

Appendix 9: Cloning steps followed to generate the P385 construct *HSP-loxP-mCherry-pA-loxP-Tgal4-vp16*. 276

Appendix 10: Diagram showing GIBSON assembly steps followed to generate the *tol2-m.flk1:NICD-GFP* plasmid P405. 277

Appendix 11: Diagram showing GIBSON assembly steps followed to generate the tol2-fli1:NICD-GFP plasmid P409. 278

Appendix 12: 5fC and 5caC are detectable by immunochemistry in mESCs. 280

Appendix 13: Global 5hmC levels are dramatically decreased in both Tet1 and Tet3 morphants 282

LIST OF TABLES

Table1.1: Notch ligand and receptor genes in *Drosophila* and their homologues in mammals and zebrafish. 38

Table 2.1: sequences of the minimal and full length *attB* and *attP* attachment sites. 76

Table 2.2: mRNAs produced and their linearization and transcription polymerases. 78

Table 2.3: PCR reaction volumes. 82

Table 2.4: PCR reaction cycling conditions. 82

Table 2.5: Typical restriction digest reactions. 83

Table 2.6: Example of a ligation reaction. 85

Table 2.7: Primers and probes used in quantitative real time PCR. 96

Table 2.8: Proteinase K treatment durations according to age of embryos. 97

Table 2.9: RNA probes used in this project. 99

Table 2.10: primers used in this project. 101

Table 4.1: Summary of Notch inhibition approaches used and percentage expected to be affected in each experiment. 129

Table 5.1: Identified *Tg(ef1α-loxP-cer-loxP-nicd*) transgenic founders. 139

Table 5.2 Identified *Tg(ef1α-loxP-cer-loxP-dnRbpj*) transgenic founders. 139

Table 5.3: *cre* mRNA titration. 144

Table:5.4 *cre* mRNA injections to the *nicd* transgenic embryos results. 146

Table:5.5: *cre* mRNA injections to the *Tg(ef1α-loxP-cer-loxP- dnRbpj)*^{qmc131} embryos does not produce Notch loss of function phenotypes. 148

Table 6.1: the table shows expected and observed embryos on day2 with the Notch activity reported with the *csl:venus* transgene. 172

Table 6.2: embryos used in single embryo genotyping. 173

Table 6.3 the table shows expected and observed embryos on day2 with the vascular system highlighted with *f.flk1:gfp Tg*. 176

Table 6.4: embryos used in single embryo genotyping. 178

Table 7.1: List of *tet* morpholinos used. 208

Table 7.2: List of confirmatory morpholinos used. 214

ACKNOWLEDGEMENTS

First and foremost, I offer my sincerest gratitude to my supervisor, Dr Martin Gering, who always believed in me, allowed me the room to do things in my own way and helped me in every circumstance throughout my PhD. His insightful discussions, critical thinking and endless patience were the key to successful completion of this work. I feel truly privileged to work with him.

I would also like to thank Dr Ruzov Alexey, for giving me the chance to work with his group in the Tet project, and to thank all members in our lab, Chris Moore, Deniz Ucanok, Maryam Jalali and Sunny Modhara, for their constructive criticism and continues support throughout my studies.

I would also like to deeply thank my parents for their belief in me, and for their honest prayer every day and night for me. Thanks also to my brothers and sisters for their unfailing love and support.

To my sons Mujtaba, Jehad, Ali and Hussein for all the joy and smiles that they brought to me, to pull me out of the life's pressure and stress. My sons, I am really sorry for every day and every moment I spent away from you. I love you.

Last but not least to my wife Fatemah: thank you for all your love and sacrifice. I could never have completed this project without your support and encouragement. Your care for children and me-you make my life complete and you are truly my "life companion".

ABBREVIATIONS

AGM	aorta-gonad-mesonephros
BSA	bovine serum albumin
CHT	caudal haematopoietic tissue
dpf	day post fertilization
DAB	diaminobenzidine
DMSO	dimethyl sulfoxide
DA	dorsal Aorta
E	embryonic day
ESC	embryonic stem cells
EHT	endothelial to haematopoietic transition
EMPs	erythroid/myeloid progenitors
EDTA	ethylenediamine tetra acetate
Gfp	green fluorescent protein
gfi1.1	growth factor independent factor 1.1
hEC	haematopoietic endothelial cells
HSCs	haematopoietic stem cells
HH	hedgehog
hpf	hours post fertilisation
ICM	intermediate cell mass
MAB	maleic acid buffer

mRNA	messenger RNA
mib	mind bomb
Mo	morpholino
NECD	Notch extra-cellular domain
Nicd	Notch intra-cellular domain
P-Sp/PAS	para-aorta splanchnopleura
PFA	paraformaldehyde
PTU	phenylthiourea
PBS	phosphate buffered saline
polyA	poly adenylation site
CV	posterior Cardinal vein
PLM	posterior lateral mesoderm
RBCs	red blood cells
RT	room temperature
Runx1	runt-related transcription factor 1
tg	transgenic line
TAE	tris acetate EDTA buffer
TE	tris EDTA buffer
VEGF	vascular endothelial growth factor
vDA	ventral wall of the dorsal aorta

CHAPTER 1

1 Introduction

1.1 Haematopoiesis

Blood is among the tissues that have the highest cell turnover in the body. Every day, it is estimated that one trillion blood cells are produced in the bone marrow to replenish old ones. More than a century ago, it was proposed that all blood cells derive from one common precursor, the haematopoietic stem cells (HSC), and that the cells derived from these precursors are organized in a hierarchy (Maximow, 1908).

This hypothesis was supported by establishing that the lethal consequences following radiation were due to bone marrow failure, and that those patients could actually be rescued by injection of spleen or marrow from non-irradiated donors (Lorenz et al., 1951). Remarkably, lymphohaematopoietic cells from donor bone marrow were also shown to repopulate the recipient haematopoietic tissues (Ford et al., 1956, Makinodan, 1956, Nowell et al., 1956). Despite the establishment of bone marrow transplantation in the early 1950s, it was still not known whether blood is derived from multiple lineage restricted stem cells or single multipotent stem cells that have the ability to give rise to all blood lineages (HSC).

In the early 1960s, Till and McCulloch (1961) injected bone marrow into irradiated mice and noticed the presence of gross nodules in their

spleens that are proportional to number of bone marrow cells injected. To demonstrate that each colony was truly derived from a single bone marrow cell, they further exposed bone marrow recipient mice to sub-lethal doses of radiation sufficient to induce karyotipic variation among the injected cells. They then noticed that each colony has a unique karyotipic pattern compared to other neighbouring nodules, and so provided the first evidence for the existence of single multipotent stem cells in the bone marrow, the haematopoietic stem cells (HSCs) that have the potential for proliferation, differentiation and self-renewal. This definition was then updated when Jones et al. (1989) discovered that cells forming colonies in the spleen were in fact progenitor cells with only short-term repopulating ability while the haematopoietic cells seeding the bone marrow are the cells that provide long-term repopulation (Figure 1.1 shows the classical haematopoietic hierarchy).

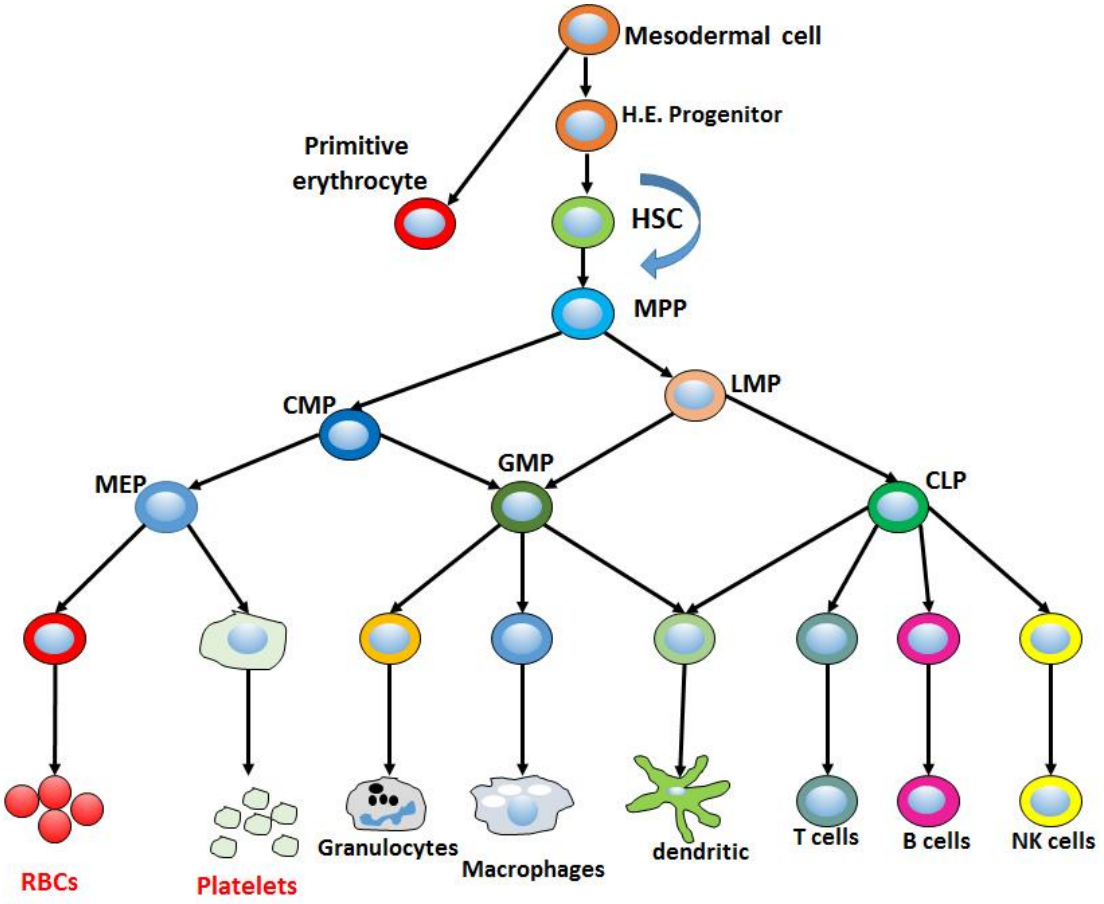

Figure 1.1: Lineage Hierarchy of blood cell progenitors.
Diagram showing the classical model for the haematopoietic development. HSCs develop from haemogenic endothelial progenitors derived from mesodermal cells that have the potential to give rise to primitive blood cells and the haemogenic endothelial progenitors that form the axial vessels' endothelium. HSCs reside at the top of the haematopoietic hierarchy, where they asymmetrically divide to give rise to committed progenitor cells that pass through several levels of differentiation to finally give rise to all mature cells of all blood lineages.

Soon after their discovery, HSCs were used in bone marrow transplantation for patients with blood system failure to restore normal blood formation and their use is now established as a standard therapy for several malignant and non-malignant diseases (Cambier et al., 2015). However, HSC transplantation has not achieved its full

potential due to the scarcity of HSCs in bone marrow and the shortage of suitable donors. The use of improperly matched donor HSCs can lead to graft rejection or graft-versus-host disease, common serious complications in the clinic (Slukvin, 2013). Despite substantial efforts by the research community, HSC derivation from human pluripotent stem cells or from reprogrammed somitic cells has not been fully accomplished yet. Knowledge about the molecular programming of HSCs during embryogenesis is an important prerequisite for achieving this goal. We study HSC formation in the zebrafish embryo to reveal the molecular programming HSC precursors undergo as they develop from haemogenic endothelium in the ventral wall of the dorsal aorta, one of the major arteries in the vertebrate embryo.

1.2 Embryonic Haematopoiesis in Vertebrates

In vertebrates, haematopoiesis occurs in two major waves. The first transient (embryonic) wave, which takes place during early development to provide oxygen and innate immunity to the rapidly growing tissue, occurs in the mammalian and avian embryos in the extra-embryonic yolk sac. The second permanent (definitive) wave, which follows the embryonic wave, and provides all blood cell lineages from multipotent self-renewing HSCs that maintain the blood system throughout life.

1.2.1 Embryonic Haematopoiesis

Embryonic haematopoiesis is the process that leads to the production of all primitive blood cells in early embryogenesis, as well as some of definitive-like blood cells. Primitive blood cells are the erythrocytes, macrophages and megakaryocytes that form during the transient wave of haematopoiesis. These blood cells are required to provide nutrient, oxygen and innate immunity to the rapidly growing tissues during early development.

Primitive blood cells are termed primitive due to the fact that they are closer in shape and characteristics to lower vertebrates' blood cells than their adult type counterparts. For instance, primitive erythrocytes are generally large in size, nucleated and they express embryonic haemoglobins (Palis and Yoder, 2001). Primitive macrophages are also functionally immature and have less phagocytic activity compared to their adult counterpart, and they lack certain markers such as F40/80 antigen and Lysozyme M (Lichanska and Hume, 2000). On the other hand primitive megakaryocytes are indistinguishable from their adult types, as they are both morphologically similar, express the same surface markers and both have the ability to produce platelets (Xu et al., 2001).

Primitive blood cells originate in the *extra-embryonic* yolk sac directly from mesodermal precursors that form blood islands, and are detectable in mouse embryos by embryonic day (E) 7-7.5 (reviewed in Medvinsky et al., 2011). This is at least half a day earlier than the

establishment of the yolk sac circulation, and one day earlier than the embryonic circulation initiating at E8 and E8.5 respectively (Walls et al., 2008). Towards the end of the embryonic wave, it is also now accepted that some definitive-like blood cells also being produced in the murine yolk sac (Palis and Yoder, 2001) and in the zebrafish CHT (Bertrand et al., 2010b). These cells develop under a different genetic control than that of primitive and true definitive blood cells, as discussed later in this chapter. Even though produced blood cells are morphologically and functionally similar to the blood cells generated in the definitive wave. Because the progenitor that these cells arise from does not have the full characteristics of the HSCs, including the ability to reconstitute haematopoiesis of irradiated mouse, and due to their disappearance later in development, they are still classified under embryonic haematopoietic stem cells.

1.2.2 Definitive Haematopoiesis

A short time after the establishment of blood circulation in the yolk sac and before its connection to the embryo proper (around E8), another wave of haematopoiesis is detected intra-embryonically. The intra-embryonic origin was first confirmed experimentally by (Dieterlen-Lievre, 1975) to correct the previous theory of the yolk sac being the origin of HSCs (Moore and Metcalf, 1970), which was based on culturing murine embryo bodies harvested on day 7 in the presence or absence of their yolk sac, and then dissecting their foetal

liver to explore colony formation. Even though only embryos cultured in presence of their yolk sac produce foetal liver colonies, this experiment does not exclude possible cell migration and the repopulating capability of the later identified AGM region. Unlike the first wave, which is only transient and mainly forms primitive blood cells, this wave leads to formation of all blood lineages throughout the life of the organism, and so it is called the definitive wave. In this wave, haematopoietic progenitors develop in an area called the para-aorta splanchnopleura (P-Sp/PAS), which later forms the aorta, gonads, and mesonephros (AGM) (reviewed in Golub and Cumano, 2013). These progenitors are the founders of the first long term haematopoietic stem cells. They gain their full self-renewal activity and autonomous ability to reconstitute haematopoiesis of adult recipient (HSCs characteristics) two days after their first appearance in the AGM with a potency like those found in the adult HSCs (Medvinsky and Dzierzak, 1996).

In the mouse embryo proper, hemangioblasts differentiate from mesodermal origin during early development and are found dispersed throughout the head mesenchyme and other areas of the embryo (Herbert et al., 2009). Based on molecular signals coming from other cells and from the microenvironment, they aggregate to form arterial and venous angioblasts, including the dorsal aorta DA and cardinal vein CV (Coultas et al., 2005). They then slowly remodel and refine into endothelial cells (ECs). A subset of the DA endothelium

"haemogenic endothelium" in the AGM region then further differentiate to generate the definitive haematopoietic stem cells that were found to form clusters that contain progenitors with the ability to reconstitute the HSC system from E10 (Medvinsky and Dzierzak, 1996).

Several other vascular tissues were also found to produce blood progenitor clusters at the same time point, including placenta, yolk sac, vetelline and umbilical arteries (Alvarez-Silva et al., 2003, Gekas et al., 2005, Ottersbach and Dzierzak, 2005, de Bruijn et al., 2002) however, only the AGM derived progenitors have the ability to reconstitute adult blood system by day 10.5 (Kumaravelu et al., 2002). A few days later, blood progenitors derived from these vascular tissues also gain the ability to reconstitute haematopoiesis in irradiated mouse, but as blood circulation has already established in the embryo at this time point, it is difficult to exclude the possibility that these cells were originating from the AGM region. As all current lines of evidence point to the AGM region as the first and major site for HSC development, in this study we are mainly focusing on definitive haematopoiesis originating in this area and the molecular programming involved in AGM derived haematopoiesis.

1.3 HSCs are derived from a sub population of endothelial cells (haemogenic endothelium) in the AGM region

Soon after the chick quil chimera experiment by Dieterlen-Lievre (1975) that provided evidence for the intra-embryonic origin of HSCs, intensive morphological and lineage tracing studies were carried out to determine the origin and nature of cells that give rise to HSCs. These studies led to identification of intra-aortic haematopoietic clusters (IAHCs) associated with the aorta in the AGM region that contain cells capable of engrafting adult recipients. The close association between these clusters and the endothelial cells lining of the DA also suggested that HSCs might be derived from endothelial origin, giving rise to the theory of haemogenic endothelium. To investigate this theory, Jaffredo et al. (1998) injected the endothelial and macrophage specific marker DiI-labelled AcLDL into chick embryos and noticed that the HSCs clusters budding from ventral wall of the DA were positive for the injected endothelial marker, thus demonstrating for the first time that HSCs are derived from endothelial origin.

The other confirmation came from the use of inducible Cre/loxP system, in which the promoter of the endothelial gene *VE-cadherin* was used to initiate recombination of a Cre reporter gene, and so label endothelial cells at E9 of mouse embryogenesis. Because the

induction is only done for a short period of time, it only labels cells positive for VE-Cadhirin at that time point. The labelled cells and their progenies were then traced throughout development and into adulthood, and result was that at least 10% of adult HSCs were labelled, and so were derived from cells expressing *VE-cadherin* during early embryogenesis (Zovein et al., 2008, Oberlin et al., 2002). Additional evidence also emerged from the experiment of Chen et al. (2009) in which they used the Cre/loxP system to specifically delete the *runx1* gene flanked by two loxPs with a *cre* expressed under the control of the *VE-cadherin* gene promoter. This resulted in the absence of intra-aortic cluster formation and of HSCs, which confirmed that all adult HSCs were derived from endothelial cells.

In vitro experiments carried out by two independent research groups also showed the formation of endothelial cells from hemangioblasts. Likewise, both groups showed expression of the endothelial specific markers *tie-2* and *c-kit*, but not CD41, *VE-cadherin* expression and DiI-Ac-LDL uptake. Subsequently these cells differentiated into blood cells expressing *c-kit*, CD41 and then CD45, but not *tie-2* (Lancrin et al., 2009, Eilken et al., 2009).

1.4 Zebrafish as a model to study haematopoiesis

Historically several vertebrate models have been used to study the development of haematopoietic stem cells, including mouse, chick, frog and fish. This has been possible because of the high genetic and phenotypic conservation of this system across vertebrates (Amatruda and Zon, 1999). Today, the mouse is still considered the gold standard model for studying haematopoietic development, however exploring the early haematopoietic events in mice are hampered by the small size of embryos and intra uterine development, added to the high costs of maintaining and breeding the animals themselves. In contrast, invertebrate models such as the fruit fly and C.elegans lack number of blood and vascular structures and organs found in vertebrates such as the multi-chambered heart and the multi-lineage haematopoietic system (Haffter et al., 1996).

In this context, the zebrafish has emerged during the last two decades as one of the preeminent complements to the study of haematopoietic stem cells development. Apart from zebrafish similarity to mammalian cardiovascular system, the zebrafish also has multi-lineage blood cells that are regulated by vascular and haematopoietic markers homologous to their mammalian counterparts such as Gata, Lmo2, Scl, c-Myb, Ikaros, Lck, c-Fms, c-Kit, Globins, Tie1, Tek, Flk1 and Flt (Paw and Zon, 2000).

These added to their external fertilization, embryo transparency during development, which makes it easy to manipulate and monitor in real time. Moreover, the short generation time and high number of embryos produced even in weekly crosses, makes it possible to get strong statistical data from experiments. Another advantage of zebrafish is the ease of introducing germ-line mutations, which make them suitable for forward genetics (Paw and Zon, 2000). Additionally, one of the unique features of the zebrafish embryo is that blood circulation is not essential for oxygen delivery, consequently, it can live on oxygen diffusion from water for days with no blood circulation (Pelster and Burggren, 1996). This feature allows tolerating and assessing conditions that compromise cardiovascular function, which opens the door for a wide range of experiments that are impossible to carryout in mice due to complications resulting from cardiovascular abnormalities under such conditions.

1.5 Haematopoietic Development in Zebrafish

In zebrafish, as in mammals, haematopoiesis occurs through two major waves, the embryonic and the definitive waves; however, unlike in mammals, both waves occur intra-embryonically in zebrafish (Detrich et al., 1995, Gering et al., 1998, Thompson et al., 1998). During the embryonic wave, haematopoiesis occurs in two places: the anterior lateral mesoderm (ALM) in which primitive myeloid cells

and head ECs form, and the posterior lateral mesoderm (PLM) in which sub-populations of cells are specified as blood and endothelial progenitors. These specified cells then migrate to the midline to form the intermediate cell mass (ICM) (Detrich et al., 1995, Gering et al., 1998, Fouquet et al., 1997, Sumoy et al., 1997). By 18hpf all these migrating cells will have arrived in the ICM and started to further differentiate into arterial angioblasts that form the dorsal aorta (DA), venous angioblasts that form the posterior cardinal vein (PCV), and erythroblasts that form primitive red blood cells. Soon after the formation of major axial vessels, primary inter-somitic vessels start to sprout from the DA, followed by similar sprouting from the PCV that then connects to half of the ISV sprouting from the DA to form a functional circulatory loop (Isogai et al., 2003).

Before the onset of blood circulation, a sub population of the arterial angioblasts present in the ventral wall of the DA are specified to form the first HSCs indicated by the consecutive expression of the transcription factors such as Runx1 and c-Myb (Lam et al., 2010, Kissa et al., 2008, Murayama et al., 2006). These markers are homologous to the markers expressed in the ventral wall of the DA in the mouse AGM. However, confocal time-lapse studies in zebrafish have shown that, unlike mammalian HSCs that bud into the lumen of the DA and eventually join circulation, zebrafish HSCs leave the DA lining and join the mesenchyme underneath the ventral wall of the DA. They then squeeze through in between the venous ECs and leave

through the cardinal vein (Bertrand et al., 2010a, Lam et al., 2010, Kissa and Herbomel, 2010). They are then carried by the circulation to an area in the ventral tail mesenchyme that develops into the caudal haematopoietic tissue (CHT), which is an intermediate haematopoietic organ equivalent to the foetal liver in mammals (Murayama et al., 2006). At this stage, some of these cells further differentiate into erythrocytes and myeloid cells, whereas others proliferate and then the T cells migrate through the circulation to seed the thymus, whereas HSCs seed the kidney, to provide all blood cell types throughout life (Murayama et al., 2006, Jin et al., 2007)(Figure 1.2).

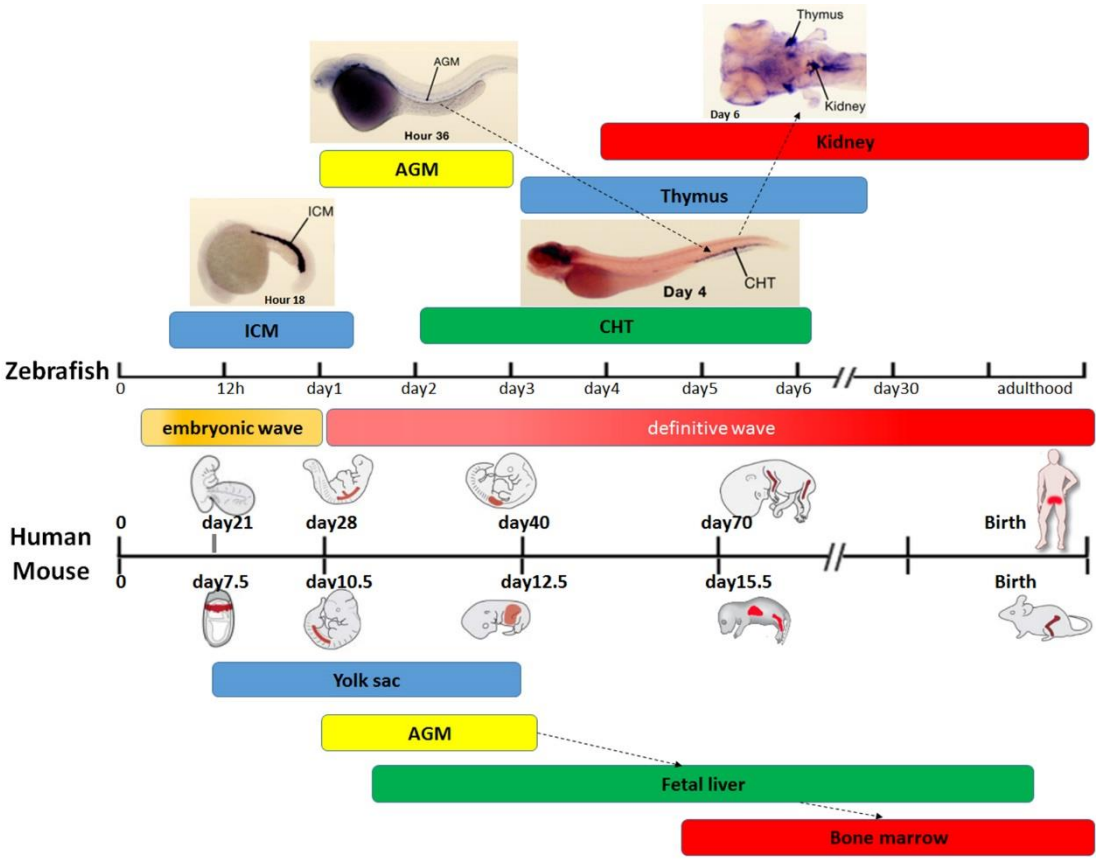

Figure 1.2: Comparison of the spatiotemporal haematopoietic ontogeny in different vertebrates.

Diagram showing the haematopoietic development and migratory root in zebrafish, compared to human and mouse. Embryonic wave that takes place in zebrafish ICM and in human and mouse yolk sac. HSCs in the three vertebrates emerge from DA endothelium in the AGM region. They then migrate to the haematopoietic intermediate tissue, which is the CHT in zebrafish and foetal liver in human and mouse. After several rounds of proliferation and differentiation, HSCs migrate to the adult site of haematopoiesis, which is the kidney and thymus in zebrafish or the bone marrow in human and mouse (Adapted from Detrich et al., 2011, Orkin and Zon, 2008, Baron et al., 2012).

Studies on *runx1* mutants and *runx1* morphants have shown that Runx1 protein depletion completely blocks definitive haematopoiesis, indicated by absence of c-Myb positive haematopoietic progenitors in all haematopoietic tissues, whereas embryonic haematopoiesis is completely unaffected. The loss of HSC formation in Runx1 depleted cells greatly support the theory that the Runx1 positive cells present in the AGM region contain HSCs (Gering and Patient, 2005, Burns et al., 2005, Jin et al., 2009).

1.6 Notch signalling distinguishes Erythroid/myeloid progenitors (EMPs) from true HSCs

In zebrafish, as in the mouse, the emergence of HSCs is preceded by specification of definitive-like progenitor cells with limited multi-lineage differentiation potential, termed Erythroid/myeloid progenitors (EMPs). These cells arise in the posterior blood island between 24-30 hpf and are first identified by co-expression of fluorescent transgenes driven by the *lmo2* and *gata1a* promoters

(Bertrand et al., 2007). In vitro assays and cellular transplantation experiments showed that these cells are only capable of differentiation into erythroid and and myeloid cells (Bertrand et al., 2007). Interestingly, it was also shown that blocking Notch signalling chemically or with *mind bomb* mutation (*mib*) does not affect the specification and differentiation of these cells while blocking expression of HSCs markers such as Runx1 and c-Myb in the vDA (Bertrand et al., 2010b). Fate mapping and transplantation assays also showed that EMPs remain in the CHT and do not have the ability to migrate and seed the thymus or kidney (Bertrand et al., 2007).

1.7 Notch signalling in definitive HSC

Three signalling molecules were found to work in a cascade required for proper vascular and HSC formation: Hedgehog (Hh), Vascular endothelial growth factor a (Vegfa) and Notch (Gering and Patient, 2005). This cascade is initiated by the release of Hh from the notochord and floor plate into the nearby somites. Upon receiving the signal, somitic cells start expressing and secreting Vegfa. The secreted VegfA protein then diffuses to the DA angioblasts in the midline, where it interacts with the Vegfa receptor Flk1. This interaction induces these cells to express Notch receptors and ligands, leading to subsequent activation of the Notch pathway (Gering and Patient, 2005). Activation of the Notch pathway involves

interaction of the Notch ligands delta and jagged with the Notch receptor extracellular domain (NECD) on adjacent cells (Figure 1.3). Upon binding, the NECD is cleaved and endocytosed by the signal sending cell in the presence of functioning ubiquitin ligase (Itoh et al., 2003). The remaining part of Notch receptor in signal receiving cell then becomes susceptible to γ-secretase, which cleaves it and releases the Notch intracellular domain (Nicd). Nicd then enter the nucleus where it forms a complex with Rbpj (Csl) and co-activators. The complex then binds Rbpj binding sites in enhancer and promoter sequences of Notch target genes.

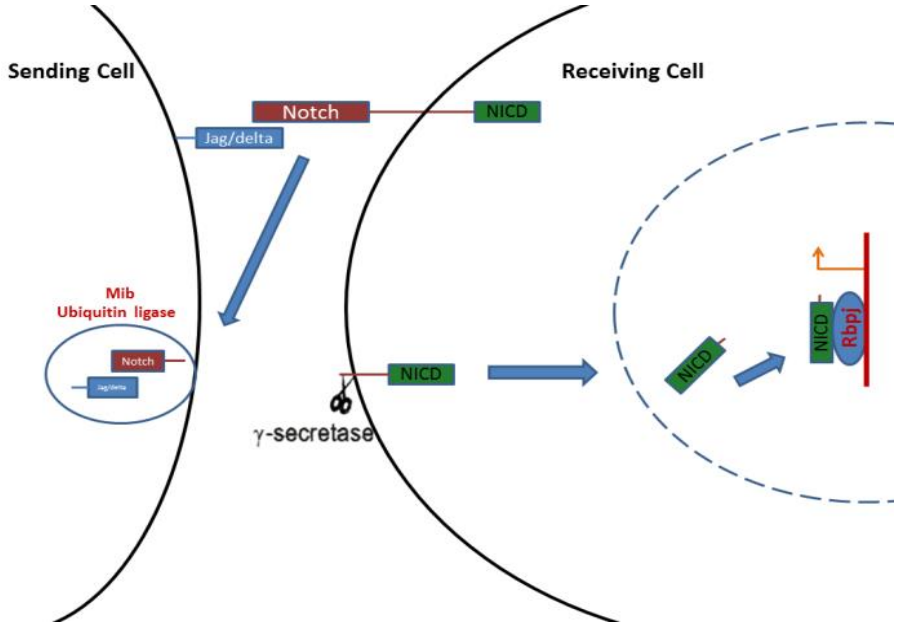

Figure 1.3: Representation of the Notch signalling pathway. Activation of the Notch pathway is triggered by the interaction of the Notch ligands (blue) with the NECD (red) on an adjacent cell. Upon binding, the NECD get cleaved and endocytosed by the signal sending cell in presence of functioning ubiquitin ligase (the blue circle on the left). The stump of Notch receptor in signal receiving cell then becomes susceptible to γ-secretase, which cleaves the stump and releases the Nicd. Nicd then enters the nucleus where it forms a complex with Rbpj and co-activators. The complex binds Rbpj (Csl)

binding sites in enhancer and promoter sequences and so activates Notch target genes.

Notch is an evolutionary conserved pathway that plays essential roles in normal embryonic development in most multicellular organisms including vertebrates. It performs this role through regulating cell fate decisions during development through a process called lateral inhibition. In this process, Notch signals to neighbouring cells to prevent them from adopting equivalent identity (Kopan and Ilagan, 2009). The pathway was first discovered in Drosophila, where mutations were found to be linked with indentations (Notches) in the fly wings (Morgan, 1917). Soon after its discovery, the pathway became a target for extensive studies. It is now known that the pathway is involved in a wide variety of cell fate decisions during development, including neurogenesis, somitogenesis, angiogenesis and haematopoiesis. In haematopoiesis Notch was shown to be involved in the regulation of HSC differentiation, proliferation, survival and apoptosis (Penton et al., 2012).

The link between Notch signalling and haematopoiesis was first discovered in the early 1990s, when defected Notch1 signalling was linked with certain types of chromosomal translocation lymphoid leukaemia (Ellisen et al., 1991). Cloning the truncated human Notch1 from this translocation leukaemia into retrovirus constructs, then injecting the construct to mice, was also shown to lead to similar lymphoid leukaemia in 50% of injected mice. Abnormal Notch

signalling was also found in myeloid leukaemia, and several studies suggested a Notch-induced suppression in myeloid progenitors differentiation (reviewed in Weber and Calvi, 2010).

Additionally, in vivo and in vitro studies in the mouse that involved blocking and over-activating the Notch pathway also confirmed the requirement for Notch in endothelial and HSCs development. For instance, when Varnum-Finney et al. (2000) infected murine bone marrow cells with a retrovirus containing a constitutive active form of *notch1* gene, they succeeded in establishing immortalized cell lines that generate progeny with either lymphoid or myeloid characteristics both in vitro and in vivo. Kawamata et al. (2002) also reported that over-activating Notch with constitutively active Nicd in mouse embryos, suppresses the B cell lineage development and increases development of thymus cells T-cells. On the other hand when (Kumano et al., 2003) surgically removed the AGM region from *notch1*$^{-/-}$ mutant mice and grew it in culture they showed that the AGM-derived cells from *notch1*$^{-/-}$ mutants were unable to produce colony forming cell (CFC) units in vitro or reconstitute the blood system of irradiated adult mice. In consistence with these early studies, Notch involvement in HSCs specification during early embryogenesis was confirmed in all studied vertebrate models including chick, frog and fish (Drevon and Jaffredo, 2014, Clements and Traver, 2013, Medvinsky et al., 2011).

In zebrafish, some of the earliest evidence on Notch involvement in HSC development came with the identification of the zebrafish *mib* mutants. These mutants were first identified in large scale zebrafish mutagenesis projects due to their neurological and somitogenic abnormalities (Jiang et al., 1996, Schier et al., 1996). Apart from their neurological and somitogenic defects, these mutants were also found to lack both arterial ECs and definitive haematopoiesis (Lawson et al., 2001, Gering and Patient, 2005). Itoh et al. (2003) then showed that these mutants lack functioning Notch due to mutations in the enzyme E3 ubiquitin ligase, required for the ubiquitination of the Notch ligands, and eventually the release of Nicd.

In zebrafish there are four Notch receptor genes that are homologous to Drosophila *notch* and nine Notch ligands genes, five *deltas* and 4 *jaggeds* that are homologous to Drosophila *delt*a and *serrate* genes respectively (Espin-Palazon et al., 2014, Janicke et al., 2007). Table1.1 shows the zebrafish Notch receptor and ligand genes and their ortholog in *Drosophila* and mammals.

Table1.1: Notch ligand and receptor genes in *Drosophila* and their homologues in mammals and zebrafish.

Drosophila		Homologous		References
		Mammals	**Zebrafish**	
Ligands	*delta*	*delta-like1*	*dla (deltaA)* *dld (deltaD)*	(Haddon et al., 1998)
		delta-like3	*dlb (deltaB)* *dlc (deltaC)*	(Haddon et al., 1998)
		delta-like4	*dll4 (delta-like4)*	(Leslie et al., 2007)
	serrate	*jagged1*	*jag1a (jagged1A)* *jag1b (jagged1B)*	(Zecchin et al., 2005)
		jagged2	*jag2a (jagged2A)*	(Zecchin et al., 2005)
			jag2b (Jagged2B)	(Janicke et al., 2007)
Receptors	*notch*	*notch1*	*notch1a*	(Bierkamp and Campos-Ortega, 1993)
		notch2	*notch2 (notch6)*	(Westin and Lardelli, 1997)
		notch3	*notch3 (notch5)*	(Westin and Lardelli, 1997)
		notch4	*notch1b*	(Westin and Lardelli, 1997)

In support of *mib* mutant data, Notch whole embryo gain of function and loss of function studies in zebrafish embryos as well as expression of Notch ligands and receptors in the AGM region at the time of HSCs formation, further confirmed the essential role for Notch in embryonic haematopoiesis. Notch whole embryo loss of function experiments involved blocking the γ-secretase enzyme with DAPT and DAPM, the use of *rbpja/b* morpholinos that prevent formation of Nicd-containing transcription complex, or the expression of the dominant negative form of *rbpj* gene (*dnrbpj*) to compete with the endogenous Rbpj protein (see Figure 1.4).

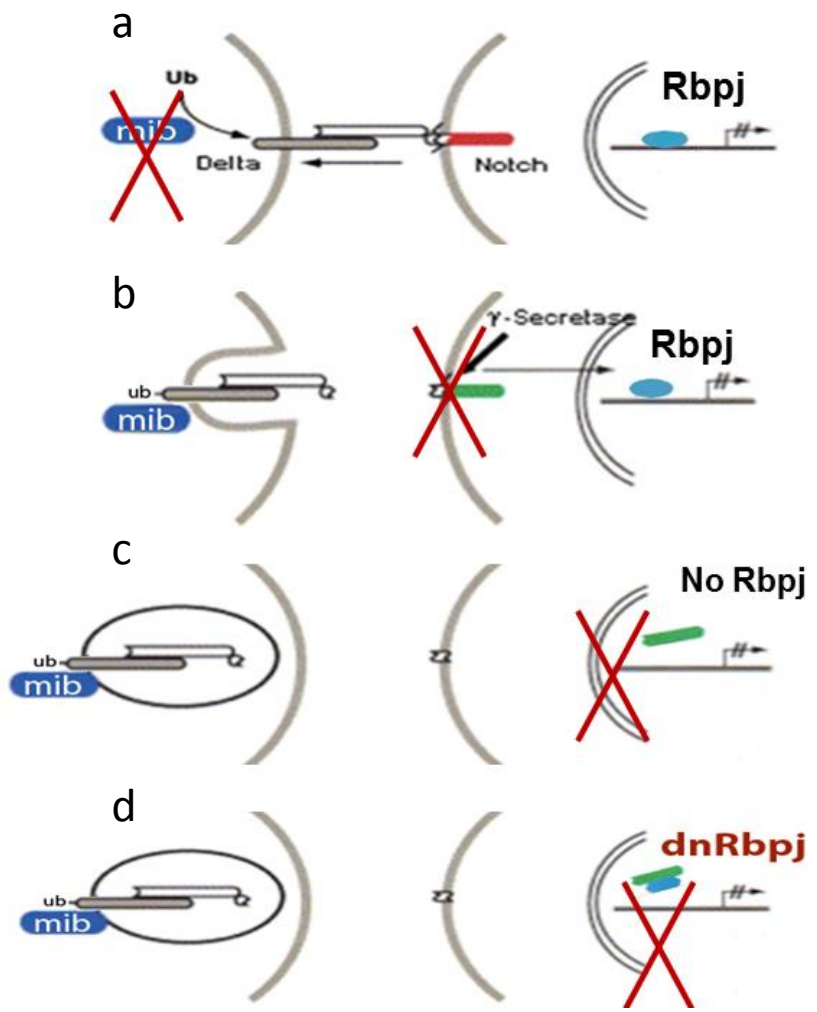

Figure 1.4: Approaches used to block Notch pathway.
(a) Deletion of the ubiquitin ligase enzyme in *mib* mutants, (B) inhibition of γ-secretase by γ-secretase inhibitors, (c) blocking Rbpj protein production with *rbpja/b* morpholinos, (D) blocking Rbpj function by occupying the binding site by the non-functioning Rbpj (DnRbpj).

Blocking Notch signalling in the whole zebrafish embryo with any of these approaches leads to phenotypes that are generally similar to those in *mib* mutants (Rowlinson and Gering, 2010). The common phenotypes observed in these embryos were somite defects, neuronal defects, and absence of HSCs. From data generated in the lab, we also showed that blocking Notch signalling with different

approaches leads to loss of the haematopoietic marker *runx1* mRNA (Figure 1.5).

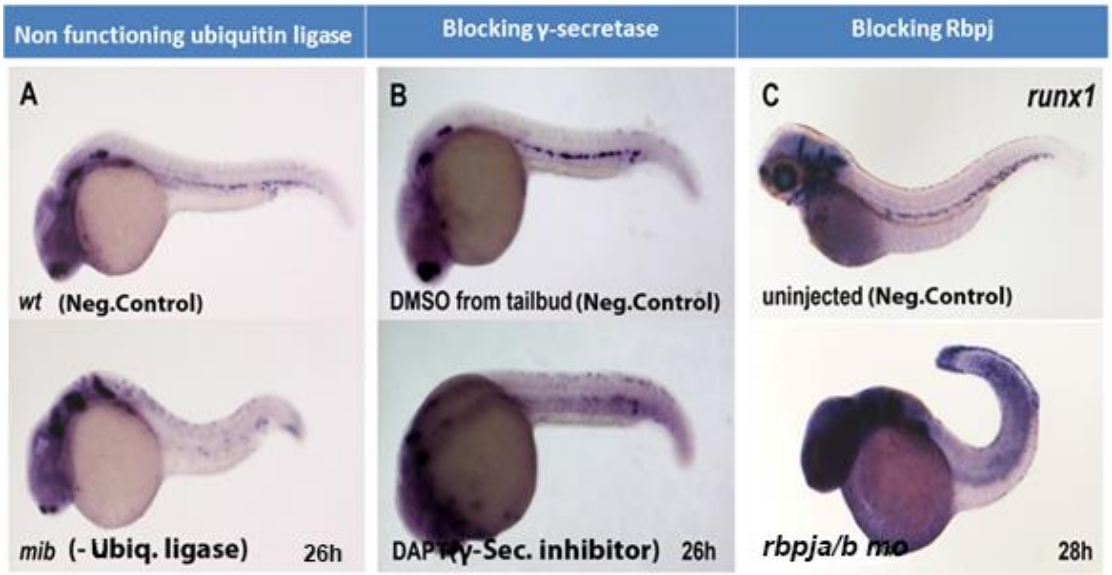

Figure 1.5: blocking the Notch pathway with different approaches blocks HSCs formation.
The Figure shows great reduction or absence of HSCs in the three approaches indicated by absence of *runx1* expression in the AGM region (the darkness in *rbpja/b* morphants in C is a stain deposition resulting from over-staining). Adapted from (Rowlinson, 2010, Rowlinson and Gering, 2010).

We also previously produced gain of function data showing that using the Gal4-Uas system to over-express the zebrafish *notch1a* intra-cellular domain (*nicd*) over-activates Notch pathway in the whole embryo, leading to ectopic expression of both arterial endothelial and HSCs markers in the cardinal vein (see Figures 1.6 and 1.7).

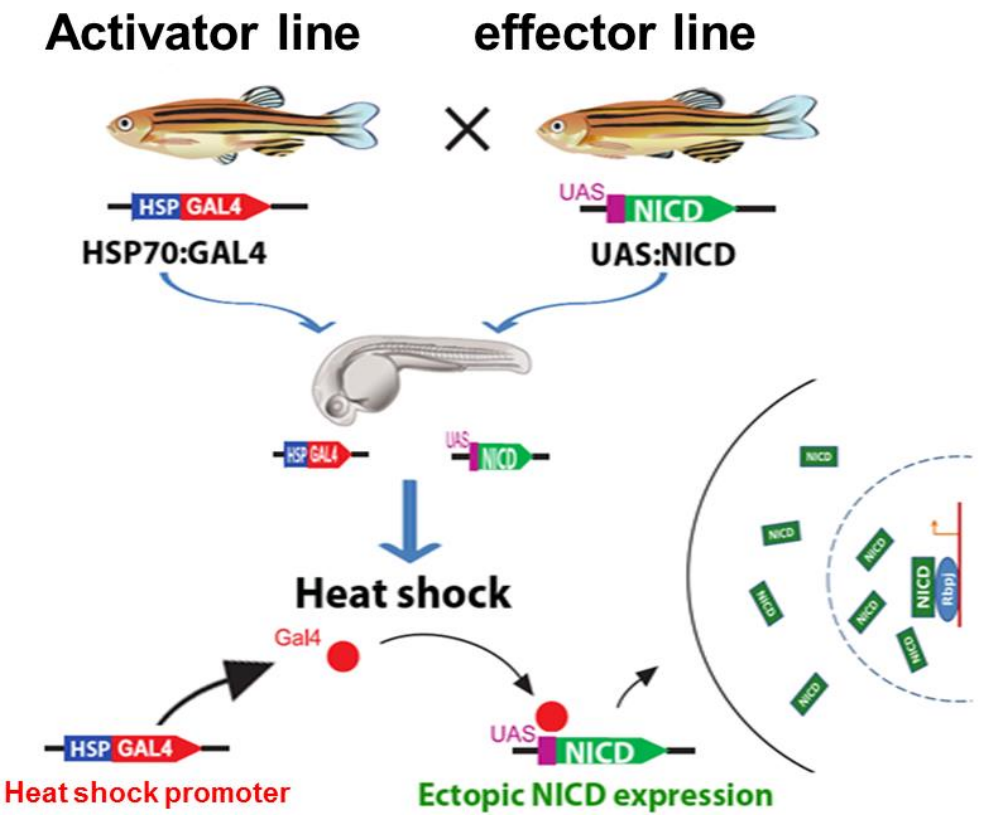

Figure 1.6: Diagram showing the heat shock over-activation of Notch pathway with the Gal4-Uas system.
Crossing the *tg(hsp:gal4*) with the tg(*uas:nicd*) lead to generation of double transgenic embryos, which when heat shocked initiated expression of the *gal4* gene. The Gal4 protein then interacts with the UAS and so activate expression of the *nicd* in the whole embryo.

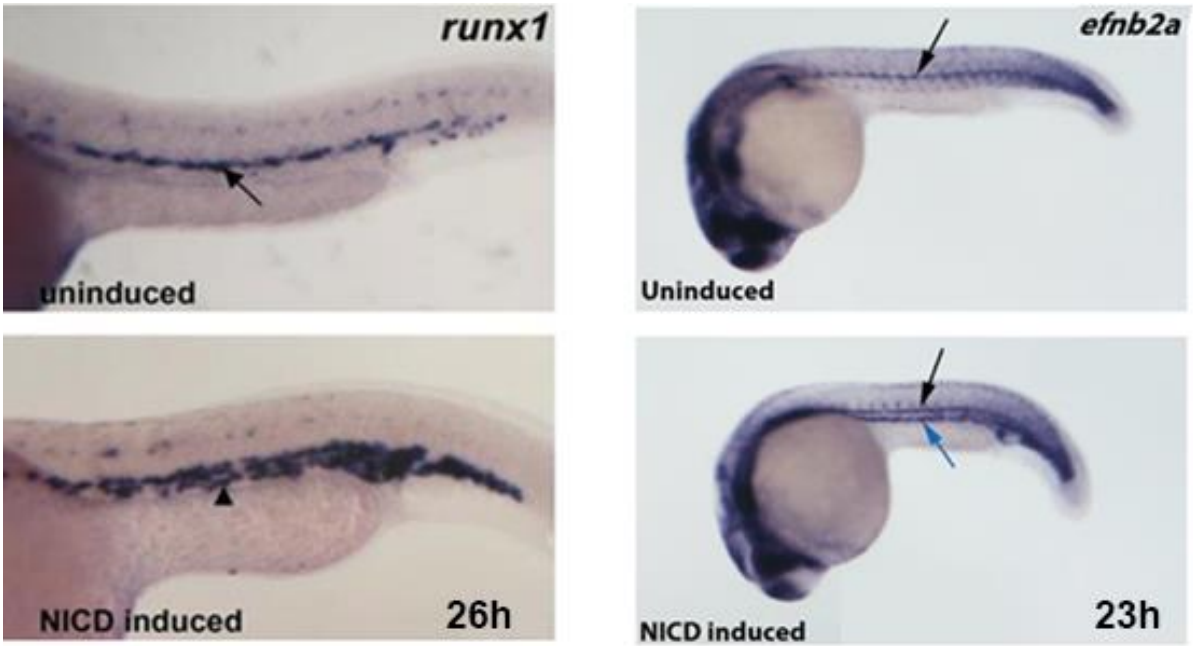

Figure 1.7: The effects of Notch over-activation on arterial and HSCs specification.
Embryos from crossing *tg(hsp:gal4*) with the tg(*uas:nicd*) transgenic fish were heat shocked at 17hpf for 30 min. the results showed increased expression of both arterial ECs and HSCs indicated by elevated expression of the endothelial marker *efnb2a* and HSCs marker *runx1*. The figure also shows that with forced activation of Notch pathway even veins become positive for these markers. Adapted from (Rowlinson and Gering, 2010, Rowlinson, 2010).

1.8 Is the requirement for Notch in definitive HSCs formation cell autonomous?

Establishment of the essential role for Notch signalling in definitive haematopoiesis by whole embryo Notch gain/loss of function studies opened up a new question, which is whether this requirement was cell autonomous or non-cell-autonomous. A first indication that the requirement was cell autonomous came from studies on chimeras that showed the in-ability of the *notch1*$^{-/-}$ mouse ES cells to contribute to definitive haematopoiesis in chimeric animals, which suggests a cell autonomous requirement for Notch in definitive haematopoiesis. However, this study does not identify the time point or developmental window at which Notch is required.

Other efforts to study the cell autonomous requirements for Notch in HSCs development, like those utilizating endothelial promoters to mis-express Notch signalling either directly or with the help of Cre-loxP recombinase system were also explored in mice, but these experiments were hampered by the severe impairment in the foetal vascular system and embryonic arrest shortly after E9 (Krebs et al.,

2004, Venkatesh et al., 2008, Uyttendaele et al., 2001, Kim et al., 2008), which is well before the time point when HSCs can be reliably detected. On the other hand, zebrafish provide an attractive animal model to study the cell autonomous requirements for Notch in definitive haematopoiesis due to their ability to survive in the absence of intact blood circulation by diffusion of oxygen and nutrients from water. However, at the time of starting this project, no published data were available about the cell autonomous requirements for Notch in zebrafish definitive haematopoiesis. This was mainly due to lack of several molecular manipulation and lineage tracing tools homologous to those available in the mouse, such as the lack of a reliable ubiquitous transgene promoter like the *rosa26* promoter which leads to ubiquitous and efficient expression of downstream genes both in embryonic and adult mouse tissues (Mosimann et al., 2011).

1.9 Recently reported non-cell autonomous requirements for Notch in definitive haematopoiesis

Despite the fact that Notch signalling was known to be active in the muscular and neural tissues in close association to the developing AGM, until recently Notch was assumed to be only required cell autonomously in HSCs formation. This assumption was based mainly on the mouse chimera experiments conducted by Hadland et al. (2004), which demonstrated failure of *notch1*$^{-/-}$ cells in contribution

to haematopoiesis. Recently, an additional non-cell autonomous Notch requirement for Notch in HSC specification was also reported (Clements et al., 2011). The reported requirement for Notch involves Wnt16/Dlc/Dld in the developing sclerotomal somites. The requirement for Notch through this pathway seems to occur earlier and in a form distinct from the previously described Hh/Vegf/Notch pathway.

Targeted deletion of *wnt16* gene with morpholinos was shown to cause severe reduction in the number of Runx1 positive cells without affecting Notch ligands and receptors in the DA (Clements et al., 2011). *wnt16* knock down was also shown to have no effect on expression of Notch components in the DA (Figure 1.8). The fact that blocking this non-cell autonomous signalling only blocks HSCs specification without affecting arterial identity, added to the early timing of signalling, raises the possibility that this signalling may interact with other signalling pathways to initiate HSC formation (Figure 1.8). Interestingly, Bmp4 signalling from the mesenchyme below the DA was also shown to be required non-cell autonomously, to polarize HSC formation in the vDA (Wilkinson et al., 2009). Similar to the Wnt16/Dlc/Dld pathway, loss of Bmp4 protein was shown to block HSC emergence without affecting the arterial fate. However, initially it was not known whether there is an interaction between the non-cell autonomous Notch and Bmp pathways to initiate haematopoiesis.

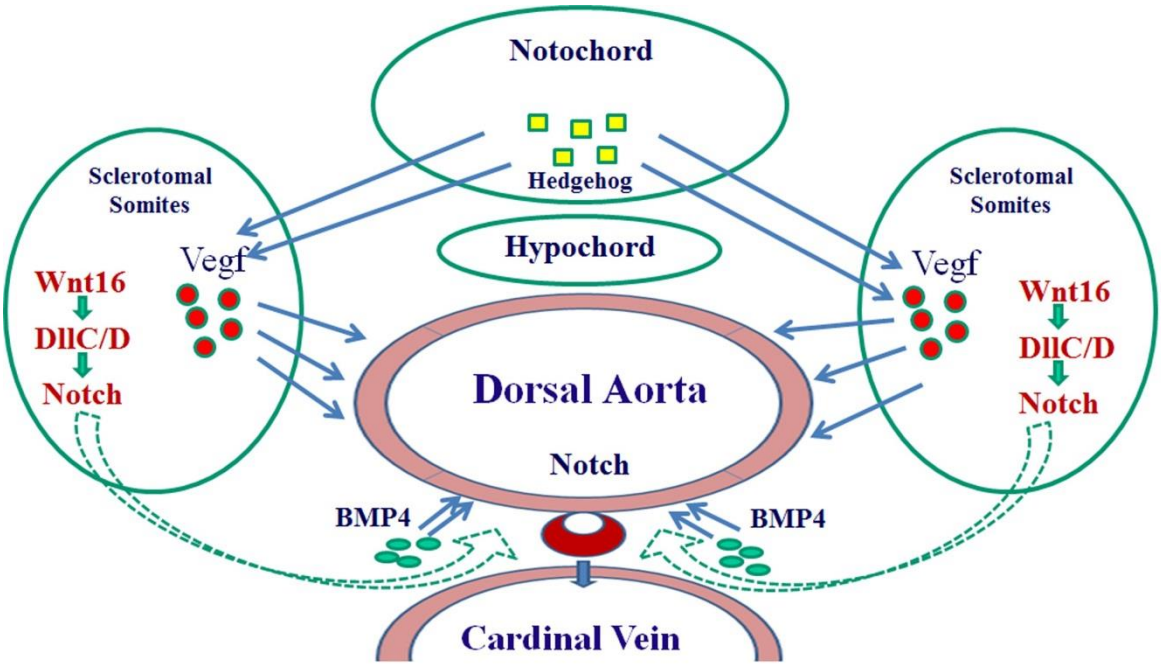

Figure 1.8: Diagram showing signalling pathways involved in HSC formation.
The diagram shows the established Hh/Vegf/Notch signalling and the non-cell autonomous signalling from the sclerotomal somites surrounding the DA, and the Bmp4 signal from the mesenchyme below the DA.

Complementary to Clements et al. (2011) work, in an efforts to understand how an early Notch signalling in the somites contributes to HSCs, Kim et al. (2014) provided data showing that this early non-cell autonomous Notch signalling is mediated by the Notch3 receptor, to promote HSCs specification. They also showed that early somite-specific Notch induction is sufficient to rescue *runx1* and *c-myb* expression in *notch3* morphants. The fact that *dlc/dld* were expressed normally in *notch3* morphants, and also the fact that *dlc/dld* mRNA

injection to the *notch3* morphants did not rescue *runx1* expression, were also used to postulate that the somitic Notch3 act downstream of the *wnt16/dlc/dld* (Kim et al., 2014).

The other addition to this Notch non-cell autonomous signalling came from the study of Lee et al. (2014), which showed early involvement for FGF signalling in HSCs specification downstream of the Wnt16, and demonstrated that the FGF receptor 4 (Fgfr4) mediates a signal between Wnt16 and Dlc, but not Dld, to regulate HSC specification. It also appears from their findings that the somitic Dlc/Dld can also interact with Notch receptors expressed on the surface of the HSC progenitors, while they are migrating to the midline along the ventral face of the somite, in a process facilitated by adhesion of the somitic Jam2a, with the HSCs progenitors' Jam1a (Kobayashi et al., 2014). This early somitic haemogenic Notch signalling is possibly required to prime these progenitor cells in a process that involves activation of the recently identified Gata2b (Butko et al., 2015).

Unlike *gata2a*, which is expressed throughout the endothelium, *gata2b* expression is restricted to the haemogenic subpopulation of the endothelium forming the DA, and this expression initiates in these cells as early as 18hpf in a Notch dependent manner (Butko et al., 2015). In birds, a later somitic contribution to haematopoiesis was also described (Pardanaud et al., 1996). In this process, the endothelial cells forming the roof of the DA were shown to originate

from a somitic mesodermal origin, then they migrate to the DA in a process regulated by Notch signalling (Pardanaud et al., 1996). Even though these cells do not appear to directly contribute to the HSCs population, their Notch activity may be essential in regulating the DA floor endothelial to haematopoietic transition. Somitic derived endothelium was also shown to restrict endothelial to haematopoietic transition to a limited developmental window by replacing the DA floor splanchnic endothelium, giving rise to haematopoietic cells (Pouget et al., 2006).

A similar somitic contribution to the DA was also recently proposed in zebrafish; as Nguyen et al. (2014) also showed that the zebrafish *meox1* mutants have an expansion in HSCs markers, and showed that this expansion resulted from an increase in somitic cells contribution to the DA in these mutants. Even though the authors were not be able to establish a link between these migrating cells and the somitic Wnt16/Dlc;Dld/Notch3 pathway, it appears from their in situ data that these migrating cells were Notch3 active, as indicated by the increase in the DA Notch3 activity in these *meox1* mutants. There is also now evidence in the zebrafish model that early Notch signalling in the somites also contributes to the polarization of HSC emergence. This is particularly true because appropriate Notch signalling is essential for somite formation and patterning, which is a prerequisite for somitic FGF signalling. In addition to FGF involvement in the Wnt16/Dlc;Dld Notch3 pathway discussed earlier (Lee et al.,

2014), the Patient lab recently reported a late FGF requirement (Pouget et al., 2014). In this newly reported signalling pathway, it was revealed that FGF acts upstream of the BMP4 localized in the sub-aortic mesenchyme, and was shown to be responsible for polarizing HSCs formation to the ventral wall of the DA (Wilkinson et al., 2009).

1.10 Reporting Notch activity in zebrafish

Notch signalling pathway is among the most widely studied pathways in most animal models. This is due to Notch involvement in various developmental roles such as neurogenesis, somitogenesis, vasculogenisis and haematopoiesis. Consequently, it is essential to precisely determine cells and tissues with Notch activity at given time point to study its involvement in these tissues development. These studies can be achieved with Notch reporter genes that highlight tissues with reporter gene activity in the experimental model of interest. However, the generation of such reporter lines for Notch signalling was hampered by the fact that Notch signalling is mediated by several Notch receptors and ligands that have various degrees of overlap in their expression pattern and redundant functions (Espin-Palazon et al., 2014).

Notch signalling also involves several other intracellular and extracellular proteins in the process of pathway activation such as Mindbomb, Tace and γ-secretase (Itoh et al., 2003). Notch signalling

is also modulated by other pathways such as Wnt, FGF and Bmp (Bigas et al., 2013). Moreover, Notch target genes are also large families with complex expression patterns such as the Her gene family (Takke and Campos-Ortega, 1999, Takke et al., 1999). As a result, it is impossible to simply report Notch activity through utilizing the regulatory elements of any of its components or downstream targets. However, activation of the Notch pathway only occurs when Notch intra cellular domain makes a complex with Csl/Rbpj, that then binds specific DNA sequences called *csl/rbpj* binding sites. This makes using reporter lines with this binding sequence an optimal alternative. Several Notch reporter lines were generated in mice in recent years (Souilhol et al., 2006, Nowotschin et al., 2013). Despite the difference in the reporting proteins and the methodologies used to generate these lines, all these lines were similar in their utilization of the Epstein Barr Virus terminal protein 1 *tp1* promoter. This promoter due to its containment of two Csl/Rbpj-like binding sites with the binding sequence "GTGGGAAA", which enables expression of the reporting proteins in cells with Notch activity. Despite the difference in origins of the Epstein-Barr virus and Notch cellular components, the similarity in their sequences, both were found to be interchangeable (Henkel et al., 1994). For instance the EBV *tp1* promoter natively contains two binding sites for the complex of Epstein Barr Virus C-promoter binding factor 1 (CBF1) and the Epstein-Barr virus nuclear antigen 2 (EBNA2). As CBF1 and Csl/Rbpj

binding sites are identical, these binding sites also act as binding sites for Csl/Rbpj (see Figure 1.9).

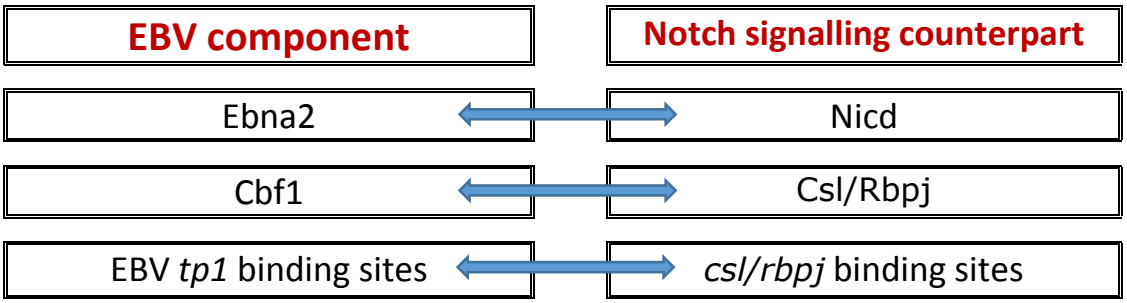

Figure 1.9 EBV components and their cellular counterparts
The first row shows the Epstein-Barr virus nuclear antigen 2 (EBNA2) that shares great similarity and interchangeability with Notch Intracellular Domain (Nicd). The second row shows the Epstein Barr Virus C-promoter binding factor 1 (CBF1) that was shown to be identical to the cellular Csl/Rbpj. The third row shows the Epstein-Barr virus EBV TP1 binding sites that were also shown to serve as binding sites for the cellular Csl/Rbpj (Henkel et al., 1994, Hsieh et al., 1996).

Henkel et al. (1994) showed that Epstein Barr Virus CBF1 is identical to Rbpj, and due to the great similarity between EBNA2 and Notch intra cellular domain (Nicd), both have the ability to bind Rbpj to activate Notch target genes (Hsieh et al., 1996).

Utilizing Csl protein binding ability to *tp1* promoter, Kato et al. (1997) generated a Notch reporter cell line using six repeats of the EVB *tp1* promoter sequence and a minimal promoter upstream of fluorescent protein gene (*luciferase*), and showed that that they reliably report Notch activity.

1.10.1 Notch reporter transgenic lines as tools to monitor and lineage trace cells with Notch activity

Several mammalian Notch reporter lines were established ex vivo and in vivo in the last few years (Gupta-Rossi et al., 2001, Joutel et al., 2004, Kohyama et al., 2005, Souilhol et al., 2006). All generated lines utilized repeats of the well characterized *tp1* promoter, to drive the reporter genes expression in Notch-active tissues. Due to the un-availability of similar lines in zebrafish at the time of starting this work, the decision was taken in our lab to establish in-house zebrafish Notch reporter lines utilizing the same promoter. To achieve this, the former technicians in our lab. (A. Haase and K. McMahon) used the *tp1-luc* construct PGa981-6 (Kato et al., 1997) to get the *csl/rbpj* like cassette and the minimal *βglobin* promoter. They then cloned this cassette and promoter sequence (we will refer to this fragment as *csl* for short) upstream of the *venus* gene. The *csl:cerulean* and *csl:mCherry* constructs were also generated by former PhD students in the lab (R. Thambyrajah and S. Modhara) by replacing the *venus* gene with either *cerulean* or *mCherry* within *tol2* backbone plasmids (Appendix 1). These plasmids were then co-injected with transposase mRNA to zebrafish embryos at one cell stage, as previously published (Kawakami et al., 2004), and embryos with mosaic fluorescent expression were grown to adulthood. Progenies of these fish were then screened for inheritance of the fluorescent protein, and positive embryos with decent expression were grown to establish stable Notch

reporter lines. This has led to establishment of three stable transgenic lines for reporting Notch activity, each with different fluorescent protein, the *Tg(csl:venus)*^{qmc61}, *Tg(csl:cerulean)*^{qmc63} and the *Tg(csl:mCherry)*^{qmc97}.

1.11 *flk1* promoter drives endothelial specific gene expression during early zebrafish development

Tissue-specific promoters are powerful tools, commonly used for tissue specific genetic manipulation in mice and zebrafish animal models. To enable studying the cell autonomous requirements for Notch in definitive haematopoiesis we decided to use the *flk1* promoter to specifically manipulate the Notch pathway in the endothelial cells, which includes the endothelial cells from which HSCs first emerge in the vDA. The following is an introduction about the expression pattern of the endogenous *flk1* gene and identification and utilization of its promoter to label, lineage trace and also to specifically genetically manipulate *flk1* active tissues.

The mammalian receptor tyrosine kinase Flk1 (also known as Kdr,Nyk, Vegfr2) is a receptor for the vascular endothelial growth factor receptor 2 Vegfr2. *flk1* is first expressed in the early lateral mesoderm on the surface of cells committed to form both the vascular and haematopoietic systems, then during later stages of embryonic development. *flk1* expression then persists in the endothelial cells,

while is lost in most cells committed to the haematopoietic lineage (Yamaguchi et al., 1993). Genetic studies showed that Flk1 plays an essential role in the establishment of the vascular and haematopoietic systems, and its deletion in the *flk1*$^{-/-}$ mutant mice leads to failure in vascular and haematopoietic development and mice death by E 9.5, (Shalaby et al., 1995). Moreover, *flk1*$^{-/-}$ ESCs were shown to be in-capable of contribution to the chimeric mouse endothelial or haematopoietic system (Shalaby et al., 1995).

The early expression and specificity of *flk1* makes it an ideal marker for the vascular and blood progenitors and endothelium through detection of its mRNA (Yamaguchi et al., 1993) as well as protein with antibodies that specifically bind and label these populations of cells (Kataoka et al., 1997). *flk1* promoter was also used to follow expression of reporter genes in live embryos through *lacz* or *gfp* knock-in down-stream of the *flk1* promoter (Shalaby et al., 1995, Ishitobi et al., 2010). *flk1* promoter was also used to specifically mis-express other genes, specifically in the *flk1* active cells and their progenies, such as expression of activated Notch directly under the *flk1* promoter by Uyttendaele et al. (2001). *flk1* promoter was also integrated with the recombinase system to enable conditional knockout, and also for genetic switching (Motoike et al., 2003). This system was shown to be useful in the mouse model to drive expression of recombinase genes such as the *cre* recombinase, with

presence of floxed genes to enable conditional knockout of target genes, specifically in *flk1* active cells.

Soon after identification of the mouse *flk1* gene, three independent groups simultaneously identified a DNA sequence with close homology in zebrafish (Fouquet et al., 1997, Sumoy et al., 1997, Liao et al., 1997). The identified zebrafish gene was found to share an overall of 60% cDNA sequence identity with the mouse *flk1*. The identified gene was initially named *flk1/kdr* by the zebrafish community. However and due to identification of a duplicate gene (discussed in *flk1* knockout) with high similarity in structure and function to the initially identified *flk1* gene (Bahary et al., 2007), the *flk1* name was changed initially to *kdra* and then to *kdrl* (Bussmann et al., 2008). This thesis still uses the term *flk1* to refer to the firstly identified zebrafish *flk1* on chromosome 4 due to the wide use of this term in the literature and the great similarity in its expression pattern to the mouse *flk1* gene.

Although the zebrafish *flk1* is expressed in the axial and ISV during early development, its knockdown was shown to be milder than that seen in mouse and it does not affect vasculogenesis or haematopoiesis (Habeck et al., 2002). Other cytoplasmic or kinase domain mutations identified in the same gene were shown to cause vascular development defects (Covassin et al., 2006) but still milder than that seen with the deletion of the Vegf signalling mediator *plcg1*

(Lawson et al., 2003) or treatment with the Vegf receptors inhibitor (SU5416), suggesting a compensation from other genes.

To resolve this issue, Covassin et al. (2006) searched the zebrafish genome for a gene with homology to the previously identified *flk1* gene, and found an orthologues gene (*kdrb/kdr*) on chromosome 20 that has a marked overlap with the previously identified *flk1*. Over-expression of the newly identified gene was found to partially rescue *flk1*, and the combined knockdown of the two genes with morpholinos, leading to more severe vascular defects, including partial loss of the main axial vessels and complete loss of ISV, but with apparently un-affected haematopoiesis (Bahary et al., 2007). Because newly identified *flk1* homologue (*kdrb/kdr*) was found to exhibit a pan mesodermal expression pattern (Bussmann et al., 2008), which makes it un-suitable for endothelial specific gene mis-expression or lineage tracing, in this thesis I am only focusing on the firstly identified *flk1* gene and its promoter.

In situ hybridization was performed by the three labs in which zebrafish *flk1* gene was first identified to analyse its expression pattern (Fouquet et al., 1997, Sumoy et al., 1997, Liao et al., 1997). All three studies showed that *flk1* specifically marks cells that follow the distribution and migration of the endothelial cells, as previously described by Al-Adhami and Kunz (1977). *flk1* expression was detectable in zebrafish embryos between 5-7 somites (about 12hpf)

in the form of two bilateral lines located in the lateral mesoderm both in the trunk and the head regions. These cells then migrate medially to form the main trunk and head vasculature, including the haemogenic endothelium in the vDA that initiates the haematopoietic system (Figure 1.10, A-C). At 15 somites two waves of migrating *flk1* expressing cells become evident, the medial *flk1* high expressing cells that mainly form the DA angioblasts followed by the *flk1* low expressing cells that mainly form the CV angioblasts (Sumoy et al., 1997, Kohli et al., 2013). At the 24 somites stage (20hpf) all migrating cells reach the midline to form the DA and the CV. Some *flk1* positive cells are now also visible between the somites and they are the early ISV forming endothelium. At 24hpf *flk1* mRNA become visible in all vascular tissues, with arterial preferability of *flk1*, unlike what is observed with the other tyrosine kinase receptor *flt4* that becomes restricted to the veins (Thompson et al., 1998, Fouquet et al., 1997). The developing vascular tissues continue to express *flk1* until at least 36hpf, then Flk1 activity is greatly reduced and becomes hardly detectable. Apart from blood and endothelial progenitors and endothelial expression of *flk1*, both Liao et al. (1997) and Sumoy et al. (1997) also reported *flk1* expression in the hindbrain and the endocardium (Figure 1.10 A), however *flk1* expression in these non-endothelial tissues only exists for a short period of time then becomes undetectable.

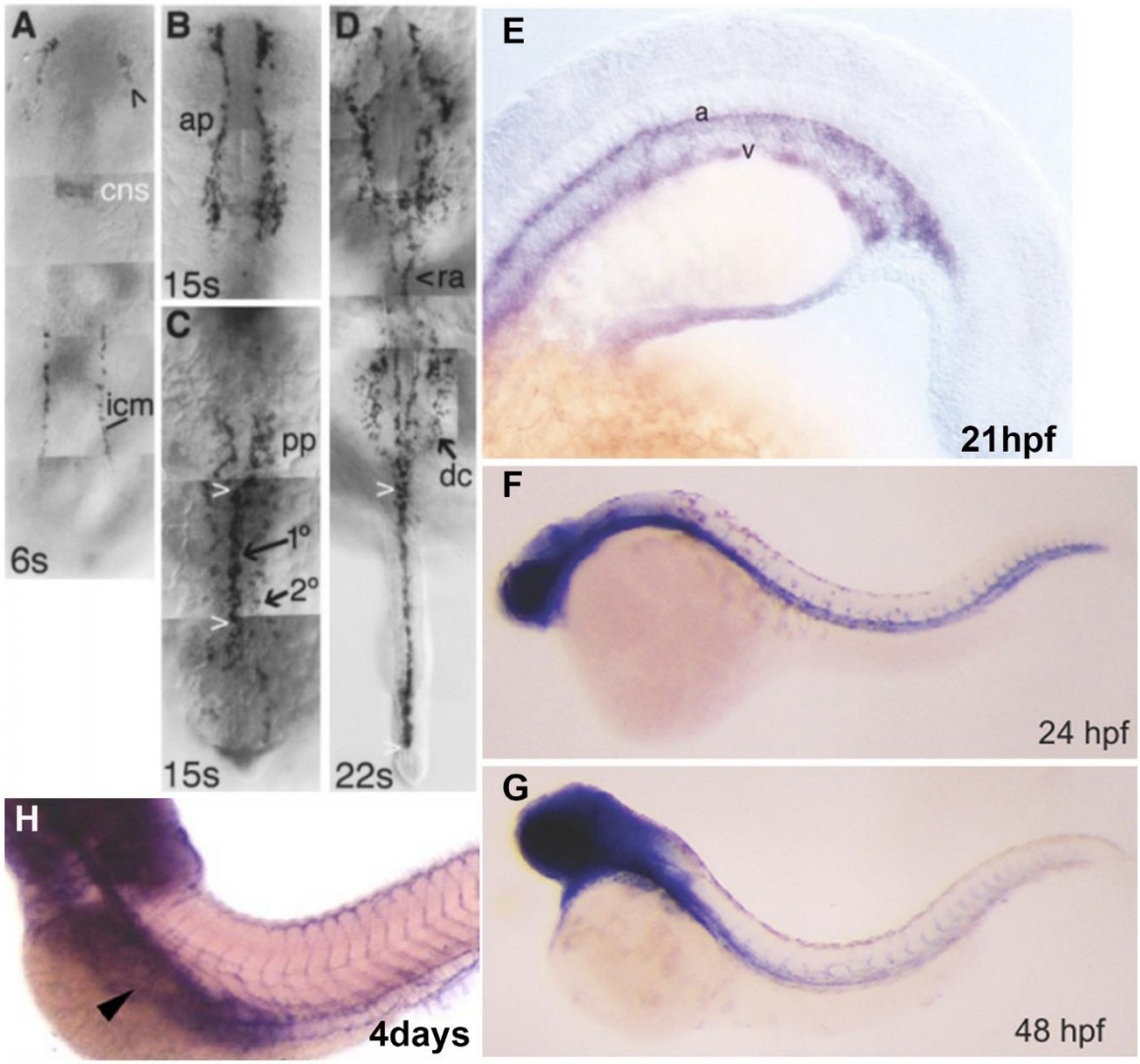

Figure 1.10: *flk1* expression pattern during zebrafish early development.
Whole mount in situ hybridization of *flk1* expression at the six somite (A), 15 somite (B-C), 22 somite (D), 21 hpf (E), 24hpf (F), 48hpf (G), 4 days (H). (A) *flk1* is expressed in two lateral lines along the intermediate cell mass (icm) and other bilateral lines of endothelial precursor cells anteriorly (arrowhead). A weak expression of *flk1* is also seen in the lower part of the central nervous system (CNS). (B-C) *flk1* expression expand both anteriorly and posteriorly. (C) Two waves of migrating cells become distinguishable (1º and 2º waves cells). (D) At 22 somites, all migrating cells in the trunk and tail arrive to the midline and the head and trunk positive cells connect at the level of the root of the aorta (ra); *flk1* positive cells also become detectable at the position of the ducts of Cuvier (dc). (D-H) Lateral view with (D) showing 21 hpf old embryo; at this stage the developing axial vessels, DA and CV become distinguishable with a higher level of expression in the DA (a) compared to that of the CV (v). (F) At 24hpf *flk1* expression is visible in all head and trunk vasculature,

including the DA, CV and ISV. (G) At 48hpf *flk1* expression is down-regulated after the vasculature is established and by 4 days it is barely detectable by in situ hybridization (H). Sources: (images A-D adapted from (Sumoy et al., 1997), image E adapted from (Fouquet et al., 1997), images F-G adapted from (Bertrand et al., 2010a), image H adapted from (Bahary et al., 2007).

Until recently, it was not easily possible to knock reporter genes into endogenous genes, which created the need to identify the *flk1* promoter and utilizes it in generating endothelial specific fluorescent reporter or recombinase lines. To achieve this, Cross et al. (2003) used a 6.5kb genome fragment 5' to the zebrafish *flk1* gene start codon to drive the green-red coral fluorescent protein (G-RCFP) expression specifically in zebrafish blood vessels. With this approach they acquired an expression pattern almost identical to that of the endogenous *flk1* gene. Following the findings of Cross et al. (2003), similar transgenic lines were independently generated in several labs with the same fragment. All labs reported expression pattern recapitulating endogenous *flk1* expression (see Appendix 2) (Beis et al., 2005, Jin et al., 2005, Choi et al., 2007, Bertrand et al., 2010a).

To enable lineage tracing of ECs, Bertrand et al. (2010a) have also generated a transgenic line with the same promoter driving expression of *cre* recombinase gene *Tg(kdrl:cre)*^{s898} and showed a tight restriction of *cre* gene expression to the endothelium (appendix 3). With this approach, they were able to permanently label the ECs and show that the ECs can give rise to HSCs that seeded the adult

kidney. However, it was also found by the same group that the used *flk1* promoter also labels the primitive blood cells (Bertrand et al., 2009).

To further characterise the original 6.5 kb *flk1* promoter fragment, Choi et al. (2007) generated a series of deletion variants of the 6.5kb fragment. These were cloned upstream of a *gfp* reporter gene and injected in zebrafish embryos. Analysis of transient *gfp* expression in the injected F0 embryos showed that a 0.8kb (−4.3,−3.5) enhancer and a 1.5kb minimal promoter (−1.5) were sufficient to drive *gfp* expression specifically in the endothelium of injected embryos (see Appendix 4).

Based on Choi et al. (2007) findings, we cloned the (−4.3,−3.5) enhancer and 1.5kb minimal promoter (−1.5) upstream of *gfp* into a *tol2* plasmid backbone, then co-injected the construct with *transposase* mRNA into WT embryos at one cell stage, as previously described (Kawakami et al., 2004). The injected embryos were raised to adulthood, and then screened for potential founders. This led to identification of founders whose progeny express *gfp* in a spatial and temporal expression pattern indistinguishable from the previously published line with the full 6.5kb *flk1* promoter fragment (Jin et al., 2005), (see Appendix 5) . Identified embryos were grown to establish our in-house generated line *Tg(flk1:gfp)*^{qmc67}.

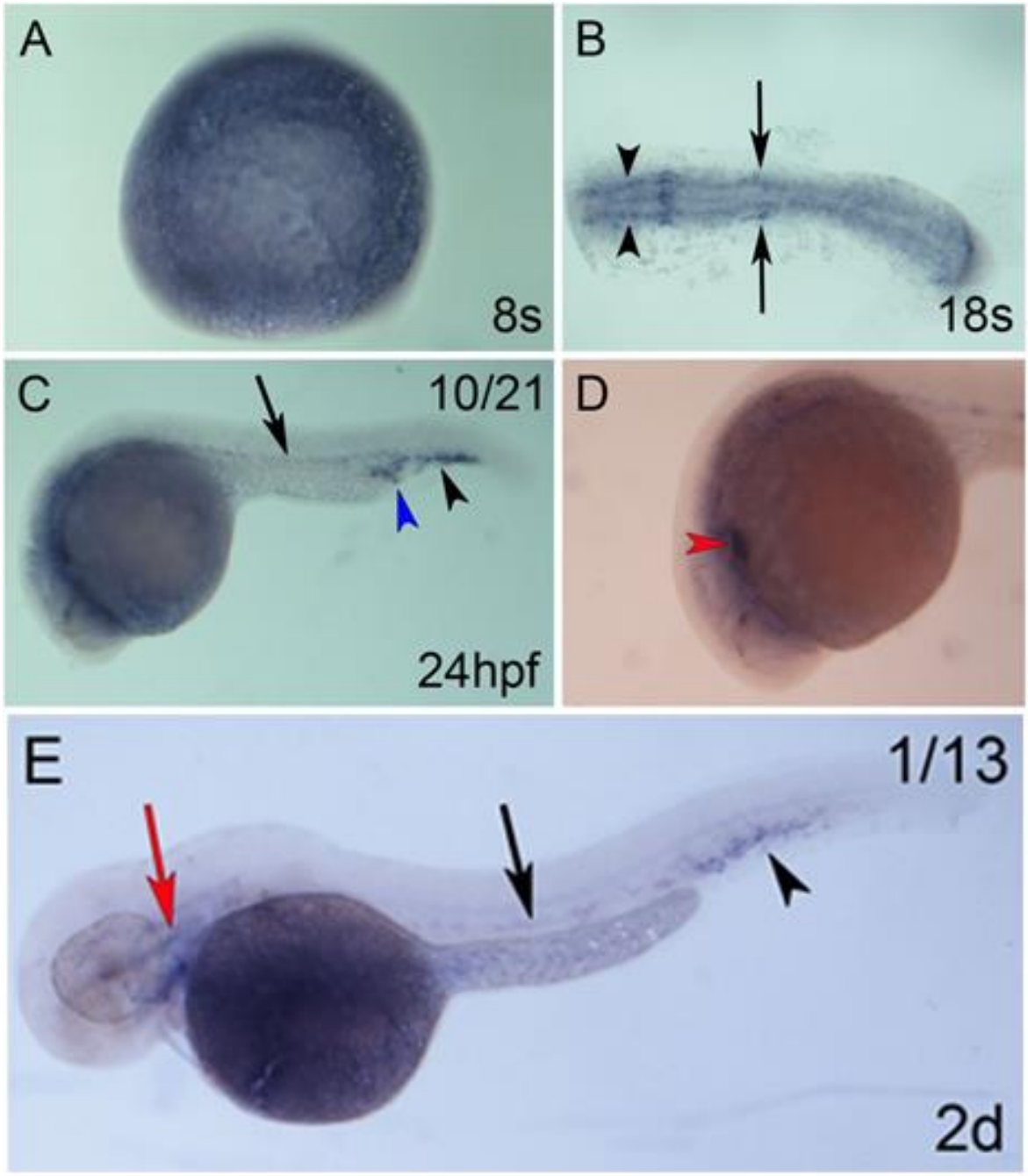

Figure 1.11: Minimal and *flk1* promoter drive *cre* expression in the endothelium.
Whole mount in situ hybridization for *cre* mRNA. (A) *cre* mRNA was undetectable at 8 somite stage. (B) at 18s *cre* mRNA become detectable in the endothelial progenitors in the ALM (black arrowheads) and the PLM (black arrows). (C-D) at 24hpf, *cre* mRNA is expressed in the developing DA (black arrow), and also in the posterior end of the ICM (blue arrowhead). *cre* mRNA is also present in the posterior blood island (PBI; black arrowhead) and the endocardium (red arrowhead). (E) *cre* mRNA persists in the dorsal aorta (black arrow), CHT (black arrowhead) and the branchial arteries (red arrow) (adapted from Drew, 2010).

To enable endothelial specific mis-expression of other genes, we then modified the *flk1:gfp* construct used to generate the *Tg(flk1:gfp)*^{qmc67} line by replacing the *gfp* gene with the *cre* gene. The generated construct was then co-injected with transposase mRNA into WT embryos at one cell stage as previously described by Kawakami et al. (2004). The injected embryos were then raised to adulthood, and screened for potential founders by PCR with the primers DB143 and DB144, which recognise and amplify a 592 bp fragment of an area made of part of the *flk1* promoter and part of the *cre* gene. This has led to the identification of founders whose progeny have the *cre* gene integrated into their genome, and establishment of the *flk1:cre* transgenic line *Tg(flk1:cre)*^{qmc101}. To analyse the expression pattern of the *cre* gene in this line, in situ hybridization analysis was performed by the former student in our lab (Drew, 2010), and the results showed an endothelial specific expression of the *cre* gene (as shown in Figure 1.11).

As in situ analysis confirmed presence of the *cre* mRNA in the endothelial tissues, we wanted to know if this mRNA leads to production of an active Cre protein, that is able to induce endothelial specific Cre recombination. To achieve this, we utilized the Cre reporter line *Tg(ef1α:loxP-gfp-loxP-dsRed2)*, which was a kind gift from Dr. Bally-Cuif's lab (Sinha et al., 2010). In the Cre reporter transgenic line, *dsRed* gene was cloned downstream a floxed *gfp-pA*

cassette under the *ef1α* promoter (Figure 1.12 B). This leads to ubiquitous expression of the floxed *gfp* gene, however in the presence of the Cre protein, the *loxP* sites get recombined and the *gfp-pA* cassette get deleted. This then makes the *dsRed* gene fall directly downstream of the *ef1α* promoter in the tissues were *cre* gene is expressed (Figure 1.12 A-C).

With this genetic reporting tool, we were able to label all cells that were *flk1* active or derived from *flk1* active progenitor, through detection of the DsRed protein with fluorescent microscopy by crossing the *flk1:cre* transgenic, *Tg(flk1:Cre)*^{qmc101} to the Cre reporter line *Tg(ef1α:loxP-gfp-loxP-dsRed2)*. This led to endothelial specific *cre* induced recombination and expression of *dsRed*, that was detectable starting from day 4. At this time point *dsRed* gene was expressed in the vascular endothelium as well as cells that are located in the CHT in the area where the HSCs are located (Figure 1.12 D), whereas un-recombined tissues were negative for *dsRed*, and still expressing *gfp* under the control of the *ef1α* promoter (Figure 1.12 E). Unlike in situ results that showed the presence of *flk1* mRNA starting from 18 somite stage, DsRed fluorescent protein was only detectable on day 4. This might be resulting from the slow maturation of the DsRed protein or the low level of produced DsRed due to down regulation of *ef1α* promoter activity, as previously reported (Hans et al., 2009).

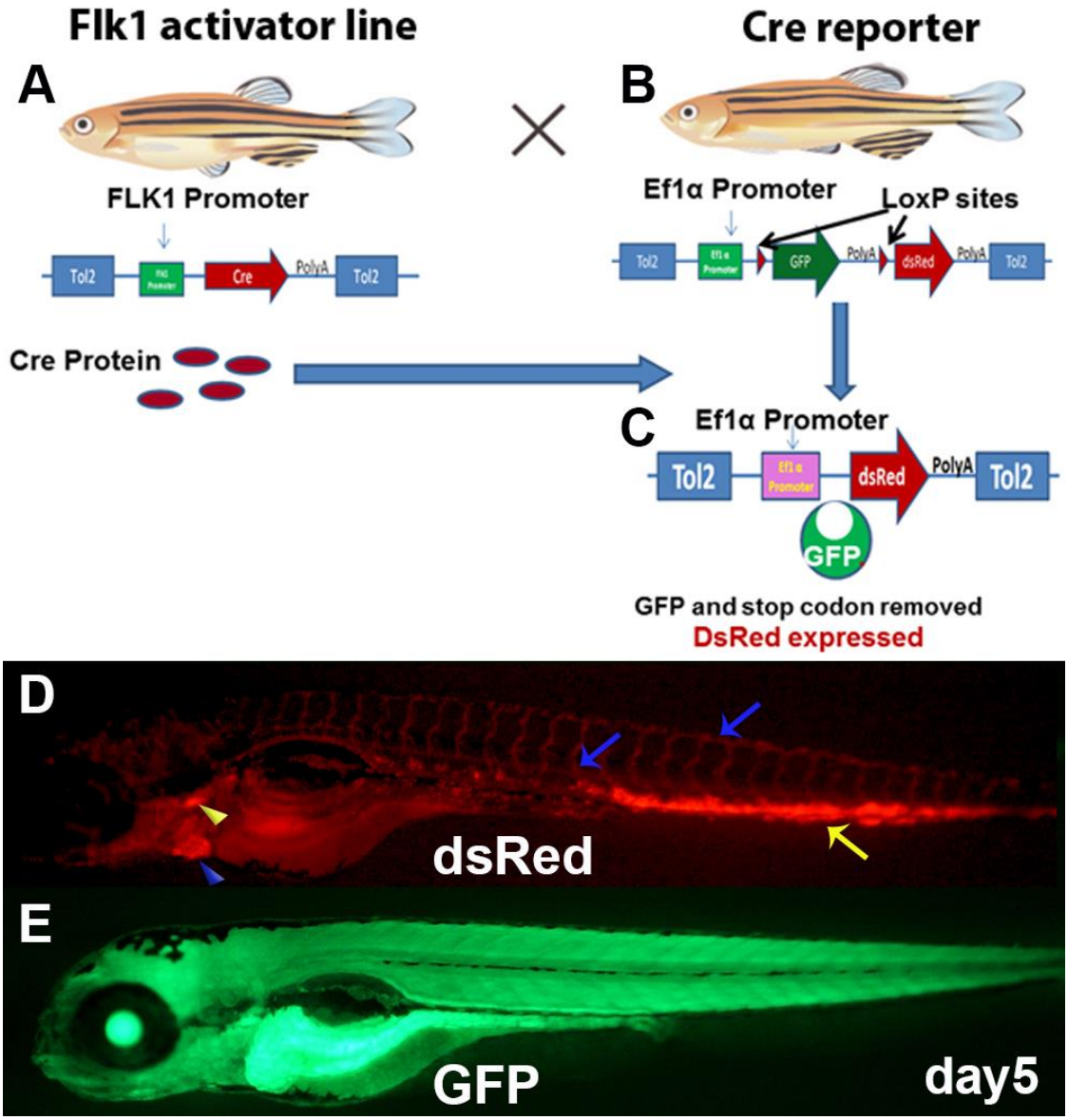

Figure 1.12: Cre-mediated endothelial specific deletion of the floxed *gfp* and expression of *dsRed* in recombined cells.
(A) Schematic diagram showing the *flk1* activator line with the minimal *flk1* promoter, *Tg(flk1:cre)*^{qmc101} that drives *cre* expression specifically in the endothelium. (B) Crossing the Cre reporter line *Tg(ef1α:loxP-gfp-loxP-dsRed2)* to the activator line enables reporting the *cre* active tissues through Cre induced removal of the floxed *gfp* and allow expression of the *dsRed* gene under the *ef1α* promoter. (D) Fluorescent microscopy showing an example of progenies resulting from crossing the *flk1* activator line *Tg(flk1:cre)*^{qmc101} to the Cre reporter line *Tg(ef1α:loxP-gfp-loxP-dsRed2*), imaged on day 5 with (D) showing DsRed fluorescent protein expression restricted to the vascular endothelial tissues (blue arrows) and the caudal haematopoietic tissues CHT (yellow arrow). DsRed is also seen in the

thymus (yellow arrowhead) and also in the heart (blue arrow head). (E) Fluorescent microscopy showing the ubiquitis expression of *gfp* under the control of the *ef1α* promoter.

To study the effects of over-activation and blocking Notch pathway in ECs, two constructs similar in their structure to the Cre reporter construct *ef1α:loxP-gfp-loxP-dsRed2* were generated in our lab by a former student (Stone, 2010). The generated constructs have either the *nicd* or the *dnRbpj* gene downstream of a floxed *cerulean* gene that is falling downstream of the *ef1α* promoter (see Figure 1.13). Just before I started this project, the generated constructs were validated by sequencing then injected by Dr. Martin Gering to establish the transgenic lines, and as a preliminary step I started this project by characterizing these injected fish to identify transgenic founders that have the injected constructs in their germline.

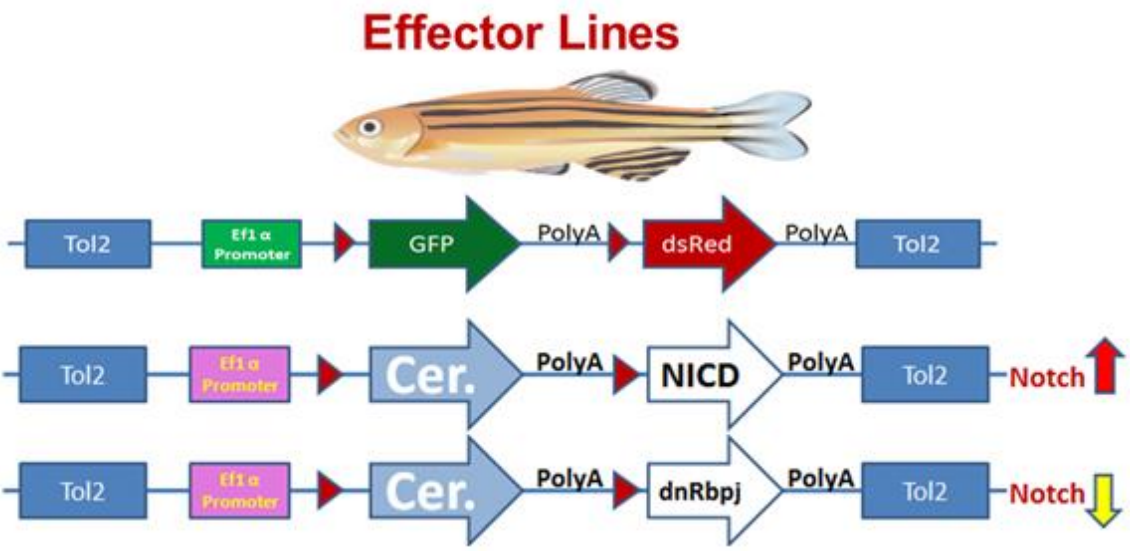

Figure 1.13: Notch endothelial mis-expression constructs. Diagram showing constructs generated and injected to establish transgenic lines to enable mix-expressing Notch signalling specifically in the endothelium when present with the *flk1:cre* construct of the transgenic line *Tg(flk1:cre)*^{qmc101}.

1.12 Tet proteins and oxidative demethylation of 5mC in vertebrate development

DNA methylation is a mechanism by which a methyl group is added to the cytosine base at its fifth carbon in a process mainly catalysed by the DNA methyl transferase enzymes (DNMTs) (Pastor et al., 2013). DNA methylation in vertebrates usually occurs in CG dinucleotide repeats upstream of genes CpG islands. Methylated promoter regions are largely associated with the suppression of downstream gene expression as transcription factors poorly bind to methylated promoters (Deaton and Bird, 2011). The methyl group can be removed passively (passives 5hmC) during cell division, or actively by the DNA oxidative ten eleven translocation (Tet) enzymes (see Figure 1.14), which further modifies the 5hmC to 5-formylcytosine (5fC) and 5-carboxylcytosine (5caC), which can subsequently be removed by base excision repair mechanism (Kriaucionis and Heintz, 2009, Tahiliani et al., 2009) . The dynamics between methylation and de-methylation states comprise one of the main regulators of pluripotency and differentiation during development (Paranjpe and Veenstra, 2015).

In consistent with this, experiments involving deletion of the three *tet* genes in mouse ESC was found to hinder the correct differentiation of the embryonic stem cells (Dawlaty et al., 2014). In contrast, mESC with individual loss of *tet1* were undistinguishable from their control

despite the slight reduction in 5hmC level and the increase in 5mC level (Koh et al., 2011). Interestingly, it was recently reported that individual *tet1* or *tet2* knockout mice are viable fertile and grossly normal (Li et al., 2011). Likewise, *tet3* knockout mice were viable through development and only dying on day 1 postnatal (Gu et al., 2011). All three *tet* genes were shown to be expressed in the developing murine brain and 5hmC was shown to be 10 times higher in mouse brain than in the ESC (Wu and Zhang, 2011). Moreover, deletion of *tet1* gene in mouse mutants was shown to result in several neurological abnormalities and brain developmental complications that were associated with reduction in 5hmC levels (Zhang et al., 2013, Rudenko et al., 2013).

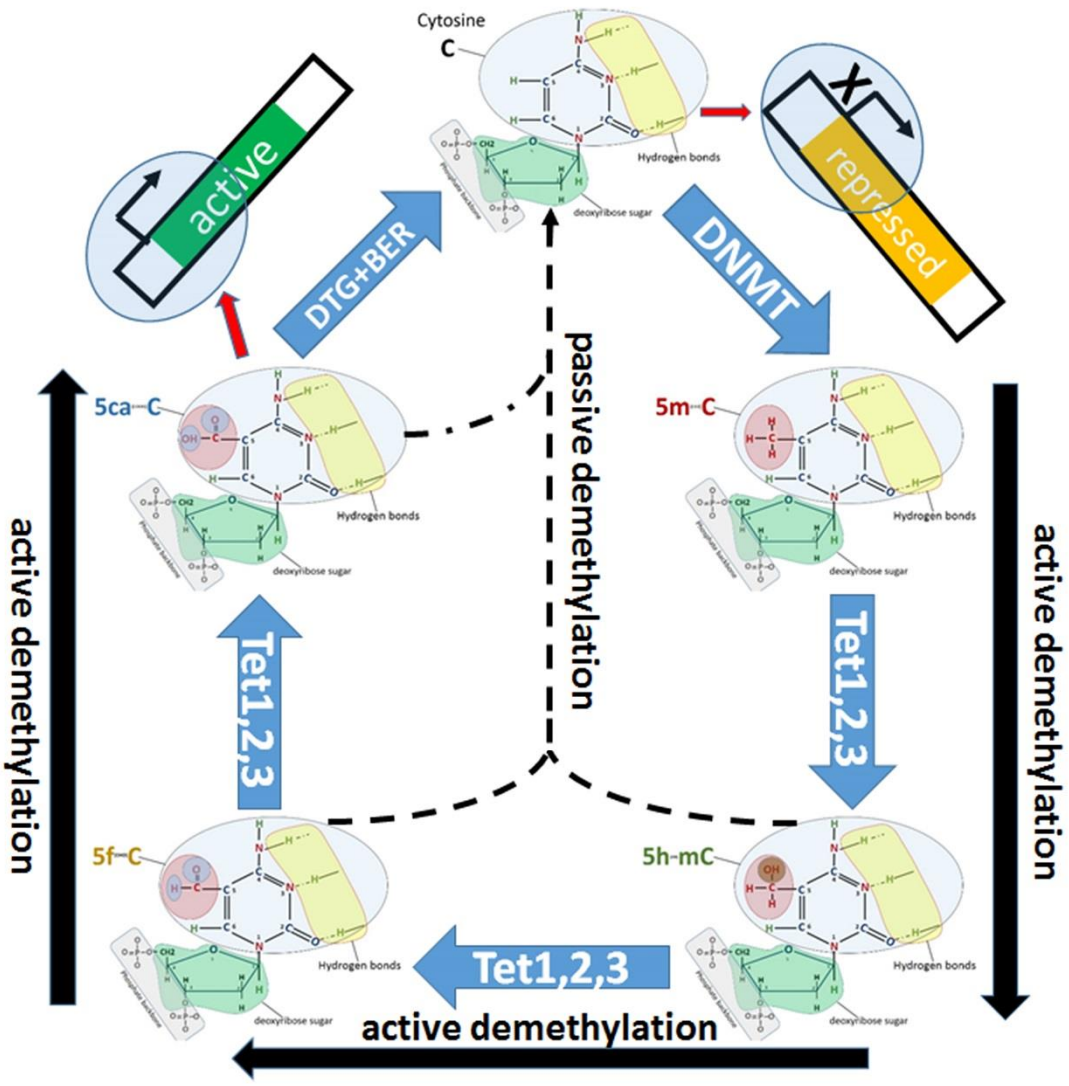

Figure 1.14: Tet enzymes mediate active DNA demethylation that affect promoters accessibility to transcription factors.
Diagram showing the chemical structures of cytosine bases at their methylated and demethylated states, the role of Tet enzymes in active cytosine demethylation and how could this process affect promoter accessibility to transcription factors and gene expression.

On the other hand, *tet2* was shown to be required for differentiation of haematopoietic stem cells and its deletion leads to increased self-renewal and was also linked to number of malignant transformations (Wu and Zhang, 2011). Further studies involving combined deletion of *tet1* and *tet2* also showed little alteration in

mouse development, while organogenesis appeared un affected, thereby suggesting a functional overlap with *tet3* (Dawlaty et al., 2013). Thus, the extent to which the the vertebrate developmental program depends on their activities is currently unclear, including their ability to oxidize 5mC.

Unlike mammalian blastocysts and ESCs that are highly enriched for 5-hmC, our lab in a collaboration with the Ruzov lab showed that chick and zebrafish embryos only gain the 5hmC mark during early organogenesis (Almeida et al., 2012). We also confirmed that the *tet* genes, known to play a rule in this epigenetic modification, only become detectable in zebrafish embryos at early somitogenesis and peak at the onset of organogenesis (Almeida et al., 2012, Collas, 1998, Rai et al., 2008).

Co-occurrence of Tet enzymes and up-regulation of the 5-hmC mark at the onset of organogenesis strongly suggests that *tet* genes mediated epigenetic modifications are essential in regulating cellular pluripotency and differentiation. Moreover, loss of function studies that involved deletion of the enzymes essential for maintaining the methylation mark, such as Dnmt1 or Dnmt3, were shown to result in severe defective organogenesis. These defects include abnormal development of the brain, eye and the intestine (Rai et al., 2006, Anderson et al., 2009, Tittle et al., 2011, Rai et al., 2010, Seritrakul and Gross, 2014). While these findings highlighted the fact that

maintaining cellular pluripotency before gastrulation is not a universal mechanism across vertebrates, these studies also showed that utilizing this feature in zebrafish animal model can provide valuable information about the role of Tet enzymes in mammalian ESCs.

Following this, to functionally test whether the Tet dependent DNA demethylation is required during embryonic organogenesis, a former student in our lab (Sabrina Boudon) performed a pilot study, in which she blocked expression of the *tet* genes during early development with anti-sense morpholinos. The morpholinos used in this experiment were designed to target the catalytic C-terminal of the dioxygenase domain in the three *tet* genes, leading to frame-shifts and premature termination of their translation. Consistent with this, she observed severe defects in organogenesis and developmental arrest after somitogenesis initiation in *tet1* and *tet3* morphants, whereas *tet2* morphants developed normally and were indistinguishable from their controls even when examined on day 3. Next, we wanted to expand this pilot study, and also to utilize our in-house Notch reporter transgenic lines together with other molecular tools to gain more insight on the mechanism by which Tet enzymes achieve this role.

1.13 Project aims

- Although Notch signalling pathway was demonstrated to be essential in HSC development from hEC progenitors in the floor of DA, it was not clear when Notch signalling initiates in these progenitor cells and how it differently affects both arterial specification and HSC development. In this project, I am utilizing in-house generated Notch reporter lines with other zebrafish molecular tools to identify when Notch signalling initiates in these hECs and how it can differently affect these two fates.

- Notch signalling was proposed to act cell autonomously in HSC in mice, but no data were available to address this question in zebrafish due to the lack of molecular tools. Recently, it was reported in zebrafish that non-cell autonomous Notch signalling is also required for HSC development. One of this project's aims is to optimise currently available zebrafish molecular tools to enable mis-expressing Notch signalling pathway, specifically in the endothelium, to study the cell autonomous requirements for Notch in HSC formation, and if cell autonomous Notch induction is sufficient to expand HSC population.

- In parallel to the Notch experiments a former student in the lab (Sabrina Boudon) identified in her preliminary data an essential rule for *tet1* and *tet3* in zebrafish organogenesis. I then took over to firstly confirm these preliminary data and then to utilize our Notch reporter lines to investigate *tet1* deletion effects on neurogenesis.

CHAPTER 2

2 Materials and Methods

2.1. Zebrafish maintenance

Embryos and adult zebrafish (Danio rerio) were raised, bred and maintained under standard conditions at 28.5°C (Westerfield and Zfin, 2000) on a 14h light/10h dark cycle. The fish were fed twice a day with dry food and brine shrimp. Approximate embryo stages were determined under the dissecting microscope, as described by Kimmel et al. (1995). Experiments on zebrafish were performed under UK Home Office Licence 40/3457.

Both live and fixed embryos to be imaged at time points later than 24hpf were treated with 1-phenyl-2-thiourea (PTU) to prevent pigmentation by addition of 1.5ml of the 0.3% PTU solution into each petri dish. To facilitate imaging of live embryos, all embryos to be imaged were pre-anesthetized by adding about 500-750µl of 4g/l pH 7-7.5 tricaine methanesulfonate (MS222) into each petri plate.

2.2 General manipulation of zebrafish

2.2.1 Microinjection

Microinjection remains the simplest and most effective method to alter gene expression and manipulate genetic contents in the zebrafish animal model. This method enables researchers to introduce RNA, DNA, proteins, antisense oligonucleotides and other

small molecules into fertilized embryo. Using this technique, an injection needle is filled with solution containing the injected molecules.

2.2.2 Microinjection needle preparation

The microinjection needles were made by pulling the glass capillaries with internal filaments into micropipettes. This is done using the micropipette puller (Sutter Instrument, Novato, CA) with the following parameters: heat (305), pull (200) time (115) and velocity (115). Needle tips were broken (just before use) with clean forceps to enable delivery of injected solution.

2.2.3 Microinjection

In general, unless specified, injections were done at one cell stage embryo. To perform injection, the collected healthy looking embryos, were lined up against a microscope slide in a petri dish lid, then kept moist with E3 buffer. Embryos were orientated so that their animal poles faced the injecting needle. The needle is then backfilled with 2-3µl of the injection solution using a microloader pipette tip (Eppendorf, Hamburg, Germany). All injections were done on the stage of a stereomicroscope equipped with the microinjector (picospritzer® III, Parker, Ohaio, USA). Injected volumes ranged

from 0.2-1.0 nl of the solution per embryo. Injection of these volumes did not interfere with embryonic development.

2.2.3.1 Co-injection of *tol2* vectors and *transposase* mRNA for transient and stable transgenesis

For all transient and stable transgene injection experiments in this project, the constructs of interest were firstly inserted into *tol2* backbone plasmids, then co-injected these *tol2* plasmids with an in vitro synthesized *transposase* mRNA into WT embryos as described below:

The injection solution mix was prepared by adding 1 µg of the *tol2* plasmid + 1µg of *transposase* mRNA, then the volume was completed to 10ul with H_2O, to make a final concentration of 100pg/nl for each. About 2-3 µl of the mix was then loaded into the microinjection needle and the rest was put on ice. I then injected 0.3-0.5nl of the solution into each embryo, making the injected amount about 25-50pg of the *tol2* plasmid + 25-50pg of the *transposase* mRNA. Injected embryos were raised at 28.5 ºC. In all constructs used in this project for transient and stable transgenesis, fluorescent reporter genes such as *gfp* or *mCherry* were included in the *tol2* plasmids either flanked by *loxP* sites or fused to the gene of interest. As a result, injection efficiency was evaluated based on the expression level and reporter protein distribution in the tissues of the injected embryo. For stable transgenesis, embryos with mosaic expression of the reporter

fluorescent proteins were raised to adulthood. These F0 fish were screened to find those that transmitted the transgene through the germline. For this purpose, the fish were outcrossed to WT and at least 100 embryos of their offspring were examined under the fluorescent microscope for inheritance of the injected transgene. Identified embryos that appeared healthy and expressed the reporter gene in expected tissues and at decent level were then given a *qmc* line number and raised to establish transgenic lines.

2.2.3.2 Co-injection of *attB* donor vector and *PhiC31 integrase* mRNA for site specific transgenesis

For all *PhiC31* mediated site-specific integration experiments, vectors were generated with either the minimal or the full attachment sites (*attB*) inserted upstream of genes of interest. *PhiC31 integrase* mRNA was also generated by in vitro transcription, then the two components were co-injected into the in-house line *Tg(gfi1.1:gfp)*^{qmc551}, which carries a single minimal *attP* landing site downstream of the endogenous *gfi1.1* promoter. Injection amounts, ratios and procedures were identical to those used in Transposase mediated transgenesis (see above). In general a solution with 100pg/nl of *attB* vector and also *PhiC31 integrase* mRNA was prepared, then 0.3-0.5nl of the solution was injected into *Tg(gfi1.1:gfp)*^{qmc551} transgenic embryos at one cell stage, then raised at at 28.5 ºC. As none of the injected vectors carried a promoter,

expression of reporter genes in the injected vectors was dependent on successful integration behind the *gfi1.1* promoter. As the *gfi1.1* promoter is active in pRBCs and the ECs in the ventral wall of DA, successful recombination should lead to reporter gene expression in these cell types. To screen for site specific integration injected embryos were screened for reporter gene expression in primitive blood cells and the vDA. PCR screening was also done using primers that amplify the sequence around the integration site to determine efficiency of integration.

Table 2.1: sequences of the minimal and full length *attB* and *attP* attachment sites.

Minimal *attB* 34bp	gtgccagggcgtgcccttgggctccccgggcgcg
Native full length *attB* 285bp	gtcgacgatgtaggtcacggtctcgaagccgcggtgcgggtgcc agggcgtgcccttgggctccccgggcgcgtactccacctcacccat ctggtccatcatgatgaacgggtcgaggtggcggtagttgatccc ggcgaacgcgcggcgcaccgggaagccctcgccctcgaaaccg ctgggcgcggtggtcacggtgagcacgggacgtgcgacggcgtc ggcgggtgcggatacgcggggcagcgtcagcgggttctcgacg gtcacggcgggcatgtcgac
Minimal *attP* 39bp (Groth 2000) 48bp	gccccaactggggtaacctttgagttctctcagttggggg
Minimal *attP* actually in *Tg(gfi1.1:gfp)*^{qmc551}	gtagtgccccaactggggtaacctttgagttctctcagttgggggcgta
Native full length *attP* 221bp (not used in this project)	Gtactgacggacacaccgaagccccggcggcaaccctcagcgg atgccccggggcttcacgttttcccaggtcagaagcggttttcggg agtagtgccccaactggggtaacctttgagttctctcagttggggg cgtagggccgccgacatgacacaaggggttgtgaccggggtgg acacgtacgcgggtgcttacgaccgtcagtcgcgcgagcgcga

2.2.3.3 Co-injection of CRISPRs donor plasmid and DNA-Cas9 & guide mRNA for site specific transgenesis

A solution made of donor plasmid, sgRNA and Cas9-encoding mRNA was prepared with varying concentrations of each components, initially starting with concentrations of 300ng/µl of Cas9 mRNA, 30ng/µl of gRNA and 100ng/µl of donor plasmid or 30ng/µl of donor fragment. The prepared solution was then injected into *Tg(gfi1.1:gfp)*^{qmc551} embryos at one-cell stage. As injected donor plasmids or fragments did not carry a promoter, expression of reporter genes in the injected vectors was dependent on successful integration behind the *gfi1.1* promoter. To screen for successful integration, Injected embryos were examined for reporter gene expression in primitive blood cells and the vDA. PCR screening was also done with primers amplifying around the integration site to determine efficiency of this technique.

2.2.3.4 cre mRNA in vitro synthesis and microinjection for whole embryo *cre* mediated recombination

Using SfiI, the *pBUT4-cre* plasmid (P161) was linearized as a template and the mRNA of the linearized construct was synthesised in vitro using the mMESSAGE *t3* kit (Ambion), according to the

manufacturer's instructions. The quality and quantity of synthesized mRNA were analysed using NanoDrop and electrophoresis. For *cre* recombination experiments, 200 pg of the *cre* mRNA were injected into transgenic embryos with *loxP* flanked sequences at one-cell stage. As all *loxP* flanked sequences in injected transgenic embryos encoded fluorescent reporter proteins, injection efficiency was determined by reduction of the excised gene's protein, and phenotypes associated with activation of downstream target.

Table 2.2: mRNAs produced and their linearization and transcription polymerases.

gene	vector	linearizing enzyme	RNA polymerase
cre	p161	SfiI	T3
transposase	p97	Not1	SP6
PhiC31 integrase	p382	SbfI	T3
cas9	p371	PmeI	T7
gfp guide RNA	p373	draI	T7

2.2.3.5 Morpholino injections

Antisense morpholino oligonucleotides were synthesized by Gene Tools, (LLC, Corvallis, Oregon), Upon delivery, stocks were dissolved then subsequently diluted in sterile H20.

The *rbpja/b* morpholino was originally published by Sieger et al. (2003), whereas *tet* genes' morpholinos were designed de novo. The working doses were determined as previously described (Nasevicius and Ekker, 2000).

2.2.4 Treatment with the γ-secretase Inhibitor XVI (DAPM)

The γ-secretase Inhibitor XVI DAPM (5mg of 10 mM powder) was ordered from Calbiochem (Cat. No. 565777, San Diego, CA, USA). Stocks were dissolved in 1024µl DMSO at a concentration of 12.5 mM and stored in 100µl aliquots at -20ºC. Embryos were treated with 100 µM of γ-secretase Inhibitor XVI starting from late epiboly stage (9hpf) until 26 hpf in batches of 25 embryos in 5ml E3 buffer to which 41µl of the 12.5mM γ-secretase stock solution was added. For negative control, siblings embryos were treated similarly but with 41µl DMSO instead of γ-secretase. Embryos were then either used for total RNA extraction or fixed in 4% PFA for in situ hybridization.

2.2.5 Heat shock experiments with the quadruple transgenic embryos *Tg(hsp:loxp-mCherry-loxp-gal4-vp16/flk1:cre/uas:nicd/csl:venus)*

To generate the quadruple transgenic embryos *Tg(hsp:loxp-mCherry-loxp-gal4-vp16/flk1:cre/uas:nicd/csl:venus)*, a triple transgenic *Tg (flk1:cre/uas:nicd/csl:venus)* fish was crossed to *Tg(hsp:loxp-mCherry-loxp-tgal4-vp16)*^{qmc138} fish, then the embryos were collected at one cell stage. The embryos were then raised at 28.5ºC until 17hpf (16-18 somite stage), then transferred into 50 ml falcon tubes in batches of 30-50 embryos, then the E3 buffer volumes

in these tubes were made up to 5ml. To perform the heat shock, the tubes were incubated in a waterbath set to 38ºC for 20 minutes, then the embryos were transferred back to petri dishes with E3 buffer at room temperature. The embryos were then raised at 28.5 ºC until they were required for examination or fixation. For late heat shock experiments, the embryos were raised until 40hpf then heat shocked for 20 minutes at 38ºC following the same procedures as with 17hpf heat shock.

2.3 General DNA and RNA work

2.3.1 DNA Phenol-Chloroform Extraction

DNA extraction from single or pooled embryos was done to separate DNA from proteins, salts and other impurities. In this procedure, the DNA and due to the negative charge on its phosphate backbone, dissolves in water, whereas all other uncharged components such as proteins, salts and fats dissolve in the phenol. In detail an equal volume of phenol:chloroform:isoamyl alcohol (25:24:1, cat no P2069, Sigma, Germany) was added to the sample. The sample was mixed vigorously and then centrifuged at 13000 rpm in a table-top centrifuge. The top layer (aqueous phase) was transferred into fresh tube and an equal volume of chloroform:isoamyl (24:1, cat no 1.02432.2500, Merck, Germany) was added to it. Subsequently, the aqueous phase was transferred into another fresh tube and then the

DNA was precipitated by addition of 0.1 volume of sodium acetate (3M, pH5.2) and 2.5 volumes of 100% ethanol, incubated at -80C° for 30min-overnight, centrifugation at 13000 rpm then removing the supernatant and keeping the DNA pellet. The pellets were then washed with 70% ethanol, dried in air for at least 20 minutes, and finally re-suspended in an appropriate volume of autoclaved water.

2.3.2 PCR amplification

Several polymerase Chain Reaction (PCR) systems were used in this project. In general, for genotyping and other genetic screening, I used the regular NEB Taq polymerase (New England Biolabs, Ipswich, USA). For TA cloning, I used the Reddy mix extensor PCR/Abgene Mastermix (Termo Scientific cat. no. AB-0794/A, MA, USA) that contain in addition to Taq polymerase activity, a thermostable proofreading activity to minimize mutations and maintaining the adenine to the 3' end of the product for TA cloning. In cases where amplified fragments need to be cut with restriction enzymes before cloning or when amplified fragments need to be submitted directly for sequencing, I used the Q5 High-Fidelity DNA Polymerase (NEB). Amplification reactions were carried out using TECHNE TC-512 (Bibby Scientific, Stafford UK) with the reaction components and volumes summarized in (table 2.3). Cycling conditions used in these PCR reactions are also summarized in (table 2.4).

Table 2.3: PCR reaction volumes.

components	Taq polymerase reaction	Q5 polymerase reaction	Thermo (Abgene) mix reaction
frwd primer (10 µM)	2 µl	2.5 µl	2 µl
revse primer (10 µM)	2 µl	2.5 µl	2 µl
Template (100ng/µl)	2 µl	2.5 µl	2 µl
dNTPs (2mM)	5 µl	5 µl	-
buffer	5 µl (10XTaq buffer)	10 µl (5X Q5 buffer)	-
Taq polymeras	0.5 µl	-	-
Q5 polymerase	-	0.5 µl	-
Thermo mix	-	-	25 µl
H_2O	33.5 µl	27 µl	19 µl
Total volume	50 µl	50 µl	50 µl

Table 2.4: PCR reaction cycling conditions.

cycling condition		Taq polymerase reaction	Q5 polymerase reaction	Thermo (Abgene) mix reaction
initialization		94^{o}C for 5 min.	94^{o}C for 2 min.	94^{o}C for 2 min.
30 X for Q5 & Thermo 40 X for Taq P.	**Denaturing**	94^{o}C for 30 sec.	94^{o}C for 15 sec.	94^{o}C for 15 sec.
	Annealing	57^{o}C for 30 sec. may be optimized	57^{o}C for 30 sec. may be optimized	57^{o}C for 30 sec. may be moptimized
	Extension	72^{o}C for (1 min./kb)	72^{o}C for (1 min./kb).	68^{o}C for (1 min./kb).
for extension		72^{o}C for 5 min.	72^{o}C for 5 min.	68^{o}C for 5 min.
for hold		4^{o}C until collected.	4^{o}C until collected.	4^{o}C until collected.

2.3.3 Restriction enzyme digestion

All DNA restriction enzymes used in this project were ordered from NEB. Restriction digests were performed using the manufacturer's recommended buffers and incubation temperature. For mini-prep screenings and plasmid analysis, a typical 20 µl digestion mix was

used and set up as shown in Table 2.5, then incubated for one hour and examined by agarose gel electrophoresis. In case of digestion for cloning purposes, a 100 µl digestion mix was used and set up as in Table 2.5. To ensure complete digestion of DNA with a minimal degradation of the DNA cohesive ends, the digestion mixes were typically incubated for four hours.

Table 2.5: Typical restriction digest reactions.

components	20 µl digestion mix	100 µl digestion mix
DNA (100ng/µl)	4 µl	20 µl
enzyme buffer	2 µl	10 µl
10X BSA (100ng/µl)	2 µl	10 µl
restriction enzyme	0.5	2 µl
H_2O (2mM)	11.5 µl	58 µl
Total volume	20 µl	100 µl

2.3.4 Agarose gel electrophoresis

DNA fragments were examined by gel electrophoresis using (0.8-2 % based on fragment size) agarose gels in 0.5 X TAE buffer (40mM Tris acetate, 5mM ethylene diamine tetraacetic acid). Agarose gels were prepared by dissolving the required agarose powder in 0.5x TAE buffer by boiling the mixture in a microwave. When cooled, Ethidium Bromide was added to enable visualization of DNA. To facilitate loading and to determine fragment sizes, NEB loading

buffers and molecular ladders (NEB) were used in all gel experiments, and gels were usually run by applying a voltage of 120V for 30 minutes, or 80V for one hour if fragments need to be recovered from the gel. The fragments were visualised by exposure to UV light using the Bio-Rad Chemi XRS Gel Documentation system and the Bio-Rad (Quantity One® software, CA, USA).

2.3.5 Extraction of DNA from agarose gels

Following the gel electrophoresis, bands of interest were located and cut out with a scalpel blade while the gel was visualised on a UV light. The DNA was then extracted from the gel using NucleoSpin kit (Duren, Germany) following the manufacturer's instructions.

2.3.6 DNA ligation and transformation

DNA ligations were carried out in 20 µL volumes (see Table 2.6), using T4 DNA ligase (NEB) following manufacturer's instructions. Reactions were incubated overnight in heat block at 16ºC, then chilled on ice and finally used to transform chemically competent bacteria. For *ta* cloning, (Promega) pGEM-T Easy plasmid and T4 ligase were used. The incubation was done overnight at 4ºC. To determine the amount of insert required in each ligation the following equation was used:

$$\text{Amount of insert} = \frac{\text{Size of insert (bp)}}{\text{Size of vector (bp)}} \times (\text{Amount of vector}) \times 3$$

Following ligation, samples were used to transform chemically competent E.coli (in-house E.coli for plasmids<6kb, or NEB high efficiency competent E.coli for larger plasmids). To determine the success of the ligation, plasmid DNA was isolated from the transformants and digested with appropriate restriction enzymes. The digests were then examined on agarose gel.

Table 2.6: Example of a ligation reaction.

COMPONENT	20 µl REACTION
10X T4 DNA Ligase Buffer	2 µl
Vector DNA (3 kb)	50 ng (0.025 pmol)
Insert DNA (1 kb)	50 ng (0.076 pmol)
Nuclease-free water	to 20 µl
T4 DNA ligase	1 µl

2.3.7 Plasmid DNA Isolation

To isolate plasmid DNA, bacterial cultures were prepared by firstly picking and inoculating transformed bacterial colonies into 3ml (mini-prep) or 50ml (midi-prep) of SOC medium containing the appropriate antibiotic (100 µg/ml ampicillin or 50 µg/ml kanamycin). Bacterial cultures were grown overnight at 37°C (14-16 hours) with shaking. Plasmid DNA was isolated from bacteria using Mini-prep or Midi-prep kits (NeucleoSpin plasmid NucleoBond Xtra Midi/Maxi, Duren, Germany), according to the manufacturer's instructions.

2.3.8 Measurement of nucleic acid concentrations

Purified DNA and RNA concentrations were determined using a NanoDrop ND-1000 (Termo Scientific, MA, USA). A260/280 wavelength ratios of ≈1.8 and ≈2.0 were used as purity criteria for DNA and RNA, respectively. In cases were the absorbance curve was skewed or showed multiple peaks, the nucleic acid was re-precipitated and its concentration was re-quantified.

2.3.9 DNA Sequencing

DNA sequencing was performed by Source Bioscience Company (Nottingham, UK).

2.3.10 Gibson assembly

Gibson assembly is a simple robust method that allows joining multiple DNA fragments with overlapping sequences in a single isothermal reaction. The assembly in this method is done by the simultaneous action of a 5' exonuclease, a DNA polymerase and a DNA ligase that are all included in one tube reaction (Figure 2.1).

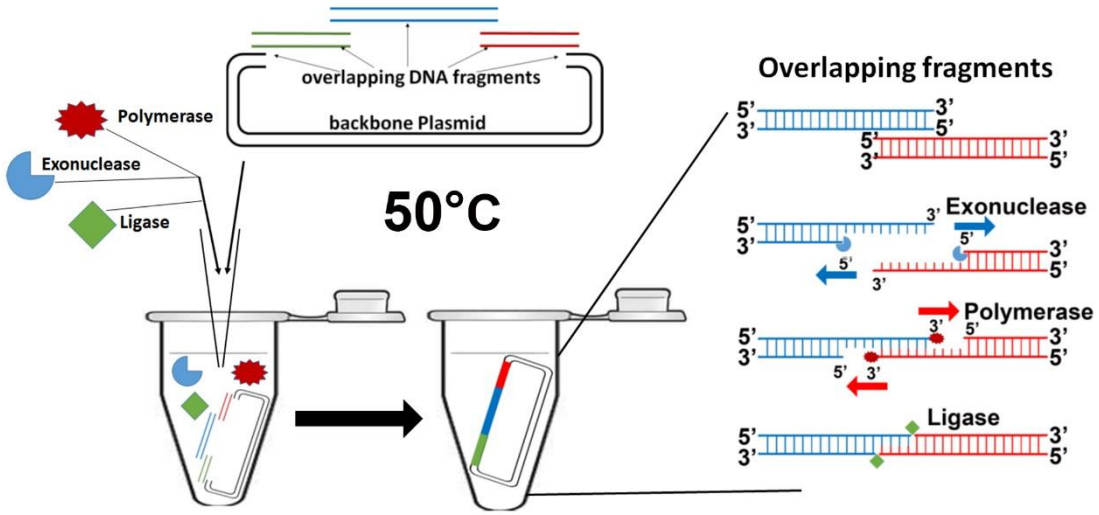

Figure 2.1: One-step assembly of fragments with overlapping sequences with the Gibson assembly approach.
Diagram showing the Gibson assembly principle and enzymes utilised. In the process, the exonuclease enzyme firstly removes nucleotides from the 5' ends to generate single strand overhangs. Complementary sequences of adjacent fragments then annealed together. DNA polymerase then extends the 3' ends to fill in any gaps. Finally, DNA ligase covalently join adjacent fragments.

The technique was first published in 2009 as an alternative to the classical approach in experiments that have led to the construction of synthetic viral and mitochondrial genomes (Gibson et al., 2009, Gibson et al., 2010, Siridechadilok et al., 2013). In this project this technique was utilised to generate several plasmids and also to fuse the *gfp* reporter gene in-frame with the 3' *nicd* gene in the *flk1:nicd-gfp* (P405) and *fli1:nicd-gfp* (P409) plasmids. The steps used to assemble plasmids using this technique are explained below.

2.3.10.1 Primer design, PCR amplification and backbone plasmid preparation

Primers used in the assembly were between 30-40 bp long. They were made of 15-20bp of the amplified fragment and preceded by the last 15-20 bp of the fragment with which the PCR fragment needed to be ligated (using 40bp primers, unless specified otherwise). When ligating to a linearized backbone plasmid, a minimum of 20bp overlap was included at both ends of the PCR product. In cases when specific sequences needed to be introduced such as restriction sites or *kozak* sequence, the sequence between the overlap was added at the 5', and the template sequence at the 3' end. For all PCR amplified fragments, Q5 high fidelity polymerase (NEB cat M0491S) was used with 57°C annealing temperature for 30 seconds and one minute/kb extension, and 30 cycles of amplification. PCR products were run on a preparative gel, cut out from the agarose gel and purified. The DNA concentration was determined on the NanoDrop. Furthermore, a small aliquot was run on a gel. To increase the assembly efficiency, the backbone plasmids were linearized using suitable restriction enzymes for four hours to ensure complete digestion with minimal degradation and nicking of the backbone plasmid.

2.3.10.2 Calculating needed fragment concentration

Gibson assembly enzymes are highly sensitive to DNA fragments concentrations and proportions. For the best outcome the fragments concentration formula of: 1 ng per 100 bp for a total reaction mix of 20 µl was used; thus, if 1kb fragment and 10 kb backbone were to be assembled, then 10ng of the insert and 100 ng of the backbone were added to 10 µl assembly mix, with the volume completed to 20 µl with H_2O.

2.3.10.3 Assembly mix incubation

Assembly incubation was done in the thermal cycler at 50°C for 1 hour. To increase efficiency, in some cases the assembly mix was divided after addition of the DNA fragments into 4 X5µl aliquots and the thermal cycler program was modified to provide a gradient with temperatures ranging from 40°C-60°C. The four tubes were then distributed in the gradient. After incubation, the four aliquots were pooled again and used to transform E.coli. The assembly mix was then incubated on ice for at least one minute before transformation. 10 µl of the chilled assembly mix was used to transform high efficiency competent E.coli (NEB) according to the manufacturer's protocol. Plating and colony screening were all done following standard procedures. Comprehensive restriction analysis and sequencing were done to confirm the correct assembly of the plasmid.

2.3.11 Zebrafish embryo sampling for quantifying remaining Notch activity in DAPM treated and mib mutant embryos by quantitative PCR

DAPM treatment was performed on embryos generated from crossing *Tg(csl:venus)*^{qmc61}+/- ♂ X WT ♀. To determine the remaining Notch activity in *mib*^{ta52b} mutants, the *Tg(csl:venus)qmc61+/-* transgene was introduced in the background of *mib*^{ta52b} carriers. Next, ♂ *Tg(csl:venus)*^{qmc61}+/-; *mib*^{ta52b} heterozygous were crossed to ♀ *mib*^{ta52b} heterozygous carriers. Due to the difficulty to identify the *mib* homozygous mutants at 26hpf, and to maintain the percentage of affected venus +ve embryos, *mib* mutants, DAPM treated and un-treated control samples were corrected as shown in (Figure 2.2). This makes the final number of embryos used for total RNA extraction in each batch 200. Before performing the RNA extraction, embryos were dechorionated, anesthetised then collected in 1.5 ml Eppendorf tubes. They were then de-yolked, washed and finally frozen at -80°C for RNA extraction. Three biological samples were collected from each group.

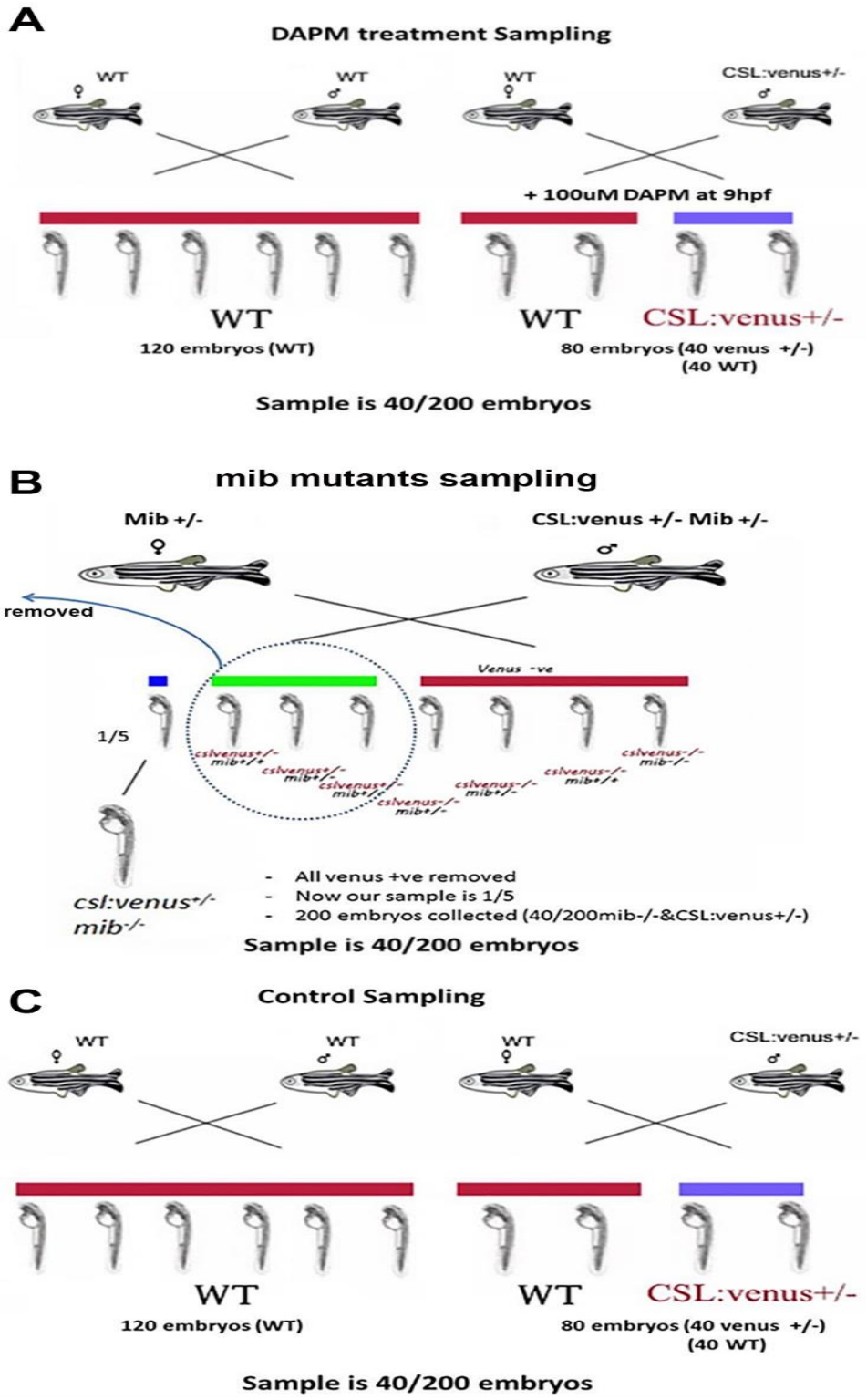

Figure 2.2: Sampling method for quantifying the remaining Notch reporter gene mRNA in DAPM treated, *mib* mutants compared to control embryos.

Schematic representation of the method used to collect equivalent samples of *Tg(csl:venus)*^{qmc61} to quantify the remaining venus mRNA with DAPM treatment (A) or *mib* mutants (B) compared to their un-treated control (C).

2.3.12 Total RNA extraction

Total RNA was isolated from pooled zebrafish embryos using the RNeasy Plus Mini Kit (Qiagen, Germany). To improve the yield in these extactions, embryos pooled in each tube were firstly homogenized with RNase-free masher in 1ml of TRI reagent (Sigma, USA) for at least five minutes. They were then incubated at room temperature for five minutes, vortexed for two minutes then spun in a benchtop centrifuge (Thermo Fisher Scientific, USA) at 13000 rpm for ten minutes. The aqueous phases were transferred into fresh tubes then 200 µl of (none-isoamyl alcohol) chloroform (Sigma, USA) was added to each tube. The tubes were vortexed again for about 30 minutes then centrifuged at 13000 rpm for 15 minutes. To remove all DNA from these samples, the top phases were transferred into gDNA eliminator columns (Qiagen, Germany) which, in combination with the high-salt buffer, selectively and efficiently removes genomic DNA, spun at 13000 rpm speed for one minute, then the gDNA columns were discarded and an equal volume of 70% ethanol was added to the filtrates. These mixes were loaded into RNA-Easy RNA extraction columns. Extractions were preceded following the manufacturer's instructions then samples were eluted in 30-50 µl H_2O, their concentrations were determined by the NanoDrop, then they were stored at -80°C.

2.3.13 Reverse transcription and cDNA synthesis

First strand cDNA was synthesized using SuperScript™ III Reverse transcriptase (Life Technologies, USA) according to the manufacturer's guidelines. For each sample, an RT- control (with no reverse transcriptase) was prepared in parallel to the cDNA sample. In general, 1.5 µg of isolated total RNA, together with 1 µl of the 10X non specific hexa-nucleotide primers (Roche, Germany) and 1 µl of 10mM dNTPs (NEB) were pipetted into a 1.5 sterile tube. Sterile water was added to a final volume of 13 µl. The mixture was heated to 65°C for five minutes and then quickly chilled on ice for one minute. The mixture was subsequently centrifuged then this step was followed by the addition of 4 µl 5X first strand buffer, 1 µl 0.1 M DTT, and 1 µl (200 units) of SuperScript™ III Reverse Transcriptase for the cDNA tubes or 1 µl H_2O for RT- tubes. The mixtures were pipetted up and down to mix the contents. They were then left at room temperature for five minutes, then incubated in the heat block at 50°C for one hour prior to inactivation in heat block at 70°C for 15 minutes. The samples were finally diluted (1 in 5) with H_2O and then stored at -20°C for PCR amplification.

2.3.14 Relative quantitative PCR (qPCR)

2.3.14.1 TaqMan

The expression of Notch reporter gene (*venus*) was quantified relative to the house keeping gene *ef1α* by using the universal Absolute qPCR ROX Mix kit (Thermo Scientific, cat. AB-1133/A, USA) with primers and TaqMan probes (Sigma) that were previously validated in our lab by a former PhD student (Modhara, 2014). The primers were designed to amplify about 100 bp fragments in *venus* and *ef1α* cDNA. The TaqMan probes used carried a FAM fluorophore at the 5' end and a TAMRA quencher at the 3' end. The master mix was prepared using the following formula per reaction: qPCR Mix 12.5 µl; forward/reverse primer (10µM) 1 µl each; probe (10µM) 0.5 µl, H_2O 5 µl. The reactions were set up in a standard 96 well plate (Life Technology, cat AB-0800). 20 µl master mix was added into each well with 5 µl cDNA. Three technical replicates were setup for each experimental sample, including the RT- and H_2O negative controls. The plate was sealed using a MicroAmp Optical Adhesive Film (Life Technology, cat 4360954) and PCR reaction was performed on the ABI 7500 Fast Real Time PCR System (Applied Biosystems, Life Technology, USA). The cycling conditions used were as follow: initial denaturing at 95°C for 15 minutes, then 40 cycles of 95°C for 15 seconds, and 60°C for one minute. Primers and probes used are listed in Table 2.7.

2.3.14.2 SYBR Green

The SYBR Green quantitative real-time PCR was carried out to quantify the reduction in *tet1* and *tet3* genes transcript's cDNA following their morpholino injections, and also to quantify enrichment for 5hmC in immunoprecipitated DNA (DIP) from *tet1* injected, *tet3* injected and uninjected control. In the DIP quantification, a preliminary 10 cycles PCR were performed to amplify the starting templates of the 12 fragments targeted (2X6 genes) and to normalize the results, we used no antibody input.

The SYBR Green PCR was setup in 96 well plates (Life Technology, cat AB-0800) and performed using SYBR Green JumpStart PCR master mix (Sigma, cat S4438-500RXN) following manufacturer instructions, using an ABI 7500 Fast Real Time PCR system (Applied Biosystems, Life Technology, USA). The cycling conditions used were as follow: initial denaturing at 95°C for 15 minutes, then 40 cycles of 95°C for 15 seconds, and 60°C for one minute. Primers and probes used are listed in Table 2.7.

Table 2.7: Primers and probes used in quantitative real time PCR.

TaqMan primers and probes				
PRIMER NAME	**DIRECTION**	**SEQUENCE**	**TARGET**	**SIZE**
DB305	F	CAGGAGCGCACCATCTTCTT	*Venus*	107bp
DB306	R	CGATGCCCTTCAGCTCGAT		
DB289	F	TGGAAATTCGAGACCAGCAAA	*Ef1a*	100bp
DB290	R	AGTCAGCCTGAGAAGTACCAGTGA		
VENUS PROBE	[6FAM]CAACTACAAGACCCGCGCCGAGG[TAM]			
EF1A PROBE	[6FAM]ACGTCACCATTATTGATGCCCCTGGA[TAM]			
SYBR Green primers				
PRIMER NAME	**DIRECTION**	**SEQUENCE**	**TARGET**	**SIZE**
DB450	F	ACCTGTGCATGTCAGGGTCT	*Tet1* cDNA Exon7—E8	223bp
DB452	R	CCTTCGGTGCAAGTCTTTTG		
DB457	F	AAGGTTTTCTTGAGTCACCATTG	*Tet3* cDNA Exon3—E4	164bp
DB458	R	TCGTCCAGATCCCAAATGAT		
DB629	F	GCGACTGCCAGATCTTTTTC	*Dlc* exon2	112bp
DB630	R	GAGTCCGCGCTCAGTATTTC		
DB631	F	AGTGTCTCGATTTGGGCAAC	*Dlc* exon7	107bp
DB632	R	ATTTTGACAGGGGTTGCTTG		
DB633	F	CACCAACCGGGAACAATAAG	*Elavl3* promoter	144bp
DB634	R	ATAATCGACAAAGGCCAACG		
DB635	F	CATCGAGAGGAAAGGCAAAG	*Elavl3* Intron1	120bp
DB636	R	TCACGAAGCATAATCGCAAG		
DB637	F	GATGTAAGAACATGCGGTTGG	*Jag1b* promoter	107bp
DB638	R	TTAAAGGGTGTGGTTTGTGC		
DB639	F	ACAGGGGGTGACAATAGCTG	*Jag1b* Intron1	138bp
DB640	R	AGGAGCCGATCTCATCACTG		
DB641	F	ATGCAAGTCAGACCCAATCC	*Notch2* Intron 1a	141bp
DB642	R	CGAGAAAGGCAAGAGAGAGG		
DB643	F	TTGCTCACATCAGCCGTTAC	*Notch2* Intron 1b	120bp
DB644	R	TTCACACCAGAGAGCAGCAG		
DB645	F	TGACCCGACTCCGATTCTAC	*Tet1* promoter	102bp
DB646	R	CATGGGTCAGTGTTGGTCTG		
DB647	F	CAATGCAAGGTCAACTGTGG	*Tet1* Intron1	135bp
DB648	R	CAGGTGCCTTACCTTTCCTG		
DB649	F	TCTCTCTCGATGCTTTGCAG	*Tet3* promoter	142bp
DB650	R	CCCTCCCTTCATTTTTCTCC		
DB651	F	AATTGCTTTGGGCTGTCAAC	*Tet3* Intron1	148bp
DB652	R	AACACGCCCAACCAGAATAG		

2.4 Histology

2.4.1 Whole mount in situ RNA Hybridization (WISH)

2.4.1.1 Embryo collection and fixation

Embryos older than 18hpf were firstly de-chorionated manually, then fixed in 4% para formaldehyde reagent (PFA) in phosphate-buffered saline tween 20 (PBSTw) overnight at room temperature. Embryos younger than 18hpf were fixed in their chorions. The next

day, embryos were washed three times with PBSTw. Embryos younger than 18hpf were de-chorionated. All embryos were dehydrated from the PBSTw in ascending concentrations (25%; 50%; 75%; 100%) of methanol and kept at -20°C.

2.4.1.2 Whole-mount RNA in situ hybridization (WISH)

Methanol preserved embryos were rehydrated into PBSTw by washing them in descending concentrations (75%;50%;25%) of methanol in PBSTw followed by five washes in only PBSTw. Embryos older than 24hpf were firstly permeabilized with Proteinase K while younger embryos were taken directly to the hybridization step. Permeabilization was done by digesting embryos with Proteinase K (10µg/ml, Sigma, Germany) for an appropriate time (Table 2.8).

Table 2.8: Proteinase K treatment durations according to age of embryos.

age of embryo	duration of Proteinase K treatment (min)
0-24hpf	0 minutes
25-31 hpf	5 minutes
2 days	20 minutes
3 days	30 minutes
4 days	45 minutes
5 days	1 hour

After permeabilization, embryos were washed three times with PBSTw then re-fixed with 4% PFA for twenty minutes at room

temperature, then washed with PBSTw for five times. Prehybridization was then performed by firstly washing embryos in 50% hybridization buffer in PBSTw then 100% hybridization buffer (Hyb) for at least one hour at 65°C. The hybridization buffer was then replaced with Hyb buffer containing DIG or fluorescein labelled RNA probe containing Hyb (500ng/1ml Hyb) and incubated overnight at 65°C (Table 2.8 shows probes used for in situ studies discussed in this work). In general, probe synthesis was done from linearized plasmids following standard in vitro transcription but with Sp6, T3 or T7 RNA polymerase primers and DIG or flourescein labelling DNTP mixes. Two hours incubation at 37°C was used, then the templates DNA was digested by DNAseI. RNA quality was analysed by running a small aliquot on agarose gel.

2.4.1.3 post hybridization

Probes were recovered, then embryos were washed in descending concentrations of Hyb in 2XSSCTw then successively washed with 2XSSCTw, followed by four washes with 0.2 SSCTw, all at 65°C. Embryos were equilibrated with ascending concentrations of MABTw, then blocked with 2% blocking solution (Roche, Germany) for one hour. They were then incubated in 2% blocking solution containing DIG or fluorescein antibodies in 1:5000 for anti-DIG Ab or 1:1000 dilution for anti Fluorescein Ab (Roche) for 30 min at room temperature, then overnight at 4°C. The next day, embryos were

washed eight times with MABTw at room temperature, washed three times with the developing buffer (BCLIII), then stained with 50% BM-purple in BCLIII and left in the dark until embryos were stained sufficiently. The reaction was then stopped by washing the embryos 3 times in PBSTw 20mM EDTA and they were then fixed in 4% PFA for 20 minutes, washed three times with PBSTw then slowly taken through ascending concentrations of glycerol in PBSTw (30%, 50% then 80%). At this stage embryos were ready for microscopic examination, thus they were stored at 4°C until needed in the future. In the case of fluorescent labelling double in situ, embryos were incubated in 100 µl of 1:25 dilution of Cy3 tyramide or fluorescein tyramide with amplification reagent (PerkElmer) for 30 minutes in the dark, then stained with tyramide substrate then washed with PBStw after that stored in glycerol as in normal in situ.

Table 2.9: RNA probes used in this project.

marker gene	vector name in Gering lab database	reference
c-myb	P77	Thompson et al., (1998)
runx-1	P86	Kalev-Zylinska et al., (2002)
efnb2a	P193	Lawson et al., (2001)
flt4	P59	Thompson et al., (1998)
gfi1.1	P287	Developed in our lab; Thambyrajah., (2011) 580 bp fragment from gfi1.1 cDNA
her4.1	P243	Takke et al., (1999)
elavl3/ zHuC	Received from Sablitzky's lab	Kim et al., (1996)
neurog1/ngn1	Received from Sablitzky's lab	Blader et al., *(1997*)
dla	P117	Haddon et al., (1998)
notch1b	P113	Kortschak., (2001)
gfp/venus	P308	In-house (whole gene)

2.5 Image acquisition and data analysis

For all bright field and fluorescent examination and imaging of embryos, I used a fluorescence dissection microscopes (Nikon, Model. SMZ1500, Japan) equipped with 100W super high pressure mercury lamp (Nikon, 100 W, C-SHG1, Japan) and FITC, TRITC and Cyan-Gfp filter set. For images and movies acquisition, coloured (Nikon DXM1200F/DS-5MC, Japan) or black and white (Hamamatsu ORCA-ER C474280, Japan) digital cameras were attached to these microscopes. All signal density quantifications were performed using imageJ software (v1.48, National Institutes of Health). Adobe Photoshop software was used to assemble and edit images where necessary. Statistical analyses and graphical representations were done with GraphPad Prism v6.0 and Microsoft Excel Software (GraphPad; Microsoft, USA), and statistical significance of results was determined using two-tailed, unpaired t test and presented as the mean ± SEM in three repeats and in all cases, any P value of < 0.05 was considered to be significant.

Table 2.10: primers used in this project.

Primer name	direction	sequence	target	Fragment size
DB414	F	cctcgtcgacgccaccatgaagctgctgagtagtat	*gal4-vp16* gene	710bp
DB415	R	gaggatcgatttatccaccgtactcatcaa		
DB162	F	catcgcgtctcagcctcac	*uas-nicd* region	459bp
DB163	R	cggaatcgtttattggtgtcg		
DB143	F	ctgaataagtagatagcctatc	*flk1-cre* region	592bp
DB144	R	cgatgcaacgagtgatgag		
DB542	F	atccgaacgtgaagtgacat	Truncated *gal4-vp16* gene	624bp
DB543	R	cgatgaggatcgatttacatatcgagcgctccgtatg		
DB608	F	gagtatcattcgggatcacagccaccatggagcaaaagct	*nicd* to fuse with *gfp*	2314bp
DB609	R	agctcctcgcccttgctcaccttgaaggcttctggaatat		
DB610	F	atattccagaagccttcaaggtgagcaagggcgaggagct	*gfp* to fuse with *nicd*	757bp
DB611	R	atcatcatcggatccgaattttacttgtacagctcgtcca		
DB612	F	aaacacaggccagatgggcccggatctcatctttgaccca	*fli1* promoter for GIBSON	2066bp
DB13	R	agcttttgctccatggtggctgcgcgtctgaattaattcc		
DB28	F	ggaattaattcagacgcgcagccaccatggagcaaaagct	*nicd-gfp*	3031 bp
DB611	R	atcatcatcggatccgaattttacttgtacagctcgtcca		
DB143	F	ctgaataagtagatagcctatc	*flk1-cre* fragment	592bp
DB144	R	ctcatcactcgttgcatcg		
DB347	F	cctcgggcccaccagcaaagttctagaatttgtcg	*Ubi* promoter	3490bp
DB348	R	cctccctgcaggctgtaaacaaattcaaagtaagattagc		
DB377	F	cctcccgcgggccaccatggtgagcaagggcgagga	*mCherry*	740bp
DB378	R	gaggcttaagttacttgtacagctcgtcca		

CHAPTER 3

3 Result I Notch reporter gene expression pattern during zebrafish early development

3.1 Introduction

At the start of this project, as described in Chapter 1, three in-house Notch reporter lines were generated in our lab: *Tg(csl:venus)^{qmc61}, Tg(csl:cerulean)^{qmc63} and Tg(csl:mCherry)^{qmc97}*. The three lines were identical in their inserted transgene structure but with different reporter fluorescent proteins. Because these three lines were dependent on artificial regulatory elements to drive expression of the reporter fluorescent protein in Notch-active cells, and the fact that they might also be influenced by the position where they were inserted in the genome, it was an essential prerequisite to re-asses the usefulness of these generated lines as tools for reporting Notch activity. Moreover, despite the accumulating evidence of Notch requirements in arterial specification and HSC development, it was still to be shown whether te presence of Notch receptors and ligands in the arterial and haematopoietic progenitors in the AGM region during early embryogenesis was associated with activation of Notch pathway, and to what level it is required.

It was also still not clear when Notch activity initiates in these arterial and haematopoietic progenitors, and how it varies from the time point of arterial specification until HSCs formation. Therefore, the aims of

this chapter were to carefully examine the in-house generated Notch reporter lines and asses their usefulness in reporting Notch activity. In addition, to utilising these lines to determine when Notch signalling initiates in the hEC progenitors forming the DA and how the level of Notch signalling in the DA varies from the time point of arterial specification to the time point of HSCs development.

3.2 The three in-house generated Notch reporter lines have identical expression patterns

Even though the Notch reporter regulatory elements were successfully used ex vivo and in vivo in mammalian model to report Notch activity, it was still necessary to examine if the system also efficiently reports Notch activity in the zebrafish. In parallel to our efforts to establish our in-house Notch reporter lines, two Notch reporter lines were published by Parsons et al. (2009) utilising the same regulatory elements, *Tg(tp1βglob:gfp)*^{um13} and *Tg(tp1βglob:hmgb1-mCherry)*^{jh11}. The published lines were verified by the authors and shown to efficiently report Notch activity in the zebrafish animal model. To test if our in-house generated lines have expression pattern, identical to the verified Parsons et al. (2009) lines, transgenic fish were crossed from our generated lines to wild type fish. I then examined their embryos at 1 dpf to firstly see if the inserted transgenes led to an identical pattern of expression in the three transgenic lines, as an indicator of promoter specificity. Careful

examination of embryos from the three lines showed that apart from the differences in type of reporting fluorescence proteins, all three transgenic lines showed identical expression pattern (Figure 3.1) with only slight variation in the level of fluorescent protein expression, which could be due to the differences in their fluorescent intensity, maturation or folding and fluorophore formation. I then compared expression pattern in the three in-house lines with that in the published transgenic line *Tg(tp1 βglob:gfp)*^{um13} and the results showed an identical expression pattern with characteristic strong reporter genes expression in the telencephalon , heart , dorsal aorta , neural tube and medial fin fold (white arrows in Figure 3.1). Moreover, blocking the Notch pathway with different approaches also blocked expression of the reporter genes in these lines as in the lines published by the Parsons et al. (2009), as shown in Figure 4.4. We also noticed some inter-embryonic variations in level of fluorescent proteins. These variations are at least in part due to the biological and environmental conditions. The other possible cause of these inter-embryonic variations is the spontaneous transgene suppression, associated with the use of 12 *csl* binding repeats. Transgene suppression, or complete silencing by adopting methylated or closed conformation, are common issues in transgenic lines that contain repetitive regulatory sequences, such as the Gal4 binding repeats (Goll et al., 2009, Thummel et al., 2006).

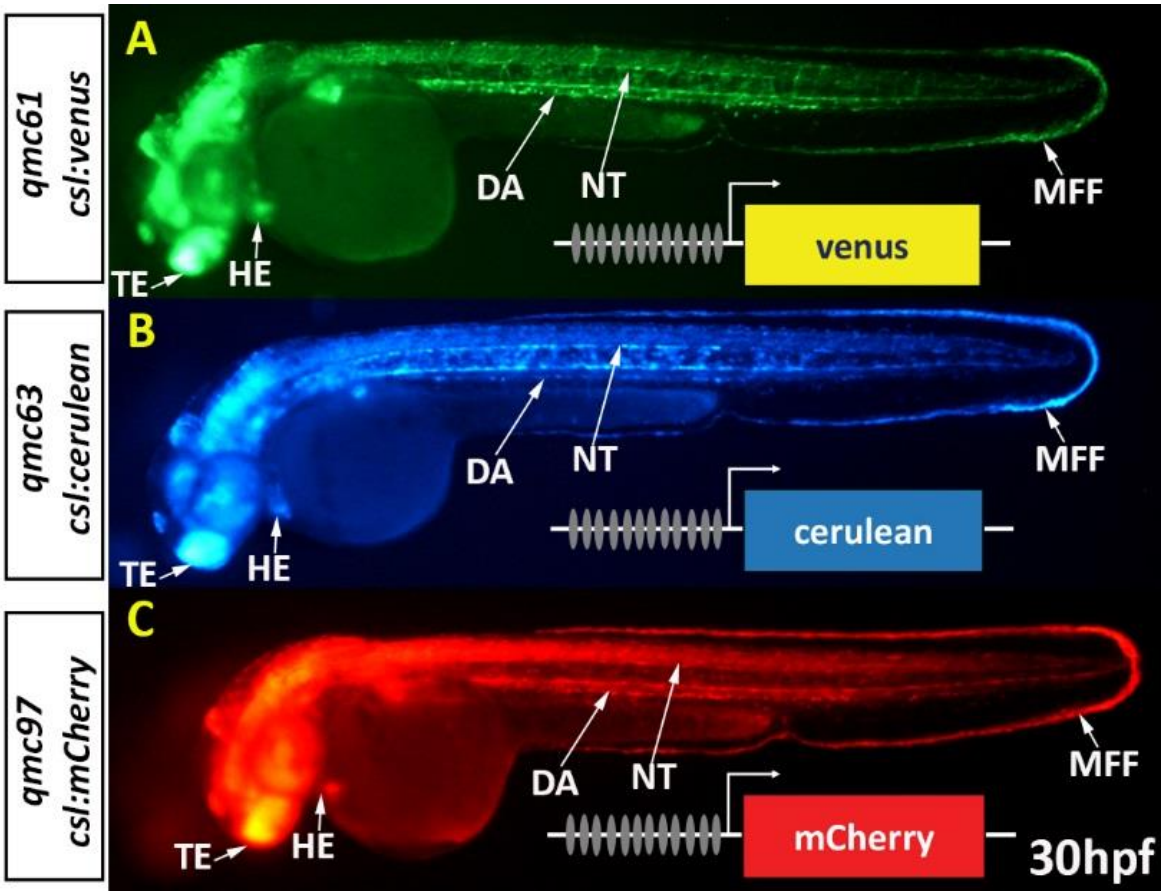

Figure 3.1: Generated in-house Notch reporter lines drive identical expression pattern.
The Figure shows embryos from the three Notch reporter transgenic lines established in our lab. A *Tg(csl:venus)*^{qmc61}, B *Tg(csl:cerulean)*^{qmc63} and C *Tg(csl:mCherry)*^{qmc97}. The three lines show identical expression pattern as indicated with the arrows. TE telencephalon, HE heart, DA dorsal aorta, NT neural tube, MFF medial fin fold.

To overcome this problem, only embryos with robust reporter gene expression were used to maintain these lines, and fish that gave progenies with notably low reporter fluorescent protein levels were excluded from Notch reporter level quantifications in Chapter 4. On the other hand, transgenic fish that gave progenies with universally low reporter fluorescent protein levels were used to report and quantify endothelial specific Notch over-activation. Together, the fact

that all three in-house Notch reporter lines have identical expression patterns and the high similarity between our lines and the lines generated and validated independently in another lab strongly suggest that the reporter genes expression in our in-house generated lines faithfully recapitulate Notch activity.

3.3 Notch signalling activity is detectable at the 5 somite stage (11.5 hpf) with fluorescent reporter proteins

To precisely determine when Notch activity appears in the embryo, male *Tg(csl:mCherry)*^{qmc97} fish were out-crossed to female WT, and to precisely determine the age of studied embryos, dividers were used to control the timing of fertilisation. The next day, the dividers were removed, then the embryos were collected 30 minutes later. Collected embryos were then quickly sorted and incubated at 28.5^{o}C. Embryos were examined under dissecting fluorescent microscope every 30 minutes to determine the earliest detectable Notch activity. Expression of the fluorescent reporter protein was first seen at the 5 somite stage (11.5hpf). Notch activity at this stage was mainly in the midline in the position of the hypochord (Figure 3.2 A'; blue arrow in A''). Notch activity was also seen in the developing somites (Figure 3.2 A'; yellow arrowheads in A''). As the somitogenesis proceeds, Notch reporter fluorescent protein become stronger in the somites

and hypochord and also become detectable at other tissues, and by16 somite stage (17hpf) several other developing organs also become Notch-active (Figure 3.2 B'). At this stage, some of the early migrating blood and endothelial progenitors had arrived to the midline. Despite the fact that Notch might be active in these early migrating cells, due to the high Notch activity in the hypochord and its close proximity to the midline, we found it difficult to clearly identify Notch-active blood and endothelial precursors at this stage with fluorescent microscopy.

These results show that the earliest zygotic Notch reporter fluorescent protein signal only becomes detectable at 11.5hpf. The earliest Notch-active tissues are mainly the hypochord and the developing somites. By the 16 somite stage a high Notch activity was reported in the nervous system and the developing somites. Other tissues that were Notch-active at 16 somites are annotated in (Figure 3.2 B’).

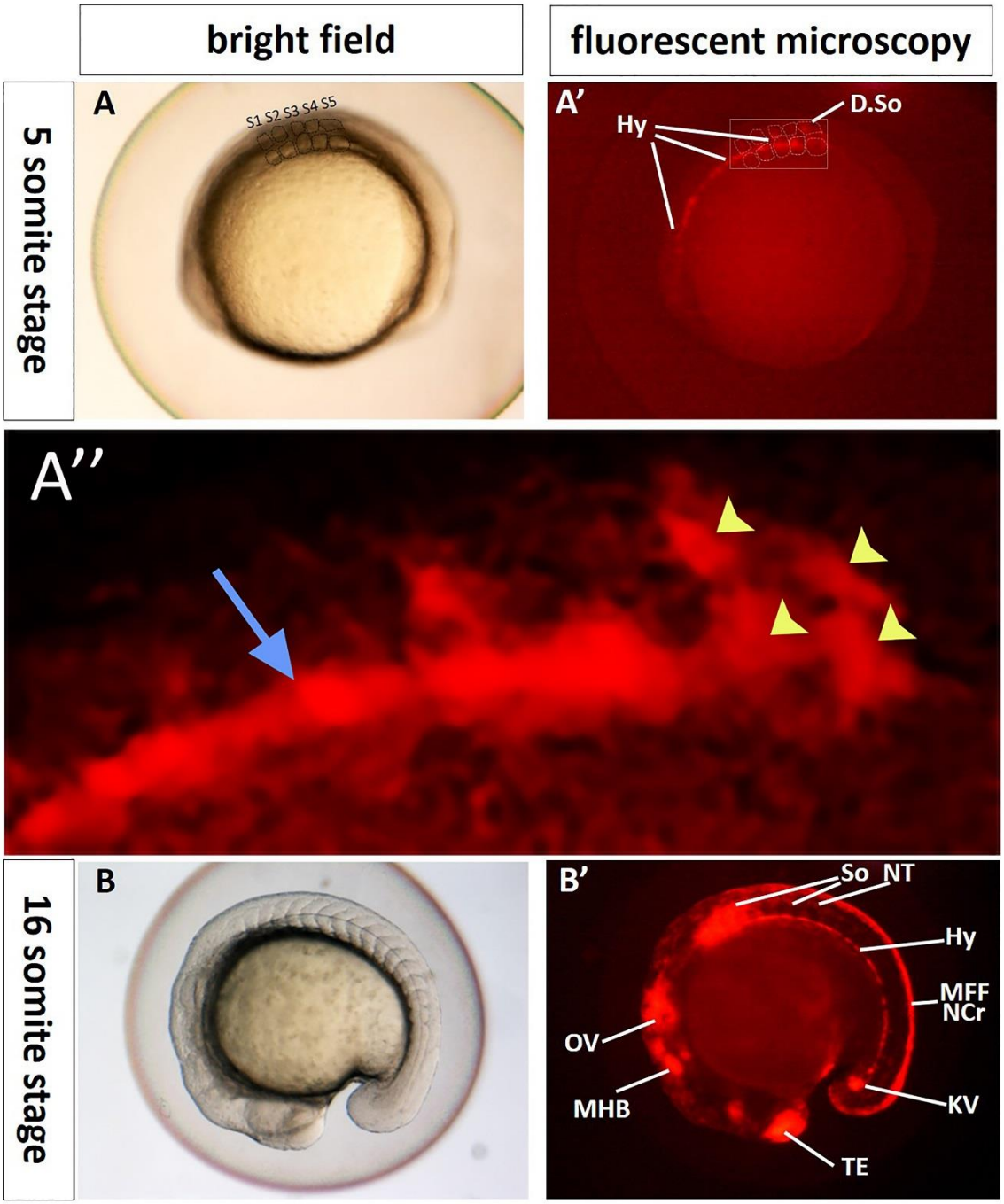

Figure 3.2: Notch activity is detectable in Notch reporter line at 5 somites stage (11.5hpf).

A bright field microscopy showing the developmental stage with somites highlighted. A' same embryo examined with fluorescent microscopy. The reporter *mCherry* protein is detectable in the hypochord (Hy) and developing somites (D.So). A'' Magnification of the boxed area in A'. the yellow arrowheads label the developing somites, blue arrow labels the hypochord. B shows the developmental stage of Notch reporter embryo under bright field microscopy. B' same embryo under fluorescent microscopy. The image shows strong Notch activity in several tissues. Labelled Notch-active tissues in image B' are somites(So), neural tube (NT), hypochord (Hy), median

fin fold (MFF), neural crest (NCr), Kuppfer's vesicle (KV), telencephalon (TE), middle and hind brain (MHB), otic vesicle (OV).

3.4 Notch reporter protein is detectable in the position of the DA by 18hpf by fluorescence microscopy

In zebrafish it was previously shown that the migrating lateral mesodermal vascular and haematopoietic progenitors express the Notch ligands *dlc* and *dll4*, and their expression persists in the developing DA (Lawson et al., 2001). However, it was not known if the presence of Notch receptors in these migrating cells was associated with active Notch signalling before they arrive to the midline to form the main axial vessels (DA and CV), which is known to occur between 17-18hpf (Medvinsky et al., 2011). To determine if these progenitors are Notch-active at this time point, the Notch reporter embryos were carefully examined starting from 17hpf for expression of Notch reporter protein just below the hypochord. Even though a weak Notch activity appeared to be present in the mid-line just below the hypochord in trunk area by 17hpf (Figure 3.2 B'). But, due to the close association of these apparently Notch active cells to the highly Notch active hypochord, and possibly the low number of cells arriving to the midline by this time point, it was difficult to clearly distinguish these cells. An hour later (18hpf), all migrating cells had

arrived to the midline to form the main axial vessels, and with early maturation of the DA, arterial and haematopoietic progenitors of the vDA become distant from the hypochord (white arrowheads in Figure 3.3). The position of the dDA remained in very close proximity to the highly Notch-active hypochord (yellow arrows in Figure 3.3), and so it is still difficult to distinguish by normal fluorescent dissecting microscope.

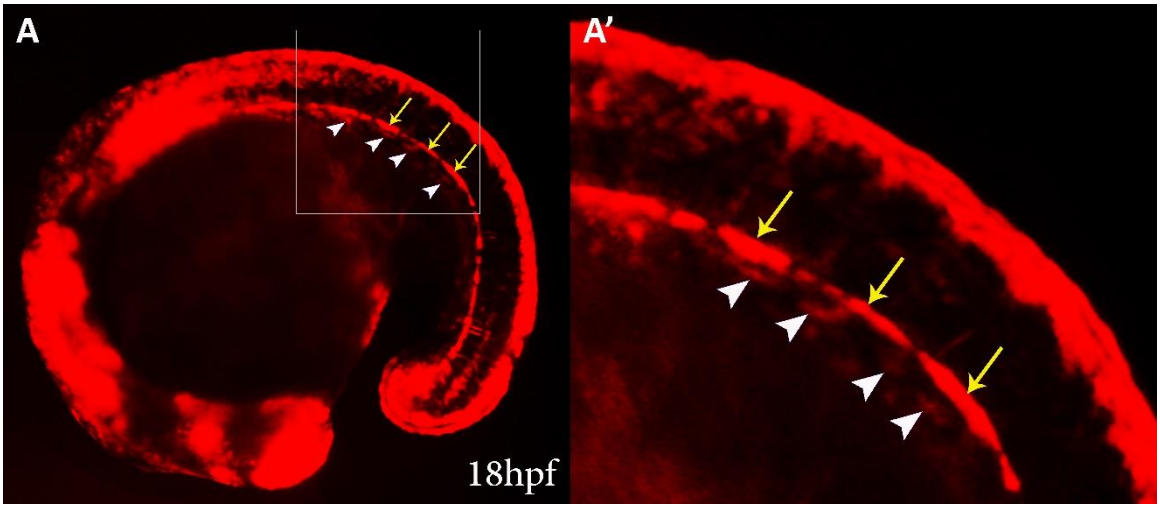

Figure 3.3: Notch signalling is detectable in the position of arterial and haematopoietic progenitors in the DA by 18hpf. Fluorescent microscopy images of live embryo of Notch reporter *Tg (csl:mCherry)qmc97* embryo. (A) lateral view of 18hpf embryo. (A') Magnified area indicated by the box in (A). Yellow arrows point to hypochord, arrowheads point to vDA angioblasts and progenitor cells.

From this experiment, it appears that Notch is active in the progenitor cells forming the DA by the time point of the DA formation, as determined by Notch reported activity below the hypochord in the position of the developing DA.

3.5 Double in situ hybridization shows co-localization of Notch and the endogenous endothelial gene (*flk1*) mRNA at 18hpf.

To further confirm our fluorescent microscopy observation at 18hpf, and also to confirm the identity of these Notch-active cells observed below the hypochord in the position of the DA, double in situ hybridization was performed to investigate whether these Notch-active cells are also expressing the endothelial marker *flk1*. To achieve this I crossed the Notch reporter line *Tg(csl:venus)*^{qmc61} to WT, raised their embryos until 18hpf then stopped and fixed in PFA. A standard double in situ hybridization was then performed on these embryos using *venus* digoxigenin- and *flk1* fluorescein-labeled probes. The the Cy3 and fluorescein tyramide were used for signal development respectively. Upon completion, embryos were examined under fluorescent dissecting microscope.

Double in situ hybridization showed a strong *venus* expression in the position of the DA (yellow arrows in Figure 3.4 A) in all of the *venus* positive embryos (50% in heterozygous). On the other hand, and as the *flk1* probe was designed to target the endogenous *flk1* gene mRNA, all examined embryos (100%) showed expression in the vascular endothelial tissues including the DA and the CV. Interestingly we noticed a higher *flk1* expression in the DA compared to the CV (blue arrowheads in Figure 3.4 A'-A''). When digitally

merged images were obtained for *venus* and *flk1* expression, the co-localization, of *flk1* expression and the *venus* expression was observed at the position of the DA in 100% of the 11 double positive embryos. (Figure 3.4 A'').

To further confirm the double in situ fluorescent microscopy results and to clearly demonstrate that the Notch-active cells at this stage were localizing within the endothelial cells forming the DA, confocal microscopy was performed on these embryos and the obtained images further confirmed these findings (Figure 3.4 B-B''). Both normal and confocal fluorescent microscopy imaging illustrated that Notch signalling is active in the DA endothelial cells upon their arrival to the midline to form the DA precursors.

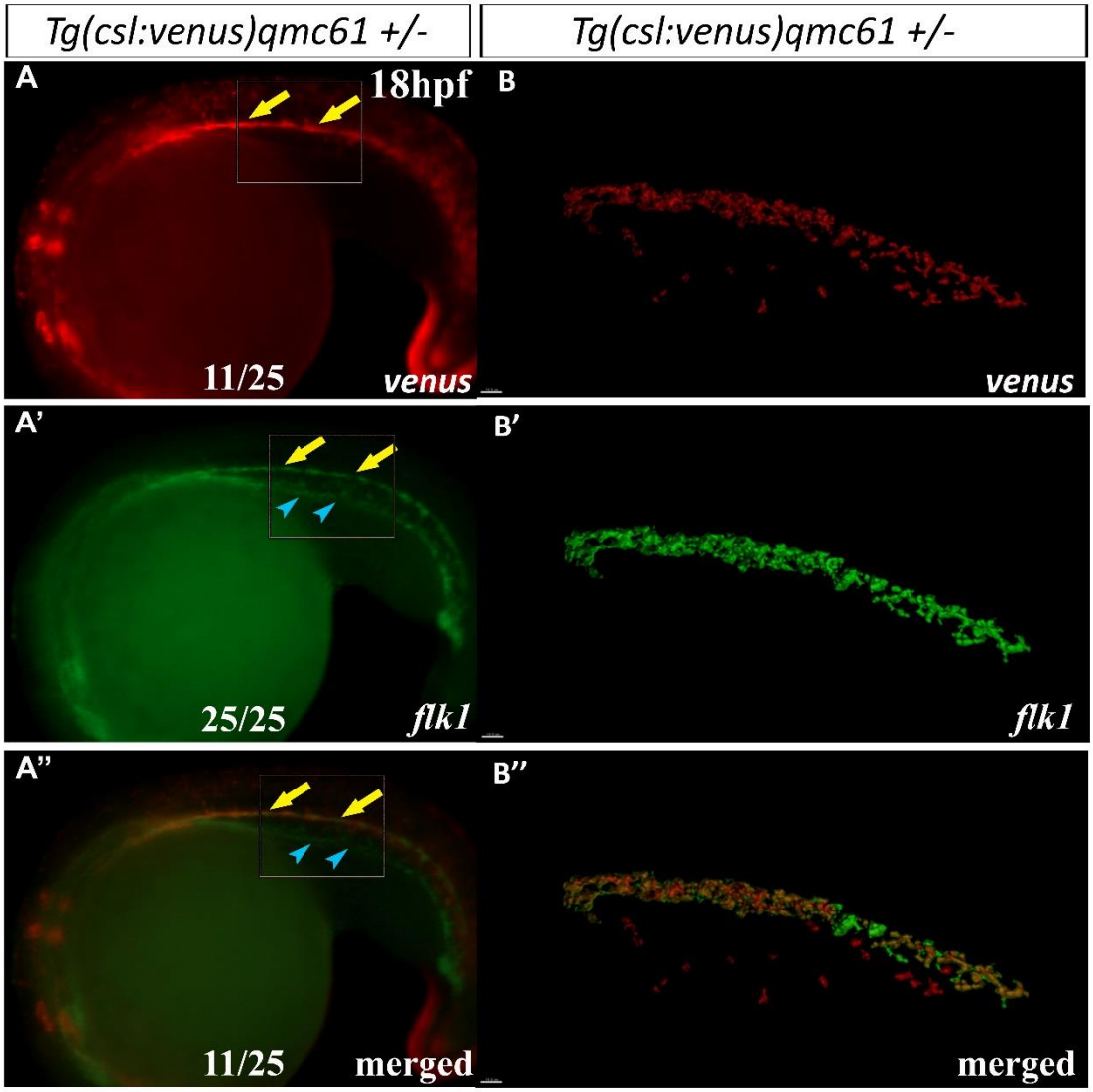

Figure 3.4: double in situ hybridization shows co-localization of the Notch reporter RNA and the endogenous endothelial marker flk1 RNA.

Double in situ fluorescent microscopy images of *Tg(csl:venus)*^{qmc61} +/- embryos at 18hpf. (A) Shows *venus* expression in Notch-active tissues. (A') Shows expression of the endogenous *flk1* gene in the endothelium. (A'') Digitally merged image of the same embryo showing co-localization of *venus* and *flk1* expression in the developing DA. Yellow arrows point to the developing DA, white arrowheads point to CV. (B-B'') Confocal imaging of *Tg(csl:venus)*^{qmc61}+/- embryos at 18hpf. (B) Shows *venus* expression in the trunk region. (B') Shows expression of the endogenous *flk1* at the same area as in (B). (B'') Merged image of (A) and A' showing co-localization of *venus* and *flk1* expression in the developing DA. The images were acquired using a confocal microscope then processed with Imaris software.

3.6 Notch activity increases in the developing DA from the time point of DA formation to the time point of HSC development

Notch is required for both arterial specification and HSC development, yet it is not clear how Notch signalling can differentially affect these two fates. While monitoring Notch activity in the AGM region we have established that Notch activity becomes detectable with the early arrival of the Haemogenic endothelial progenitors to the midline. At this stage, Notch reporter gene expression of the developing DA appears as a weak signal. Continued monitoring of Notch reporter expression after its appearance, revealed a rapid increase in its activity in the DA as the embryo grows older (Figure 3.5 A-E).

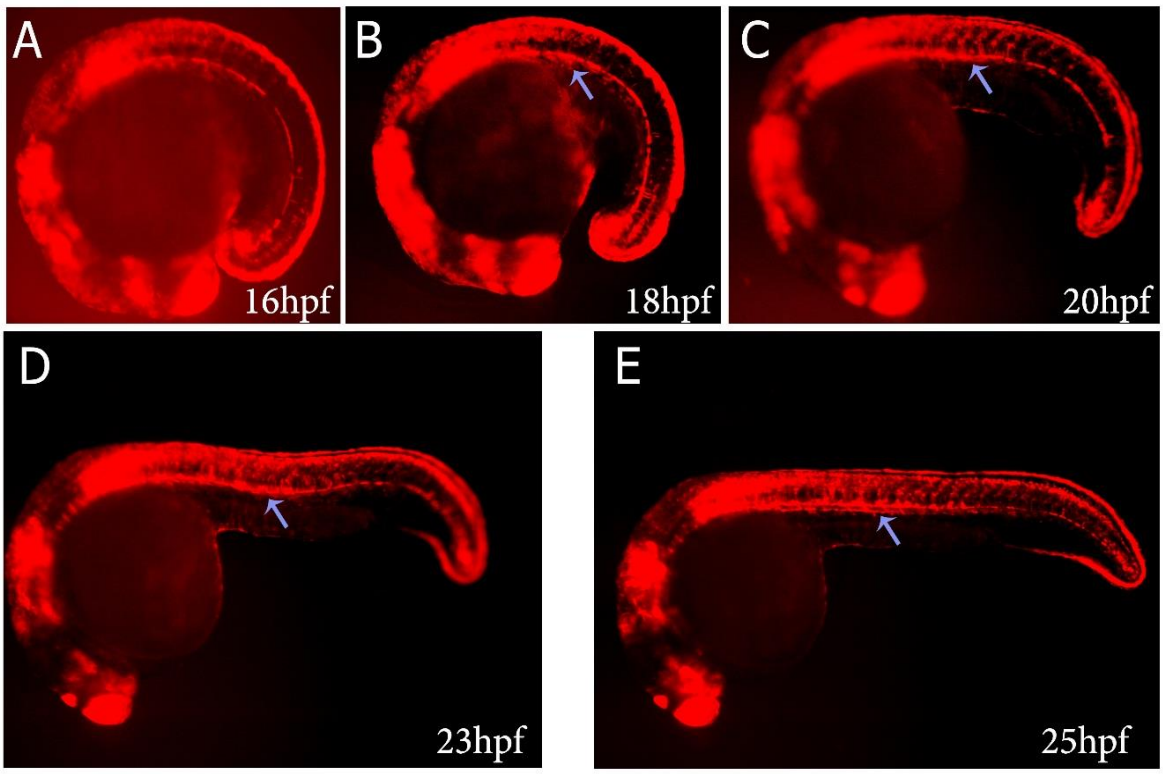

Figure 3.5: Notch activity in the DA increases after arterial specification.
Fluorescent microscopy images of live embryo of Notch reporter *Tg(csl:mCherry)*^{qmc97} embryo from 16-25hpf (A-E). The images show a rapid increase in Notch activity in the DA (indicated by the blue arrows) after the time point of arterial specification, which continues to increase until the time point of HSC emergence at 25hpf, as indicated by the blue arrow.

3.7 In situ hybridization of Notch reporter mRNA expression strongly suggests initiation of Notch activity in the migrating hEC progenitors before their arrival to the mid-line

Previously it was shown that before a fluorescent protein gains the ability to absorb energy and emit light its chromophore needs a period of time to mature (Sniegowski et al., 2005). The maturation process starts with the translation of the mRNA message followed by the correct protein folding and finally acquiring the fluorescing property. According to Sniegowski et al. (2005), at least one hour is required for Gfp protein maturation in E.coli at 37°C. Due to the wide number of variables affecting maturation time added to the technical variables associated with exciting and detecting fluorescent proteins we decided to estimate the time difference between first detection of Notch reporter mRNA and the time when reporter fluorescent protein can be detected with fluorescent microscopy. To achieve this, embryos were stopped and fixed from Notch reporter line *Tg(csl:venus)*^{qmc61} at different time points starting from 6hpf then

carried out in situ hybridization. In situ hybridization results showed that Notch reporter mRNA becomes detectable in the neural progenitor cells as early as 8hpf, which is 3.5 hours earlier than the time point when the reporter fluorescent protein become detectable with fluorescent microscopy (Figure 3.6).

Considering the 3.5 hours delay associated with the Notch reporter protein maturation, these findings strongly suggest that the migrating hECs progenitor cells must have active Notch signalling activity a few hours before their arrival to the midline to form the DA, i.e. at least starting from 14 hpf.

Interestingly, our in situ data shows that while Notch activity rapidly increase in the DA after arterial specification and persists at a high level during the time window at which HSCs emerge from the vDA, Notch activity sharply falls by 48hpf to hardly detectable levels (see Figure 3.6).

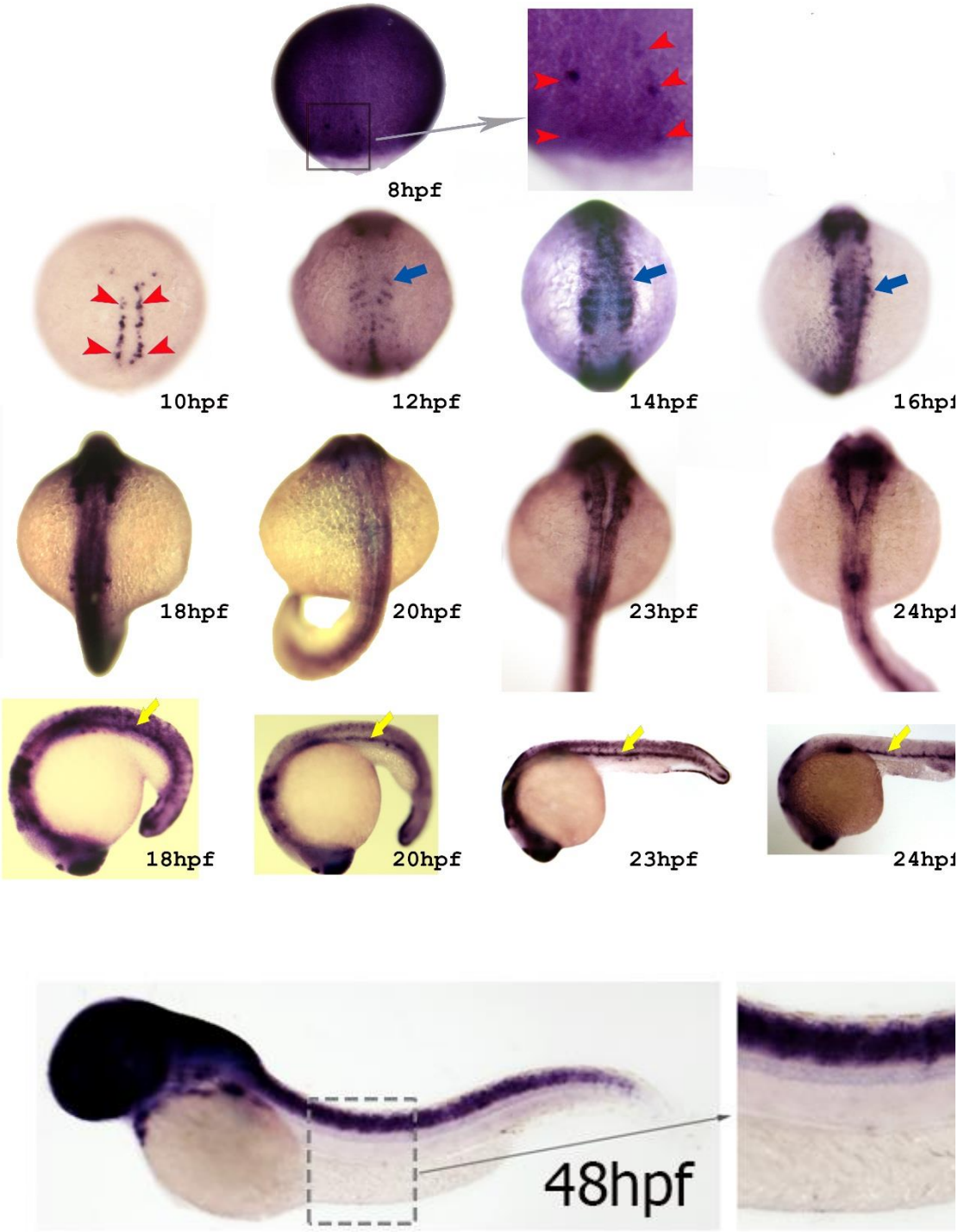

Figure 3.6: Notch reporter mRNA become detectable at 8hpf. In situ hybridization for *Tg(csl:venus)*^{qmc61} embryos showing expression of the reporter mRNA in the position of neural progenitor cells starting from 8hpf (red arrow heads) and extent along the migrating cells that form the hypochord by 10hpf. At 12 hpf the developing somites also become Notch-active (blow arrows). At 18 hpf Notch activity in the hypochord become hardly detectable while the DA Notch activity become clearly detectable and then increases

towards the time point of HSC formation at 24hpf (yellow arrows). At 48hpf Notch activity in the DA sharply down-regulated to hardly detectable levels.

3.8 Discussion of results

Comparative analysis of the expression pattern in the in-house Notch reporter lines revealed high specificity of reporter gene expression. In the three in-house generated Notch reporter lines, reporter gene expression was restricted to tissues of known Notch activities, such as the telencephalon and heart dorsal aorta (Scheer et al., 2001) in identical pattern, and also to the Notch reporter lines generated and published independently by the Leach Lab (Parsons et al., 2009). We also noticed occasional suppression of the reporter gene expression in embryos generated from known Notch reporter transgenic fish. Nevertheless, such suppression is a common issue with transgenes containing multiple repeats in their promoters (Goll et al., 2009, Thummel et al., 2006), but due to the extremely low number of embryos with suppressed expression, the impact of this variation is extremely low, especially when large sample sizes are used or the same embryos are followed over time.

Utilizing these Notch reporter lines, we presented data showing mature and detectable fluorescent reporter protein in the DA as early as 18hpf. By comparing the time point of earliest reporter gene mRNA and the earliest fluorescent protein detection, we

estimated the time required for the reporter protein translation, maturation and accumulation to a detectable level to be 3-4 hours. Based on this, we concluded that the haemogenic endothelial progenitors (derived from the mesoderm then migrated to the midline) must have become Notch-active a few hours before their arrival to the midline to from the DA. Due to the close association between the developing DA and the highly Notch active hypochord, we performed double in situ hybridization at 18 hpf with venus and flk1 probes, to determine the identity of these Notch active cells.

Our double in situ hybridization analysis confirmed the endothelial identity of these Notch active cells, as both fluorescent and confocal microscopy showed overlap between venus and flk1 expression. Fluorescent microscopy examination also showed the persistence of the reporter fluorescent protein in the DA after arterial specification. Due to high protein stability, it was essential to investigate if the observed reporter protein resulted from continuous Notch activity in the DA and not from earlier Notch activity. For this, we examined expression of the reporter gene at the mRNA level with in situ hybridization and the results showed high expression of the reporter gene in the DA, even when examined eight hours after arterial specification. Interestingly, unlike with fluorescent microscopy, we noticed a dramatic reduction in the Notch reporter mRNA on day two.

Together, our findings suggest an early Notch activity in the progenitor cells forming the DA, including the haemogenic endothelium in its ventral wall. The on-going prolific Notch activity in the DA after arterial specification until the point of HSCs specification, then its reduction to a hardly detectable level, suggests that high Notch signalling could be required for HSCs specification from the ventral wall of the DA.

CHAPTER 4

4 Result II Low level of Notch is sufficient for arterial specification whereas high level is required for HSCs formation

4.1 Introduction

In vertebrates, HSCs are specified from arterial endothelial cells in the ventral wall of the Dorsal Aorta (Bertrand et al., 2010a, Kissa and Herbomel, 2010, Lam et al., 2010). Studies on zebrafish, birds and mammals have shown that both arterial and HSC specification are both derived from one common precursor, the haemangioblasts. Soon after formation of the DA, a sub-population of the cells forming the vDA further differentiate into HSCs. This differentiation step is dependent on type and level of signal they receive added to the competency of these cells. Notch is one of the signalling pathways that are known to be essential for both arterial endothelial and HSCs development (Lawson et al., 2002, Gering and Patient, 2005). In zebrafish, several Notch receptors and ligands are expressed in the Angioblasts fated to form the DA (Lawson et al., 2001), suggesting an early role for Notch in arterial specification. However, Notch activity is maintained after arterial gene induction until the time point of HSCs cluster formation in the DA.

This is reflected by persistence of Notch reporter mRNA and fluorescent protein in Notch reporter transgenic lines. Due to their

close association and the shared requirement for Notch in arterial specification and HSCs development, it was still not understood how Notch differently specify these two fates in the DA. Notch gain of function studies show that high level of Notch is sufficient to expand HSCs formation in WT embryos as well as Notch over-activation could also rescue Hh, Vegf and Hey2 depleted embryos (Rowlinson and Gering, 2010). These findings suggest that high level of Notch may be needed for HSCs development. Notch loss of function studies with different approaches including *mib* mutant homozygosity, have also shown loss of HSCs specification (Gering and Patient, 2005). Interestingly we noticed that only some approaches interfere with arterial specification. Our careful analysis of the Notch activity reported by expression of the reporter genes in our zebrafish transgenic lines revealed a clear up-regulation of Notch reporter expression in the DA angioblasts and endothelial cells from 20 to 26 hpf. This up-regulation was also confirmed in our lab at the mRNA level by RT-PCR experiments performed on FAC-sorted Flk1:Gfp+ trunk endothelial cells harvested from *flk1* reporter transgenic embryos at different time points (Modhara, 2014). Together, these observations suggest that different levels of Notch are required for arterial specification and hEC induction, and that low level of Notch activity is sufficient for arterial specification, whereas a high level of Notch is needed for hEC induction. In this study I used our in-house developed Notch reporter line *Tg(csl:venus)*^{qmc61} to measure the level

of Notch activity during DA development and hEC induction in wild-type and Notch-depleted embryos. I also used in situ hybridization as well as quantitative RT-PCR to measure the remaining Notch reporter gene expression in *mib* mutants, *rbpja/b* morphants and DAPM-treated embryos, and its correlation with maintaining or losing arterial and HSC marker genes expression.

4.2 Notch activity is up-regulated in the DA after arterial specification to the time point of HSCs development

From our observation of the fluorescent protein expression in our Notch reporter lines, we noticed that the Notch reporter protein becomes detectable in the endothelial progenitors located just below the hypochord between 17-18hpf (see Figures 3.2 and 3.3). At this stage Notch reporter expression is low and barely detectable in these progenitor cells with normal fluorescent microscopy. In situ hybridization analysis showed that these progenitors were specified as arterial, indicated by their expression of arterial markers such as *efnb2a* (Gering and Patient, 2005). Interestingly, after arterial specification we noticed an increase in Notch reporter protein expression, and this up-regulation continued until the time point of HSCs development (see Figures 3.4,3.6 and 4.1). To exclude the contribution of inter-embryonic variation in Notch reporter protein

level that we reported earlier (chapter 3) and to quantify the up-regulation of the reporter fluorescent protein, ImageJ software was used to measure the intensity of fluorescent protein at 20hpf, 24hpf and 27hpf all from same embryo and same imaging and analysis settings. Average intensity means of the sample measured showed about three fold increase in *venus* intensity from 20hpf to 24hpf and another two fold increase from 24hpf to 27hpf as shown in Figure 4.1 D. Even though these quantifications came from one embryo, when added to fluorescent microscopy and in situ hybridization that showed upregulation in the reporter fluorescent protein and reporter gene mRNA, this suggests a true upregulation in Notch activity rather than the expected inter-embryonic variation in the Notch reporter activity.

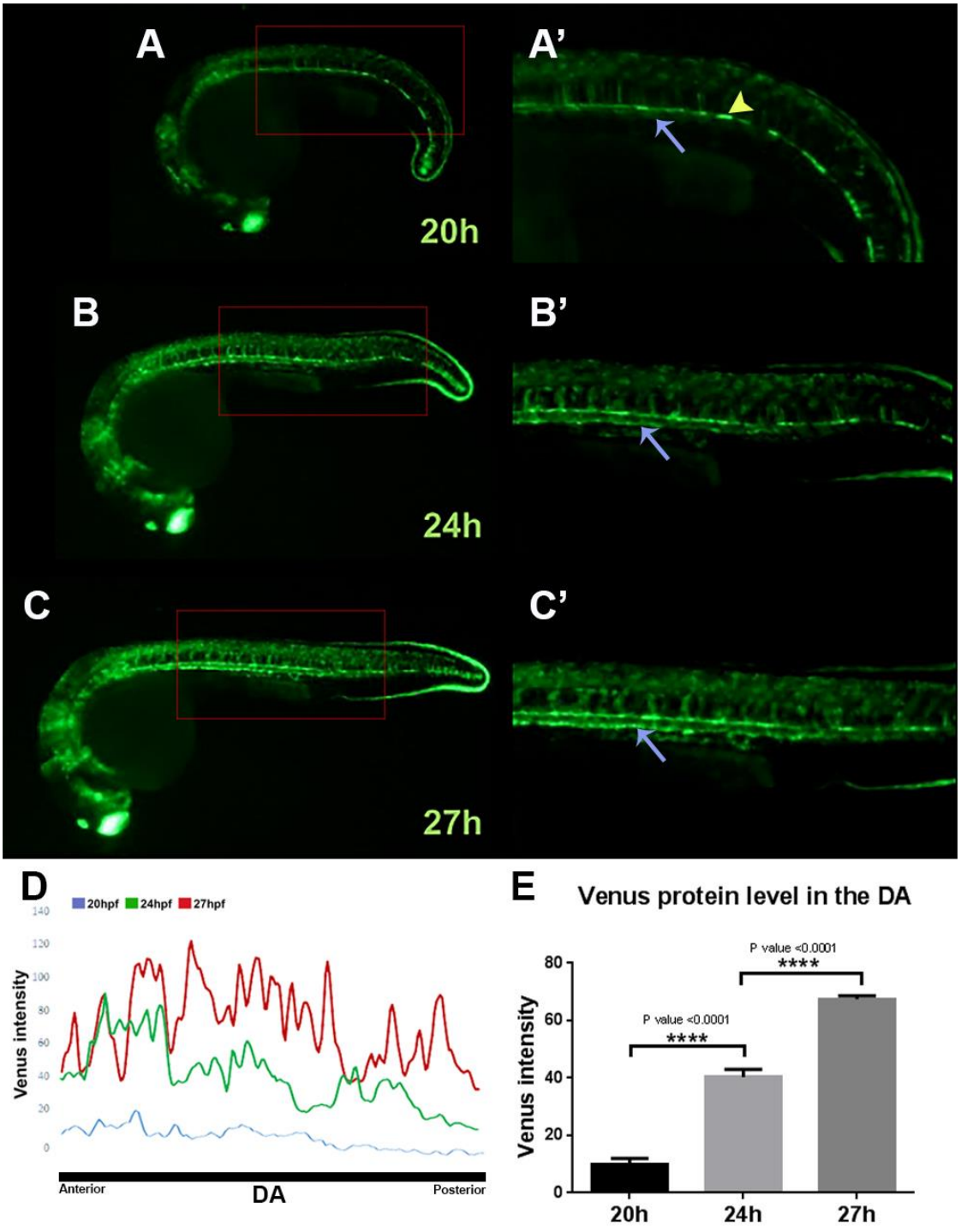

Figure 4.1: Notch reporter fluorescent protein expression is up-regulated after arterial specification of the DA to the time point of HSC development.

(A-C) Venus fluorescent protein expression in *Tg(csl:venus)*^{qmc61} showing an increase in the Venus fluorescent protein expression from 20hpf-27hpf. (A) Shows a very weak *venus* expression in the developing DA located just below the hypochord (yellow arrowhead) that is high in Venus at this stage. Boxed area in A is magnified in (A'). (B-B') Venus fluorescent protein level at 24hpf become very

prominent along the DA. Boxed area in B is magnified in (B'). (C-C') Venus fluorescent protein expression increases in the DA at 27hpf compared to 24hpf. Boxed area in C is magnified in (C'). (D) Comparison of the Venus fluorescent protein intensity along the DA at 20hpf, 24hpf and 27hpf measured by obtaining the fluorescence intensity along the DA using a line tool in imageJ drawn through the dorsal aorta endothelium. (E) Comparison of the average aortic Venus fluorescence intensity, showing a 3-fold increase in Venus level from 20hpf to 24hpf and another a 2-fold increase from 24hpf to 27hpf. Data are shown from five measurements done on images from a single embryo imaged at different time points on the same day using the same conditions and settings (mean ± SEM; unpaired t test; **** = $p<0.0001$).

4.3 High level of Notch coincides with loss of Flt4 in the DA at the time point of HSC development

Previously, Lawson et al. (2001) showed that Notch signalling is needed for Flt4 suppression in the DA and that *flt4* mRNA persists in *mib* mutants DA. They also showed the persistence *of flt4* mRNA in the DA coincides with loss of HSC markers expression in the vDA. On the other hand, Rowlinson (2010) showed that Notch over-activation in the whole embryo leads to *flt4* mRNA suppression not only in the DA, but also in the CV. Moreover, Rowlinson (2010) showed that Flt4 suppression coincides with expansion of HSC marker expression to include the CV.

Interestingly, we noticed that the developing DA endothelium expresses *flt4* as well as arterial markers such as *efnb2a* at 18-20hpf in the presence of low Notch activity as indicated by low level of the reporter fluorescent protein in our reporter line *Tg(csl:venus)*^{qmc61} (Figure 4.2). However, as the Notch activity increases in the DA at

24h, *flt4* expression becomes much weaker (Figure 4.2), and is completely lost at 27hpf. These findings suggest a correlation between up-regulation of Notch activity and suppression of *flt4* expression in the DA at the time point of HSC development.

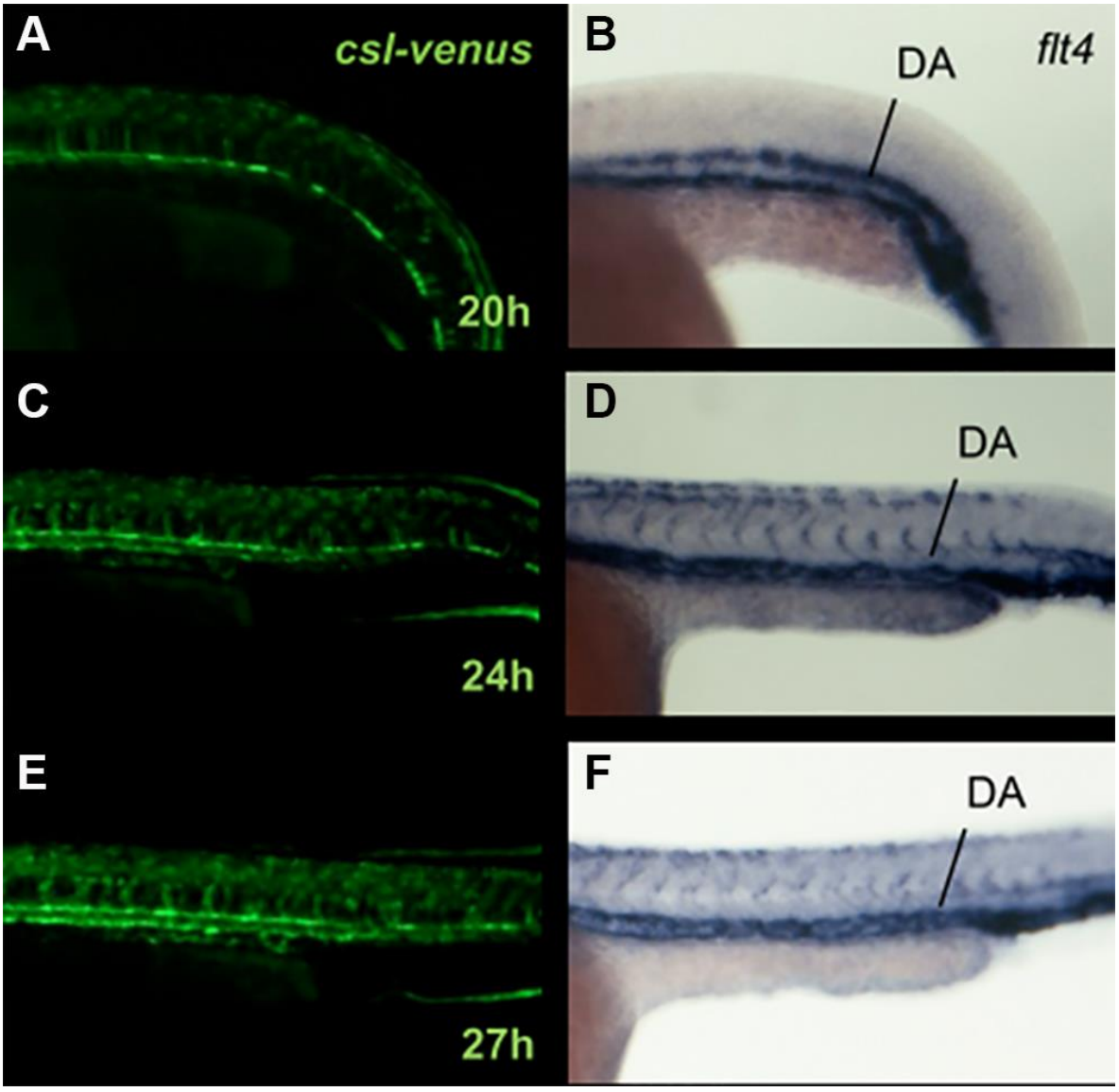

Figure 4.2: High level of Notch activity correlates with Flt4 downregulation in the DA at the time point of HSC development.
(A,C,E) Venus fluorescent protein expression in *Tg(csl:venus)*^{qmc61} showing an increase in the Venus fluorescent protein from 20hpf (A), 24hpf (C), and 27hpf (E). (B,D,F) In situ hybridization of *flt4* expression showing strong *flt4* expression in the DA at 20hpf (B). *flt4*

expression become hardly detectable in the DA as the Notch activity increase in the DA (D), *flt4* expression become completely lost at 27hpf (F).

4.4 Blocking Notch pathway with different approaches leads to absence of HSCs markers in the vDA but with differential effects on arterial specification.

In our lab it was noticed that blockade of the Notch pathway in the *mib* mutants or *rbpja/b* morphants leads to loss of expression of both arterial and haematopoietic markers, whereas blocking Notch pathway pharmacologically with γ-secretase inhibitor (DAPM) leads only loss of haematopoietic markers but with intact arterial specification. To confirm earlier findings, a double transgenic/mutant fish was generated by crossing an identified mind bomb (mib^{ta52b}) carrier to a heterozygous *Tg(csl:venus)*^{qmc61} fish, then the Venus positive embryos were grown to adulthood. At adulthood, these fish were characterised to carry the *mib* mutation by crossing them to known *mib* carriers and observing the distinct neurogenic, somitogenic and vasculogenic phenotypes, and also the absence of pigmentation in their trunk and tail (white tail) starting from day2 (Jiang et al., 1996, Schier et al., 1996).

The identified $mib^{+/-}$/$venus^{+/-}$ males were then crossed to *mib* $mib^{+/-}$ females and embryos were collected from these crosses at 24hpf for *efnb2a* in situ hybridization, and at 26hpf for *flt4* and *runx1* in situ

hybridization and for fluorescent microscopy. I also crossed *Tg(csl:venus)*$^{qmc61+/-}$ male to WT females and separated collected embryos into three batches, then injected the first batch with *rbpja/b* morpholinos (see Methods), and treated the second batch with the γ-secretase inhibitor DAPM from 9 hpf till the time collected for in situ, while the third batch was left un-treated as negative control. Embryos from the three batches were also collected at 24hpf for *efnb2a* in situ and at 26hpf for *flt4* and *runx1* in situ hybridization and also for fluorescent microscopy.

Table 4.1: Summary of Notch inhibition approaches used and percentage expected to be affected in each experiment.

sample	crosses	treatment	affected embryos	affected and Venus +ve
mib mutants	*mib*$^{+/-}$*/csl:venus*$^{+/-}$ ♂ X *mib*$^{+/-}$ ♀	*mib* mutation	25%	12.5%
DAPM treated	*csl:venus*$^{+/-}$ ♂ X WT ♀	DAPM treatment	100%	50%
rbpja/b Morphants	*csl:venus*$^{+/-}$ ♂ X WT ♀	*rbpja/b* Mo.	100%	50%
Control	*csl:venus*$^{+/-}$ ♂ X WT ♀	None	100%	50%

4.5 Blocking Notch pathway with different approaches differentially affect Notch reporter expression in the DA.

Even though the three approaches shown in Table 4.1 dramatically reduced Notch signalling in the whole embryo, I noticed that some Venus protein remained with each of the approaches used, with the *mib* mutants having the least *venus* expression, as only some cells in

the heart and the inner ear were still expressing the reporter gene (Figure 4.3 A-B'). On the other hand, parts of the brain remained Notch-active in the *rbpja/b* morphants and DAPM treated embryos (Figure 4.3 C-F'). Moreover, in DAPM treated embryos some remaining Notch reporter expression was still detectable in the DA (Figure 4.3 E-F').

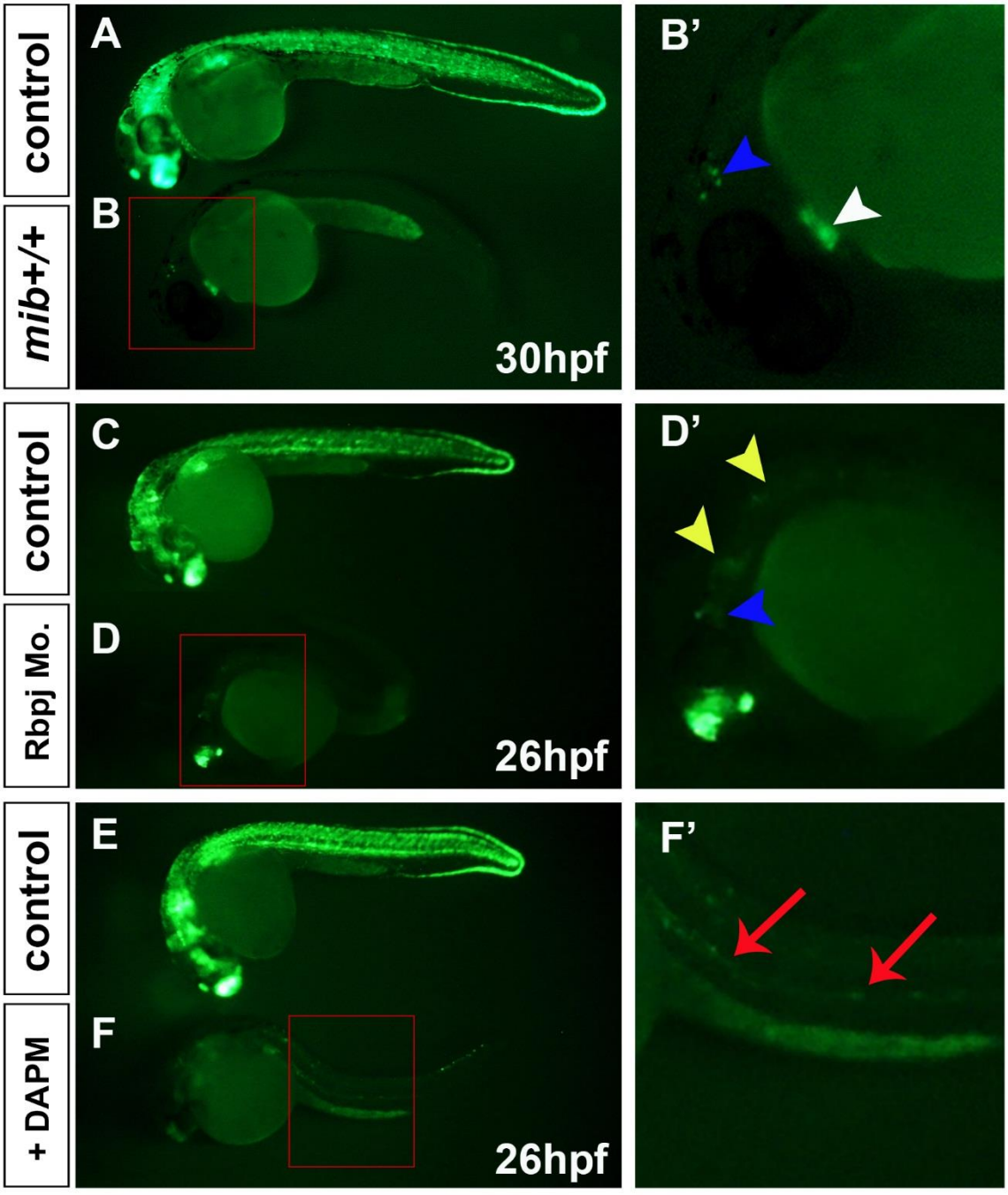

Figure 4.3 Blocking Notch pathway with different approaches differentially affects Notch reporter expression.
(A-B) Comparison of Venus fluorescent protein expression at 30hpf in *Tg(csl:venus)*$^{qmc61+/-}$ (A) compared to *mib*$^{ta52b+/+}$*/Tg(csl:venus)*$^{qmc61+/-}$ (B) showing a complete loss of Venus protein in the whole embryo except the heart (white arrowhead in B') and the inner ear (blue arrowhead in B'), which showed Venus fluorescent protein starting from 30hpf. B' is amplification of the boxed area in B. (C-D) Comparison of Venus fluorescent protein at 26hpf in *Tg(csl:venus)*$^{qmc61+/-}$ (C) compared to their *rbpja/b* morphant siblings(D), showing a complete loss of Venus fluorescent protein in the trunk and tail, whereas there is some remaining *venus* expression in the brain, inner ear (blue arrowhead in D') and hind brain (yellow arrowhead in D'). D' is magnification of the boxed area in D. (E-F) Comparison of Venus fluorescent protein at 26hpf in *Tg(csl:venus)*$^{qmc61+/-}$ (E) compared to their DAPM treated siblings (F), showing a weak *venus* expression in the DA (red arrows) and the medial fin fold. A weak *venus* expression is also seen in the head and neck region, the brain and the inner ear. F' is magnification of the boxed area in F.

To understand how the remaining Notch signalling using each of these approaches affects arterial specification and HSC development, in situ hybridization was performed on embryos from the four batches for endothelial and haematopoietic markers expression in these embryos (Figure 4.4). In situ hybridization results showed a complete loss of the HSC marker *runx1* in all treated embryos. While consistent with fluorescent microscopy data, the arterial marker *efnb2a* was maintained in DAPM treated embryos, while lost in *mib* mutants and *rbpja/b* morphants. Moreover, the *venus* marker *flt4* suppression in the DA failed in all three approaches.

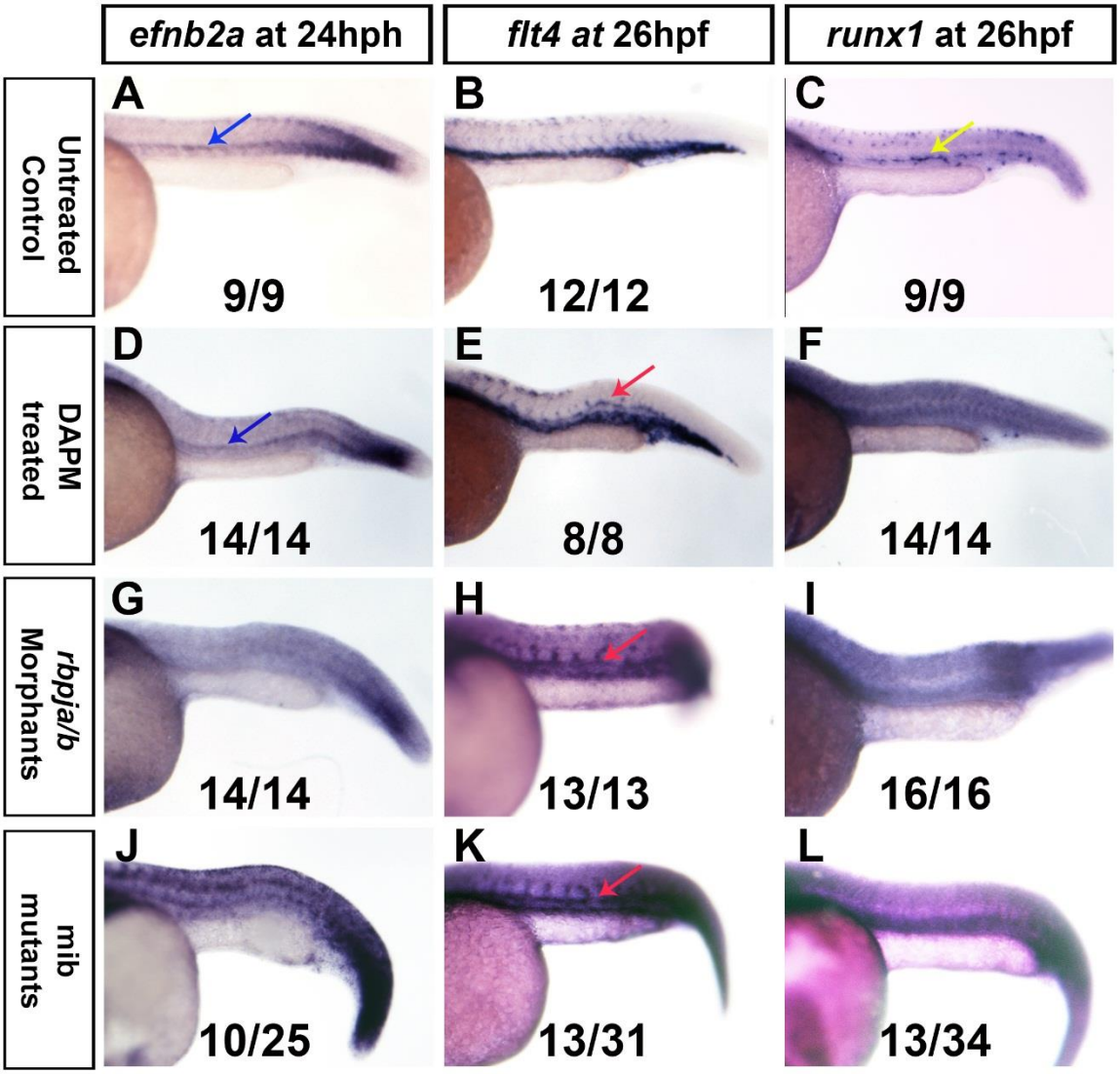

Figure 4.4 Blocking Notch pathway with different approaches differentially affect arterial and haematopoietic specification. Whole mount in situ hybridization of *efnb2a, flt4 and runx1* expression of WT (A-C) and Notch inhibited embryos (D-L). In WT *efnb2a* expression is restricted to the DA at 24hpf (blue arrow in A), while *flt4* is suppressed from DA and only present in the CV at 26hpf (B), whereas *runx1* is only seen in the vDA at 26hpf. Inhibiting Notch pathway with DAPM does not affect the arterial identity of the DA and expression of *efnb2a* is still seen in the DA (blue arrow D), but it fails to suppress *flt4* (red arrow in E), and also losses expression of the haematopoietic marker *runx1* (F). Blocking Notch pathway with the *rbpja/b* morpholinos leads to complete loss of arterial marker expression in the DA (G), failing to suppress *flt4* in the DA (H), and also losing the haematopoietic marker *runx1* (I). In *mib* mutants, the arterial marker *efnb2a* was lost in the DA (J), suppression of *flt4* in same tissue failed (K), and also expression of the haematopoietic marker *runx1* was lost (L).

4.6 Quantification of the residual Notch activity revealed that low level of Notch is sufficient for arterial gene expression while high levels are required for hEC induction

To quantify the residual Notch activity in DAPM treated embryos and *mib* mutants compared to un-treated controls, the sampling protocol included in materials and methods was followed, then total RNA was extracted from all three groups, reverse transcribed, then the remaining Notch levels was quantified with real time PCR on cDNA from three biological samples for each of the three groups. The results showed that the most efficient inhibition of Notch pathway was with *mib* mutation, while Notch activity was partially maintained in DAPM treated embryos. A summary of the results is shown in Figure 4.5.

Together, quantitative RT-PCR data, in agreement with both in situ hybridization and fluorescent microscopy, suggest that high levels of Notch are required in the DA after arterial specification to suppress venous fate and to initiate HSCs specification, while low level of Notch activity is sufficient to support the arterial fate of the DA.

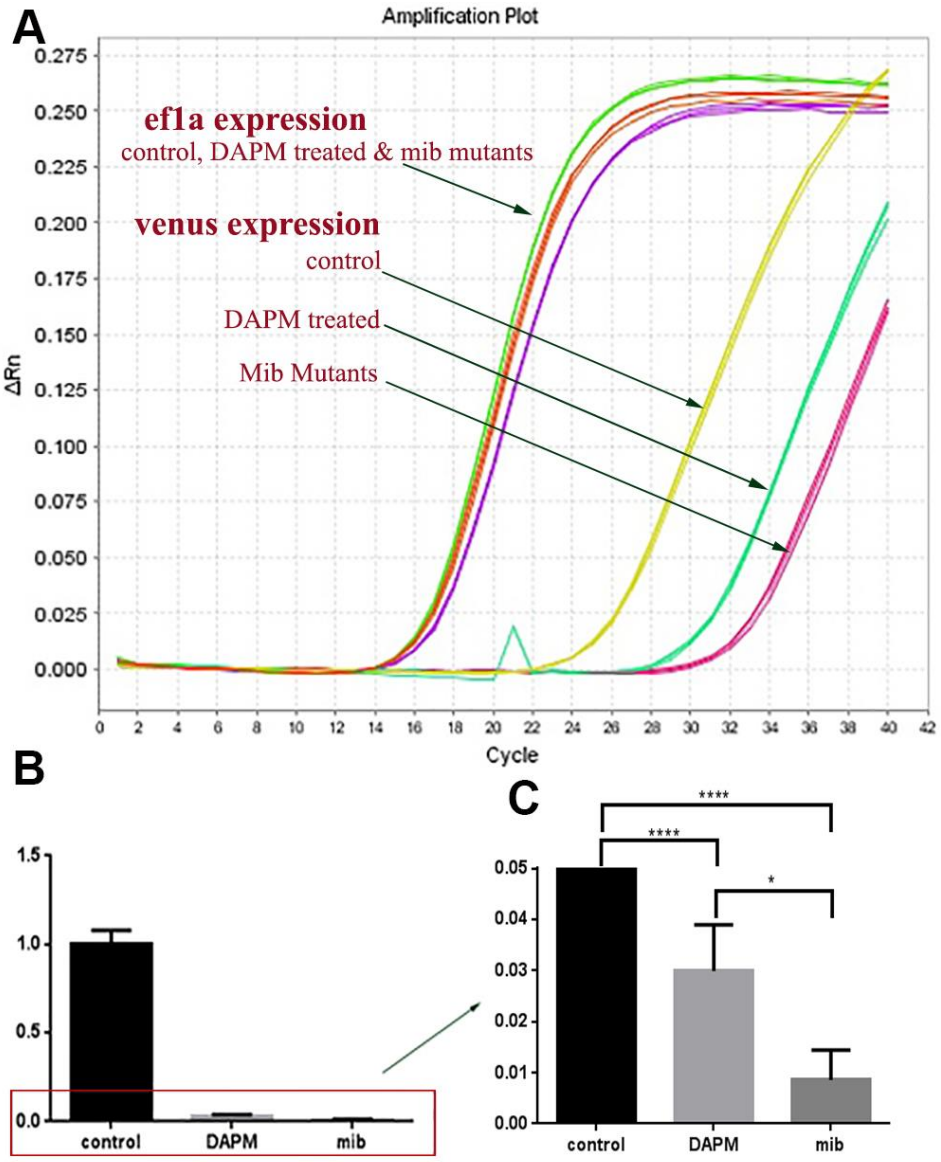

Figure 4.5 Notch reporter remaining levels in DAPM treated and *mib* mutants compared to un-treated control.
(A)Amplification plot showing cycles difference between DAPM treated and *mib* mutants compared to un-treated control. (B) Histogram of remaining Notch reporter mRNA compared to *ef1α* mRNA by RT-PCR. (C) Magnification of the boxed area in (B).

4.7 Discussion of results

During zebrafish development, the haemogenic endothelial progenitors specified from the posterior lateral mesoderm migrate to the midline to form the main axial vessels, the DA and the CV. At 18hpf, these progenitor cells further specify into arterial or venous endothelial and organize to form the developing DA and CV. Arterial and venous specification are determined by expression of the arterial markers such as efnb2a for arterial specification, and flt4 for venous specification.

Notch is known to act upstream of efnb2a to regulate arterial specification at this developmental stage. In the previous chapter we showed that Notch activity persists at a high level in the DA after arterial specification, thus suggesting that a high Notch signal is required for HSCs specification from the vDA. In this chapter we performed a semi-quantification analysis of DA fluorescent protein intensity after arterial specification and until the time point of HSCs specification. Our analysis showed a remarkable increase in the reporter protein intensity from 20hpf to 27hpf, which further supports the theory that high Notch signal is required for HSCs specification.

During the early stages of arterial specification of the DA, both efnb2a and flt4 are expressed in this region, then flt4 expression becomes undetectable in the DA by the time of HSCs emergence. Notch was shown previously to act upstream of flt4 suppression (Lawson et al., 2001). Our in situ data show that downregulation of flt4 after arterial

specification coincides with the upregulation in Notch activity. The fact that flt4 expression is maintained in the DA when Notch activity is low while it is lost at higher levels suggests that a high Notch activity may be required after arterial specification to suppress flt4 expression in the DA.

Consistent with this, we found that blocking Notch pathway in mib mutants or rbpja/b morphants led to loss of both arterial specification and HSCs development, while blocking Notch pathway with the less efficient approach (DAPM treatment) only interferes with HSCs specification. To confirm fluorescent microscopy and in situ hybridization data, we also quantified the remaining Notch reporter mRNA in mib mutants and DAPM treated embryos by RT-PCR and found less remaining Notch activity in mib mutants.

CHAPTER 5

5 Result III Developing a molecular tool to over-activate/ block Notch pathway in the endothelium

The efforts to develop molecular tools that enable mis-expressing Notch signalling pathway specifically in the endothelium started in the Gering lab a few years before starting this PhD project. These efforts yielded the generation and characterization of several transgenic lines, including *Tg(flk1:cre)*^{qmc101} and *Tg(flk1:cre-ERT)*^{qmc104}. Crossing these lines to the (Sinha et al., 2010) *cre* reporter line *Tg(ef1α:loxP-gfp-loxP-dsRed2*) which was received as a kind gift from Dr. Bally-Cuif's lab. The line was shown to drive *cre* induced recombination, specifically in the endothelial progenitors and the cells derived from them in temporal and spatial manners (Jalali, 2012). The next step was when the former student in the lab (H. Stone) replaced the dsRed in the *cre* reporter line with either *nicd* or *dnRbpj* genes shown to over-activate/block Notch pathway in zebrafish respectively (Latimer et al., 2002, Scheer and Campos-Ortega, 1999). The new constructs were then injected by Dr. M. Gering to establish the lines then grown to adulthood. At this stage, I took over and started by characterising the injected fish to identify F0 founders that have the injected constructs in their germlines. The plan was then to cross the identified transgenic fish to the *Tg(flk1:cre)*^{qmc101} or *Tg(flk1:cre-ERT)*^{qmc104} lines to specifically recombine and over-

activate/block Notch pathway in the endothelium and study the cell autonomous requirements for Notch in zebrafish HSCs formation.

In addition to the described experiments, I also cloned the mouse *rosa26* promoter and used to replace the *ef1α* in the Sinha et al. (2010) Cre reporter after successful use of *rosa26* as a ubiquitous promoter in frogs (Gross et al., 2006) however no zygotic expression of the floxed fluorescent gene was detected. I also tried the emerging genome editing tools CRISPR and PhiC31 Integrase to specifically integrate the *cre* gene or the *gal4-vp16* downstream of the *gfi1.1* promoter in our *gfi1.1* gene trap line *Tg(gfi1.1:gfp)*^{qmc551}, however none of these efforts were successful.

5.1 Identification of *ef1α nicd* and *Ef1α dnrbpj* transgenic founders.

Embryos with mosaic *cerulean* expression after injection with the *tol2* constructs (*ef1α-loxP-cer-loxP-dnRbpj* and *ef1α-loxP-cer-loxP-nicd*) were grown to adulthood. These fish were then crossed with wild type fish and their progenies were observed for *cerulean* expression on day one. Out of 7390 embryos examined, 72 embryos from 6 transgenic founders were identified, as shown in Tables 5.1 and 5.2).

Table 5.1: Identified *Tg(ef1α-loxP-cer-loxP-nicd*) transgenic founders.

ef1α nicd Identified founders					
Founder Name	Cerulean+ embryos	Normal embryos	Level of expression	Survived to day 5	Line established
qmc121	3	Yes	Low	Yes	Yes
qmc122	1	Yes	Low	Yes	Yes
qmc123	5	No	Strong	No	No
qmc124	4	Yes	Extremely low	Expression lost	No

Table 5.2 Identified *Tg(ef1α-loxP-cer-loxP-dnRbpj*) transgenic founders.

ef1α dnRbpj Identified Founders					
founder Name	Cerulean+ embryos	Normal embryos	Level of expression	Survived to day 5	Line established
qmc131	23	yes	Strong	Yes	Yes
qmc132	33	yes	Strong	Yes	Yes

As shown in Tables 5.1 and 5.2, even though four transgenic founders were identified for *Tg(ef1α-loxP-cer-loxP- nicd)*, only two lines were established, *Tg(ef1α-loxP-cer-loxP- nicd)*^{qmc121} and *Tg(ef1α-loxP-cer-loxP-nicd)*^{qmc122}; see Figure 5.1). This was because the transgenic embryos from the other founders either had extremely weak *cerulean* levels and their expression was lost on day 4 *(qmc124),* or they did not survive due to the severe abnormalities associated with strong *cerulean* expression, *(qmc123*; see Figure 5.1).

On the other hand, four transgenic founders were identified for the other construct, the *ef1α-loxP-cer-loxP-dnRbpj*. Their progenies showed decent and stable *cerulean* expression and displayed no visible abnormalities. The fact that the *Tg(ef1α-loxP-cer-loxP-nicd)* embryos with strong *cerulean* expression were abnormal, and

developed severe phenotypes and died early in development raised the possibility of premature Notch over-activation from a readthrough the *polyA* in the loxP floxed fragment and expression of *nicd* even before the Cre recombination. Read-through the *SV40 polyA* termination signal was previously detected by in situ hybridization in transgenic embryos with similar constructs (Drew, 2010). Based on these observations, we expected that the established lines, *Tg(ef1α-loxP-cer-loxP-nicd)*^{qmc121} and *Tg(ef1α-loxP-cer-loxP-nicd)*^{qmc122}, despite their low *ef1α* activity, are still able to over-activate the Notch pathway in the endothelium after the Cre recombination.

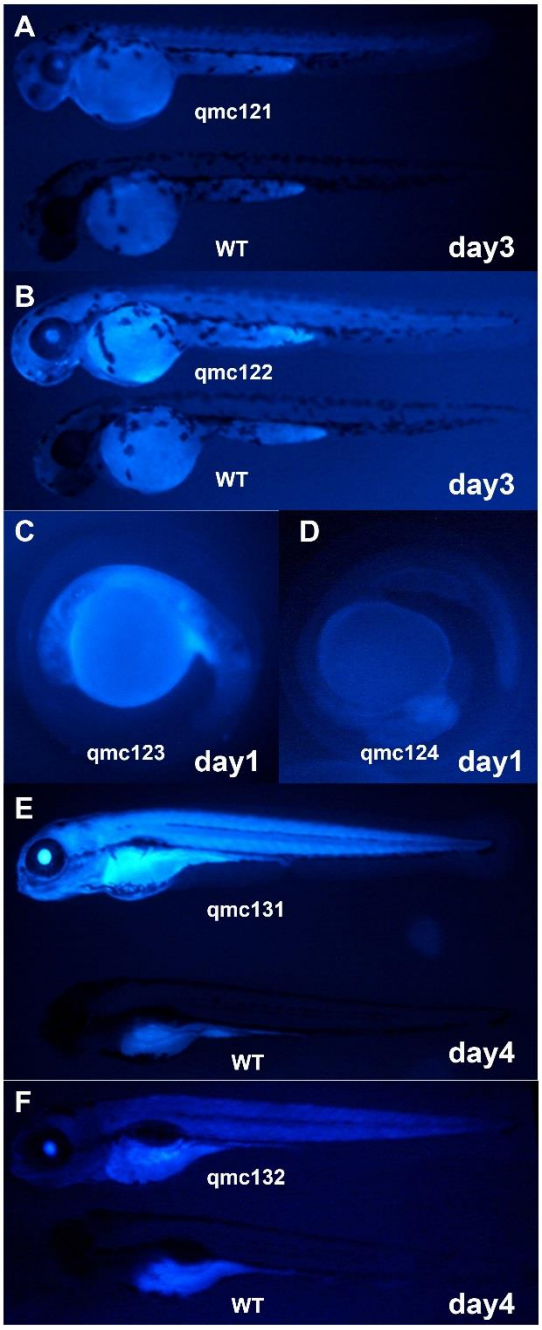

Figure 5.1 identified *Tg(ef1α-loxP-cer-loxP-nicd)* and *Tg(ef1α-loxP-cer-loxP-dnRbpj)* transgenics.
(A-F) Fluorescent images of identified F1 *nicd* and *dnRbpj* transgenics. (A-B) The established transgenic lines *Tg(ef1α-loxP-cer-loxP-nicd)*^{qmc121} and *Tg(ef1α-loxP-cer-loxP-nicd)*^{qmc122} F1 showing weak ubiquitous *cerulean* expression compared to their WT siblings. (C-D) Embryos from the other two founders with (C) showing strong *cerulean* expression but with severe defects and (D) showing extremely weak ubiquitis cerulean expression. (E-F) Established transgenic lines *Tg(ef1α-loxP-cer-loxP-dnRbpj)*^{qmc131} and *Tg(ef1α-loxP-cer-loxP-dnRbpj)*^{qmc132} F1 showing strong ubiquitous *cerulean* expression compared to their WT siblings.

5.2 Injecting the transgenic *Tg(ef1α-loxP-cer-loxP-nicd)* and *Tg(ef1α-loxP-cer-loxP-dnRbpj)* F1 embryos with *cre* mRNA

To test whether the *loxP* sequences in the generated transgenics are intact and can be recombined by the Cre enzyme to enable activation of downstream genes (*nicd* or *dnRbpj*), I first injected *cre* mRNA into two cell stage embryos from these lines. The expected outcome was removal of the floxed fragments and over-activation/blocking the Notch pathway in the whole embryo. Notch over-activation in the whole embryo with the *hsp70:gal4-uas:nicd* system was previously shown to lead to severe somite defects, with embryos of short and stumpy appearance (Scheer and Campos-Ortega, 1999). On the other hand, Notch inhibition in the whole embryo both with non-functioning Ubiquitin Ligase or with γ-secretase inhibitors, leads to abnormality in somitogenesis, loss of pigmentation in the tail (white tail) and defected vascular and HSCs formation (Jiang et al., 1996, Schier et al., 1996). The following steps were undertaken to prepare, complete and validate this experiment.

5.2.1 *cre* mRNA efficiently recombines the *loxP* sites in the Cre reporter line *Tg(ef1α:loxP-gfp-loxP-dsRed2)* and activates expression of downstream gene

Before injecting the in-house generated *cre* mRNA (see Material Methods) to the *Tg(ef1α-loxP-cer-loxP-nicd)* and *Tg(ef1α-loxP-cer-loxP-dnRbpj)* lines. The *cre* mRNA was firstly injected to the Cre reporter line *Tg(ef1α:loxP-gfp-loxP-dsRed2)* to check whether the in-house generated *cre* mRNA can be efficiently translated and whether the produced Cre protein is able recombine the *loxP* sites and so remove the floxed *gfp* in the reporter line to activate the downstream *dsRed*. It was also necessary to determine the *cre* mRNA amount required to efficiently drive the recombination with minimal toxicity to the embryos. To achieve this, *Tg(ef1α:loxP-gfp-loxP-dsRed2)* fish were in-crossed, then different batches of their embryos were injected with 100 pg and 200 pg of *cre* mRNA at 1-8 cell stage, as shown in Table 5.3.

Table 5.3: *cre* mRNA titration.

stage of injection	*cre* mRNA injected	*gfp* expression (day 1)	*dsRed* expression (day 1)	abnormal embryos
1-2 cell stage	200 pg	100% (36)/36	94% (34/36)	8% (3/36)
2 cell stage	200 pg	100% (48/48)	85% (41/48)	4% (2/48)
4 cell stage	100 pg	100% (58/58)	84% (49/58)	2% (1/58)
4-8 cell stage	100 pg	100% (41/41)	85% (35/41)	2% (1/41)
Non-injected	Not injected	100% (110/110)	0% (0/110)	0% (0/110)

cre mRNA injections confirmed that our in-house synthesised *cre* mRNA was efficiently translated and it efficiently removed the floxed *gfp*-polyA fragment, enabling expression of the downstream *dsRred* gene. This experiment also showed that the general injection efficiency was about 87% (94%+85%+84%+85%/4=87%). The results also demonstrated that *cre* mRNA has a high diffusion capacity, even when injected at slightly later stages in development. It was also found that *cre* mRNA has low toxicity, as even with injecting 200 pg the death rate of injected embryos did not exceed 8%. Together, these findings suggest that the optimal injection amount is 100 pg injected at 1-2 cell stage.

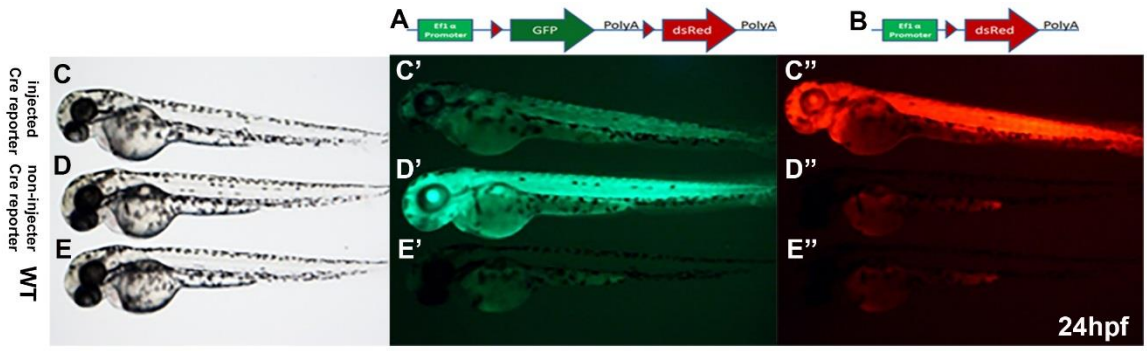

Figure 5.2 *cre* mRNA injection to the Cre reporter line.
(A)Diagram showing the un-recombined structure of the Cre reporter line. (B) Diagram showing the Cre recombined structure of the Cre reporter line. (C-E) Bright field image showing Cre reporter embryo injected with 100pg at 1 cell stage compared to their uninjected Cre reporter embryos (D) and uninjected WT embryos (E) with no observed abnormalities. (C'-E'') Same embryos imaged with fluorescent microscopy with a FITC (C'-E') and aTRITC filter sets (C''-E'').

5.2.2 Injecting the generated *Tg(ef1α-loxP-cer-loxP-nicd)^{qmc122}* with *cre* mRNA does not produce specific phenotypes

Before over-activating Notch signalling in the endothelium, we wanted to test whether we could over-activate Notch in the whole embryo by inducing recombination and expression of *nicd* in all embryonic tissues by injecting embryos with amount of *cre* mRNA that we have established in previous step. Consequently, I crossed *Tg(ef1α-loxP-cer-loxP-nicd)^{qmc121}* to WT fish then injected their progenies with *cre* mRNA following procedures and amounts injected to the Cre reporter line in previous step. Transgenic embryos injected with the *cre* mRNA showed a reduction in *cerulean* expression that

was relative to the amount of *cre* mRNA injected. A summary of injections amounts and observed phenotypes are shown in Table 5.4.

Table:5.4 *cre* mRNA injections to the *nicd* transgenic embryos results.

batch	amount injected	No. of embryos	Notch over-activation phenotypes
1st batch	100 pg	75	no clear phenotypes
2nd batch	90 pg	134	no clear phenotypes
3rd batch	100-200 pg	82	no clear phenotypes

5.2.3 Injecting the generated *Tg(ef1α-loxP-cer-loxP-dnRbpj)^{qmc131}* with *cre* mRNA does not block Notch signalling

Next, I examined whether the Notch pathway could be blocked in the whole embryo by inducing recombination and expression of the dominant negative version of *Rbpj* gene *(dnRbpj)* in all tissue. For this purpose, I injected the transgenic embryos *Tg(ef1α-loxP-cer-loxP- dnRbpj)^{qmc131}* with *cre* mRNA. In this experiment, six batches of transgenic embryos were injected with *cre* mRNA concentrations ranging from 100-200 pg. These injected embryos showed a reduction in *cerulean* fluorescent protein that is relative to the amount of *cre* mRNA injected (Figure 5.3 A-B). Injecting higher amounts of *cre* mRNA (200-400pg) seems to increase the efficiency

of recombination, but it results in higher death rates and severe unspecific defects on injected embryos (Figure 5.3 C-D). These observations are likely to be resulting from the interference of the high *cre* mRNA with the cellular activities in injected embryos. The fact that injecting amounts ranging between 200-400pg *cre* mRNA led to toxic defects while earlier experiments with injection of 200pg did not, may result from inter-experimental variation and related difficulties in precisely determining and controlling the amount of injected molecules. For example, injecting a drop size of six graticules instead of five on a normal dissecting microscope (estimated by the examiner) doubles the amount of injected volume. The other possibility is that the increased defective embryos were partly resulting from injecting needles with different tip widths. Wider needle tips create larger holes in the embryo and the chorion, which increases damage to the developing embryonic tissues, and so increases abnormalities and death rates in embryos.

Table:5.5: *cre* mRNA injections to the *Tg(ef1α-loxP-cer-loxP-dnRbpj)^{qmc131}* embryos does not produce Notch loss of function phenotypes.

Batch No.	Amount injected	No of embryos	Presence of phenotypes	Type of phenotypes
1st batch	125pg	58	No phenotypes	-
2nd batch	100pg	73	50% abnormal	control showed 20% abnormal (non-specific) (batch issue)
3rd batch	90pg	49	No phenotypes	-
4th batch	200pg	26	17/26 (65%) looks abnormal	control showed 6% abnormal (non-specific) **Cerulean completely lost**
5th batch	100pg	47	No phenotypes	- **Cerulean greatly reduced**
6th batch	150&200pg	81	No phenotypes	- Crossed to the *cre* reporter Tg (can't see Cer. as Gfp very strong and no vascular defects)
7th batch	200-400pg	36	Severe phenotypes in most embryos, death was high	Non-specific phenotypes **Cerulean either lost or greatly reduced**

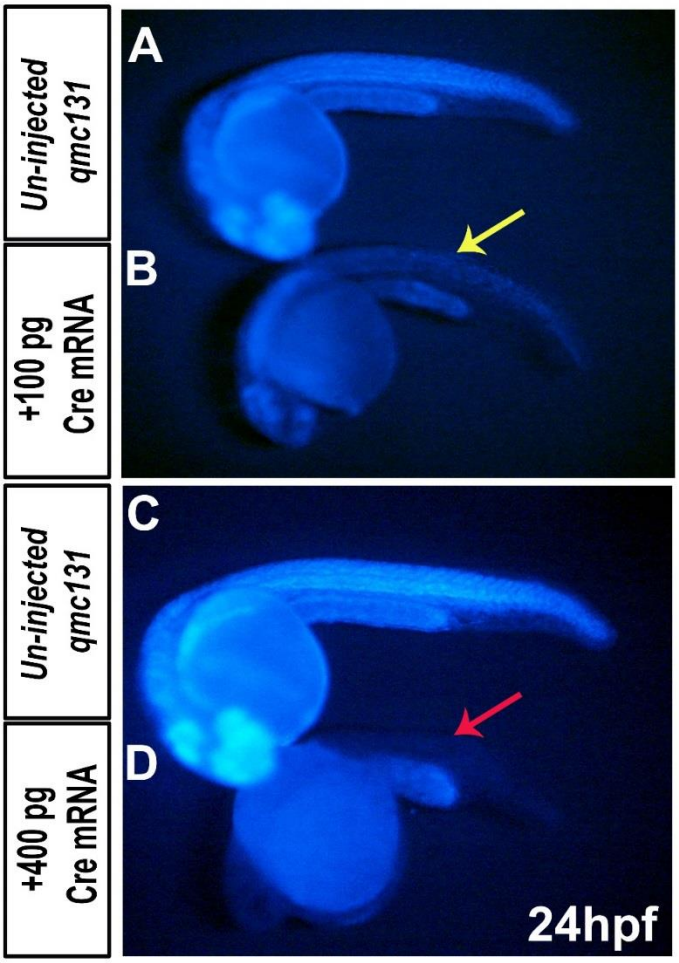

Figure 5.3 *cre* mRNA injection to *Tg(ef1α-loxP-cer-loxP-dnRbpj)*^{qmc131} embryos.
Fluorescent microscopy for *Tg(ef1α-loxP-cer-loxP- dnRbpj)*^{qmc131} uninjected controls (A,C) compared to their *cre* mRNA injected siblings (B,D) showing some remaining ubiquitis Cerulean fluorescent protein (yellow arrow) and normal embryological development with injection of 100pg of *cre* mRNA (B). Injecting higher amounts of *cre* mRNA on the other hand leads to almost a complete loss of Cerulean fluorescent protein (red arrow) and is associated with severe embryological development, but does not appear similar to *mib* mutants (D).

5.2.4 Embryos generated from crossing the *Tg(ef1α-loxP-cer-loxP-nicd)*^{qmc122} to Tg(*flk1:cre*)^{qmc101} appeared normal

Mouse studies that involved Notch over-activation in the endothelium showed severe defects in the endothelium and absence of HSCs formation and eventually early death before the time point of definitive HSCs formation (Venkatesh et al., 2008). Because zebrafish embryos can live normally on diffusion in absence of blood circulation, we expected the survival of zebrafish embryos, despite the severe vascular and haematopoietic defects after endothelial Notch over-activation. To test this hypothesis, I setup several crosses involving *Tg(ef1α-loxP-cer-loxP-nicd)*^{qmc122} fish to Tg(*flk1:cre*)^{qmc101}, then collected embryos were examined under microscope at 24hpf. Careful microscopic examination of these embryos at 24hpf showed no distinguishing differences between them and their controls with only slight delay in the initiation of blood circulation at 26hpf (which could be a biological difference).

Examining the embryos with delayed circulation a few hours later, showed the restoration of functioning blood and vascular system. Moreover, inter-somatic vessels had developed normally in all examined embryos. Together these data suggest that endothelial specific recombination of the *loxP* sites and expression of *nicd* under *ef1α* in *Tg(ef1α-loxP-cer-loxP-nicd)*^{qmc122} embryos and over-

activaation of Notch in the does not lead to distinguished blood or vascular defects. These findings also agree with whole embryo Cre mediated recombination in *Tg(ef1α-loxP-cer-loxP-nicd)*^{qmc122,} which did not show any clear Notch specific phenotypes. Together, the two experiments suggest that the amount produced of Nicd protein was not sufficient to overcome the homeostasis in embryos. A higher amount of endothelial specific Nicd protein may be need to be produced to over-come endothelial toleration for the produced Nicd in the embryo.

5.2.5 Embryos generated from crossing the *Tg(ef1α-loxP-cer-loxP- dnRbpj)*^{qmc131} to Tg(*flk1:cre)*^{qmc101} appeared normal

In order to block Notch pathway specifically in the endothelium, I setup several crosses with *Tg(ef1α-loxP-cer-loxP- dnRbpj)*^{qmc131} crossed to Tg(*flk1:cre)*^{qmc101}. No published data are currently available about blocking Notch specifically in the endothelium in the zebrafish animal model. In mice, blocking the Notch pathway either in the whole embryo in Notch -/- mutants or specifically in the endothelium both lead to severe vascular remodelling defects and early death of mouse embryos at E.10.5 (Kumano et al., 2003, Krebs et al., 2004). Blocking Notch pathway in in zebrafish whole embryo with different approaches is also associated with severe vascular and

haematopoietic defects (Gering and Patient, 2005, Lawson et al., 2001). These studies strongly suggest that blocking Notch pathway in the endothelium affects vascular and hematopoietic development, however none of the embryos resulting from crossing the *Tg(ef1α-loxP-cer-loxP- dnRbpj)*^{qmc131} to Tg(*flk1:cre)*^{qmc101} showed vascular or haematopoietic defects, even when examined at later times in development (days2-5).

This observation, together with earlier findings, all suggest that the amounts of Nicd or DnRbpj proteins produced in the endothelium in both experiments were not sufficient to over-activate/block the Notch pathway.

A stronger promoter may be required for production of higher levels of both Nicd and DnRbpj proteins to overcome cellular tolerance.

Recently, Mosimann et al. (2011) identified a 3.6 kb DNA fragment in the zebrafish genome that is homologous to human ubiquitin promoter (zebrafish *ubi* promoter). Generation of transgenic lines having this *ubi* promoter upstream of fluorescent proteins genes showed strong ubiquitous expression of downstream genes as soon as the zygotic genome transcription begins. The expression of fluorescent proteins then persisted in in all examined tissues throughout the embryonic development (Mosimann et al., 2011). To improve our Notch mis-expressing constructs, we decided to replace the *ef1α* promoter in our constructs with the zebrafish ubiquitin promoter.

5.2.6 Using the zebrasish *ubi* promoter instead of the *ef1α* promoter

A plasmid containing the zebrafish *ubi* promoter was received as a kind gift from Dr. R. Wilkinson, Sheffield University. To enable replacing the *ef1α* promoter in our *tol2- ef1α-loxP-cerulean-pA- loxP-nicd* and the *tol2-ef1α- loxP-cerulean-pA- loxP-dnRbpj* constructs, I amplified the *ubi* promoter with addition of restriction sites that enable its insertion instead of the *ef1α* promoter (see Appendix 6 for cloning procedures). The final new constructs were then verified by restriction analysis and partial sequencing, then they were given the database names *tol2-ubi-loxP-cerulean-pA-loxP-nicd* (P325) and *tol2-ubi-loxP-cerulean-pA-loxP-dnRbpj* (P323).

5.2.7 Injecting the P323 and P325 constructs and establishment of the *Tg(ubi-loxP-cer-loxP-nicd)* and *Tg(ubi-loxP-cer-loxP-dnRbpj)* lines

WT in-crosses were setup with dividers then embryos were collected the next day as soon as they were laid. Next, about 25pg of the P323 or P325 constructs were co-injected with transposase mRNA to these WT embryos soon after their collection and before the cellular division was initiated. The next day, injected embryos and non-injected controls were examined under fluorescence microscope for mosaic Cerulean fluorescent protein in their developing tissues. As

predicted, the majority of injected embryos showed mosaic *cerulean* expression and appeared normal. The results also showed that Cerulean positive cells contribute to the growing tissues with no signs of toxicity. Positive embryos were then sorted and kept in 28.5^{o}C untill day5, then 50 embryos of each batch were grown in the aquarium to establish the transgenic lines *Tg(ubi-loxP-cer-loxP-nicd)* and *Tg(ubi-loxP-cer-loxP-dnRbpj)*.

5.2.8 Screening the P323 and P325 injected fish for *Tg(ubi-loxP-cer-loxP-nicd)* and *Tg(ubi-loxP-cer-loxP-dnRbpj)* founders.

The putative founders of the two transgenic lines *Tg(ubi-loxP-cer-loxP-nicd)* and *Tg(ubi-loxP-cer-loxP-dnRbpj)* were checked frequently until adulthood. Among the 50 embryos grown for *Tg(ubi-loxP-cer-loxP-nicd)*, 34 survived until adulthood. On the other hand only 18 fish reached adulthood for *Tg(ubi-loxP-cer-loxP-dnRbpj)*. The surviving putative founders were then out-crossed to WT fish and their progenies were examined for *cerulean* expression on day one. Screening embryos from nine successful crosses of the *Tg(ubi-loxP-cer-loxP-nicd)* with WT resulted in identification of one founder that gave living embryos with good ubiquitous *cerulean* expression starting from day 1 and remained positive till day 5 (Figure 5.4 A). From this cross, 424 embryos were examined, and 84 were found

positive (about 20% transgenesis). Identified fish were then given the name *Tg(ubi-loxP-cer-loxP-nicd)*^{qmc125} F0 and 50 Cerulean positive embryos of its progeny were grown in the aquarium as F1 generation of this line. On the other hand, out of the 18 *Tg(ubi-loxP-cer-loxP-dnRbpj)* putative founders, only 10 were found to be fertile and gave aliving embryos, however screening all embryos from these 10 putative founders, revealed that none of them was positive for Cerulean fluorescent protein.

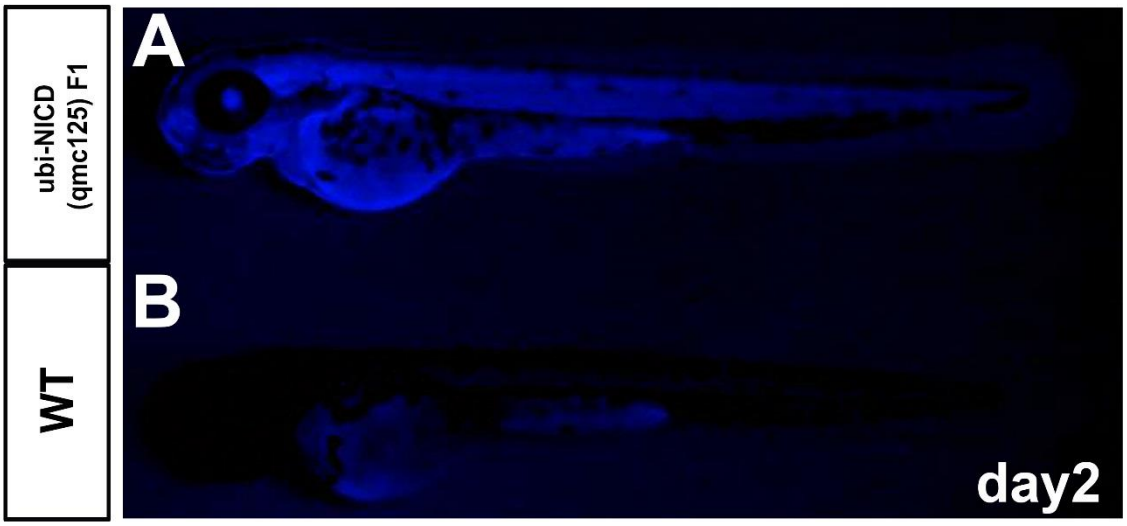

Figure 5.4 *ubi* promoter drive ubiquitous *cerulean* expression in *Tg(ubi-loxP-cer-loxP-nicd)*^{qmc125} F1.
(A-B) Fluorescent microscopy of *Tg(ubi-loxP-cer-loxP-nicd)*^{qmc125} F1 embryos (A) compared to WT on day 2. *ubi* promoter in *Tg(ubi-loxP-cer-loxP-nicd)*^{qmc125} line leads to decent ubiquitous expression of the *cerulean* gene.

5.2.9 Injecting the *Tg(ubi-loxP-cer-loxP-nicd)*^{qmc125} embryos with *cre* mRNA

To investigate whether recombining the *loxP* sites in the whole embryo would lead to phenotypes similar to those previously published with the Gal4-Uas system by Scheer and Campos-Ortega (1999). For this, I injected *cre* mRNA into *Tg(ubi-loxP-cer-loxP-nicd)*^{qmc125} embryos at one cell stage as with earlier similar experiments, then the embryos were observed for blood and vascular endothelial defects and for loss of *cerulean* expression. *cre* mRNA injected *Tg(ubi-loxP-cer-loxP-nicd)*^{qmc125} embryos showed a reduction in *cerulean* expression relative to the amount of *cre* mRNA injected. When higher amounts of *cre* mRNA (200 pg) were injected, a significant loss in *cerulean* expression was observed with phenotypes similar to that seen in Notch over-activation in the whole embryo with the Hsp70 GAL4-UAS Nicd system by Scheer and Campos-Ortega (1999). Observed phenotypes were neural and somatic deformation with a short and stumpy appearance (Figure 5.5 B-B'). Unlike the phenotypes observed with Notch over-activation with Gal4-Uas system, the phenotypes observed in injected embryos appeared less severe and were partially reversed later in development.

Figure 5.5 Injecting *cre* mRNA to the *Tg(ubi-loxP-cer-loxP-nicd)*^{qmc125} embryos produce neurological and somatic phenotypes.
(A-B) Bright field microscopy of uninjected (A) and *cre* mRNA injected *Tg(ubi-loxP-cer-loxP-nicd)*^{qmc125} embryo on day one. Injected embryos appeared shorter and with neural and somatic abnormalities. (A',B') Fluorescent microscopy of the same embryos showing reduction in cerulean expression in *cre* mRNA injected embryo (B') compared to non-injected sibling (A').

Following these observations, I crossed *Tg(ubi-loxP-cer-loxP-nicd)*^{qmc125} to *Tg*(*flk1:cre*)^{qmc101} and examined their progenies for vascular and haematopoietic defects. Yet, out of more than 300 embryos examined, none appeared distinguishable from WT controls. Careful examination of these embryos also showed normal vascular development and normal blood circulation, which suggests that endothelial produced Nicd after endothelial recombination was tolerable for the embryos.

Putting together the data collected from the first two lines generated with *ef1*α promoter that showed high death rates among embryos with high *cerulean* expression and the high death and low fertility rate

among grown the *Tg(ubi-loxP-cer-loxP-dnRbpj)* fish. This is added to the read-through reported by the former student in the lab concerning embryos having similar transgenic structures (Drew, 2010), read-through and premature expression of *nicd/dnRbpj* genes before recombination and removal of the floxed *cerulean-polyA* fragment in our injected embryos is evident. Consequently, we were not be able to generate transgenic lines with strong, ubiquitous *cerulean* expression or the downstream *nicd/dnRbpj* after the recombination. The read-through issue was also previously reported with experiments in the mouse model, and several strategies were devised to overcome this problem.

One of the strategies used, was including more than one polyA stop signal in the floxed cassette, such as the using a super stop cassette by Jackson et al. (2001). In Jackson's super stop cassette, four consecutive SV40 *polyA* signals were employed and shown to provide much higher efficiency in blocking read-through. A similar super stop cassette was also shown to be effective in the zebrafish animal model (Bertrand et al., 2010a). To further improve our *tol2-ubi-loxP-cerulean-pA-loxP-nicd* (P325) and *tol2-ef1α-loxP-cerulean-pA-loxP-dnRbpj* (P323), I decided to replace the single *polyA* signal in these constructs with the four *polyA* cassette described by Jackson et al. (2001). This is to efficiently silence the *nicd and dnRbpj* genes before the recombination, and so enable the survival of embryos in cases at which these constructs get integrated in open chromatin and in higher

supportive regions, thus achieving higher levels of expression of the studied genes after recombination.

5.2.10 Generation of the *tol2-ubi-loxP-mCherry-s.stop-loxP-nicd* (P351) and *tol2-ubi-loxP-mCherry-s.stop-loxP-dnRbpj* (P352) Constructs

In order to replace the *polyA* sequence in both P323 and P325 constructs with the *s.stop* cassette, I ordered the plasmid published by Jackson et al. (2001) from Addgene (ID 11584). The *s.stop* cassette and the *mCherry* gene was then used to replace the *cerulean polyA* fragments in P323 and P325 constructs following the cloning steps described in Appendix 7. This resulted in the generation of the constructs: *tol2-ubi-loxP-mCherry-s.stop-loxP-nicd* (P351) and *tol2-ubi-loxP-mCherry-s.stop-loxP-dnRbpj* (P352).

5.2.11 Injecting the P351 and P352 constructs and establishment of *Tg(ubi-loxP-mCherry-s.stop-loxP-nicd)* and *Tg(ubi-loxP-mCherry-s.stop-loxP-dnRbpj)* lines

P351 and P352 constructs injections were performed following the steps used to generate earlier described transgenic lines. Injected embryos were then examined for mosaic *mCherry* expression and positive embryos were sorted (see Figure 5.6). 50 normal *mCherry*

positive embryos were picked and grown from each batch to establish the transgenic lines *Tg(ubi-loxP-mCherry-s.stop-loxP-nicd)* and *Tg(ubi-loxP-mCherry-s.stop-loxP-dnRbpj)*.

When the grown embryos reached adulthood, they were screened for potential founders, and several lines were identified with slight variation in the levels of the ubiquitously expressed *mCherry* gene. Out of the several identified founders, one representative founder for the Nicd experiment was selected and named *Tg(ubi-loxP-mCherry-s.stop-loxP-nicd)*^{qmc127} and one representative of the founder for *dnRbpj* was selected and named *Tg(ubi-loxP-mCherry-s.stop-loxP-dnRbpj)*^{qmc129}*; mCherry* positive embryos from these two founders (Figure 5.6 E-F F) were grown as F1 of these lines.

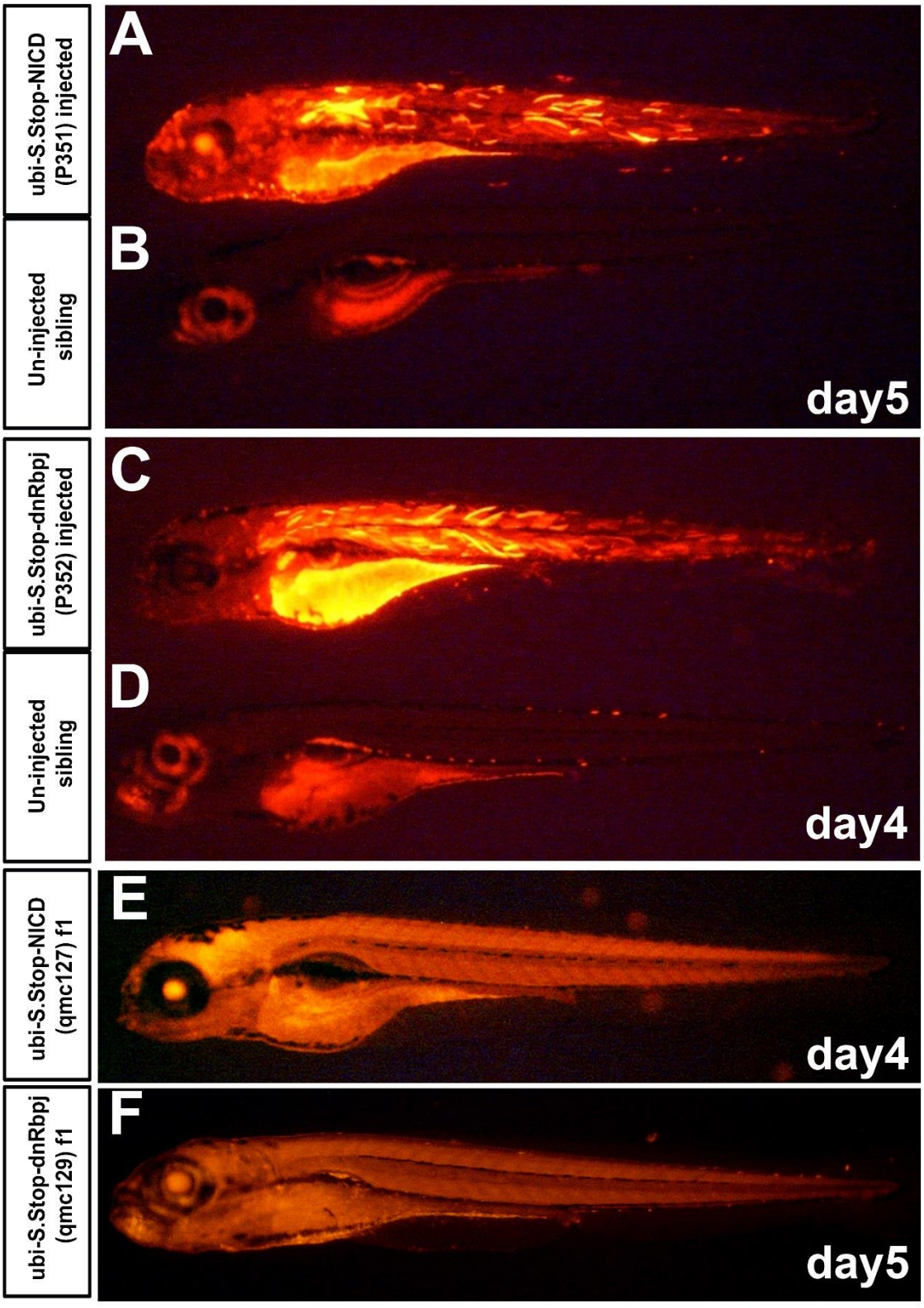

Figure 5.6 Establishment of the *Tg(ubi-loxP-mCherry-s.stop-loxP-nicd)^{qmc127}* and *Tg(ubi-loxP-mCherry-s.stop-loxP-dnRbpj)^{qmc129}* lines

(A-B) Fluorescent microscopy of WT embryos co-injected with the constructs P351 and transposase (A) or P352 and transposase (C)

compared to uninjected siblings (B,D). (E-F) Fluorescent microscopy images showing embryos from the established transgenic lines *Tg(ubi-loxP-mCherry-s.stop-loxP-nicd)*^{qmc127} and *Tg(ubi-loxP-mCherry-s.stop-loxP-dnRbpj)*^{qmc129}.

Following this, I crossed *Tg(ubi-loxP-mCherry-s.stop-loxP-nicd)*^{qmc127} and *Tg(ubi-loxP-mCherry-s.stop-loxP-dnRbpj)*^{qmc129} fish to *Tg*(*flk1:cre)*^{qmc101} fish, then examined their progenies for vascular and haematopoietic defects. They all appeared normal with normal vascular development and normal blood circulation, suggesting that the produced Nicd or DnRbpj proteins in the endothelium were as in previous experiments still tolerated by the embryos.

5.3 Discussion of results

Data presented in previous chapters suggested that the migrating haemogenic endothelial progenitor cells become Notch active soon after somitogenesis, and that the early low Notch signal in these cells is sufficient for arterial specification, as indicated by expression of efnb2a by 18hpf. Maintaining Notch in the DA endothelium at high levels also suggests that a high Notch level is required for HSCs specification from the vDA. Recently, several reports have also demonstrated a non-cell autonomous requirement for Notch in HSCs specification. To improve our understanding about Notch requirements in haematopoietic stem cell development, we

generated transgenic lines to enable endothelial specific Notch over-activation/blocking, utilizing the Cre LoxP system.

While in mice rosa26 promoter is used to reliably drive ubiquitous expression of downstream genes, no similar tool is available in zebrafish. rosa26 promoter was also shown to drive strong ubiquitous expression in frogs (Gross et al., 2006), however when we injected constructs with rosa26 promoter up-stream of fluorescent protein genes into zebrafish embryo, no expression was observed in these embryos. We then tried to optimize currently available tools and used the ef1α promoter as a ubiquitous promoter in the effector transgenes together with the flk1:cre transgene as activator for that transgene.

The read-through of the pA signal in the floxed loxP cassette was one of the obstacles faced during this process, which likely led to premature expression of the downstream genes and death of embryos with good expression. To overcome this obstacle, we replaced the single pA in the floxed fragment with a super-stop cassette made of four pA signals to ensure complete silencing of the downstream gene. Another obstacle we faced was the low expression level of downstream gene after the Cre induced recombination and removal of the floxed cassette. To address this, we replaced the ef1α promoter in the effector transgene with the ubi promoter that was recently identified in the zebrafish genome by Mosimann et al.

(2011), and proposed to drive strong ubiquitous expression of downstream genes during embryogenesis and until adulthood.

Nevertheless, activating expression of downstream genes by the ubi promoter was still compensated by the embryos. It was concluded that a system that provides a higher level of endothelial Nicd or DnRbpj proteins may be required to overcome embryonic compensation. Therefore, we decided to further improve our constructs to allow production of higher levels of Nicd or DnRbpj proteins in the endothelium after recombination. The Gal4-Uas system is among the genetic tools that have been used successfully to over-activate Notch signalling in zebrafish whole embryo (Scheer and Campos-Ortega, 1999), and the system showed very efficient expression of genes downstream of the Uas binding sites in the presence of the Gal4 protein. Due to the time constraints we limited cloning and transgenesis experiments to endothelial specific Notch gain of function studies. These experiments are the main focus of the next chapter.

Chapter 6

6 Result IV Endothelial Notch induction is sufficient to expand HSCs

6.1 Introduction

In continuation of the optimization efforts aiming to mis-express Notch signalling specifically in the endothelium, and due to the likelihood of low expression levels of *nicd* or *dnRbpj* under the *ef1α* or *ubi* promoters after the endothelial Cre recombination that might be tolerated by the embryo. It was planned to combine both the Gal4-Uas system and the Cre-loxP system to amplify the amount of produced Nicd in endothelial cells and examine whether this would expand HSC formation in the axial vessels and the CHT as indicated by expansion of the HSC marker genes like *runx1*, *c-myb* and *gfi1.1.*

6.2 Haemogenic endothelial Notch over-activation by combining the GAL4-UAS and Cre-loxP systems

6.2.1 Generating the *Tol2-ubi-loxP-mCherry-s.stop-loxP-gal4-vp16* construct

The *ubi-loxP-mCherry-s.stop-loxP-gal4-vp16* construct was generated by inserting a full length codon optimized *gal4-vp16* downstream of the floxed *mCherry-s.stop* fragment to enable expression of the inserted *gal4-vp16* in tissues where the floxed

cassette got removed by the Cre enzyme. Activation of the Gal4-vp16 in the endothelium in the presence of the *uas:nicd* transgene in the background then leads to activation of Notch pathway specifically in recombined tissues. Following the cloning steps shown in (Appendix 8), we generated the *tol2* plasmid *ubi-loxP-mCherry-s.stop-loxP-gal4-vp16* and entered it in our database under the name P356.

6.2.2 Injecting the P356 and establishment of the *Tg(ubi-loxP-mCherry-s.stop-loxP-gal4-vp16)* transgenic lines

To establish transgenic lines with the newly generated *tol2* plasmid P356, the plasmid was co injected with transposase, then embryos with mosaic *mCherry* expression were analysed for and abnormalities, then 50 appearingly normal embryos were grown in the aquarium to adulthood to establish the transgenic line.

6.2.3 Identification of the *Tg(ubi-loxP-mCherry-s.stop-loxP-gal4-vp16)* founders *qmc130, qmc133, qmc134, qmc135*

At adulthood, 33 fish were screened for expression of the floxed *mCherry* downsteam of the *ubi* promoter. The screen yielded identification of four transgenic F0 founders. The transgenic founders were used to establish the *qmc* lines *qmc130, qmc 133*, *qmc134* and

qmc135. Out of these four identified founders, two lines were found to express the *mCherry* at low levels (*qmc133-qmc134*), while the other two (*qmc130, qmc135*) expressed *mCherry* and potentially *gal4-vp16* at stronger levels (see Figure 6.1).

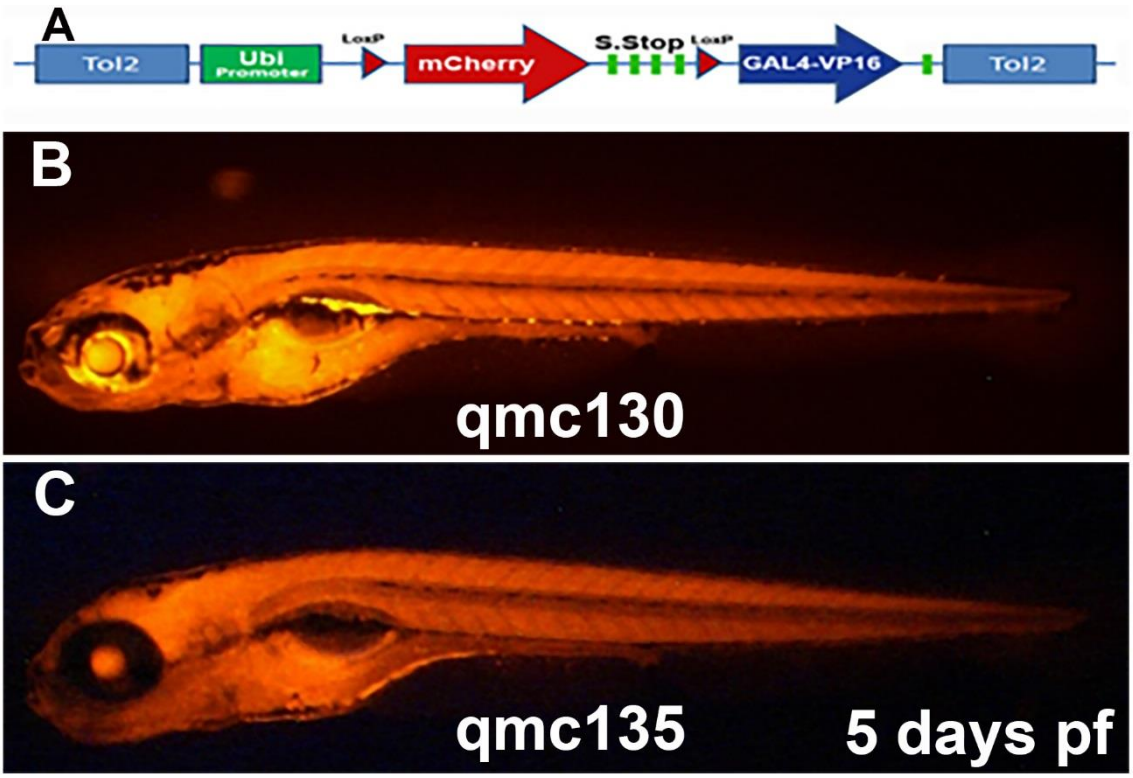

Figure 6.1 identification of embryos with strong ubiquitous expression of *mCherry* from outcrossing injected fish to WT and establishment of the transgenic lines *Tg(ubi-loxP-mCherry-s.stop-loxP-gal4-vp16)*^{qmc130}, and *qmc135*.
(A) Diagram showing the main components of the P356 construct. (B-C) Fluorescent microscopy images of live 5days old embryos from outcrossing injected fish to WT. The images show strong ubiquitous and homogenous *mCherry* in all tissues. The identified fish were given the founder names of *qmc130* and *qmc135* and their *mCherry* positive embryos were grown as (F1) generations of these lines.

6.2.4 Generation of the triple transgenic fish *Tg*(*f.flk1:cre;uas:nicd;csl:venus)*

To enable endothelial Notch induction and to enable reporting this over-activation, I firstly crossed a *Tg*(*uas:nicd)* fish (Scheer and Campos-Ortega, 1999) to our in-house *Tg(csl:venus)*^{qmc61} fish and grew their embryos to adulthood. I then crossed the identified *Tg*(*uas:nicd;csl:venus)* double transgenic fish to the Bertrand et al. (2010a) Cre line that expresses the *cre* gene under the control of the full length *flk1* promoter in the endothelium *Tg*(*f.flk1:cre)*^{s898}. Embryos were grown to adulthood then characterized for carrying the three transgenes *Tg*(*f.flk1:cre;uas:nicd;csl:venus)*. The identified triple transgenic fish was then used in combination with the *Tg(ubi-loxP-mCherry-s.stop-loxP-gal4-vp16)* to enable over-activating Notch in the endothelium and reporting any alteration in Notch activity in these embryos.

6.2.5 Endothelial Notch induction up-regulates expression of the Notch reporter gene specifically in the endothelium

To over-activate Notch specifically in the endothelium, the triple transgenic activator fish *Tg*(*f.flk1:cre;uas:nicd;csl:venus)* was crossed to the effector transgenic fish *Tg(ubi-loxP-mCherry-s.stop-*

loxP-gal4-vp16)^{qmc135}. Utilising the Notch reporter transgene in the background of 50% of produced embryos wherein the effect of endothelial recombination and activating expression of the *nicd* in the endothelium on the level of the Notch reporter fluorescent protein was studied. The results showed a clear up-regulation in the Venus fluorescent protein level in the DA and the ISV starting from day 1 (Figure 6.2). Examining these embryos on day 1 showed even stronger expression of the *venus* gene and no expression was reported outside the endothelium. Quantifying the up-regulation showed about ten fold difference in Notch reporter fluorescence intensity along the DA in induced compared to un-induced embryos (Figure 6.3, A-D). Undesirably, we also observed that about half of the embryos produced from these crosses do not have a functioning blood circulation by day 2 (Table 6.1 shows the expected and observed numbers of embryos from one of these crosses).

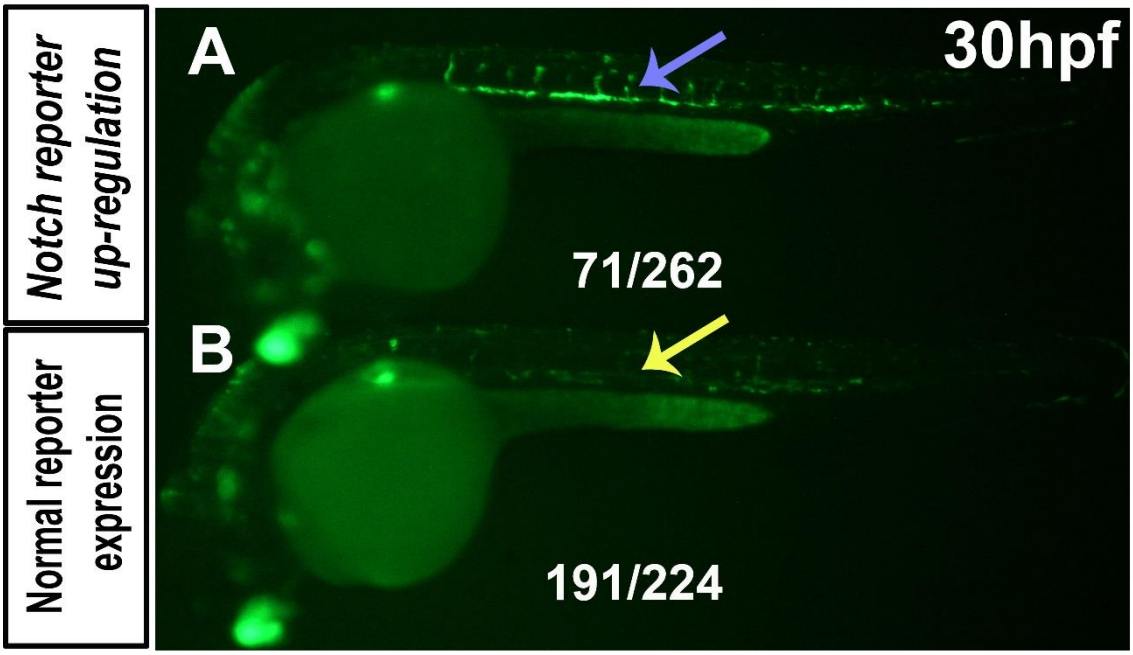

Figure 6.2 Endothelial Notch induction up-regulates expression of the Notch reporter gene.
Fluorescent image of live 30hpf embryos from crossing the triple transgenic *Tg*(*f.flk1:cre;uas:nicd;csl:venus)* to the transgenic fish *Tg(ubi-loxP-mCherry-s.stop-loxP-gal4-vp16)*^{qmc135} f1 fish. (A) Shows a sample of a quarter of the *mCherry* positive-venus positive embryos that have also shown a strong up-regulation of the Notch reporter fluorescent protein Venus in the DA and ISV, as indicated by the blue arrow compared to their counterparts (yellow arrow) in 3/4 of the embryos, as shown in (B).

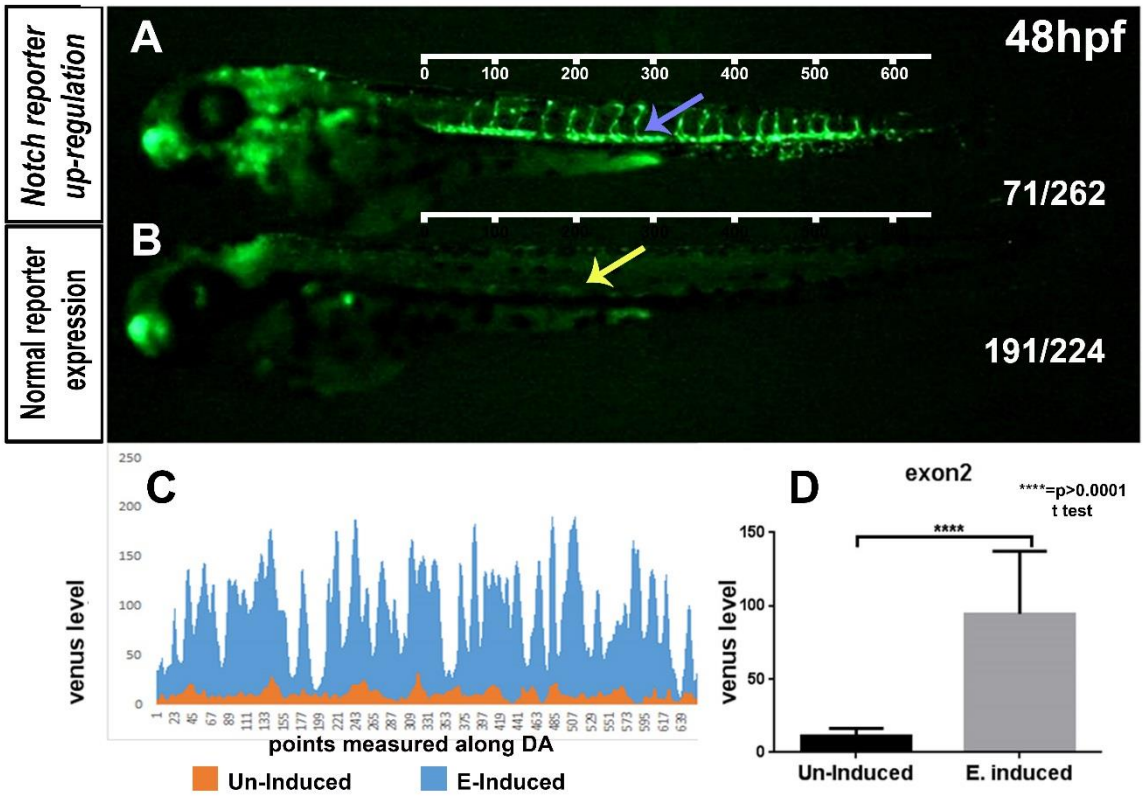

Figure 6.3 Quantification of the difference in Notch reporter fluorescent protein level between un-induced and endothelial Notch-induced embryos.

(A-B) Fluorescent image of live 48hpf embryos from crossing the triple transgenic *Tg*(*f.flk1:cre;uas:nicd;csl:venus)* to the effector *Tg(ubi-loxP-mCherry-s.stop-loxP-gal4-vp16)*^{qmc135} f1 fish. (A) Shows sample of a quarter of the *mCherry* positive embryos that have also shown strong up-regulation of the Notch reporter gene in the DA and ISV compared to the 3/4 counterpart embryos (B) that have low *venus* expression in the DA and ISV. (C) Comparison of intensity of the Venus fluorescent protein in Un-Induced and Endothelial Notch-induced in 650 points systematically picked along the DA. (D) Comparison of the means of points measurements in (C) showing about 10 fold increase in fluorescent protein intensity in the DA (Mean and SEM; **** $p<0.0001$; t test).

Table 6.1: the table shows expected and observed embryos on day2 with the Notch activity reported with the *csl:venus* transgene.

Tg(ubi-loxP-mCherry-s.stop-loxP-gal4-vp16)^{qmc135} **X** *Tg(f.flk1:cre;uas:nicd;csl:venus)* **Total no of embryos collected = 555 all were *mCh*+ve**				
tg	**Fluorescent Microscopy**	**phenotype**	**expected**	**observed**
- cre ***+ gal4*** ***- nicd*** ***- venus***	**Red**	**Normal**	**69.4**	**Normal Circulation 147**
- cre ***+ gal4*** ***+ nicd*** ***- venus***	**Red**	**Normal**	**69.4**	
+ cre ***+ gal4*** ***- nicd*** ***- venus***	**Red**	**Normal or Circulation??**	**69.4**	**No Circulation 146**
+ cre ***+ gal4*** ***+ nicd*** ***- venus***	**Red**	**High Notch Circulation??**	**69.4**	
- cre ***+ gal4*** ***- nicd*** ***+ venus***	**Red+green**	**Normal**	**69.4**	**Notch low Normal circulation 130**
- cre ***+ gal4*** ***+ nicd*** ***+ venus***	**Red+green**	**Normal**	**69.4**	
+ cre ***+ gal4*** ***- nicd*** ***+ venus***	**Red+green**	**Normal Circulation??**	**69.4**	**Low Notch No Circulation 61**
+ cre ***+ gal4*** ***+ nicd*** ***+ venus***	**Red+ high green**	**High Notch Circulation??**	**69.4**	**High Notch No Circulation 71**

To investigate whether loss of circulation was due to recombination and endothelial expression of *gal4-vp16*, and also to investigate whether observed up-regulation in Notch reporter fluorescent protein (Venus) was due to endothelial Notch induction and not due to loss of circulation. For these reasons, I performed single embryo DNA extraction then PCR genotyping for transgenes, as shown in Table 6.2.

Table 6.2: embryos used in single embryo genotyping.

Observed phenotype	No. of embryos used for single embryo DNA extraction and PCR genotyping
Venus low with normal circulation	10 embryos
Venus low with lost circulation	10 embryos
Venus high with lost circulation	10 embryos

6.3 Single embryo PCR results confirmed that endothelial Notch reporter up-regulation was due to endothelial Notch induction while lack of circulation might be caused by Gal4-vp16 protein accumulation

Utilising primers that specifically recognise and amplify fragments of the *uas:nicd* and the *flk1:cre* transgenes, I found a 100% n=10/10 correlation between up-regulation in Notch reporter activity and the presence of the four constructs (see Figure 6.4 C-C'). I also found a 100% n=10/10 correlation between the absence of circulation and endothelial recombination leading to expression of the *gal4-vp16* in the endothelium (see Figure 6.4, B-C').

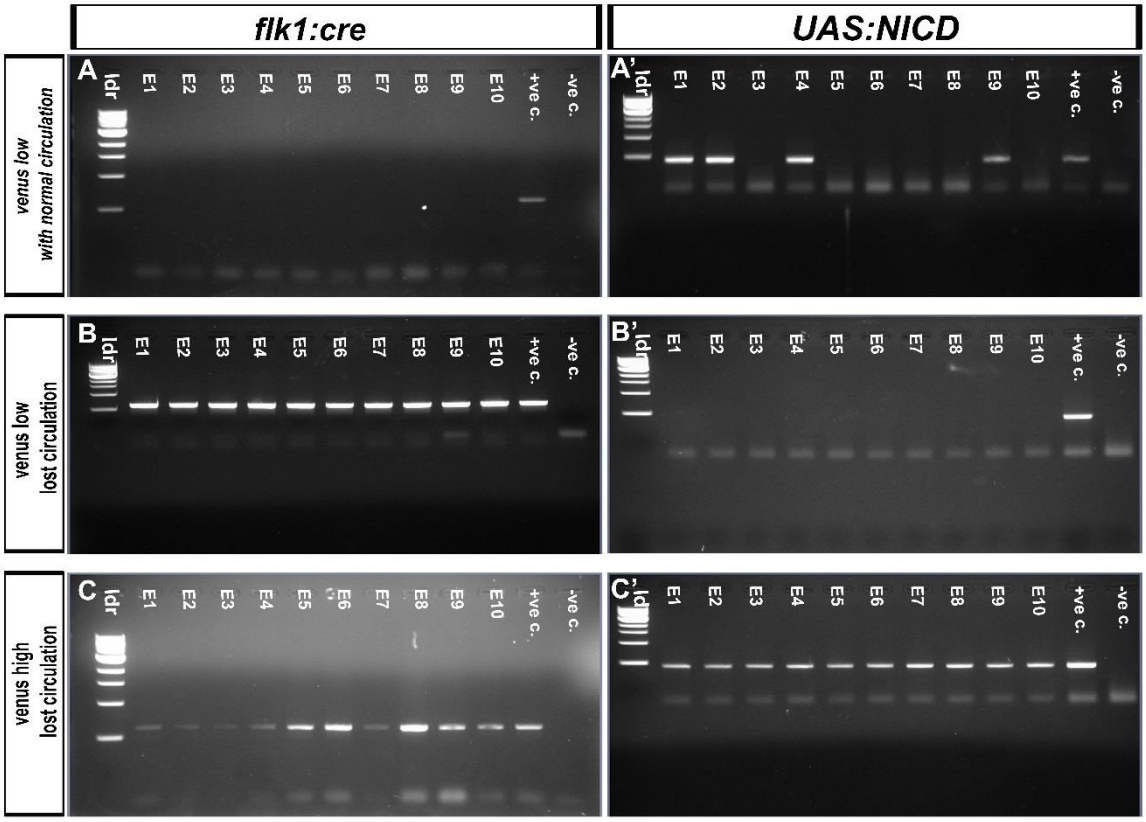

Figure 6.4 Single embryos PCR genotyping shows a strong correlation between endothelial Notch induction and Notch reporter fluorescent protein up-regulation.
Two sets of primers were used (DB143 and DB144; DB162 and DB163) to detect and amplify ~600bp fragment of the *flk1:cre* transgene and ~460bp fragment of the *uas:nicd* transgene respectively. (A-A') Shows that none of the embryos with low Notch reporter gene expression and normal blood circulation 0% (0/10) carried the *flk1:cre Tg*. Irrespective of presence of the *uas:nicd* tg. (B-B') Shows that 100% (10/10) embryos lost blood circulation have the *flk1:cre* tg. and that loss of blood circulation was not sufficient to up-regulate the Notch reporter fluorescent protein in absence of the *uas:nicd* tg. (C-C') Shows that 100% (10/10) of the embryos that have high Notch reporter fluorescent protein are positive for both *flk1*:*cre* and *uas:nicd* tg. (First lanes in all gel images show NEB 100bp ladder, whereas lanes 11 and 12 are known positive and negative controls).

It was previously reported that accumulation of Gal4-vp16 protein in the cells might result in interference with other genes, however as the cells in these embryos appeared viable and they were contributing to the DA and ISV, I wanted to know if the endothelial Notch induction has an effect on vascular formation similar to that previously published in zebrafish chimera (Siekmann and Lawson, 2007), which indicated a loss of tip cell formation in cells with over-activated Notch activity. To investigate this, I generated the triple transgenic activator *Tg*(*f.flk1:cre;f.flk1:gfp;uas:nicd)* to highlight the endothelial cells and to enable studying their behaviour when Notch is induced specifically in these cells.

Table 6.3 the table shows expected and observed embryos on day2 with the vascular system highlighted with *f.flk1:gfp Tg*.

Tg(ubi-loxP-mCherry-s.stop-loxP-gal4-vp16)^{qmc135} **X** *Tg(f.flk1:cre; f.flk1:gfp;uas:nicd)* **Total no of embryos collected = 125 all were *mCh*+ve**				
tg	**Fluorescent Microscopy**	**phenotype**	**expected**	**observed**
- cre ***+ gal4*** ***- nicd*** ***- gfp***	**Red**	**Normal**	**15.6**	**Normal Circulation 25**
- cre ***+ gal4*** ***+ nicd*** ***- gfp***	**Red**	**Normal**	**15.6**	
+ cre ***+ gal4*** ***- nicd*** ***- gfp***	**Red**	**Normal or no Circulation**	**15.6**	**No Circulation 31**
+ cre ***+ gal4*** ***+ nicd*** ***- gfp***	**Red**	**High Notch Circulation**	**15.6**	
- cre ***+ gal4*** ***- nicd*** ***+ gfp***	**Red+green normal vessels**	**Normal**	**15.6**	**Notch low Normal circulation 37**
- cre ***+ gal4*** ***+ nicd*** ***+ gfp***	**Red+green normal vessels**	**Normal**	**15.6**	
+ cre ***+ gal4*** ***- nicd*** ***+ gfp***	**Red+green normal vessels**	**Normal Circulation**	**15.6**	**Low Notch No Circulation 17**
+ cre ***+ gal4*** ***+ nicd*** ***+ gfp***	**Red+ green defected vessels**	**High Notch Circulation**	**15.6**	**High Notch No ISV 15**

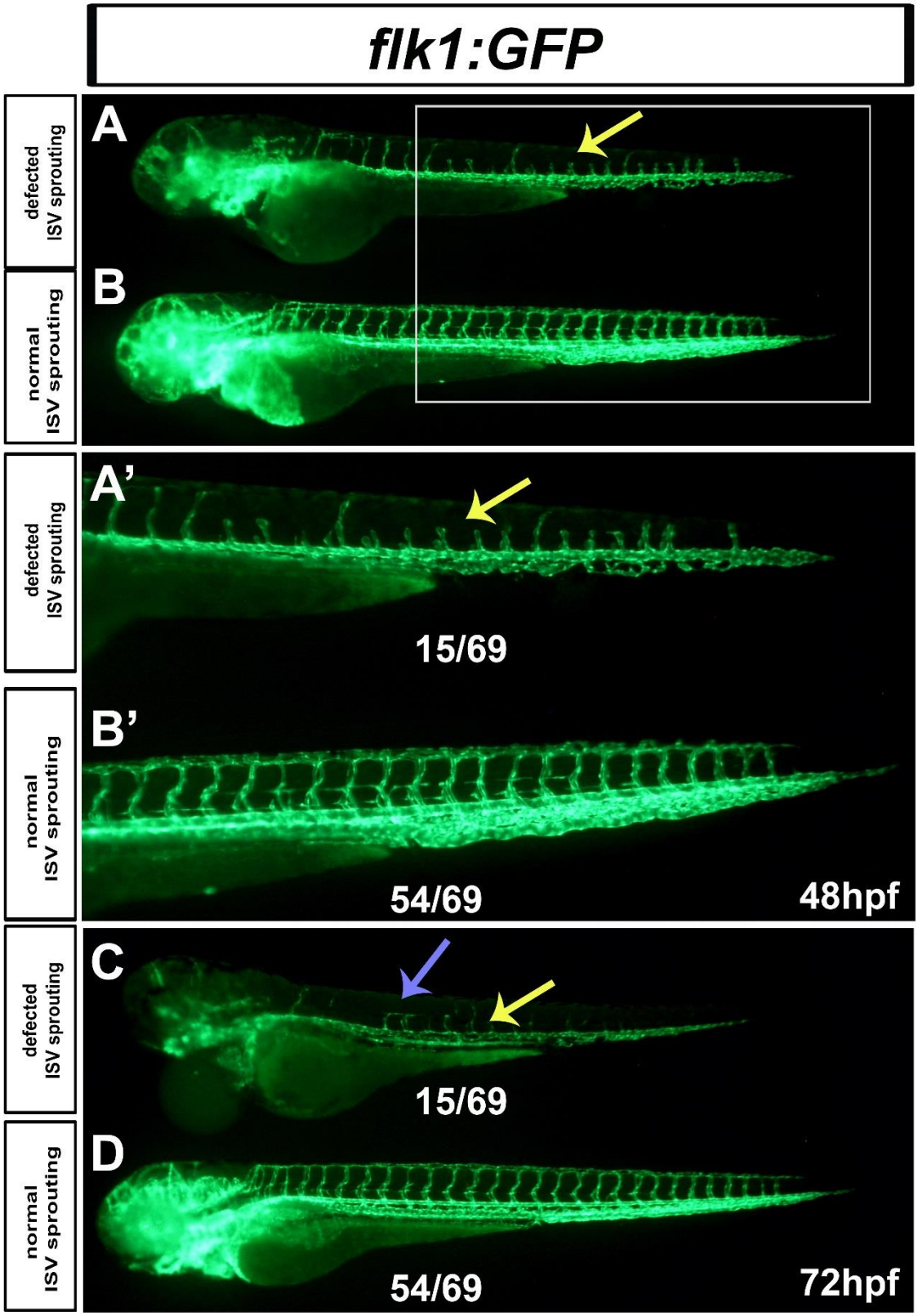

Figure 6.5 Endothelial Notch induction perturbs normal tip cell migration in response to VEGF signal and leads to defective ISV sprouting.

Fluorescent images of live 48hpf embryos from crossing the triple transgenic *Tg*(*f.flk1:cre;f.flk1:gfp;uas:nicd)* to *Tg(ubi-loxP-mCherry-s.stop-loxP-gal4-vp16)*^{qmc135} f1 fish. (A) Shows sample of a quarter of the MCherry;Gfp positive embryos that have also shown failure of proper ISV formation and restriction of branches to mid somites. (B) A sample of the three quarters of embryos with normal ISV formation (A' and B' are higher magnification views of the boxed region in A and B. (C-D) are samples of embryos on day 3 with (C) showing a clear failure in ISV sprouting (yellow arrow) and shunting at the mid somites (blue arrow) compared to normal ISV sprouting in (D).

Interestingly, only half of embryos with lost circulation had defected ISV formation and absence of tip cells (Figure 6.5), so we wanted to know whether this phenotype was due to over-activation of Notch in these cells. To address this question, I performed single embryo genomic DNA extraction then PCR genotyping, as in the previous experiment from embryos, as summarised in Table 6.4.

Table 6.4: embryos used in single embryo genotyping.

Observed phenotype	No. of embryos used for single embryo DNA extraction and PCR genotyping
Normal ISV formation with normal circulation	10 embryos
Normal ISV with lost circulation	10 embryos
Defected ISV with lost circulation	10 embryos

6.4 PCR results showed strong correlation between endothelial Notch induction and ISV defects and loss of tip cells:

While the PCR results showed 100% n=10/10 of embryos that lack *the* transgene *uas:nicd* have proper ISV formation regardless of maintaining or absence of blood circulation, 80% n=8/10 of the embryos with defective ISV and lack of tip cells had the four transgenes; the *ubi-loxP-mCherry-s.stop-loxP-gal4-vp16; f.flk1:cre;*

f.flk1:gfp; uas:nicd (Figure 6.6, A-C'). However, the negative PCR results for two embryos shown in Figure, 6.6 C' may be due to technical problems due to incorrect sorting or PCR failure. The other possibility is that these two embryos had higher endothelial Gal4-vp16 activity, which led to earlier defects in the vascular system and prevented ISV and tip cells formation.

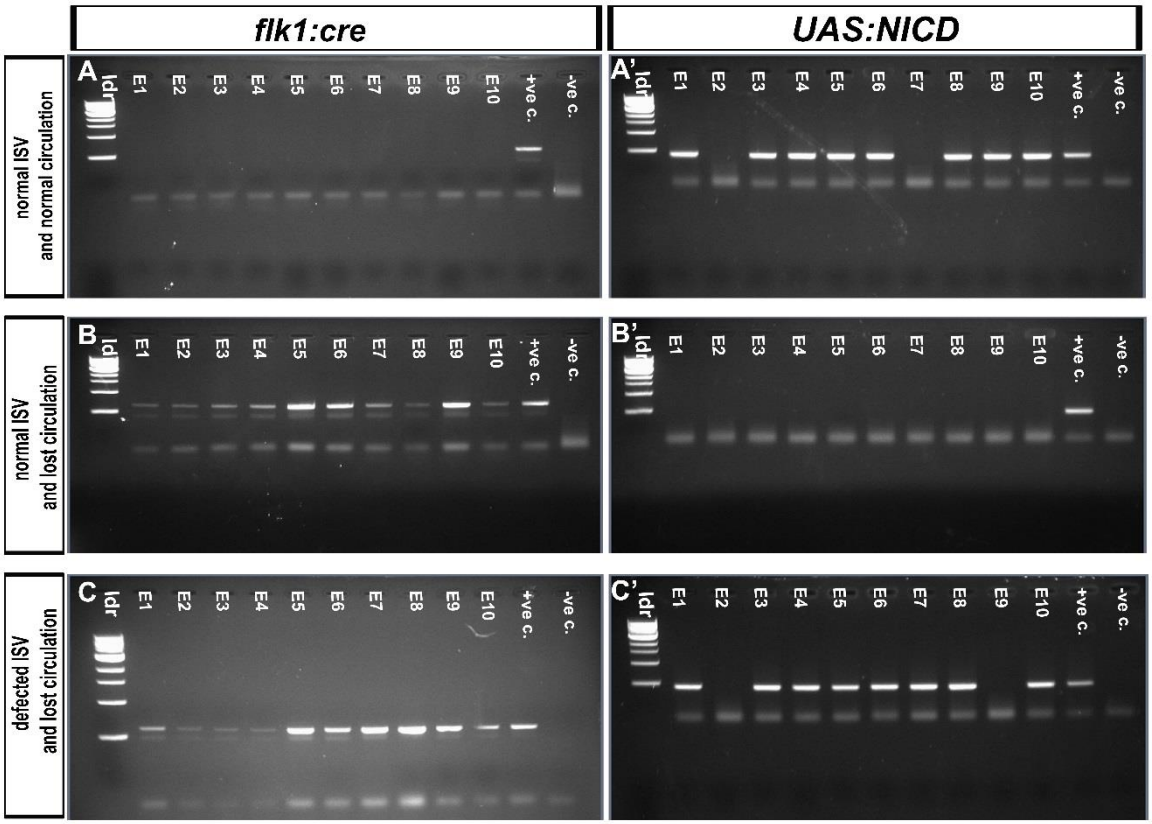

Figure 6.6 Single embryos PCR genotyping shows a strong correlation between endothelial Notch induction and defected ISV sprouting and absence of tip cells.
Two sets of primers were used (DB143 and DB144; DB162 and DB163) to detect and amplify ~600bp fragment of the *f.flk1*:*cre* transgene and ~460bp fragment of the *uas:nicd* transgene respectively. (A-A') Shows that none of the embryos with normal ISV formation and normal blood circulation 0% (0/10) carry the *f.flk1:cre Tg*, irrespective of the presence of the *uas:nicd* transgene. (B-B') Shows that 100% (10/10) embryos that lost blood circulation have the *f.flk1:cre* transgene and that loss of blood circulation does not affect ISV sprouting in absence of the *uas:nicd* transgene. (C-C') Shows that 100% (10/10) of the embryos with lost blood circulation and defected ISV sprouting have the *f.flk1:cre* and most of them 80% (8/10) also have the *uas:nicd* transgene (the first lane in all gel

images shows NEB 100bp ladder, lanes 11 and 12 are known positive and negative controls).

We then wanted to investigate whether Notch endothelial induction in these embryos lead to up-regulation of HSCs formation, so in situ hybridization was performed on embryos from the same crosses stopped and fixed at 26 hpf (Figure 6.7).

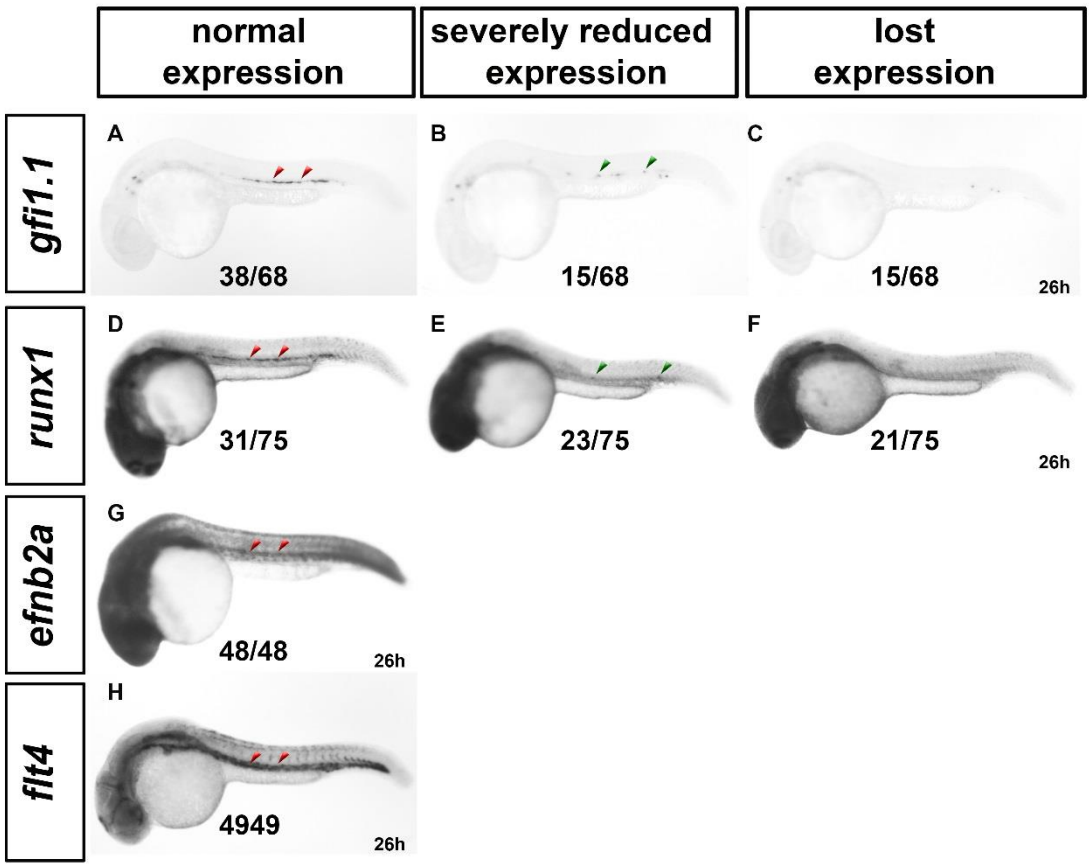

Figure 6.7 Endothelial Notch induction partially recue the loss of HSC formation caused by accumulation of Gal4-vp16 protein in the endothelium.
Whole mount in situ hybridization of *gfi1.1, runx1, efnb2a and flt4* expression at 26hpf in mCherry positive embryos resulting from crossing *Tg(ubi-loxP-mCherry-s.stop-loxP-gal4vp16)* to *Tg(f.flk1:cre; uas:nicd*) fish. (A) Red arrow heads show normal *gfi1.1* expression in the vDA compared to severely reduced expression indicated by the green arrowheads (B) or complete loss of *gfi1.1*

expression in the vDA (C). (D) Red arrow heads show normal *runx1* expression in the vDA compared to reduced expression indicated by the green arrowheads (E) or complete loss of *runx1* expression in the vDA (F). (G) Red arrow heads show normal *efnb2a* expression in the DA. (H) Red arrow heads show normal *flt4* expression in the CV.

From in situ hybridization analysis, it appears that both DA and CV were specified correctly as indicated by maintaining their normal expression of arterial and venous genes in all embryos (Figure 6.7 G-H). On the other hand, in situ hybridization data suggest that accumulation of Gal4 in the endothelial cells that we found to affect blood circulation also severely reduce HSCs markers expression as indicated by the severe reduction in *runx1* and *gfi1.1* expression (see Figure 6.7, A-F). The fact that around a quarter of these embryos have partially maintained *runx1* and *gfi1.1* (Figure 6.7, B-HE) also suggests that over-expressing Notch in the endothelium partially rescues HSCs in these embryos. However, genotyping of embryos with partial HSCs markers expression is still needed to confirm these findings.

6.5 Generating the *hsp-loxP-mCherry-pA-loxP-tgal4-vp16* construct P385

To eliminate the undesired effects of the Gal4-vp16 accumulation in the endothelium, and to add a temporal control on when to over-activate Notch in the endothelium. For this, I further modified the construct by attenuating the effect of Gal4-vp16 protein through

truncating its last 20 amino acids sequence as previously published (Davison et al., 2007, Inbal et al., 2006, Koster and Fraser, 2001, Sagasti et al., 2005, Scott et al., 2007). I then replaced the *ubi* promoter with the heat shock promoter (see Appendix 9 for cloning steps), which led to generating the *tol2* construct *hsp-loxP-mCherry-pA-loxP-tgal4-vp16* and entered it into our database under the construct name P385.

6.6 Injecting the P385 construct and establishment of *Tg(hsp-loxP-mCherry-pA-loxP-tgal4-vp16)* lines

The P385 construct co-injection with transposase and identification of potential founders to grow were all done as in previously generated lines. Screening the embryos produced from these potential founders was done after a brief heat shock of these embryos at 37ºC, then they were examined for ubiquitous expression of *mCherry*. This led to the identification of three founders with varying levels of mCherry fluorescent protein. Embryos from these three founders were given the transgenic names *qmc136, qmc137* and *qmc 138*, with *qmc136* being the lowest in *mCherry* expression and *qmc138* being the highest (Figure 6.8).

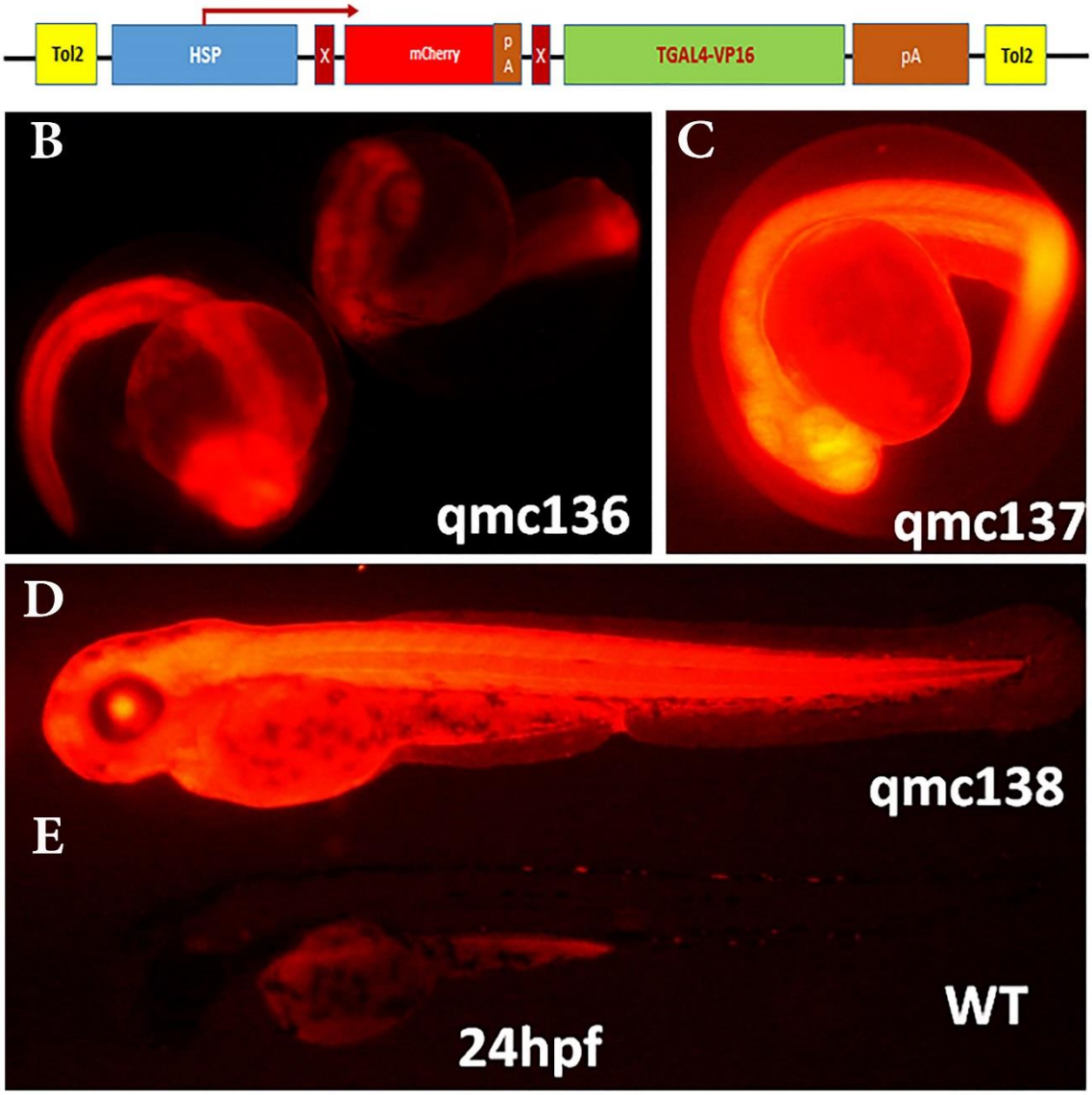

Figure 6.8 Establishment of the transgenic lines *Tg(hsp-loxP-mCherry-pA-loxP-tgal4-vp16) qmc136*, *qmc137* and *qmc138*. (A) Diagram showing the main components of the P385 construct. (B-D) Fluorescent images of live 24hpf embryos from outcrossing P385 injected fish to WT that were briefly heat shocked at 17hpf. The images show strong ubiquitous and homogenous *mCherry* expression in all tissues with *the qmc138* line being the highest in *mCherry* expression. The identified fish were given the founders names *qmc136*, *qmc137* and *qmc138* and their *mCherry* positive embryos were grown as (F1) of these lines. (D-E) Comparison between a *qmc138* transgenic embryo compared a non-transgenic sibling (E).

6.7 Endothelial Notch induction after heat shock leads to prominently high Notch activity in the endothelium

To investigate the usability of our generated *Tg(hsp-loxP-mCherry-pA-loxP-tgal4-vp16)* in over-activating Notch in the endothelium, I crossed *Tg(hsp-loxP-mCherry-pA-loxP-tgal4-vp16)*^{qmc138} to *Tg(f.flk1:cre;uas:nicd;csl:venus)*. The resulting embryos were then heat shocked, then examined by fluorescent microscopy for *venus* expression. Examining these embryos showed that with this approach, we efficiently over-activated Notch in the endothelium, indicated by up-regulation of the Venus fluorescent protein in the DA and the ISVs (Figure 6.9).

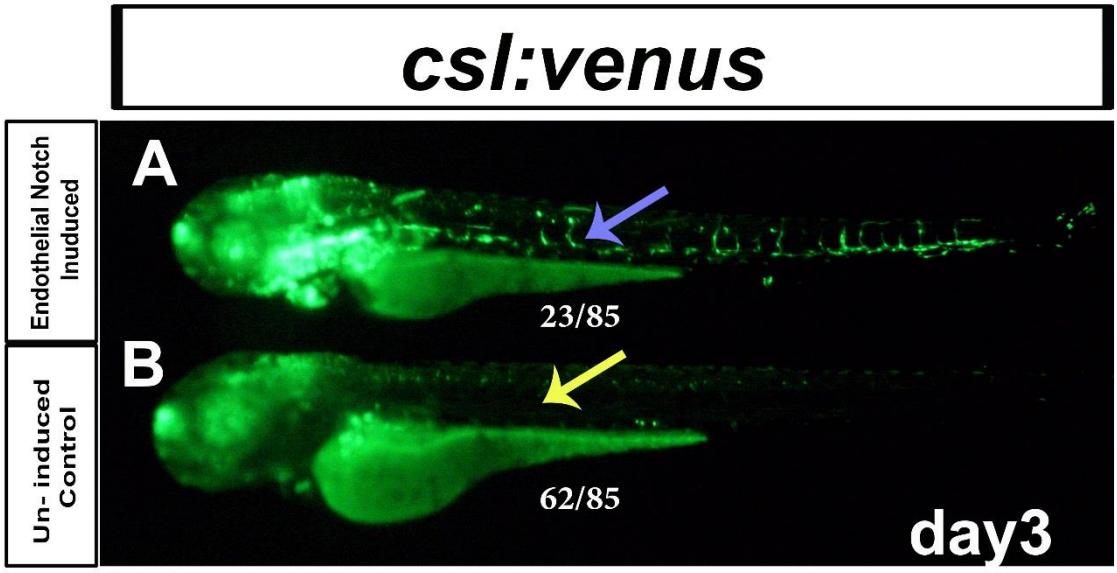

Figure 6.9 Endothelial Notch induction up-regulates expression of the Notch reporter gene specifically in the endothelium.
Fluorescent image of live 3-day-old embryos from crossing *Tg(hsp-loxP-mCherry-pA-loxP-tgal4-vp16)*^{qmc138} to *Tg(f.flk1:cre;uas:*

nicd;csl:venus) fish then heat shocking embryos at 17hpf then at 40hpf. (A) A quarter of the mCherry-Venus double positive embryos have also shown strong up-regulation of the Notch reporter gene expression in the DA and ISV (the blue arrow), compared to their un-induced counterparts (yellow arrow) in 3/4 of the embryos (B).

6.8 Notch endothelial induction moderately expands HSC markers but most cells do not leave the DA to seed the CHT.

Following fluorescent microscopy, we wanted to examine how Notch endothelial upregulation affects HSCs development. Endothelial Notch-induced embryos were stopped at 26hpf then analysed by in situ hybridization for expression of the haematopoietic markers *gfi1.1, runx1*and *c-myb*. In situ hybridization on day one showed only moderate up-regulation in the HSCs markers' expression. Interestingly, despite the normal blood circulation, it could be seen that most of the positive cells were arrested in the vDA and the mesenchyme beneath instead of seeding the CHT (Figure 6.10).

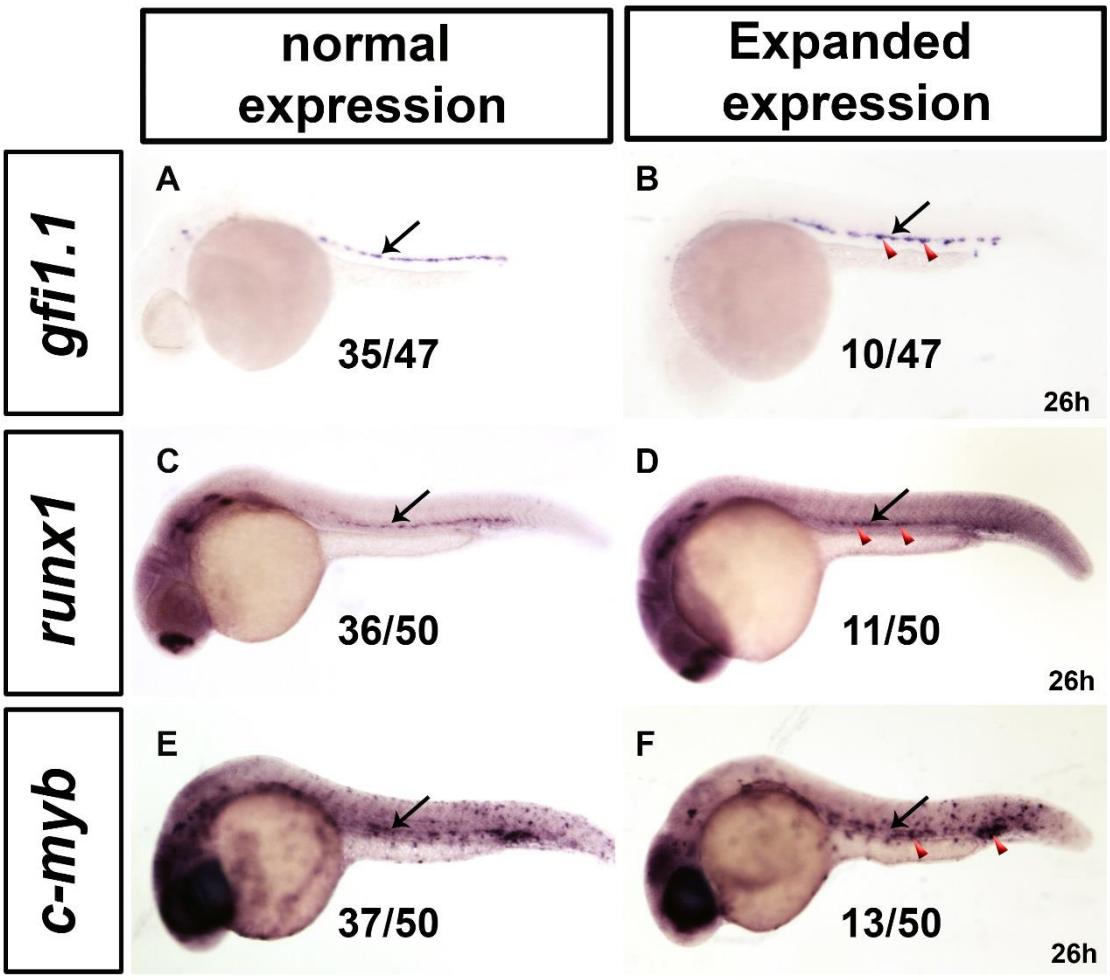

Figure 6.10 HSC specification is altered with endothelial Notch induction.
Whole mount in situ hybridization of *gfi1.1, runx1 and c-myb* expression at 26hpf in mCherry positive embryos resulting from crossing *Tg(hsp-loxP-mCherry-pA-loxP-tgal4-vp16)*^{qmc138} to *Tg(f.flk1:cre;uas:nicd;csl:venus)* fish then heat shocking their embryos at 17hpf. (A) Shows the normal *gfi1.1* expression in the vDA (black arrow) compared to (B). In addition to *gfi1.1* expression in the vDA (black arrow) also shows aggregation of *gfi1.1* expressing cells in the mesenchyme below (red arrow heads). (C) Normal expression of *runx1* in the vDA. Compared to (D), where in addition to *runx1* expression in the vDA (black arrow) also shows aggregation of *runx1* expressing cells in the mesenchyme below (red arrow heads). (E) Normal expression of *c-myb* in the vDA and CHT. Compared to (F) that in addition shows aggregation of *c-myb* expressing cells in the mesenchyme below, and the more positive cells in the CHT (red arrow heads).

Consistent with day 1 results, we also reported an expansion of the same HSC markers in the CHT and in the vDA on day 2. Interestingly, we also found that, unlike in WT that lost *gfi1.1* at this developmental stage, *gfi1.1* expression was maintained in a quarter of the transgenic embryos (Figure 6.11). Accumulation of positive cells in the vDA on day 1 and failure to downregulate *gfi1.1* by day 2 both suggest that the continuous expression of *nicd* in the endothelium arrested these cells soon after they gained the haematopoietic fate. Thus the sharp drop in Notch signalling we showed earlier in this thesis may be critical for HSCs maturation and migration to the CHT.

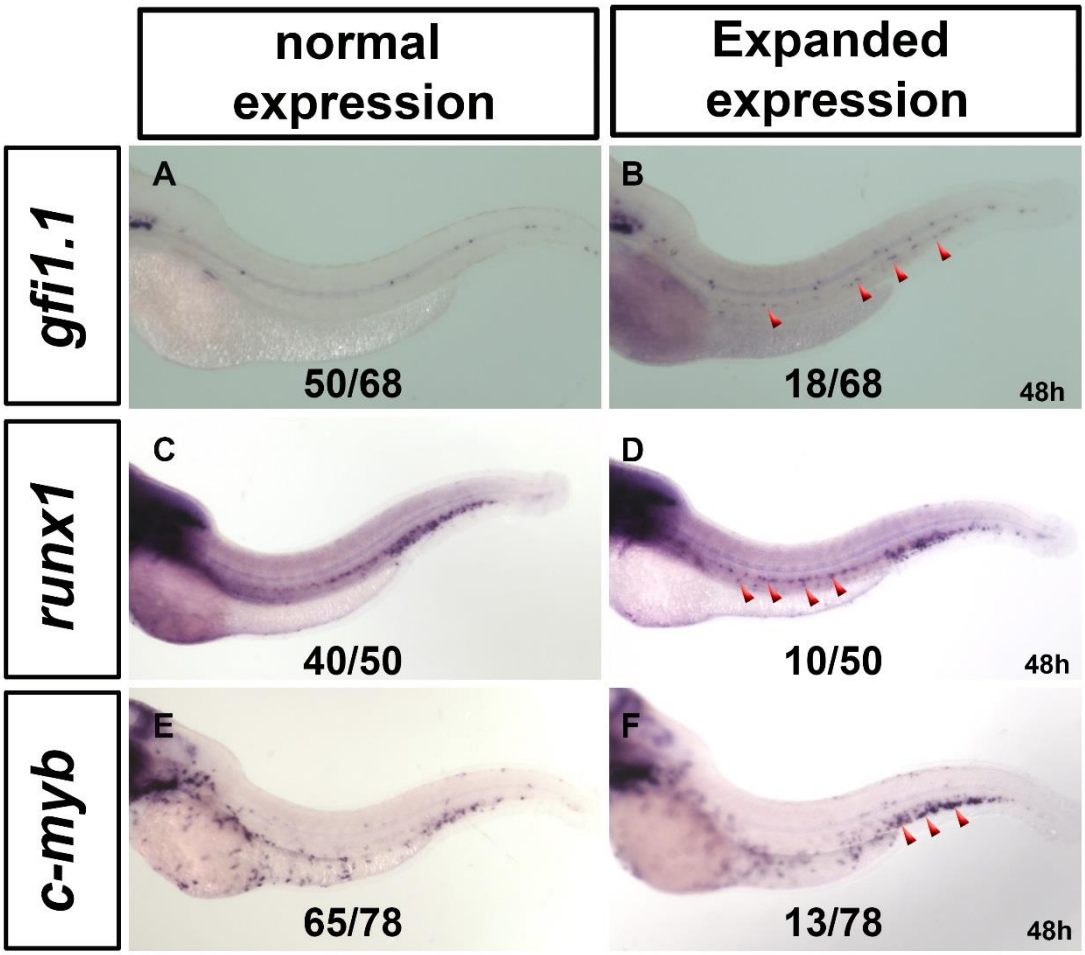

Figure 6.11: HSC expansion persists until day 2 with Notch endothelial induction.
Whole mount in situ hybridization of *gfi1.1, runx1 and c-myb* expression at 48hpf in mCherry positive embryos resulting from crossing *Tg(hsp-loxP-mCherry-pA-loxP-tgal4-vp16)*^{qmc138} to *Tg(f.flk1:cre;uas:nicd;csl:venus)* fish then heat shocking their embryos at 17hpf then at 40hpf. (A) Shows the normal down-regulation of *gfi1.1* expression in the vDA and CHT, compared to (B) that shows the persistence of *gfi1.1* expression along the vDA (red arrow heads). (C) Shows the normal expression of *runx1* in the vDA and CHT compared to (D) that in addition shows aggregation of *runx1* expressing cells in the vDA and the mesenchyme below. (E) Shows the normal expression of *c-myb* in the vDA and CHT. Compared to (F) that in addition shows aggregation of *c-myb* expressing cells in the vDA and mesenchyme below and more positive cells in the CHT (red arrow heads).

Next, we wanted to know if endothelial to haematopoietic transition is restricted to the developmental window between 28-48hpf as previously proposed by Bertrand et al. (2007). For this, I repeated the experiment but with late endothelial Notch induction. Therefore, in this experiment I heat shocked the embryos 40hpf then stopped and fixed them at 48h for in situ hybridization. In agreement with proposed developmental window for endothelial to haematopoietic transition, we also found that late endothelial Notch induction has no substantial effect on HSC formation (see Figure 6.12), thus giving direct evidence on restricting the effect of Notch induction on endothelial to haematopoietic transition to a confined developmental window.

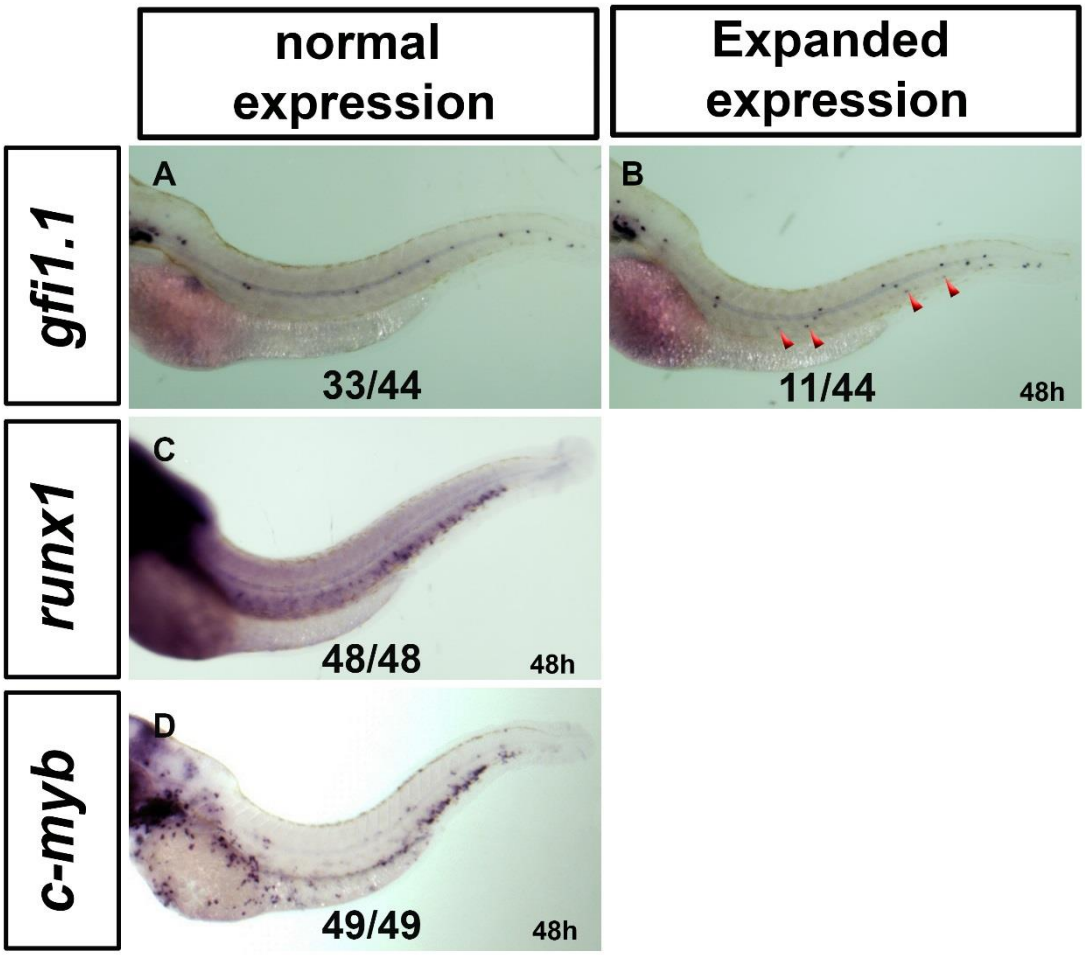

Figure 6.12 Late endothelial induction does not expand HSC. Whole mount in situ hybridization of *gfi1.1, runx1 and c-myb* expression at 48hpf in mCherry positive embryos resulting from crossing *Tg(hsp-loxP-mCherry-pA-loxP-tgal4-vp16)*^{qmc138} to *Tg(f.flk1:cre;uas:nicd;csl:venus)* fish then heat shocking their embryos at 40hpf. (A) Shows the normal down-regulation of *gfi1.1* expression in the vDA and CHT compared to (B) that shows only a few cells with *gfi1.1* expression along the vDA and CHT (red arrow heads). (C) Shows the normal expression of *runx1* in the vDA and CHT in all examined embryos. (D) Shows the normal expression of *c-myb* in the vDA and CHT in all examined embryos.

From our previous work in the lab we noticed that transgenic fish with the minimal *flk1* promoter *m.flk1* only start expressing the downstream genes after 18 somites (Drew, 2010), compared to 12-

14 somites in transgenic with the *f.flk1* promoter (Bertrand et al., 2010a). To investigate how the delay in recombination affect HSCs formation and if the recombination the m.*flk1* promoter driven Notch induction is sufficient to expand HSC, I generated double transgenic fish *Tg(m.flk1:cre;uas:nicd)*. I then crossed these double transgenic fish to *Tg(hsp-loxP-mCherry-pA-loxP-tgal4-vp16)*^{qmc138} then heat shocked one batch of their embryos at 17hpf and the other at 40hpf. The embryos were then stopped at 48hpf and fixed for in situ. In line with earlier data, *m.flk1:cre* mediated recombination and Notch induction showed more *gfi1.1* expressing cells in the vDA and the mesenchyme with early heat shock (Figure 6.13 A-B) and far less positive cells with late induction (Figure 6.13, C-D).

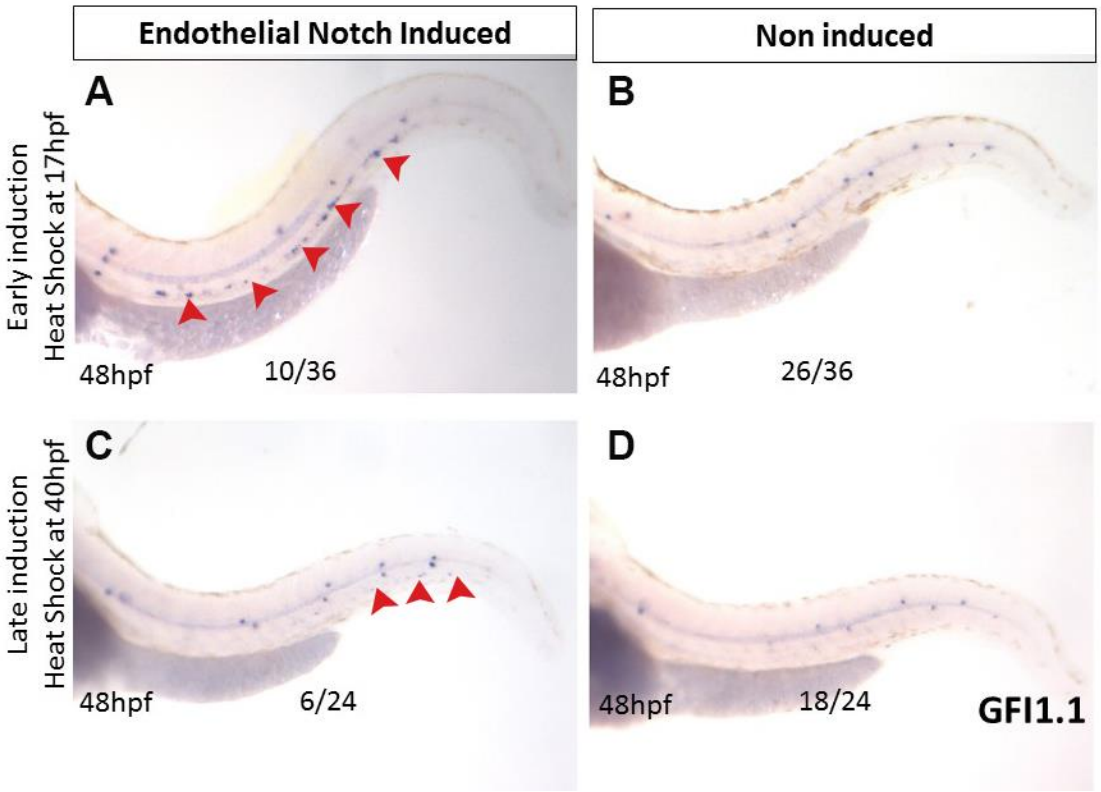

Figure 6.13 Early endothelial Notch induction with *m.flk1:cre* promotes HSCs self-renewal while late induction does not.
Whole mount in situ hybridization of *gfi1.1* at 48hpf in mCherry positive embryos resulting from crossing *Tg(hsp-loxP-mCherry-pA-loxP-tgal4-vp16)*^{qmc138} to *Tg(m.flk1:cre;uas:nicd;csl:venus)* fish then heat shocking their embryos either at 17hpf (A-B) or at 40hpf (C-D). (A) Shows persistent of *gfi1.1* expression along the vDA (red arrow heads) compared to (B) that shows the normal down-regulation of *gfi1.1* expression in the vDA and CHT. (C) Shows a very low *gfi1.1* expression in the vDA in late heat shocked embryos compared to (D) that shows the normal down-regulation of *gfi1.1* expression in the vDA and CHT at this time point.

Even though with this strategy we demonstrated that endothelial specific Notch induction is sufficient to expand HSC markers in the CHT. Yet, the fact that *gfi1.1* was maintained in the DA even on day 2 further indicates that Notch induction might only be needed transiently, then get switched off. This hypothesis is also supported by our observation of a sharp fall in Notch expression in WT DA on day 2. To enable transient endothelial specific Notch induction, I decided to generate constructs that enable expression of *nicd* downstream of *m.flk1* promoter transiently before they get diluted and finally degraded by the raped cellular division and the cellular nucleases.

6.9 Generation and injection of the *tol2-m.flk1:nicd-gfp* construct P405.

To enable assembly of the *tol2-m.flk1:nicd-gfp* components into one construct, I utilised the Gibson assembly approach (Gibson et al.,

2009). In this process, I firstly fused the *nicd* gene after exclusion of its stop codon in-frame with the *gfp* gene then ligated these fused genes downstream of the 2.3kb *flk1* minimal promoter *m.flk1*. To facilitate construct integration to host DNA and consequently increase the construct half-life, and so increase expression efficiency, *tol2* backbone plasmids were used in generating the final construct P405 (as shown in Appendix 10). I then co-injected the P405 plasmid with Transposase to one cell stage embryos resulting from in-crossing the *Tg(csl:mCherry)*^{qmc97} Notch reporter fish. Embryos were then then analysed under fluorescent microscope for Gfp fluorescent protein and also for up-regulation of the Notch reporter protein mCherry in the endothelium. Examining injected embryos at 24hpf showed a strong endothelial specific expression of *the gfp* fused to the *nicd* (Figure 6.14, A-B), thus indicating the level of Nicd protein produced in these tissues. I then examined these embryos for up-regulation of the Notch reporter protein mCherry in the endothelium in response to *nicd* expression. Consistent with expression of the fused *nicd-gfp* there was also a strong up-regulation in *mCherry* expression along the DA in most injected embryos (Figure 6.14, A'-B'). We also noticed a slight variation of mCherry expression, which is normal with ejection efficiency, but importantly, the level of *mCherry* in all examined embryos corresponded to *the level of gfp* expression. The co-localization of Gfp and MCherry further confirmed the correlation

between the up-regulation in Notch reporter and endothelial Notch induction by the injected construct (Figure 6.14, A''-B'').

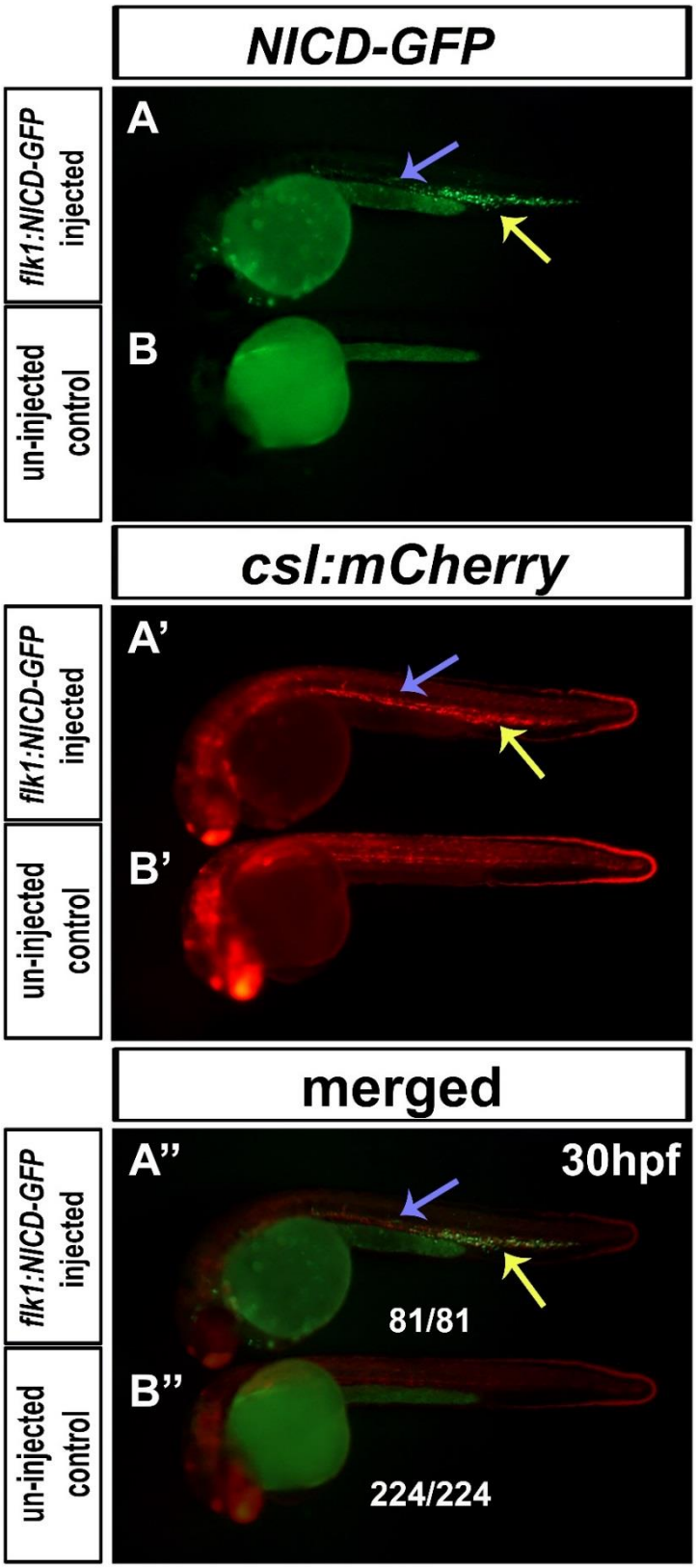

Figure 6.14 Transient endothelial Notch induction after injecting the *tol2-m.flk1:nicd-gfp* construct P405 up-regulates Notch reporter fluorescent protein in Notch reporter embryos.
Fluorescent images of live 30hpf Notch reporter *Tg(csl:mCherry)*^{qmc97} embryos co-injected with the *tol2-m.flk1:nicd-gfp* plasmid P405 compared to their uninjected siblings. (A) Shows expression of the *gfp* fused in-frame with the *nicd* specifically in the endothelial tissues including the DA (the blue arrow) and the ICM (yellow arrow) under the *m.flk1* promoter, compared to complete absence of *gfp* expression in their uninjected siblings (B). (A') Shows an endothelial specific up-regulation of the Notch reporter fluorescent protein mCherry in injected embryos including the DA (blue arrow) and ICM (yellow arrow), compared to their uninjected siblings (B'). (A'') merged image of same embryos showing co-localization of *gfp* expression and *mCherry* up-regulation in injected embryos DA (blue arrow) and ICM (yellow arrow) compared to uninjected siblings.

Interestingly, we observed a great reduction in *gfp* expression by 48hpf (Figure 6.15) and complete loss of Gfp fluorescent protein by day 3. A possible explanation for this sharp down regulation of Gfp is the dilution of the injected construct due to the rapid cell division adding to the degradation of un-integrated DNA by the cellular machinery. On the other hand, we noticed that Notch reporter gene expression peaked on day 2, which is a day after Gfp (Figure 6.15). This delay may reflect the time needed for the Nicd-Gfp fusion protein to bind the *csl* binding sequence in the Notch reporter transgene and activation of *mCherry* expression, and the time required to convert produced mRNA into mature and detectable mCherry protein.

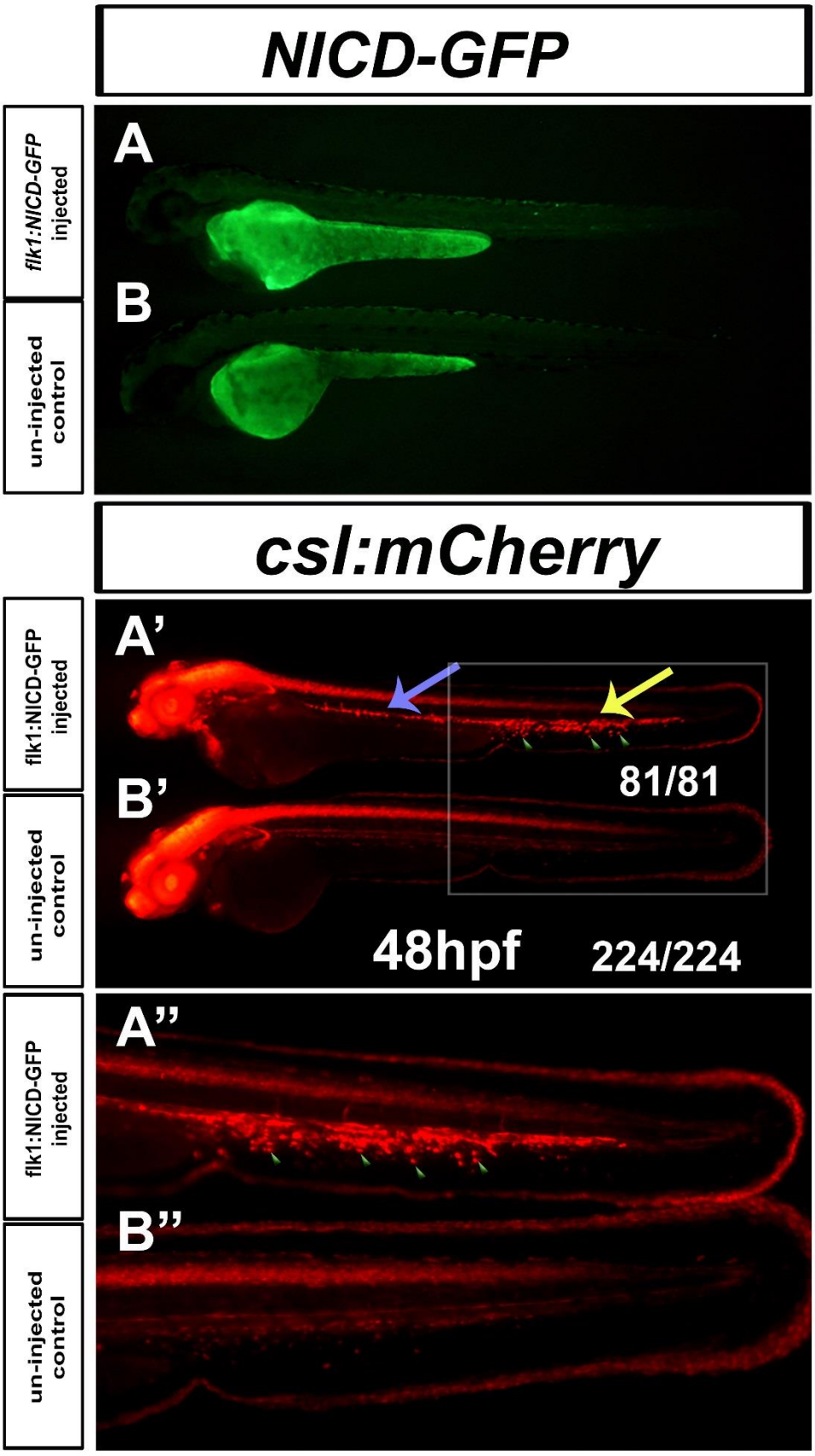
NICD-GFP
flk1:NICD-GFP injected
un-injected control
A
B
csl:mCherry
flk1:NICD-GFP injected
un-injected control
A'
B'
81/81
48hpf
224/224
flk1:NICD-GFP injected
un-injected control
A''
B''

Figure 6.15 Transient endothelial Notch induction after injecting the *tol2-m.flk1:nicd-gfp* plasmid P405 expand Notch reporter expression in CHT.
Fluorescent images of live 48hpf Notch reporter *Tg(csl:mCherry)*^{qmc97} embryos co-injected with the *tol2-m.flk1:nicd-gfp* plasmid P405 compared to their uninjected siblings. (A-B) Show a sharp decline in Notch induction by day2, reflected by loss of Gfp in injected embryos. (A') Shows a very high endothelial specific up-regulation of the Notch reporter fluorescent protein mCherry in injected embryos both in the DA (blue arrow) and the CHT(yellow arrow), compared to their uninjected siblings (B'). Boxed area in (A'-B') is magnified in (A''-B'') which shows high *mCherry* expressing round cells in the CHT (green arrow heads) that resemble the shape and location of the HSC.

In addition, blood circulation was maintained in the majority of injected embryos (71/78), and even the loss of blood circulation in (7/78) was likely due to injection complications rather than the Nicd protein up-regulation. To investigate whether this endothelial Notch induction was sufficient to expand the HSCs in the DA and the CHT, I stopped these embryos at 48hpf and performed in situ hybridization on them for the HSCs markers *runx1* and c-myb. In situ hybridization results revealed that expression of the HSCs markers *runx1* and c-myb were dramatically increased with this transient endothelial Notch induction, and the result showed seemingly intact HSCs differentiation in which more cells were able differentiate and leave the DA to seed the CHT (Figure 6.16).

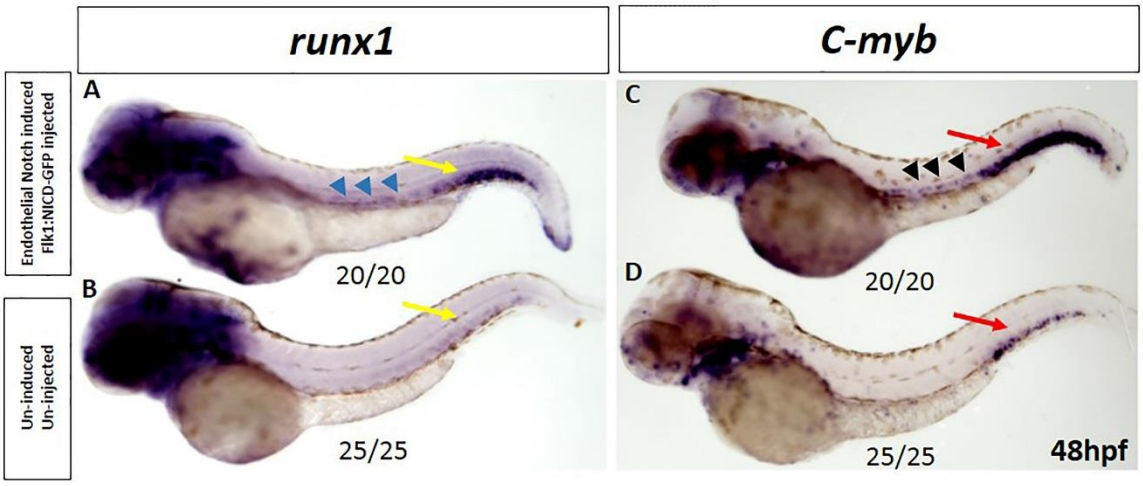

Figure 6.16 Transient endothelial Notch induction in *tol2-m.flk1:nicd-gfp* injected embryos expand expression of the haematopoietic markers *runx1* and *c-myb*.
Whole mount in situ hybridization showing expression of *runx1 and c-myb* at 48hpf in *tol2-m.flk1:nicd-gfp* injected embryos (A and C) compared to their uninjected siblings (B and D). (A) Shows dramatic expansion in *runx1* expression in both the DA (blue arrow heads) and the CHT (the yellow arrows) compared to their uninjected siblings (B), which only showed low *runx1* expression in the CHT (yellow arrows). (C) Shows dramatic expansion in *c-myb* expression in both the DA (black arrow heads) and the CHT (red arrows) compared to their uninjected siblings (D), that only showed *c-myb* expression in the CHT (red arrows).

6.10 Generation and injection of the *tol2-fli1:nicd-gfp* construct P409.

Even though *flk1* promoter is highly active in haemogenic endothelial progenitors, its activity is greatly down regulated in the AGM endothelial cells fated to become HSC (North et al., 2002). This down regulation occurs through the direct suppression of the *flk1* promoter by the HSC transcription factor *runx1*, which becomes active in these cells (Hirai et al., 2005). To overcome this suppression, and to investigate the role of Notch induction in these *runx1* positive cells

and whether maintaining Notch signalling in HSCs will further expand this population, we replaced the *flk1* promoter with *fli1* promoter in the tol2 backbone plasmid.

Plasmid construction was done by the Gibson assembly method, in which I firstly amplified the *fli1* promoter with a 5' overlap to the *tol2* backbone plasmid and 3' overlap to *nicd-gfp* fusion. I then amplified the *nicd-gfp* fusion gene with a 5' overlap to fli1 promoter and 3' overlap to the *tol2* backbone, and finally all fragments were assembled in one plasmid with the Gibson approach (see Appendix 11). The final construct *tol2-fli1:nicd-gfp* was then entered in the database as P409.

I then co-injected the construct P409 with transposase into *Tg(csl:mCherry)*^{qmc97} embryos, as in the previous experiment. Injected embryos were then analysed under fluorescent microscope for Gfp in the endothelium as an indicator of the fused Nicd and for up-regulation of the Notch reporter fluorescent protein mCherry in the endothelium. Examining these injected embryos revealed that the fused *gfp* expression fell dramatically on day 2, whereas expression of the reporter gene mCherry peaked at this period. These findings further confirmed the data generated by injecting the *tol2-m.flk1:nicd-gfp* plasmid, and suggested that both approaches led to generally similar outcomes (Figure 6.17). Interestingly, with we noticed enlargement and pocket formation in in the vessels forming the CHT in a quarter of *tol2-fli1:nicd-gfp* injected embryos, this

phenotype may have been caused by prolonged activation of the Notch pathway in the endothelial cells (Figure 6.18).

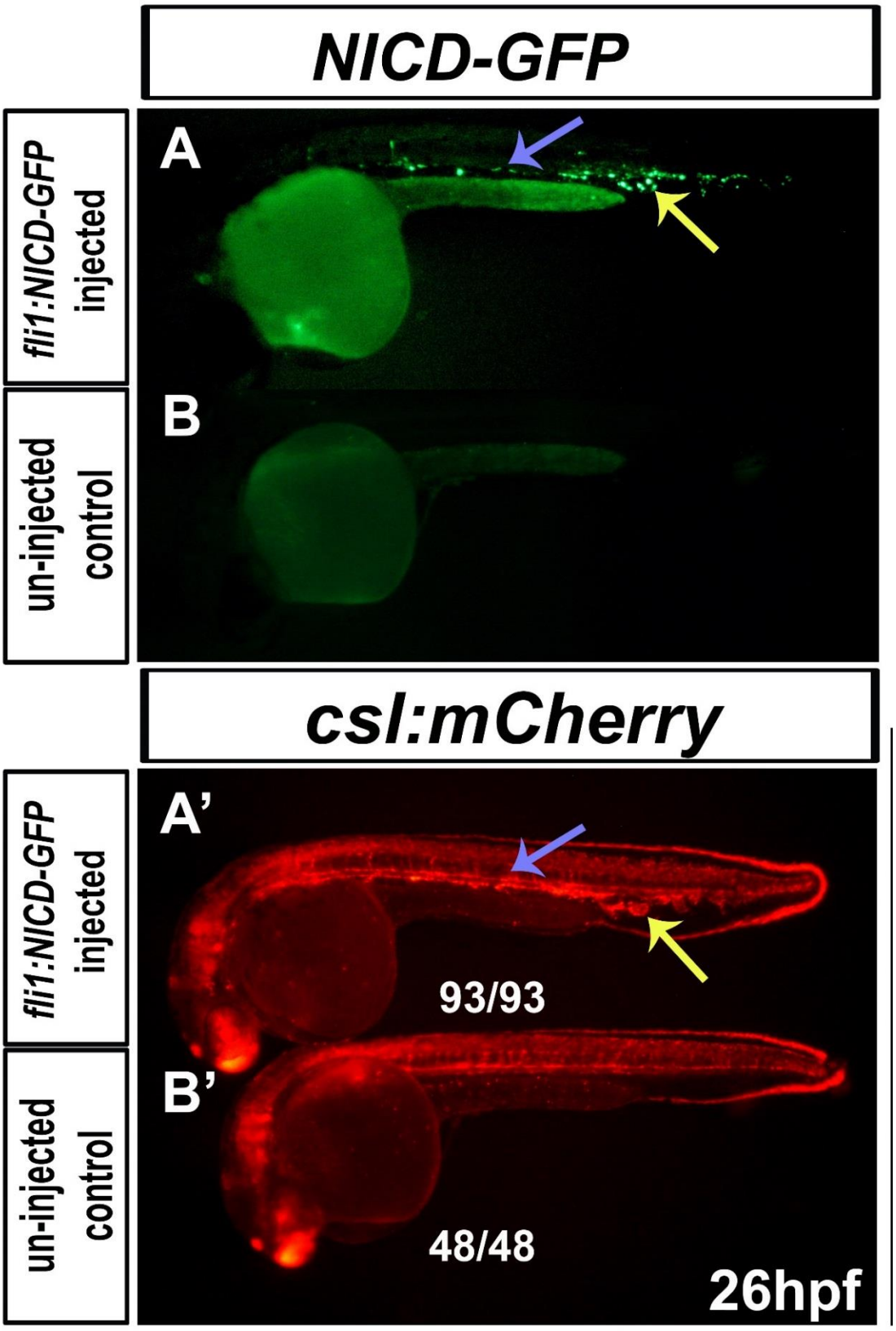

Figure 6.17 Transient endothelial Notch induction in *tol2-fli1:nicd-gfp* injected embryos up-regulates Notch reporter fluorescent protein.

Fluorescent microscopy images of live 26hpf Notch reporter *Tg(csl:mCherry)* embryos co-injected with the *tol2-fli:nicd-gfp* plasmid P409 compared to their uninjected siblings. (A) Shows expression of the Gfp protein fused in-frame with the *nicd* specifically in the endothelial tissues. This includes the DA (the blue arrow) and the CHT (yellow arrow), under the *fli1* promoter compared to complete absence of Gfp in their uninjected siblings (B). (A') Shows an endothelial specific up-regulation of the Notch reporter fluorescent protein mCherry in injected embryos including the DA (blue arrow) and CHT (yellow arrow), compared to their uninjected siblings (B').

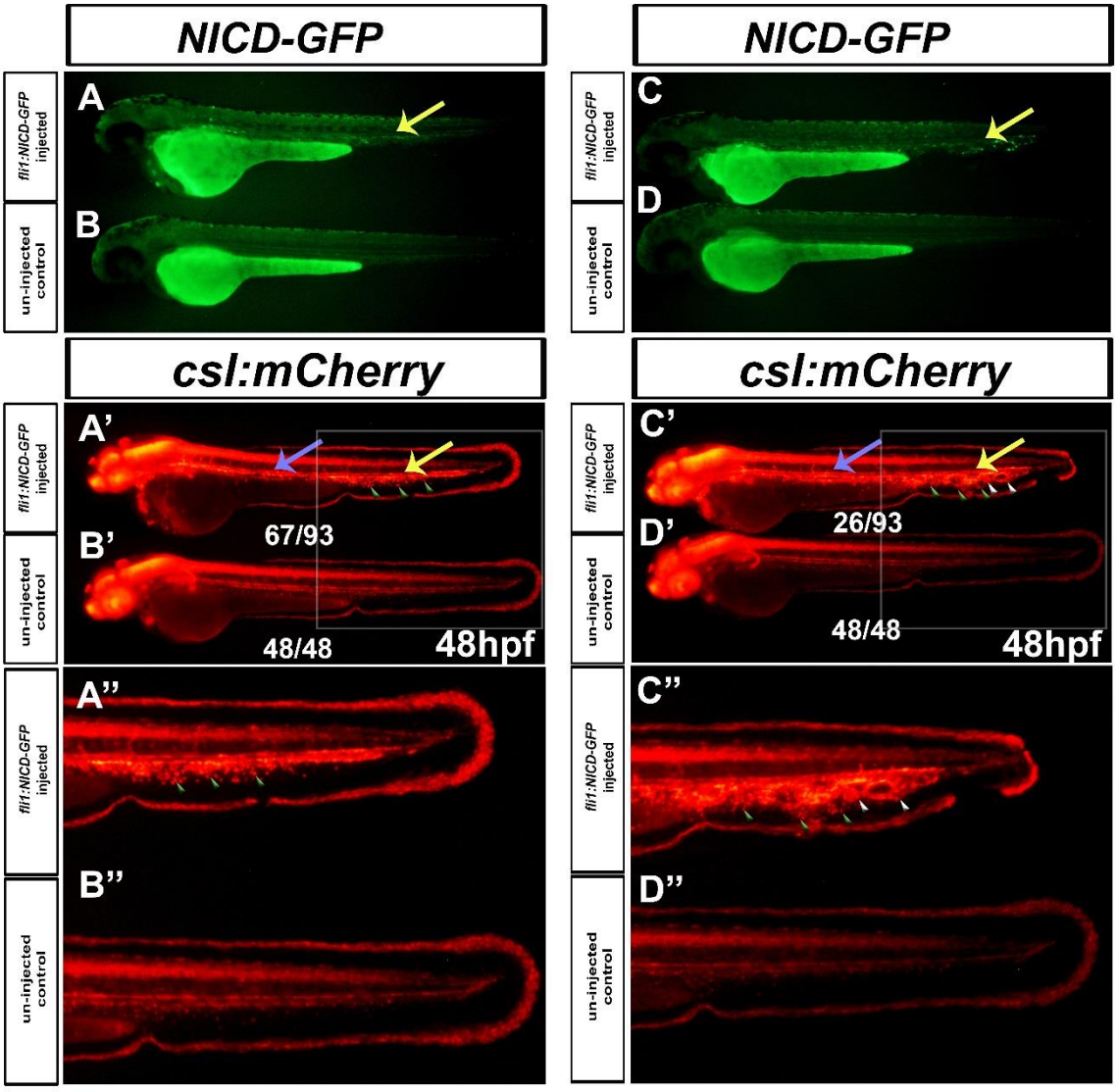

Figure 6.18 Transient endothelial Notch induction by injecting the *tol2-fli1:nicd-gfp* plasmid P409 expand HSCs in the DA and CHT.

Fluorescent images of live Notch reporter *Tg(csl:mCherry)* embryos co-injected with the *tol2-fli1:nicd-gfp* plasmid P409 were compared to their uninjected siblings at 48hpf. (A-B) Show a decline in Notch induction by day2, reflected by down regulation of the Gfp in injected embryos. (A') Shows a high endothelial specific up-regulation of the Notch reporter fluorescent protein,mCherry in injected embryos in the DA (blue arrow) and also in the CHT (yellow arrow) compared to their uninjected siblings (B'). The boxed area in (A'-B') is magnified in (A''-B'') and shows high *mCherry* expressing round cells in the CHT (green arrow heads) that resemble the shape and location of the HSC. (C-D) Show an example of about 1/3 of injected embryos in which Gfp persisted in day2 compared to uninjected siblings. (C') Shows high endothelial specific up-regulation of the Notch reporter fluorescent protein mCherry in injected embryos in both axial vessels DA and CV (blue arrow) and also in the CHT (yellow arrow). There was also notable enlargement of blood vessels and pocket formation in the CHT (white arrow heads). The boxed area in (C'-D') is magnified in (C''-D''), showing high *mCherry* expressing round cells in the CHT (green arrow heads) that resemble the shape and location of the HSC, added to the enlarged and deformed vessels (white arrows heads).

6.11 Discussion of results

This chapter explained that combining the Cre/LoxP system and the Gal4/Uas system remarkably amplified the amount of produced Nicd protein in the endothelium, evidenced by the significant up-regulation in Notch reporter fluorescent protein produced in these cells. It also revealed that high Notch signal in the DA inhibits endothelial cells migration in response to the Vegf signal to form the ISVs, and instead remain in the DA as previously described (Siekmann and Lawson, 2007).

Undesirably, we noticed that accumulation of the Gal4-vp16 protein in transgenes with the full length Gal4-vp16 interfered with the maturation of blood vessels, leading to loss of blood circulation. In situ hybridization results also suggest that this accumulated Gal4-vp16 protein also interferes with HSCs specification from the vDA endothelium, and that this defect can be partially rescued by endothelial specific Notch over-activation. To minimize the toxic effect of the Gal4-vp16, we generated transgenic fish with attenuated Gal4-vp16, in which we truncated the last 20 amino acids (Davison et al., 2007, Inbal et al., 2006, Koster and Fraser, 2001, Sagasti et al., 2005, Scott et al., 2007). We also replaced the ubi promoter in this transgene with the hsp promoter to add a control on when to over-activate Notch signalling in the endothelium. With this approach, we presented data suggesting that continuous endothelial expression

of nicd, and thus continuous up-regulation of Notch pathway in the endothelium only slightly expands HSCs that can migrate to seed the CHT.

In situ hybridization analysis also showed that most HSC specified cells in these embryos remain in the DA and fail to down-regulate the early HSCs marker gfi1.1, which suggests that after HSCs specification the marker must be down-regulated to allow specified cells to mature and leave the vDA. To test this hypothesis, we over-activated Notch pathway transiently in the endothelium, and reported remarkable expansion in the haematopoietic markers runx1 and c-myb, both in the DA and also in the CHT. Utilizing the fli1 promoter instead of flk1 promoter for endothelial Notch induction showed similar up-regulation in Notch reporter fluorescent protein in the DA and CHT, but with the presence of some defective blood vessels in some of injected embryos that may be resulting from earlier expression of the nicd-gfp in the injected construct.

Expansion of the round Notch reporter positive cells in the CHT in these embryos also suggested similar HSCs expansion with the use of fli1 promoter as with the flk1 promoter. Together, these findings show that transient endothelial specific Notch over-activation is sufficient to expand HSCs formation both in the DA and the CHT. In this model we showed that while high Notch endothelial signal is required for HSCs specification from the vDA endothelium, the low

Notch signal after specification is essential for their differentiation into mature HSCs that can leave the DA and seed the CHT.

CHAPTER 7

7 Results V Both Tet1 and Tet3 enzymes are essential for organogenesis in zebrafish

In zebrafish, we have previously shown existence of three *tet* genes as in mammals (Almeida et al., 2012). The enzymes produced by these genes are also identical to their mammalian counterparts, with the only exception that Tet3 lacks its dioxygenase domain. To understand the regulatory roles for the Tet enzymes in embryogenic development, we decided to block expression of the three *tet* genes individually or in combination with morpholinos and study the effects resulting from losing these genes on embryogenic development. Utilising our in-house Notch reporter line, we also intended to determine the role of Tet enzymes on the development of Notch-active tissues such as the nervous and cardiovascular systems.

7.1 Zebrafish *tet* genes morpholinos design and injection

To precisely target the catalytic C-terminal dioxygenase domain in the three *tet* genes, we designed morpholinos that target the splice junctions of exons preceding the dioxygenase domain exons in the three *tet* genes (Figure 7.1, A-L). Removal of targeted exons was predicted to lead to frame shifts and pre-mature termination of the proteins, and so deletion of the dioxygenase domains in the three *tet*

genes (Figure 7.1, C-D, G-F, K-L). Morpholinos sequence design was performed by Dr. Martin Gering and Dr. Alexey Ruzov, and then verified and synthesized by Gene Tools (see Figure 7.1 and Table 7.1 for morpholinos design and targeted exons).

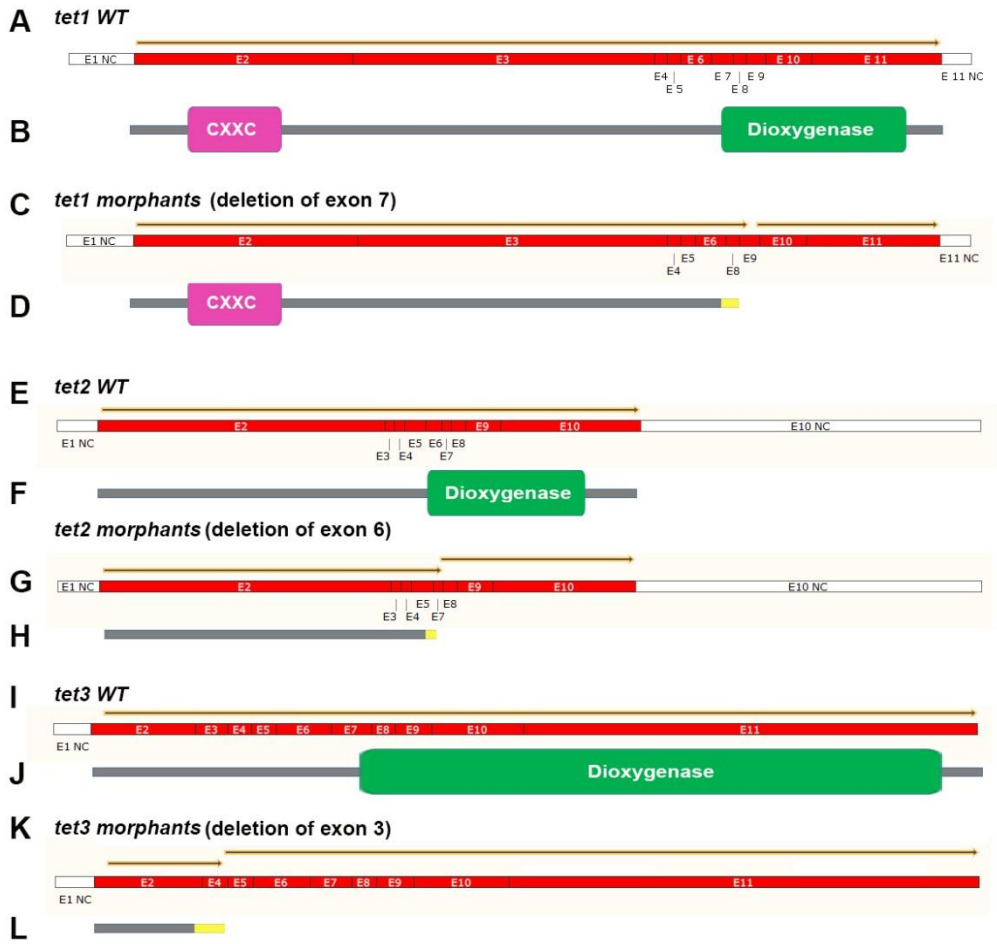

Figure 7.1 *tet* morpholinos designed to delete the dioxygenase domains sequences in the *tet* genes.
(A-L) Schematic diagrams of zebrafish *tet1, tet2* and *tet3* cDNA and their proteins in WT embryos, compared to predicted *tet* genes in the morphants. The white boxes in (A, C, E,G,I,K) are the non-coding exons, while red boxes are the coding exons. Orange arrows show the open reading frames that are intact in WT, and prematurely terminated in the morphants. (B, D, F, H, J, L) Are the Tet protein domains in WT and *tet* morphants, showing the main functional domains and the dioxygenase domains in all WT Tet proteins (green boxes) and its loss in all their *tet* morphants counterparts. The pink boxes are for the CXXC domains that present in *tet1* WT as well as

tet1 morphants. The grey lines indicate the WT amino acids, while the yellow lines indicate the frame shift and protein termination resulting from splicing to next exons. The cDNA schematics were produced with SnapGene software (from GSL Biotech; available at snapgene.com). The t*et* genes sequences were from ENSEMBL versions (*dtet1*, ENSDARG00000075230.4), (*dtet2*, ENSDARG00000076928.6), (*dtet3*, ENSDARG00000062646.6).

Table 7.1: List of *tet* morpholinos used.

Mo name	**sequence**	**Target**	**Reference sequence**
tet1 E7 ac	5′-TTCTTCATCTCTCCTGTTAGTCGTA-3′	*tet1* exon 7 splice acceptor	ENSDARG00000075230
tet1 E7 do	5′-CCATCCAATGCTCACCTCCTTAGGA-3′	*tet1* exon 7 splice donor	
tet2 E5 ac	5′-TTCTCCTAAGGACAGTGATCGAAAT-3	*tet2* exon 5 splice acceptor	ENSDARG00000076928
tet2 E5 do	5′-TTTGTGTGAGCATCTCACCTCCTT-3′	*tet2* exon 5 splice donor	
tet3 E3 ac	5′-AAGGTGAGGAGGGAAAGATATCCTT-3′	*tet3* exon 3 splice acceptor	ENSDARG00000062646
*tet*3 E3 do	5′-TTGTATTATCTCACTTACCTACGCA-3′	*tet3* exon 3 splice donor	

The morpholinos were then co-injected (0.5 ng of each) into WT embryos at two cells stage and observed for phenotypes (these preliminary injections were performed by a former student in our lab Sabrina Boudon). When examined under bright field microscopy at early development (8hpf), injected embryos appeared identical to their uninjected siblings (Figure 7.2 A). However, soon after initiation of somitogenesis, injected embryos showed a clear arrest in development and failure in organogenesis that resulted in death before 24hpf. Interestingly, the observed developmental arrest

coincided with the time point at which *tet1*/2/3 expression become detectable in the embryo (Almeida et al., 2012).

We then wanted to study the effect of knocking down individual *tet* genes, so we injected WT embryos with *tet1, tet2* and *tet3* morpholino pairs separately, and then examined injected embryos both at early somitogenesis, and at 24hpf. Our analysis of injected embryos showed a significant developmental arrest in embryos injected individually with *tet1* and those injected individually with the *tet3* morpholinos, 25% and 80% respectively. The remaining 75% and 20%, that appeared normal at early somitogenesis, also developed specific developmental abnormalities when examined at 24hpf. By comparing the severity of the observed phenotypes, we found that *tet3* morphants developed generally more severe phenotypes compared to those of *tet1* morphants (Figure, 7.2 B). The observed abnormalities in *tet1* morphants included reduced and malformed head structures, abnormally developed eyes, considerably shortened and curved bodies. This is added to missing pigmentation and formation of anomalous U-shaped (instead of chevron-shaped) somites in most injected embryos (65%). The head and posterior structures were also poorly formed in the remaining 10% of *tet1* morphants. On the other hand, the 20% surviving *tet3* morphants showed very severe failure in organogenesis and did not develop any anterior or posterior structures, and they also failed to form the regular patterning of the somites (Figure 7.3, A-D).

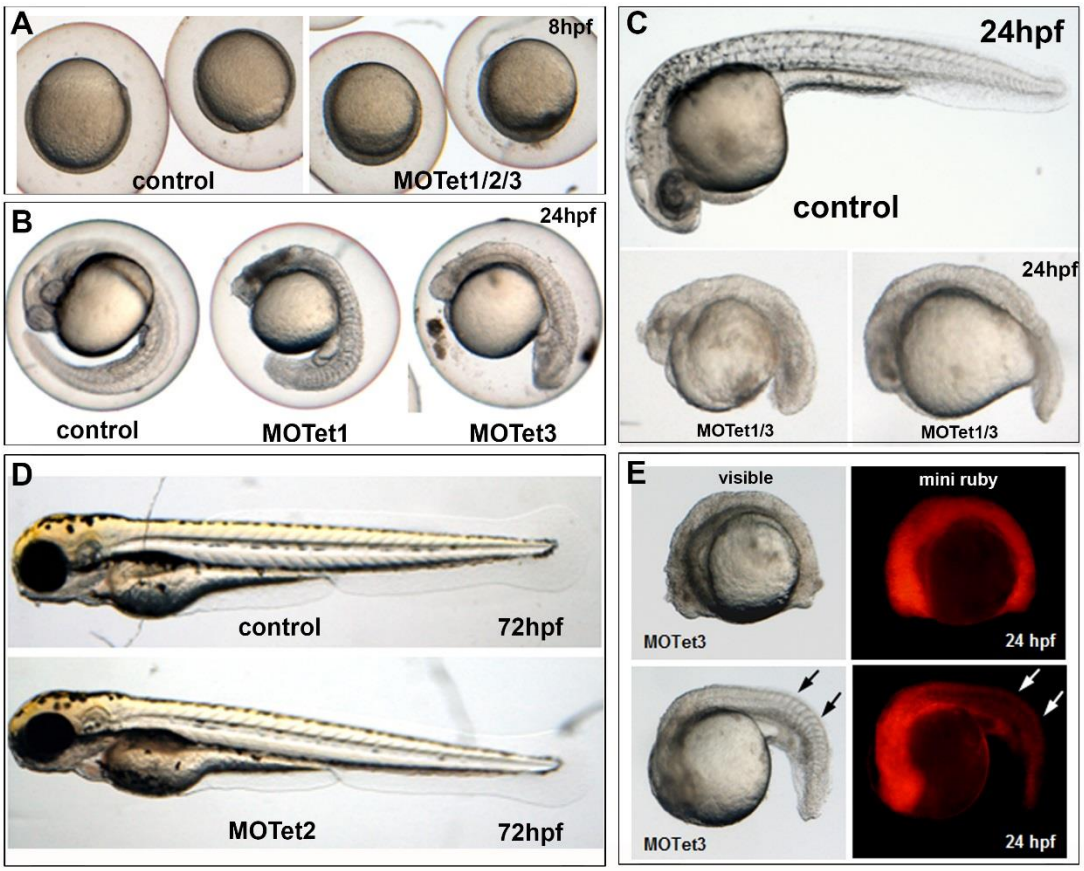

Figure 7.2 Tet1 and Tet3 but not Tet2 are essential for zebrafish organogenesis.
(A-E) Bright field microscopy of *tet* morphants compared to their uninjected controls. (A) Embryos co-injected with *tet1*/2/3 morpholinos appear normal and un-distinguishable from their uninjected controls at 8hpf. (B) Both *tet1* and *tet3* morphants showed generally similar phenotypes at 24hpf compared to their uninjected controls. (C) Co-injection of *tet1/3* morpholinos lead to more severe phenotypes at 24hpf than with individual knockdown of individual genes. (D) *tet2* morphants appeared normal and un-distinguishable from their uninjected controls, event when examined at 72hpf. (E) Including the tracking dye (mini Ruby) in the *tet3* morpholinos injection mix indicates that the phenotype severity correlates with the injected amounts.

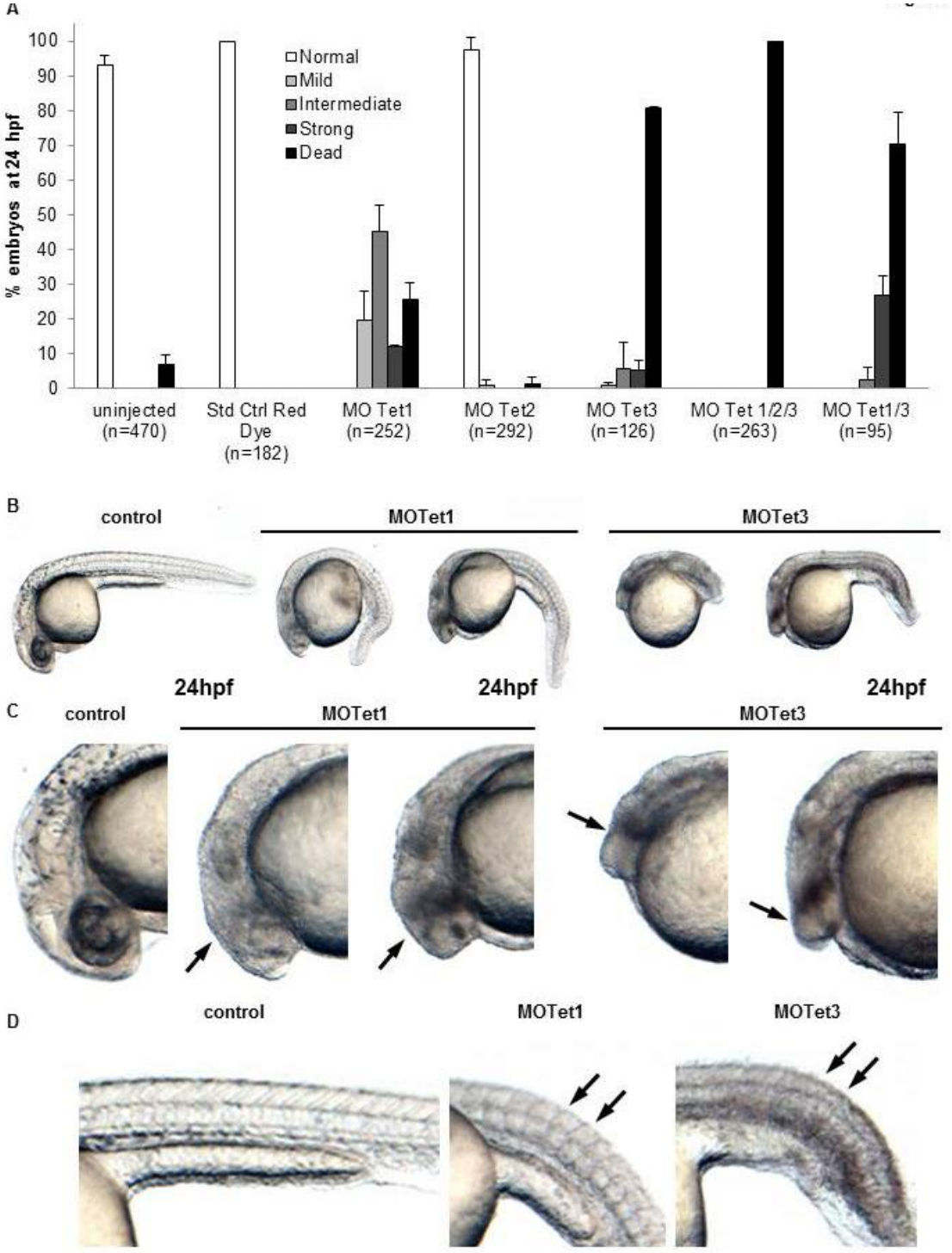

Figure 7.3 *tet1* and *tet3* morphants develop severe abnormality in organogenesis.

Analysis of *tet1/2/3* morphants phenotypes compared to uninjected or mini Ruby dye only injected controls at 24hpf. The embryos were categorized based on the severity of their phenotypes under bright field microscope, into: Normal with no observed abnormalities. Mild for embryos that lost pigmentation, have reduced body axis and small malformed eyes. Intermediate for embryos with small abnormal

head, missing eyes, considerably reduced and curved body and irregular somitogenesis and strong for embryos with more severe defects that include no anterior and posterior structures and no recognizable patterning. Mean percentages for at least three experiments are shown for each MO combination. Experimental error is expressed as s.e.m. Total numbers of assessed embryos are presented for each morpholinos combination. (B) *tet1* and *tet3* morphants phenotypes compared to their uninjected control at 24hpf. (C) Enlarged images of anterior region of *tet1* and *tet3* morphants phenotypes compared to their uninjected controls. (D) Enlarged images of posterior region of same embryos. The black arrows in (C,D) indicate absent or underdeveloped head structures and abnormal patterning of somites in the posterior region.

Interestingly, both *tet1* and *tet3* morphants were not viable beyond one day post fertilisation, which suggests the developmental arrest of these injected embryos. To assess the possible causes of observed variation among injected embryos, mini-Ruby dye was included in the morpholino injection mix, and we noticed that the severity of observed phenotypes correlates with the intensity of the dye in injected embryos (Figure 7.2, E), which shows that the observed variation in phenotype was dose dependent. We then wanted to know whether knocking *tet1* and *tet3* genes simultaneously leads to more severe phenotypes, and we found that with combined *tet1* and *tet3* blockage, the phenotypes become more severe, as most injected embryos showed failed tissue differentiation and loss of both anterior and posterior structures (Figure 7.2 C). On the other hand, injecting *tet2* morpholinos even with much higher amounts compared to *tet1* and *tet3* was found to be tolerated by embryos as injected embryos appeared normal even when examined on three days post fertilization

(Figure 7.2, D, Figure 7.3, A). Together, our morpholino study suggests an essential role for *tet* genes in zebrafish tissue differentiation.

7.2 Observed *tet1* and *tet3* morphants phenotypes are specific to depletion of *tet1* and *tet3* transcripts and not due to binding to un-intended targets

To test for morpholino specificity, one option was to rescue the phenotypes by injecting the targeted genes mRNA (Bedell et al., 2011). However, as endogenous *tet1/2/3* mRNAs are only expressed in the after embryonicsomitogenesis, injecting the *tet* mRNAs would lead to premature expression of the *tet* genes in these morphants and so premature 5mC modification, which may invalidate the results. Other confirmatory options that could be used include generating mutants with similar phenotypes, or recapitulating these phenotypes by injecting morpholinos targeting non-overlapping sequences in the same mRNA (Eisen and Smith, 2008). Due to the unavailability of published *tet* mutant lines at the time of designing the experiment. Added to the time and costs associated with generating and characterising new mutant lines, we decided to design and inject WT embryos with *tet1* and *tet3* morpholinos targeting splice sites in different exons in *tet1* and *tet3* genes (Table 7.2).

Table 7.2: List of confirmatory morpholinos used.

Mo. name	sequence	Target
tet1 E10	5′-AAGTGCATACCTGTGGTTTACAGGA-3′	*tet1* exon 10 splice acceptor
tet3 E4	5′- TCTCTCTGACTCCCTTAGACCAAGT-3′	*tet3* exon 4 splice acceptor
p53 Mo	5′-GCGCCATTGCTTTGCAAGAATTG-3′	Translation blocking

The first morpholino was designed to target the splice acceptor of exon 10 in the *tet1* gene, leading to splicing of exon9 to exon11, which is predicted to introduce a frameshift and premature termination of *tet1* transcript (Figure 7.4, A-D). The other morpholino was designed to target the splice acceptor of exon4 in *tet3* gene, leading to splicing of exon3 to exon5, which was predicted to also introduce a frameshift and premature termination of *tet3* transcript (Figure 7.4 E-H).

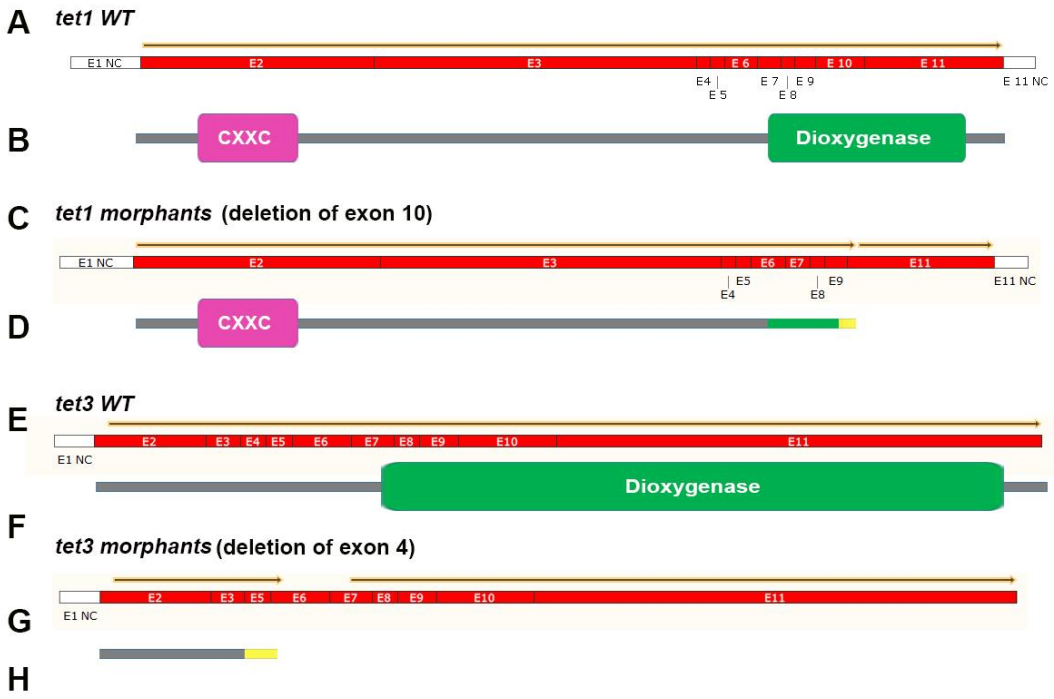

Figure 7.4 Confirmatory *tet1* and *tet3* morpholinos with different targets and similar predicted outcome.
(A-H) Schematic diagrams of zebrafish *tet1*, and *tet3* cDNA and proteins in WT embryos compared to predicted *tet* genes morphants. The white boxes in (A, C, E,G) are the non-coding exons while red boxes are the coding ones. Orange arrows show the open reading frames that are intact in WT and prematurely terminated in the morphants. (B, D, F, H) are the Tet protein domains in WT and *tet* morphants, showing the main functional domains, the dioxygenase in all WT tet proteins (green boxes) and their loss in their *tet* morphants counterparts. The pink boxes are for the CXXC domains that present in *tet*1 WT as well as *tet1* morphants. The grey lines indicate the WT amino acids, the green line indicates the in-frame part of the dioxygenase domain, while the yellow lines indicate the frame shift and protein termination resulting from splicing to next exons. The cDNA schematics were produced with SnapGene® software (from GSL Biotech; available at snapgene.com). The *tet* genes sequences were ENSEMBL versions (dTet1, ENSDARG00000075230.4) and (dTet3, ENSDARG00000062646.6).

I then injected the *tet1* and *tet3* morpholinos individually to WT embryos and examined the injected embryos both at 8hpf and also at 24hpf. At 8hpf, as with the former morpholinos, both *tet1* and *tet3* morphants appeared normal and in-distinguishable from their

uninjected siblings. Moreover, both also developed phenotypes identical to those observed with previously used morpholinos at 24hpf (Figure 7.5, A-F, Figure 7.6, A-D).

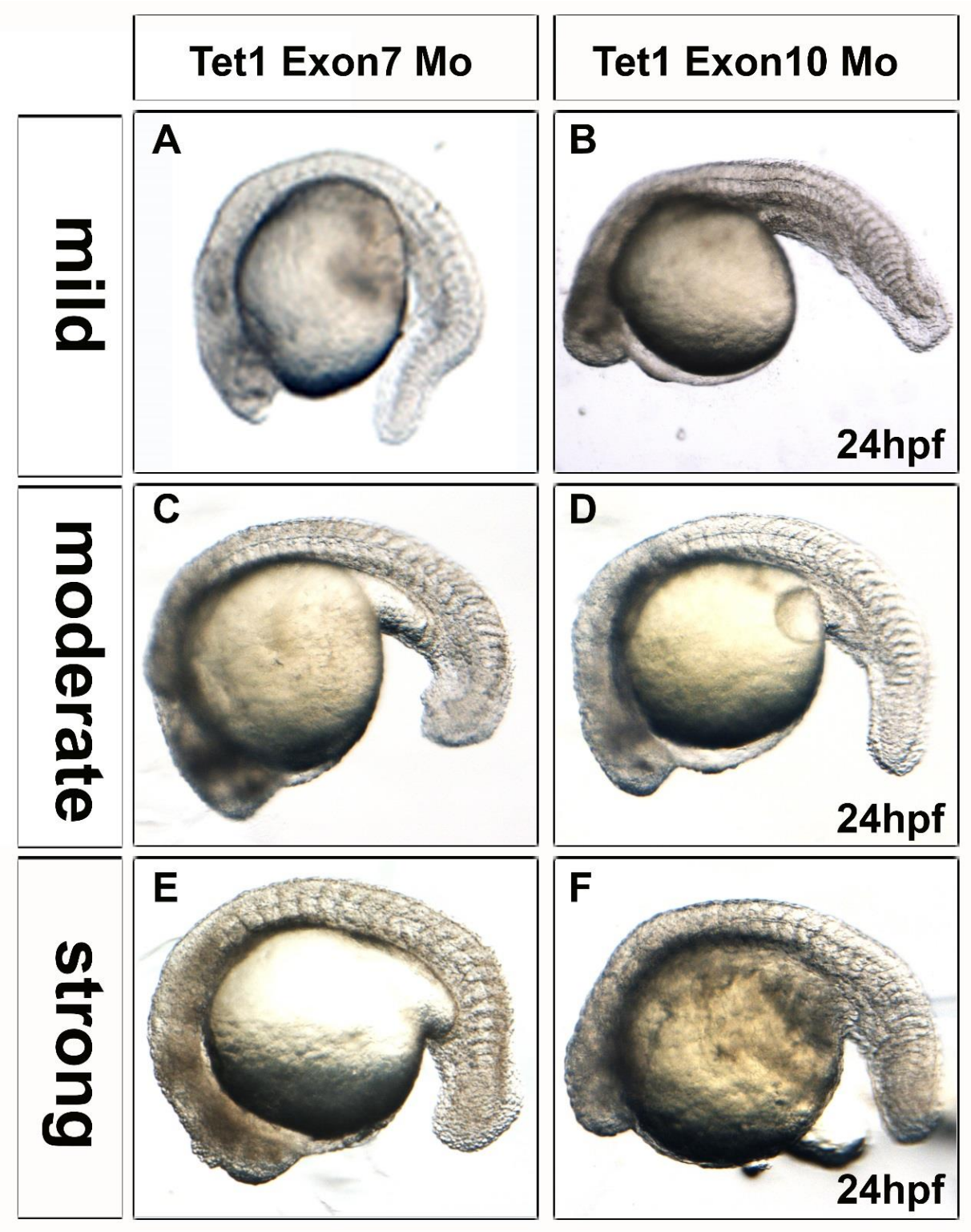

Figure 7.5 Targeting different sequence in *tet1* gene produce identical phenotypes.
(A-F) Bright field microscopy of *tet1* exon7 morphants mild (A), moderate (C) and strong (E) phenotypes compared to their *tet1* exon10 morphants counterparts (B, D, F).

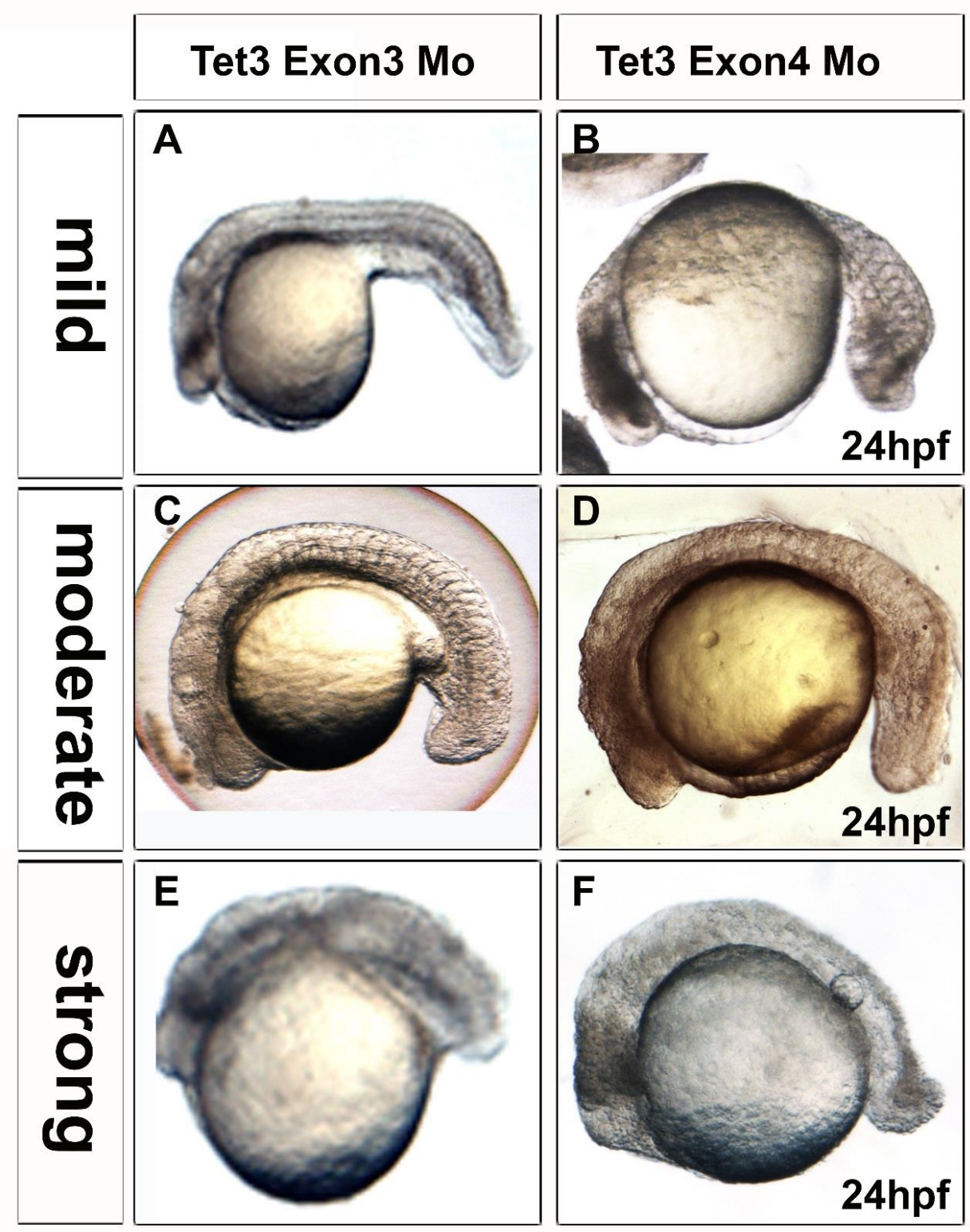

Figure 7.6 Targeting different sequence in *tet3* gene produce identical phenotypes.
(A-F) Bright field microscopy of *tet3* exon3 morphants mild (A), moderate (C) and strong (E) phenotypes compared to their *tet3* exon4 morphants counterparts (B, D, F).

I also repeated injecting the *tet2* morpholinos at higher concentrations and results were similar to previous data. Injected embryos as in the previous experiment appeared normal until 72hpf. Because the severity of morpholinos was higher with *tet1* splice acceptor 7 and *tet3* splice acceptor 4, I decided to use these two morpholinos for all subsequent *tet1* and *tet3* morpholino experiments.

Reproducing the phenotypes with injecting morpholinos targeting non-overlapping sequences in *tet1* and *tet3* mRNA highly suggested that observed phenotypes are caused by specific targeting of *tet1* and *tet3* genes and not due to non-specific binding to other places in the genome. In addition, to examine if the observed phenotypes were caused by activation of the *p53* mediated apoptosis, I co-injected the *tet1* and *tet3* morpholinos with *p53* morpholinos in the ratio of 2:1 (Robu et al., 2007), and examined the embryos at 8hpf and then at 24hpf for the phenotypes. Even though addition of the *p53* morpholinos to the injection mix reduced the severity of observed phenotypes, their persistence in co-injected embryos further eliminated the possibility of non-specific toxicity (Figure 7.7).

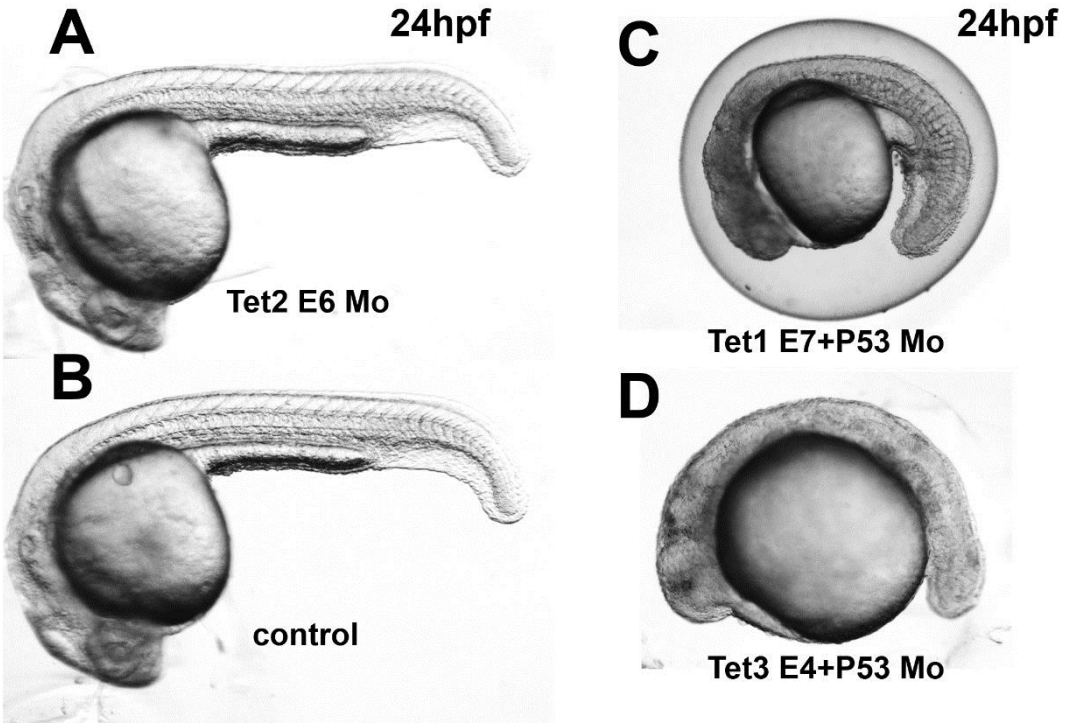

Figure 7.7: *tet2* morpholino injection with high amount does not affect embryonic development, and addition of *p53* Mo does not rescue *tet1* or *tet3* morphants.
(A) WT embryo co-injected with *tet2* exon 6 splice donor and exon 6 acceptor morpholinos. The embryos appear normal and in-distinguishable from uninjected controls (B). (C) WT embryo co-injected with *tet1* exon7 splice acceptor morpholino and *p53* morpholinos with persisting phenotypes. (D) WT embryo co-injected with *tet3* exon 4 splice acceptor morpholino and *p53* morpholino with persisting phenotypes.

7.3 Injecting *tet1* or *tet3* leads to deletion of targeted exons, frame shifts and premature termination of *tet1* and *tet3* genes

To study the effect of injecting *tet1* or *tet3* morpholinos on the normal splicing of these genes transcripts, I designed two pairs of primers, one to bind the exons before and after the targeted *tet1* exon 7 (DB658 and DB452; Figure 7.8, A). The other to bind the exons

before and after the targeted *tet3* exon 4 (DB457 and DB659; Figure 7.9, A). Next, I performed total RNA extraction and R.T. first strand cDNA synthesis from *tet1* morphants, *tet3* morphants and uninjected control embryos, all collected at 24hpf. Normal PCR amplification was then performed with the two sets of primers, followed by gel analysis of produced fragments (Figure 7.8, B, Figure 7.9, B respectively). Comparing *tet1* or *tet3* morphants cDNA results to their uninjected siblings, it is apparent that the majority of targeted transcripts were altered, indicated by the smaller bands with *tet1* and *tet3* morphants compared to their uninjected siblings. Comparing these bands to the molecular ladder, it is likely that the entire targeted exons were skipped in both *tet1* and *tet3* morphants during the splicing process, as predicted (Figure 7.8, A and Figure 7.9, A respectively). To further confirm gel results, and to rule out the possibility of splicing to cryptic splice sites in the area around targeted exons, which might result in partial insertion or deletion in-frame with the targeted *tet1* or *tet3* genes. For this, I extracted the fragments with altered sizes from the gel, and then submitted these fragments for sequencing, utilizing the same primer pairs for sequencing from both directions. Sequencing results showed no cryptic splicing with either *tet1* or *tet3* morphants, and so confirmed the complete deletion of targeted exons, and splicing between the outside (5' and 3') neighbouring exons and introduction of frame shifts and premature termination of the *tet1* and *tet3* genes as predicted (Figure 7.8, C-E and Figure 7.9, C-E

respectively). On the other hand, gel results for *tet3* morpholinos showed a significant remaining normally spliced *tet3* transcript in *tet3* morphants (the * in Figure 7.9 B), however this may be resulting from the difficulty associated with injecting low doses of morpholino, and pooling the morphants with some that might have less efficient *tet3* knock down.

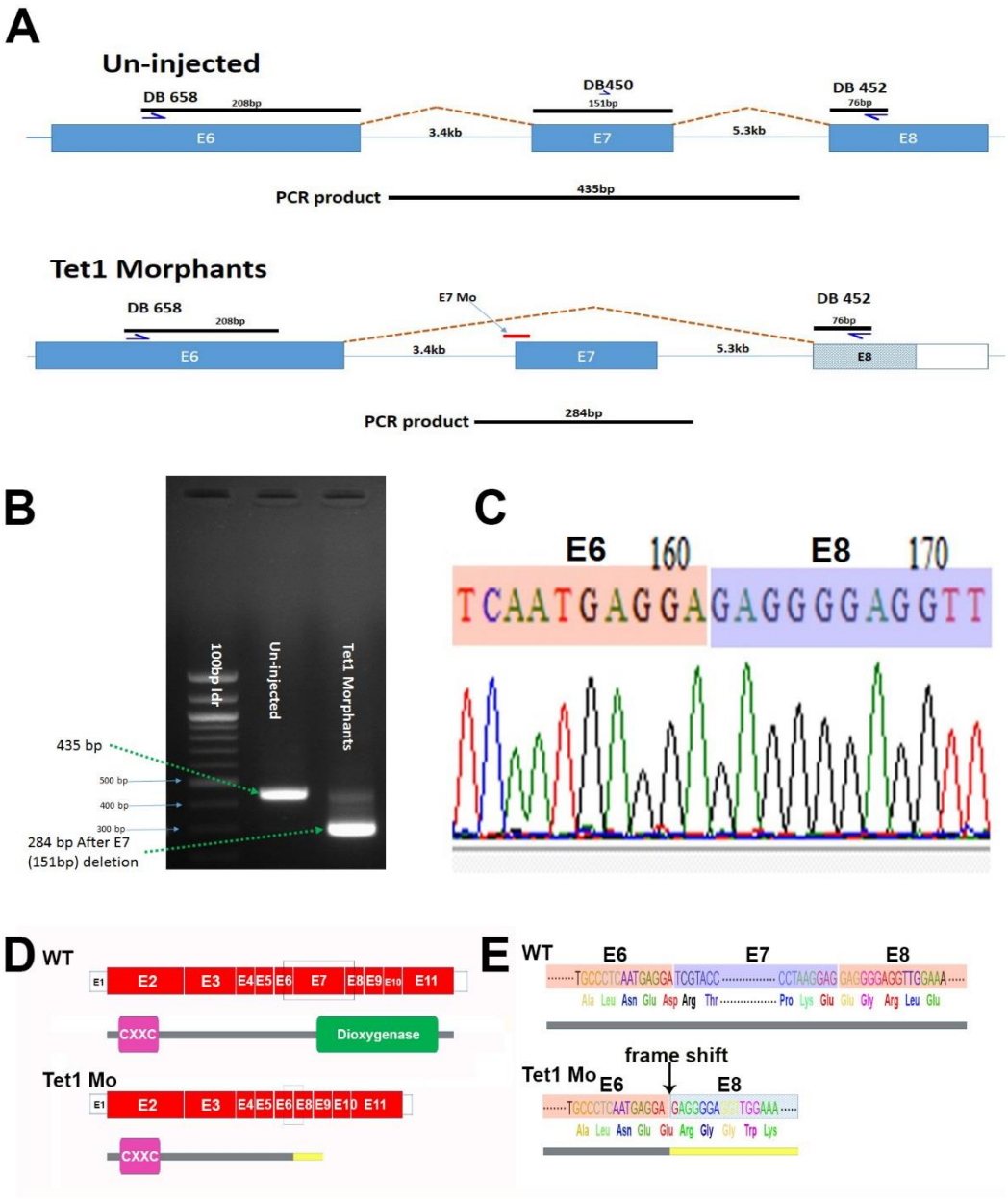

Figure 7.8 *tet1* exon 7 splice acceptor morpholino leads to deletion of exon 7, frame-shift and premature termination of Tet1 protein translation.
(A) Annealing of exon 7 splice acceptor antisense morpholino to exon7 splice acceptor site in the *tet1* pre-mRNA is intended to prevent the normal spliceosomal recognition of targeted exon (top), skipping exon 7 and splicing between exon 6 and exon 8. Blue arrows show locations of primers used to validate morpholino efficiency (DB658 and DB452) and for mRNA quantification with RT-PCR (DB450 and DB452). Black lines depict expected fragment sizes in uninjected control (top) and *tet1* exon 7 splice acceptor morphants (below). (B) The gel result showed fragments of expected sizes (as indicated with the green arrows) after performing normal PCR with the primers depicted in (A) with cDNA templates prepared from *tet1* morphants total RNA isolated at 24hpf, and uninjected controls siblings. The gel results showed almost complete loss of normally spliced *tet1* transcript in *tet1* morphants (the top 435bp) and a strong band with expected (284bp) fragment. (C) Screenshot of sequencing result (viewed in BioEdit software) of the *tet1* morphants cDNA PCR fragment (the 284bp in B) after excision from gel. Sequencing result confirmed the complete deletion of exon 7 and splicing of exon 6 with exon 8 in *tet1* morphants (as depicted in A). (D) Schematic presentation of *tet1* morphants transcript with skipping exon 7 that leads to frame-shift (indicated by the yellow line). Premature termination of the transcript, and production of truncated protein that lack the functioning deoxygenase domain. This is compared to the uninjected control transcript and protein product with the active deoxygenase domain (the green box). (E) Magnification of the boxed area in (D) showing the frameshift caused by deletion of exon 7 and the changes in amino acid sequence caused by this frame-shift. The grey line indicates the in-frame translation, whereas the yellow line indicates the out-of-frame translation.

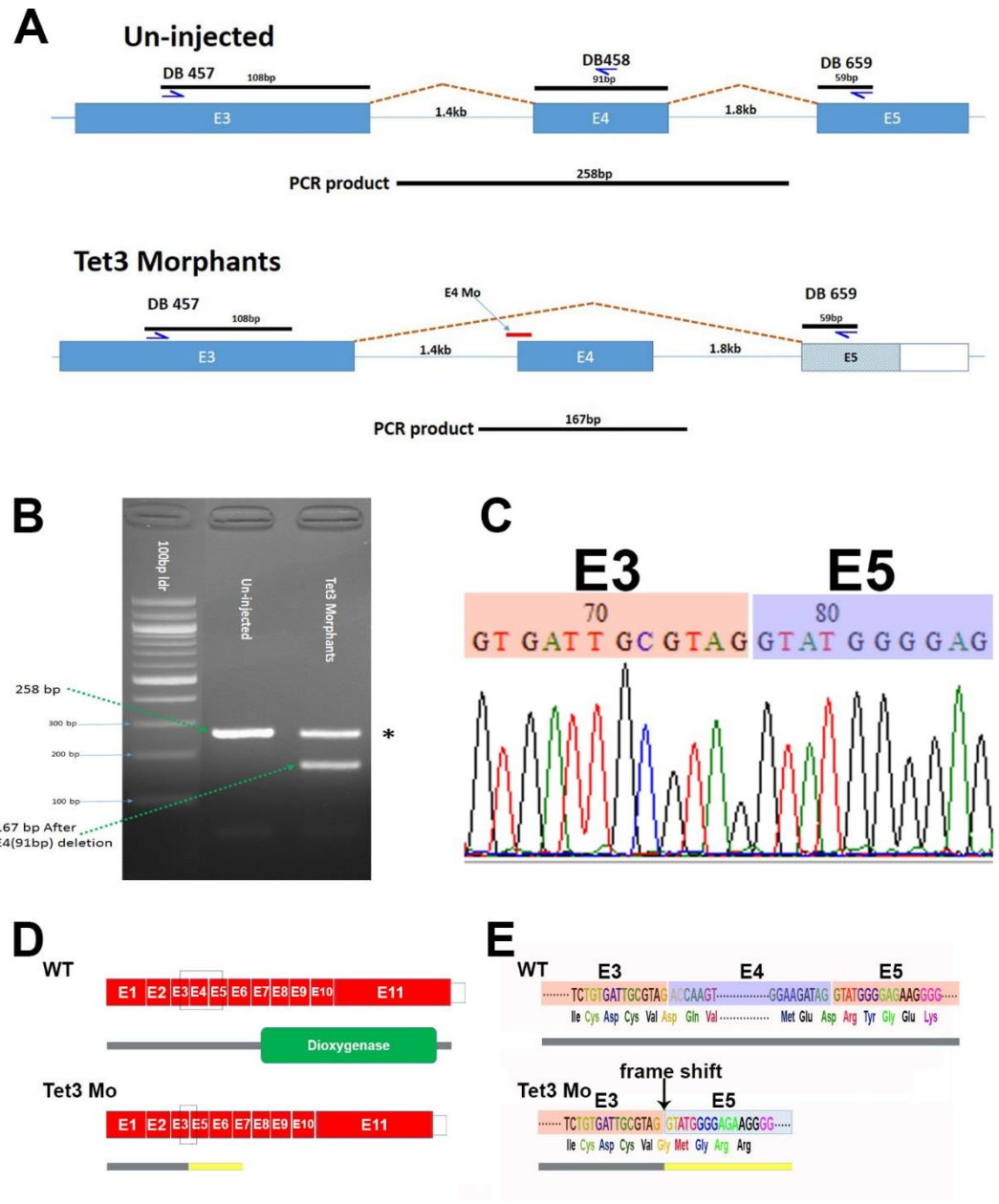

Figure 7.9 *tet3* exon 4 splice acceptor morpholino leads deletion of exon 4, frame-shift and premature termination of Tet3 protein translation.

(A) Annealing of exon 4 splice acceptor antisense morpholino to exon 4 splice acceptor site in the *tet3* pre-mRNA is intended to prevent the normal spliceosomal recognition of targeted exon (top), skipping exon 4 and splicing between exon 3 and exon5. Blue arrows show locations of primers used to validate morpholino efficiency (DB457 and DB659) and for mRNA quantification with RT-PCR (DB457 and DB458). Black lines depict expected fragment sizes in uninjected control (top) and *tet3* exon 4 splice acceptor morphants (below). (B) The gel result showed fragments of expected sizes (as indicated with the green arrows) after performing normal PCR with the primers depicted in (A) with cDNA templates prepared from *tet3* morphants

total RNA isolated at 24hpf and uninjected siblings cDNA. The gel results showed significant reduction of normally spliced *tet3* transcript in *tet3* morphants (the top 258bp) and a strong band with expected (167bp) fragment. (C) Screenshot of sequencing result (viewed in BioEdit software) for the *tet3* morphants cDNA PCR fragment (the 167bp in B) after excision from gel. Sequencing result confirmed the complete deletion of exon 4 and splicing of exon 3 to exon5 in *tet3* morphants (as depicted in A). (D) Schematic presentation of *tet3* morphants transcript with skipping exon 4 that leads to frame-shift (indicated by the yellow line) and premature termination of the transcript, and production of truncated protein that lacks the functioning deoxygenase domain. This is compared to the uninjected control transcript and protein product with the active deoxygenase domain (the green box). (E) Magnification of the boxed area in (D) showing the frame-shift caused by deletion of exon 4 and the changes in amino acid sequence caused by this frame-shift. The grey line indicates the in-frame translation, whereas the yellow line indicates the out-of-frame translation. * The remaining normally spliced transcript in *tet3* morphants cDNA PCR that may be resulting from the low injected dose that may have reduced the efficiency in some injected embryos.

7.4 Quantitative RT-PCR shows significant reduction in *tet1* transcript in *tet1* morphants and significant reduction in both *tet1* and *tet3* transcripts in *tet3* morphants

Due to the similarity of phenotypes observed in *tet1* or *tet3* morphants, we wanted to know if the two proteins act together to mediate the 5mC oxidation, or whether one of the genes regulates the other. To achieve this, I measured the level of the two transcripts in *tet1* and *tet3* morphants then compared their levels to their uninjected controls. In this process total RNA was firstly isolated at 24hpf, reversed transcribed, then quantified by RT-PCR with primers (DB450 and DB452; Figure 7.8, A) for *tet1* quantification, and (DB457 and DB458 Figure 7.9, A) for *tet3* quantification. In *tet1* morphants, real time quantification showed a significant reduction in

tet1 transcript but no effect on *tet3* transcripts (Figure 7.10, A). On the other hand, I noticed significant reduction in the two transcripts in *tet3* morphants (Figure 7.10, B). Even though the result suggests dependency of *tet1* on presence of *tet3*, we found it difficult to exclude the possibility that the reduction in *tet1* transcript was a complication associated with the failure in organogenesis.

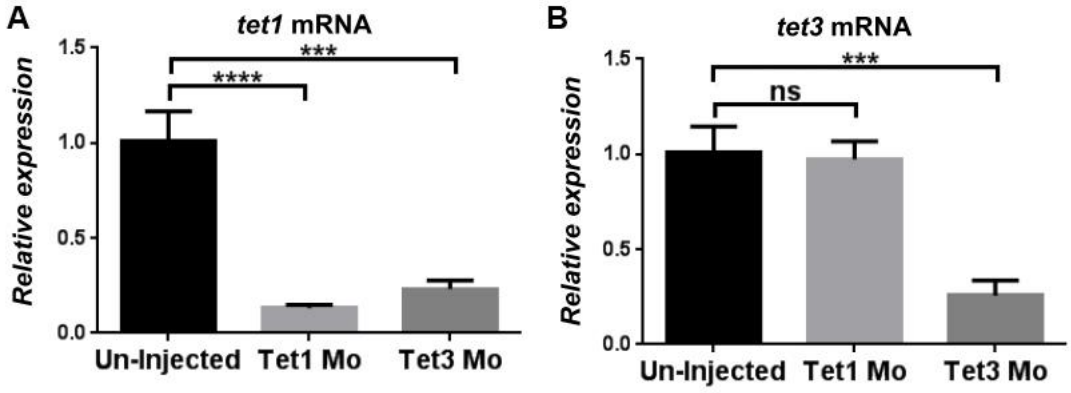

Figure 7.10 *tet1* mRNA significantly reduced in both *tet1* and *tet3* morphants whereas *tet3* transcript only reduced in *tet3* morphants.
(A-B) Histograms showing quantitative real time PCR results of *tet1* and *tet3* transcripts in uninjected, *tet1* morphants and *tet3* morphants. Blocking *tet1* expression only reduced *tet1* mRNA level (middle bar in A and B), while blocking *tet3* expression reduced both *tet1* mRNA and *tet3* mRNA (right bar in A-B) (Mean and SEM; ***p<0.001; ****p<0.0001; t test).

7.5 Notch signalling is altered in *tet1* and *tet3* morphants

Given the severe developmental phenotypes observed in *tet1* and *tet3* morphants, which included malformation of the head structure and improper somitogenesis added to the abnormality in multiple organs, we wanted to test whether the Notch signalling pathway was

affected in these morphants. Notch signalling is a key regulator controlling cell specification and tissue patterning, and plays an essential role in the development of various organs, including neurogenesis, somitogenesis, cardiovascular and haematopoiesis (Koch et al., 2013). To study the effects of blocking *tet* genes on Notch signalling, we injected the *tet1/2/3* morpholinos into our in-house Notch reporter transgenic line *Tg(csl:venus)*^{qmc61} then monitored expression of the reporter fluorescent protein (Venus) by fluorescent microscopy in these injected embryos, compared to their uninjected siblings. While expression of the Notch reporter gene in *tet2* morphants was almost identical in the level and expression pattern to their uninjected siblings, when examined at 24hpf and 48hpf, *tet3* morphants showed a strong reduction in the reporter gene expression when examined at 24hpf (Figure 7.11, A-E').

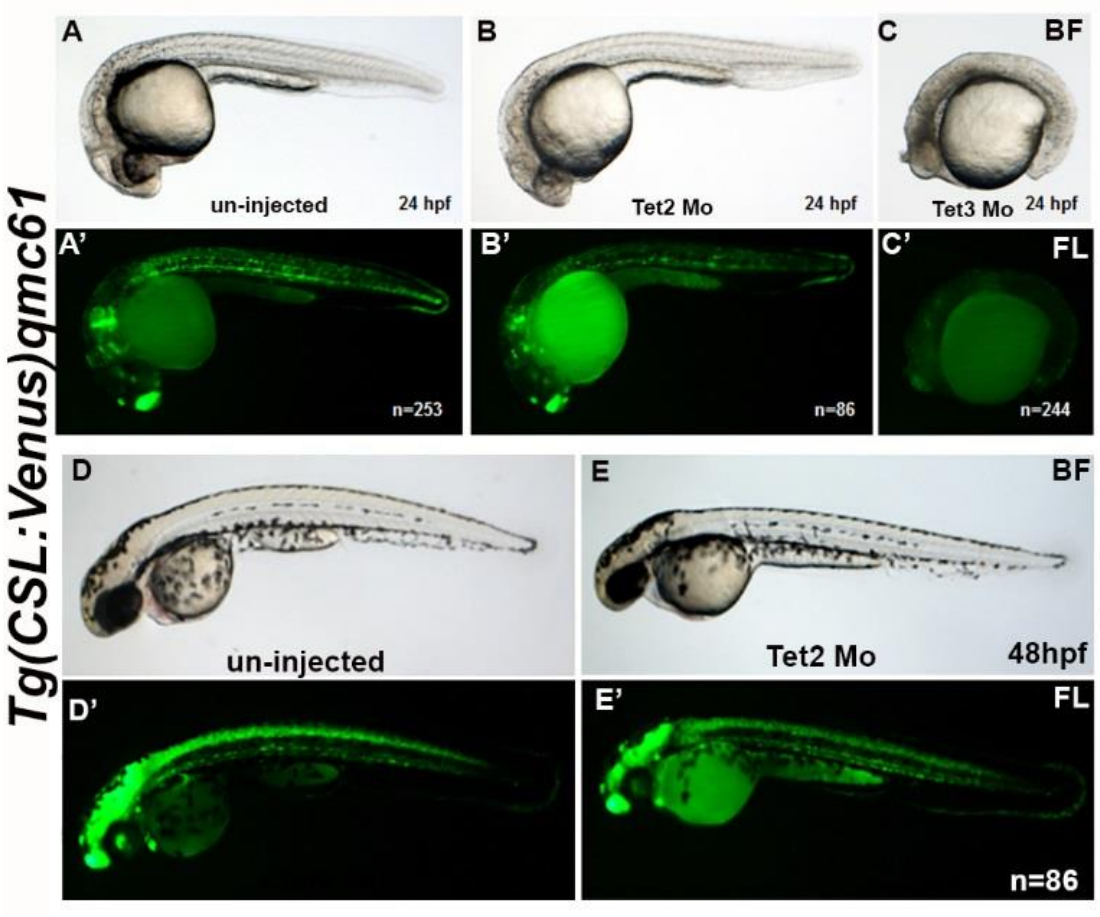

Figure 7.11 Notch activity severely reduced in *tet3* morphants and not affected in *tet2* morphants.
(A-E') Bright field and fluorescent microscopy of uninjected and *tet2/3* injected *Tg(csl:venus)*^{qmc61} embryos at 24hpf (A-C') and 48hpf (D-E'). Expression of the Notch reporter gene (*venus*) in *tet2* morphants appeared identical to uninjected controls both at 24hpf (A-B') and at 48hpf (D-E'). *tet3* depletion in *tet3* morphants leads to severe reduction in Notch reporter gene expression at 24hpf (C-C').

Interestingly, when we examined the moderately affected *tet1* morphants, we found that Notch reporter expression was still maintained in these embryos, but with different distribution among tissues with known Notch activity. For instance, whereas Notch reporter fluorescent protein was reduced throughout the notochord in uninjected controls at 23hpf, its expression was maintained at high level in *tet1* morphants (yellow arrow in Figure 7.12 B). On the other

hand, expression of the reporter gene was much lower in the hindbrain and axial vessels in these *tet1* morphants compared to their uninjected controls (red arrows in Figure 7.12 A).

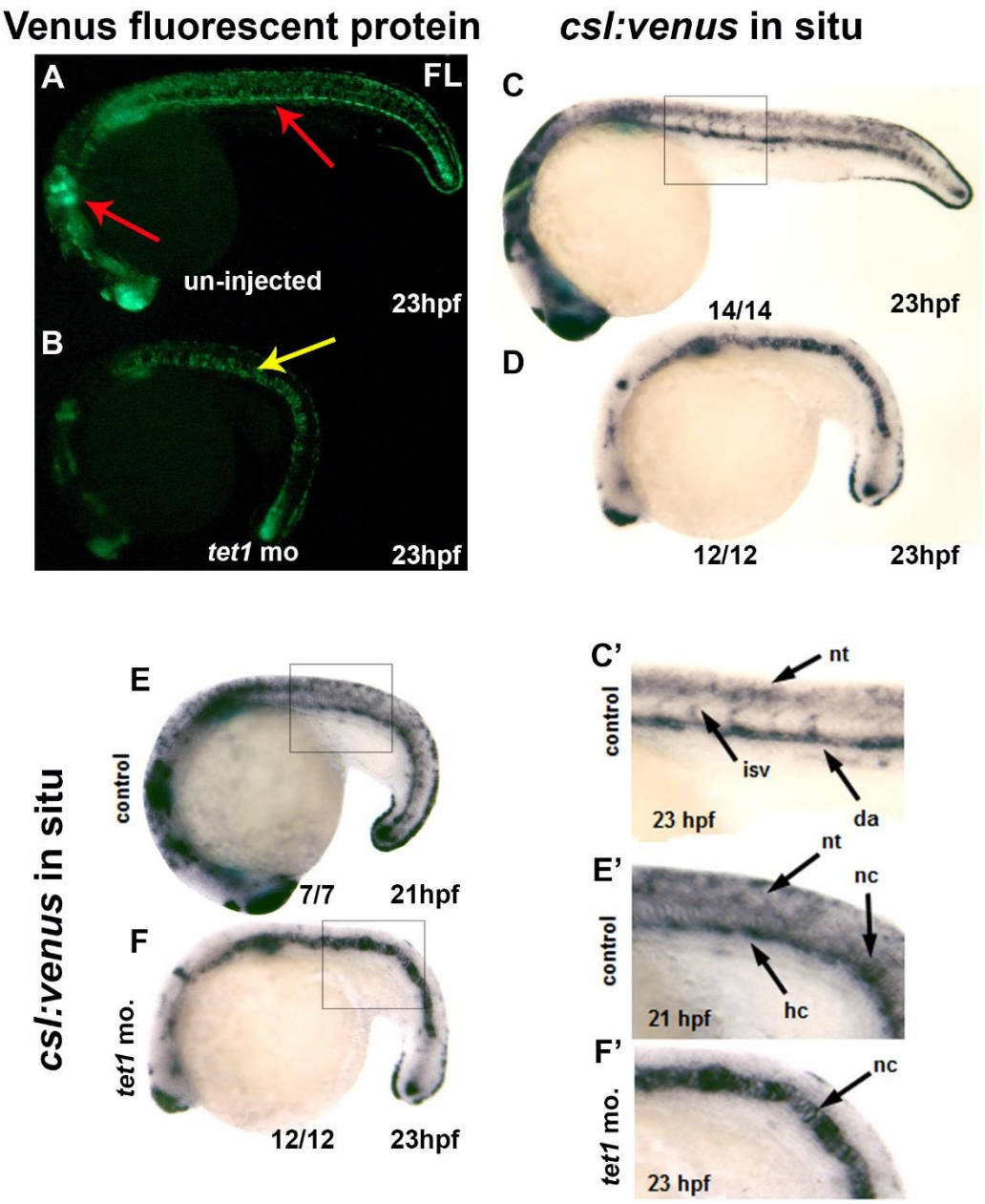

Figure 7.12 Notch activity is altered in *tet1* morphants.
(A-F') Fluorescent microscopy and in situ hybridization images of uninjected and *tet1* morpholino injected *Tg(csl:venus)*^{qmc61} embryos at 23hpf (A-D,E-F) and 21hpf (E-E'). (A) Expression of the Notch reporter gene *venus* in *tet1* morphants is maintained at a high level in the notochord (yellow arrow) at 23hpf compared to the uninjected controls. The normal *venus* expression in the DA and hindbrain (red

arrows in B) is either un detectable or severely reduced in *tet1* morphants. (C-D) Fluorescent microscopy results are recapitulated by *venus* mRNA. (E-F) *venus* mRNA distribution *tet1* morphants at 23hpf (D) does not match the *venus* mRNA distribution in younger uninjected controls. (C', E', F') are magnifications of the boxed areas in (C, E, F).

Because fluorescent microscopy only reports the fluorescent protein accumulated in the tissues over the period before examination, rather than the time point of examination, we decided to stop and fix *tet1* morphants for in situ hybridization to test for the *venus* mRNA expression pattern and so Notch activity at 23hpf.

Our in situ results further confirmed the fluorescent microscopy findings, as in situ also showed strong up-regulation of the Notch reporter mRNA in the notochord and its absence in the DA region. It is also evident that Notch activity in the hindbrain is much lower than that of uninjected siblings (Figure 7.12 C-D). We then wanted to know if the observed alteration in Notch activity was due a general developmental delay, so we compared the 23hpf mRNA expression of the *tet1* morphants to uninjected controls stopped 2 hours earlier (21hpf). Even though, the younger uninjected controls appeared morphologically similar to the 23 hpf *tet1* morphants, the expression pattern was completely different in the two groups. Unlike in the uninjected controls, where Notch was highly active in the hypochord and barely detectable in the notochord area, no clear Notch activity was reported in the *tet1* morphants' hypochord, and high activity was observed in the notochord (Figure 7.12, E-F, black arrows in E'-F'),

which suggests a *tet1* depletion dependent mis-regulation of the Notch signalling pathway.

tet1 morphants, appear normal and in-distinguishable from their uninjected controls when examined under bright field microscopy until early somitogenesis. This time point corresponds with the time when *tet1* gene is expressed in the developing embryo. Therefore, we wanted to see if the alteration in Notch activity is also happening at the time point when Tet1 protein is required in these morphants. For this, we examined the expression pattern of the *venus* gene mRNA in our Notch reporter line *Tg(csl:venus)*^{qmc61}. We also examined expression of the Notch downstream target *her4.1* by in situ hybridization at the 1-3 somite stage in *tet1* morphants and compared them to their uninjected controls, and also to *mib* mutants homozygous or heterozygous embryos (Figure 7.13, A-D). In agreement with bright field microscopy findings, and unlike the *mib* homozygous or heterozygous, Notch reporter mRNA and the Notch downstream target *her4.1* were both normally expressed in these tissues in *tet1* morphants, and their expression was indistinguishable from uninjected controls (Figure 7.13, A-D). Moreover, when examining the expression pattern of the Notch components *notch1b* and *dla* at 10 somite stage, their expression in *tet1* morphants were similar to uninjected controls (Figure 7.13, E-F). Interestingly, when examining expression of the Notch components *notch1b* and *dla* at 23hpf in *tet1* morphants, we noticed persistence of their transcripts

in the neural tube (Figure 7.13 G-H), which further suggests an epigenetic control on Notch activity in this tissue.

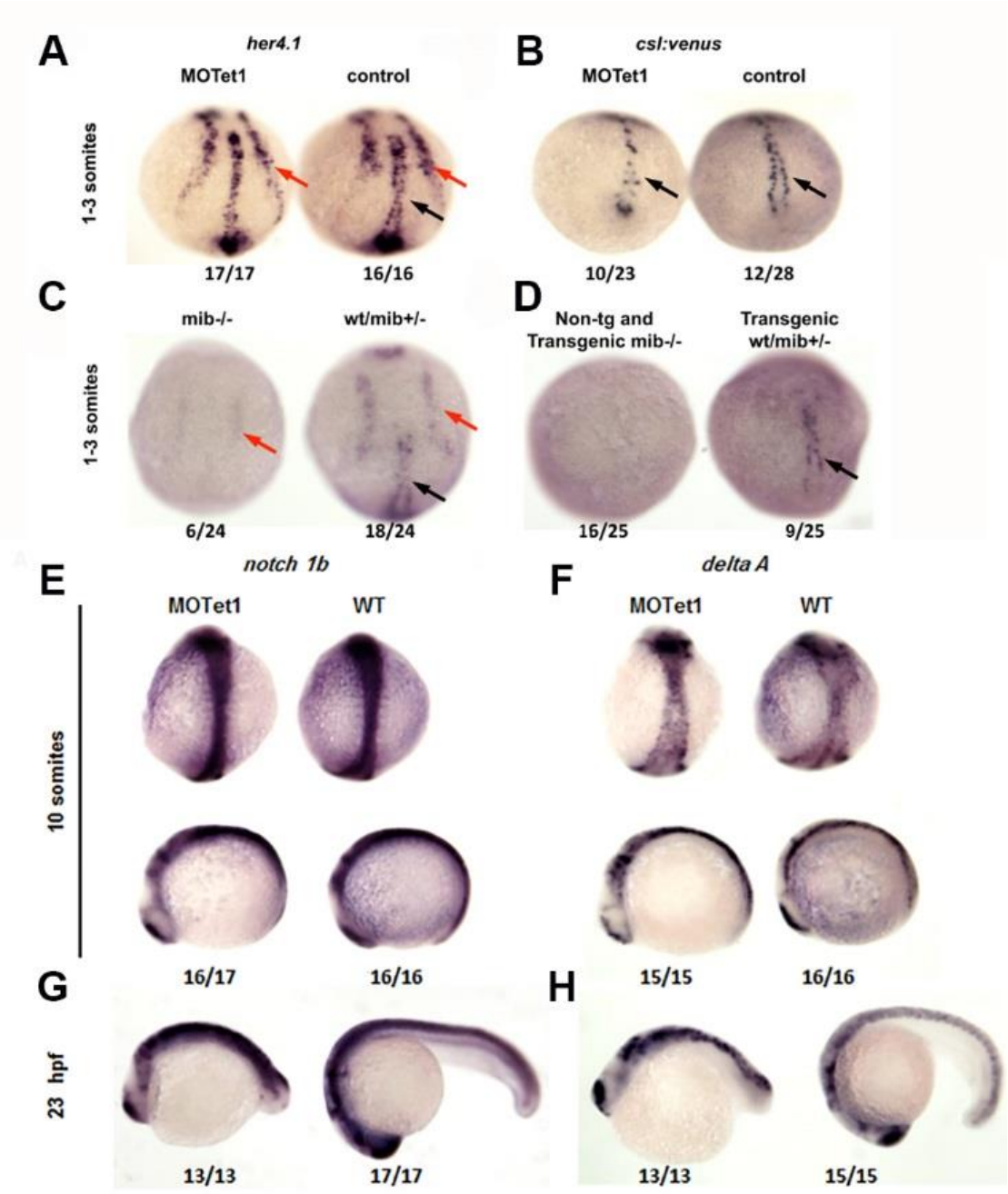

Figure 7.13 Notch signalling persists in *tet1* morphants despite alteration in its expression pattern in late somitogenesis.
(A-H) Whole mount in situ hybridization for *her4.1* expression in uninjected and *tet1* injected embryos at 1-3 somite stage (A), compared to its expression in *mib* mutants (C). Expression of *venus*

reporter gene in uninjected and *tet1* injected *Tg(csl:venus)*^{qmc61} embryos at 1-3 somite stage (B), compared to its expression in *mib* homozygous with the same transgene in the background (D). (E-H) Whole mount in situ hybridization for *notch1b* and *dla* expression in uninjected and *tet1* injected embryos at 10 somite stage (E-F) and 23hpf (G-H). Unlike in *mib* mutants, *her4.1* and *venus* mRNAs are maintained in the neural tube progenitors (red arrows in A-D) hypochord progenitors (black arrows in A-D). Notch components *notch1b* and *dla* expression persistsed in *tet1* morphants and were comparable to their uninjected siblings both at 10 somite stage (E-F) and 23hph (G-H).

Taken together, the normal development of embryos until the time point when *tet1* gene expression appears in the embryo at early somitogenesis, and the persistence of Notch activity but with altered pattern and defective organogenesis thereafter, collectively suggest a global role for *tet* genes in tissue patterning and organogenesis, and that this role may include implementing the Notch pathway.

7.6 *tet1* knockdown alter neurologic program in zebrafish embryos

Notch signalling is known to play key role in embryonic neural development, and its mis-regulation is known to disrupt the normal patterning and differentiation of the neurological tissues. To analyse the effect of knocking down *tet1* on the neurological development, we examined the expression of neuronal lineage markers in *tet1* morphants both at 1-3 and 10 somite stages. In agreement with our previous findings, in situ analysis of the *tet1* morphants revealed no significant changes in the expression of either proneural marker

*neurog*1 (*neurogenin*) or the early post-mitotic neuronal marker *elavl3* (*embryonic lethal abnormal vision; Elavl3/HuC*) (Figure 7.14 A-B). However, by 23 hpf, *tet1* morphants showed a markedly increased expression of *elavl3* in several regions of the neural tube, suggesting an alteration of neurogenesis program occurring in these embryos (Figure 7.14 C-D). Even though these results strongly suggest a *tet1* depletion dependent alteration in the neurogenesis program, it is still not identified whether Tet1 protein is interacting directly with the examined neurological markers through altering their methylome marks or through altering the epigenetic marks of components involved in Notch signalling pathway in order to regulate and co-ordinate neurogenesis.

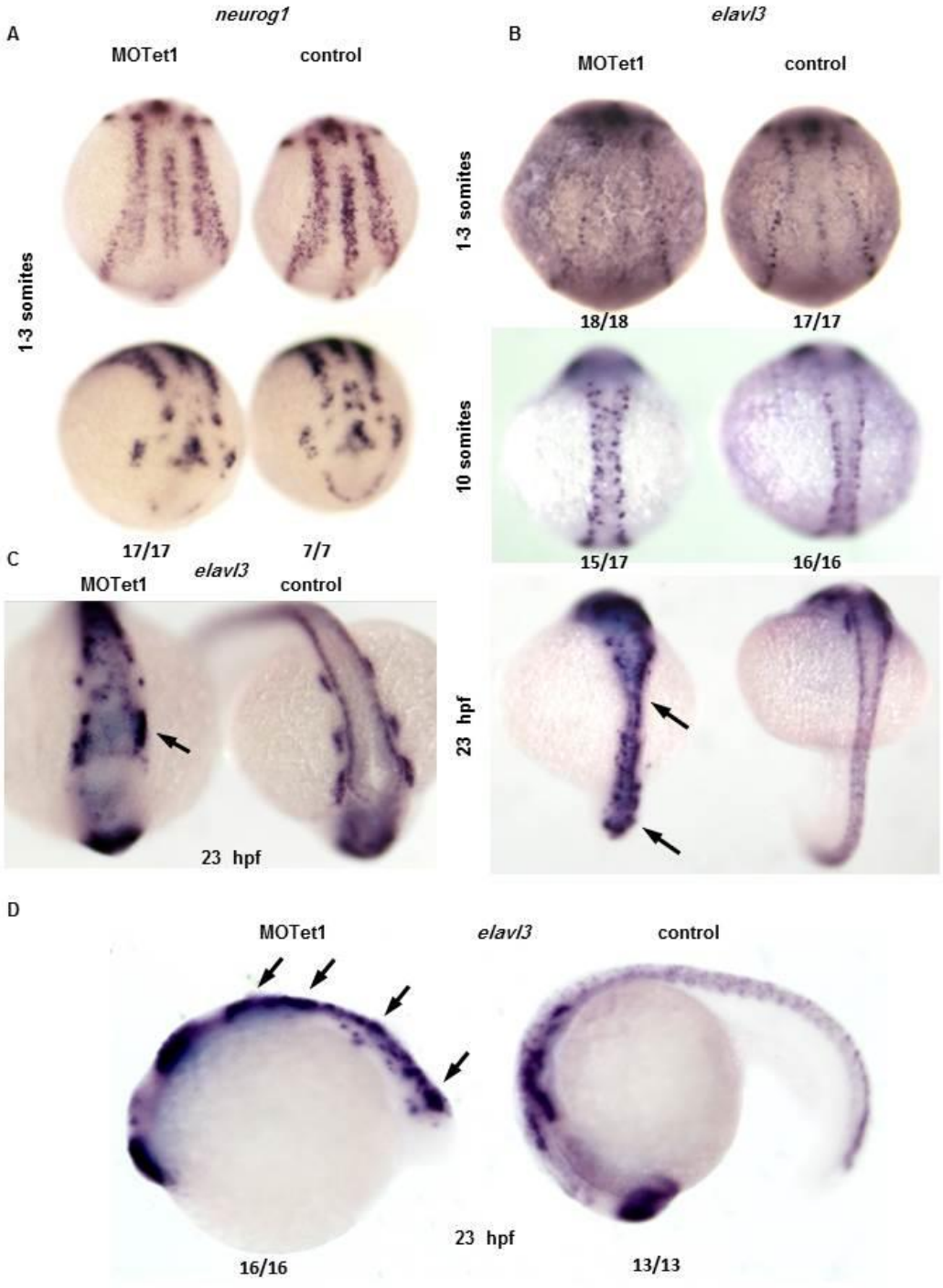

Figure 7.14 *tet1* knockdown leads to atypical neurogenesis in zebrafish embryos.
(A-D) Whole mount in situ hybridization for *neurog*1 expression in *tet1* morphants, compared to their uninjected controls at 1-3 somites stage (A) and for *elavl3* expression at 1-3 somites, 10 somites (B) and at 23hpf (C-D). Dorsal (top) and anterior (bottom) views in (A-B) show identical expression pattern of *neurog*1 and *elavl3* in uninjected embryos and *tet1* morphants at early somitogenesis.

Anterior, dorsal and lateral views of *elavl3* expression in *tet1* morphants compared to their uninjected controls showing an increased expression of *elavl3* mRNA in several regions of the neural tube (indicated by black arrows in C and D).

7.7 5hmC levels decrease in the *elavl3* promoter in both *tet1* and *tet3* morphants

DNA methylation was proven to be critical in regulating gene expression and tissue patterning. *tet* genes through their oxygenase domains have also been shown to promote the conversion of the 5mC to 5hmC and then to the more oxidized forms 5-formylcytosine and 5-carboxylcytosine that play passive and active demethylation roles (Tahiliani et al., 2009, Ito et al., 2010, He et al., 2011, Gu et al., 2011, Zhang et al., 2013). To determine whether injecting *tet1* or *tet3* alters the methylation levels of Notch components, the neurological marker *elavl3* or the *tet* genes themselves, we utilised antibodies specific for the 5mC and 5hmC to enrich for these cytosine modifications and carried out DNA immune-precipitation (DIP) on DNA from *tet1* morpholino injected, *tet3* morpholino injected and uninjected controls.

Enrichment was then quantified using quantitative PCR (qPCR) at 12 candidate loci whose selection was based on their CpG enrichment and always upstream or within the first introns of selected genes. Most of the qPCR results were difficult to interpret, which may be resulted from the ambiguity associated with the heterogeneity of cell

types in 24hpf embryos (Figure 7.15). However, we noticed a significant decrease in the 5hmC levels in the *elavl3* promoter region both in the *tet1* and *tet3* morphants, which may indicate a functional relationship between the status of methylation in *elavl3* promoter region and the abnormal expression pattern observed in *tet1* morphants.

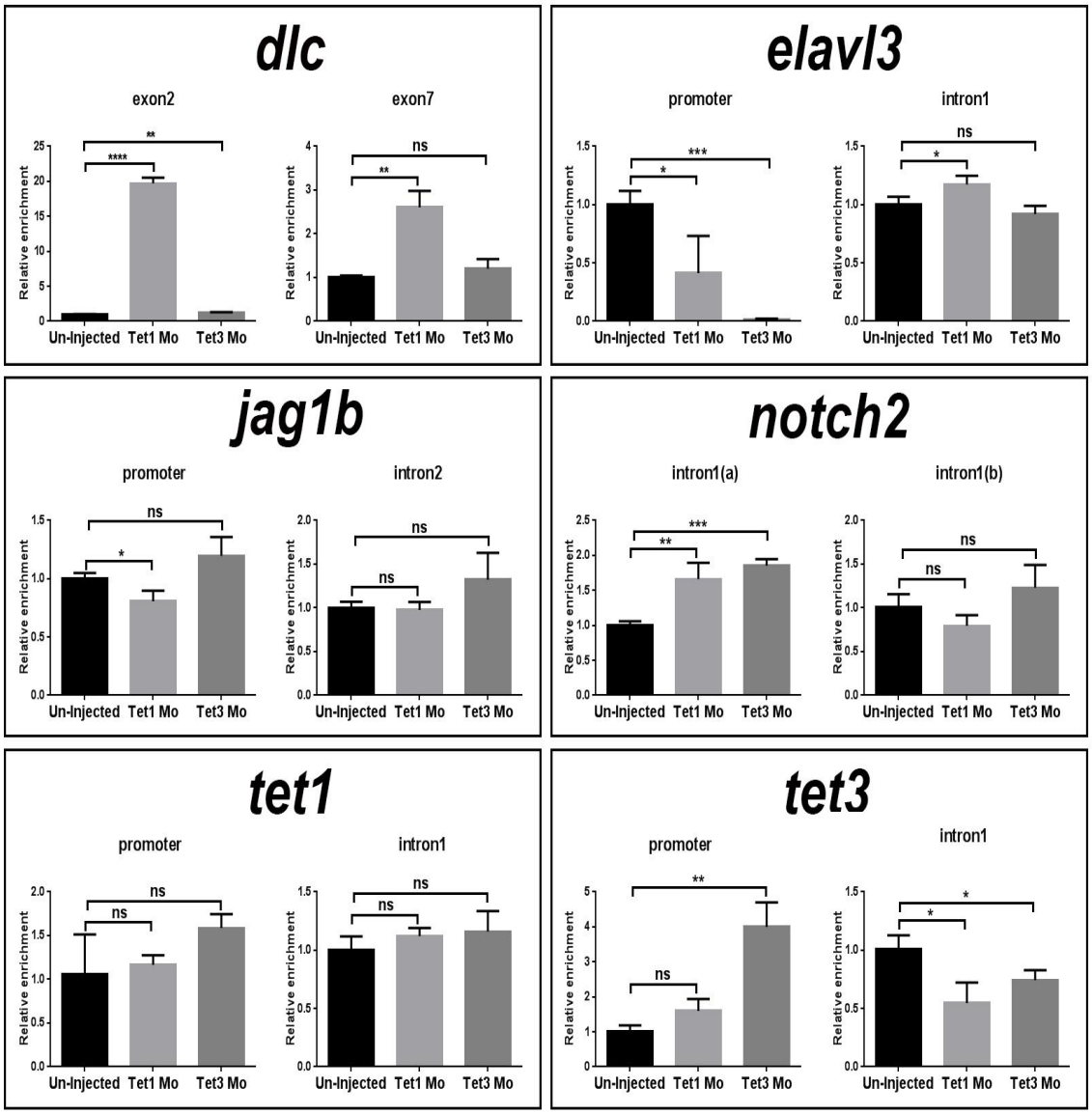

Figure 7.15 Real time PCR quantification results of 5hmC DNA immunoprecipitation (DIP) of indicated genomic regions in *tet1*, *tet3* morphants compared to their uninjected controls, all examined at 24 hpf.

Histograms showing relative enrichment values normalised to the DIP reactions without 5hmC antibodies. Significance was determined using student t test, **** p<0.0001; *** p<0.001; ** p< 0.01; * p< 0.05; ns – not significant.

7.8 Global 5hmC level dramatically decrease in *tet1* morphants

The very oxidized forms of the tet mediated 5mC modifications are the 5fC, and 5caC which are known targets for DNA repair enzymes such as the thymine-DNA glycosylase (Tdg) (Shen et al., 2013). The repair process is known as the base excision repair (Ber), and leads to excision 5fC or the 5caC and replacing them with un-methylated ones, as part of the active DNA demethylation. Based on *tet* dependence on presence of the Ber enzymes for active de-methylation, we expected the Tet and Ber enzymes to have a similar expression profile. When analysed, the zebrafish transcriptome data, we identified a number of Ber enzymes related transcripts (*gadd45g, lig3, pcna* and *tdg*) that showed expression profiles similar to that of *tet1/2/3* mRNAs, with their mRNA levels peaking during organogenesis stages between 24-48 hpf (Appendix 12, A).

We then wanted to investigate if individual or combined ablation of *tet1/tet3* in *tet* morphants can alter the global levels of the oxidized forms of 5mC in zebrafish embryos. For this, we examined fixed sections from these morphants by immuno-staining, and compared the results to uninjected control sections. The anti-5hmC, anti-5fC and anti-5caC antibodies used in the sensitive version of

immunochemistry, were the antibodies we previously used for detection of 5hmC in fish and mammalian tissues (Ruzov et al., 2011). Interestingly, unlike in human and mouse ESCs which showed decent staining for 5fC and 5caC (Appendix 13, B). Expression of these 5mC derivatives were un-detectable in zebrafish embryo sections taken at 24 hpf (Appendix 13: B). On the other hand, our immunostaining has shown a strong staining for the 5hmC mark and this mark is strongly reduced not only in combined *tet1/tet3* or *tet3* morphants that leads to reduction of *tet1* and *tet3* transcripts, but even individual *tet1* morphants show strong reduction in staining (Appendix 13: B).

To verify the immunostaining results and also to quantify the levels of 5hmC and 5mC in *tet1/tet3* morphants and compare them to those of uninjected controls, we submitted samples of the three groups for mass spectrometry. Consistent with our previous immunostaining findings, the 5hmC/5mC ratio was 6-7 times lower in both *tet1* and *tet3* morphants' DNA compared to their uninjected control, while no difference was reported in the 5mC levels between injected and uninjected embryos (Appendix 13, C-E). Surprisingly, despite the similarity in 5fC/5hmC ratios between the zebrafish embryonic DNA and mouse ESCs (mESCs) DNA, our results showed that the 5hmC and 5fC levels were approximately 10 times lower in zebrafish embryonic DNA compared to mESCs (Appendix 13, F).

7.9 Discussion of results

This chapter showed that injecting zebrafish embryos with morpholinos designed to block expression of tet1 or tet3 genes, but not tet2, leads to severe developmental defects soon after somitogenesis. Reproducing the same phenotypes with different morpholinos targeting non-overlapping sequences in the same genes strongly suggested that observed phenotypes were due to loss of tet1 or tet3 genes and not due to off-target effect. Observed phenotypes are also unlikely to be an apoptotic effect caused by injected morpholinos, as these phenotypes were maintained even with co-injecting the p53 morpholinos.

RT-PCR, gel analysis and sequencing all demonstrated that injecting tet1 and tet3 morpholinos lead to complete deletions of targeted exons, frame-shifts and the introduction of premature termination and production of truncated proteins that lack the functional Dioxygenase domain. To investigate if Tet1 and Tet3 enzymes act together or regulate one another, we quantified tet1 and tet3 mRNA both in tet1 and tet3 morphants and compared it to their uninjected siblings. Quantification RT-PCR results suggest that injecting tet1 morpholino leads to reduction of tet1 mRNA level and no effect on tet3, whereas injecting tet3 morpholino leads to reduction of both tet1 and tet3 transcripts. While these findings suggest that tet3 acts

upstream of tet1, it is essential to consider the possibility that mRNA alteration has resulted from the severely defected organogenesis

Utilizing our in-house Notch reporter, we presented both fluorescent microscopy and in situ hybridization data showing that blocking tet1 gene expression alters Notch activity in the developing embryo. This alteration appeared to be tet1 depletion-specific and did not result from developmental delays, as the expression pattern of the reporter gene does not match that of younger uninjected siblings. Unlike with tet1 morphants, expression of the reporter gene was indistinguishable from uninjected siblings in tet2 morphants, and completely lost in tet3 morphants.

To investigate if blocking tet1 affects normal embryonic neurogenesis, we performed in situ hybridization on tet1 depleted embryos and the results showed an up-regulation of the neural marker elavl3 when examined at 23hpf. Quantification of the 5hmC levels of selected Notch components, elavl3, tet1 and tet3 promoters in tet1 and tet3 morphants compared to their uninjected siblings was generally difficult to interpret, likely due to the abnormal development of tet1 and tet3 morphants. Interestingly, these data imply that loss of Tet1 or Tet3 led to a reduction in the 5hmC in elavl3 promoter.

Analysing the zebrafish transcriptome data showed that tet genes and several BER related enzymes have similar expression profiles, thus

cytosine de-methylation is likely to occur through a repair mechanism involving BER enzymes. Immunostaining and mass-spectrometry done on WT and tet1/tet3 morphants both showed clear 5hmC mark at 24hpf in WT embryos, and this mark sharply reduced with the combined or individual knock-down of tet1 or tet3 genes.

Together, our morpholino data showed an important rule for Tet proteins in zebrafish organogenesis. Our results also suggest that the proposed redundancy between different Tet enzymes in mice is not conserved in zebrafish. While our morpholino validation results and the dramatic decrease in 5hmC levels in these morphants suggest that observed phenotypes were specific to depletion of Tet1 or Tet3 enzymes, the possibility that observed phenotypes were resulting from morpholino non-specific toxicity cannot be excluded. Supporting mutants data is still necessary to assign observed findings to loss of tet1 and tet3 genes.

CHAPTER 8

8 Discussion

8.1 Analysing Notch activity during zebrafish early development

To improve our understanding of Notch requirement in haematopoietic stem cells development, we previously generated three transgenic lines that are identical in their structures but with different reporting fluorescent proteins, *Tg(csl:venus)*^{qmc61} *Tg(csl:cerulean)*^{qmc63} and *Tg(csl:mCherry)*^{qmc97}. Our careful analysis of fluorescent protein expression in these three lines showed that the reporter proteins in these three lines truly recapitulates tissues with Notch activities. This was based on the reporter genes reproducible expression in specific tissues such as the telencephalon, heart, dorsal aorta, neural tube and medial fin fold (Figure 3.3), some of which with previously known Notch activities, such as the developing central nervous system (Scheer et al., 2001). Moreover, the expression patterns seen in these lines were also identical to those in the Notch reporter lines developed and verified independently at the same period of time (Parsons et al., 2009).

We then utilised our in-house generated Notch reporter lines to profile Notch activities during zebrafish early development with the focus on the time point and the region where HSCs first appear in the embryo. Our analysis showed that the earliest zygotic Notch reporter mRNA

was detected in the neural tube at 8hpf, while the fluorescent protein become detectable three and a half hours later both in the hypochord and the developing somites. This delay in detecting the fluorescent protein can be attributed to the time required for accumulation and maturation of the synthesised protein to detectable levels. It was previously reporter that at least one hour is required for Gfp maturation at 37°C (Sniegowski et al., 2005). However, as zebrafish embryos are usually raised at 28.5°C, fluorescent protein maturation may take a longer period of time to become detectable in these embryos.

By 18hpf, we reported Notch activity in the arterial progenitor cells at the time of their arrival to the midline to form the dorsal aorta. Notch activity then appeared to increase in these cells after their gain of the arterial fate and continues to 26hpf (the time point at which haematopoietic stem cell precursors are starting to emerge from the dorsal aorta). On day 2 post fertilization, Notch activity sharply decreased in the arterial vasculatures to hardly detectable levels. Persistence of Notch signalling and its expansion after arterial fate determination further supports the concept of an additional role for Notch signalling in vascular maturation and haematopoietic stem cell development. Our data confirmed that the previously reported expression of Notch receptors and ligands in the DA principally leads to functioning Notch signalling.

Recently, a study published by the Lawson lab (Quillien et al., 2014), utilising a similar Notch reporter line also showed that Notch is active in the progenitor cells forming the developing DA, and that Notch activity increases after the time point of arterial specification. Quillien et al. (2014) also suggested persistence of Notch activity in the DA and arterial ISV based on persistence of the reporter Gfp fluorescent protein in these tissues. Unlike in the data of Quillien et al. (2014), our in situ hybridization data showed a sharp reduction in Notch activity in the DA and arterial ISV (Figure 3.7). The observed difference between our findings and those of Quillien et al. (2014) data may be resulting from the fact that in our in situ data, we examined the mRNA, which is less stable and appears earlier than the reporter fluorescent protein.

On the other hand, Quillien et al. (2014), examined the persistence of the highly stable reporter fluorescent protein on day 7 post fertilisation. This makes it unsurprising to detect the accumulated stable fluorescent protein from the basal level expression and its detection with normal or confocal microscopy. The authors also suggested that arterial and haematopoietic progenitor cells have Notch activity well before their arrival to the midline to form the DA. They provided a double in situ data showing an overlap between the Notch reporter mRNA and the endothelial marker *etv2* mRNA at early somitogenesis. Their findings also were supported by the proposed expression of *dlc* in these migrating progenitor cells (Smithers et al.,

2000). Consistent with Quillien et al. (2014) data, our ability to detect the Notch reporter protein in the cells forming the developing DA at 18hpf also indirectly suggests that Notch activity must have initiated in these progenitor cells at least 3-4 hours earlier, i.e. around 14hpf. However, our indirect observation and the double in situ data from Quillien et al. (2014) do not conclusively show co-localization within single cells, leaving the possibility that Notch activation is occurring in adjacent cells.

Therefore, a more conclusive experiment may be desirable to clearly determine when Notch signalling becomes active in these progenitor cells. Recent advances in single cell transcriptome analysis enabled a higher degree of resolution that make it possible to study individual cell fates as soon as they are acquired. Applying these techniques on individual cells sorted with the help of an endothelial reporter fluorescent protein at early somitogenesis. Analysing these cells for the Notch reporter gene mRNA, could provide a direct and powerful evidence for Notch activity in these progenitor cells during early somitogenesis.

8.2 High level of Notch is required for *flt4* suppression and HSCs formation in the DA whereas low level is sufficient for arterial specification

Previously, it was suggested by Lawson et al. (2001) that a major role of Notch signalling in the DA at the time point of HSC formation, is to repress the venous fate of the developing DA by repressing *flt4* expression. We, and others, have also shown that the whole embryo Notch over-activation with the Gal4-Uas system, suppress *flt4* expression in the CV and expands both arterial and haematopoietic markers such as *efnb2a*, *runx1* and *c-myb* in these tissues (Rowlinson, 2010, Lawson et al., 2001, Lawson et al., 2002). In agreement with these findings, we reported in Chapter 3 an up-regulation in Notch signalling in the DA after arterial fate determination. In Chapter 4 we also showed that the venous marker *flt4* is expressed in the developing DA at 18-20hpf at high level.

This high *flt4* coincides with low Notch activity as indicated by low level of the reporter fluorescent protein in our reporter lines. As the Notch activity become higher in the DA at 24h, we found that *flt4* expression become much weaker and completely disappears from the DA by 26hpf. This up-regulation was also confirmed in our lab at the mRNA level by RT-PCR experiments performed on FAC-sorted *flk1:gfp* positive trunk endothelial cells (Modhara, 2014). These data strongly suggest that high levels of Notch are required to suppress

flt4 expression in the DA to allow HSC development. In addition, the fact that residual Notch signalling in DAPM-treated embryos was sufficient to support the arterial fate as determined by *efnb2a* expression, but was not adequate to suppress *flt4* expression in the DA further support this hypothesis.

On the other hand, we found that with the more efficient Notch blocking approaches, such as mib mutation and *rbpja/b* morpholinos, even arterial specification was blocked. In line with this, a former PhD student in our lab also reported a morpholino study showing that blocking individual Notch receptors that are dominantly expressed in the DA (*notch1a, notch1b and notch3*) lead either to severe reduction or complete loss of the haematopoietic program in the embryo, with intact or minimally reduced arterial specification. On the other hand, complete deletion of the three Notch receptors blocked both arterial and haematopoietic programs (Rowlinson, 2010).

Recently, a similar study was carried out, but with the main focus on arterial specification (Quillien et al., 2014), which showed no significant reduction in Notch activity in developing DA with individual morpholino knockdown of *notch1a* and *notch1b* or minimal and temporary reduction with *notch3* knockdown (that was mostly restored by 24hpf). Quillien et al. (2014) also reported a severe reduction in the arterial marker *efnb2a* expression when injected the *notch3* mutants with the *notch1b* morpholinos, and less severe

reduction with injecting the combined *notch1a* and *notch1b* morpholinos. The Quillien et al. (2014) data, despite its slight discrepancy with our findings, does not exclude the possibility that a low level of Notch is sufficient to support arterial specification. This slight discrepancy, possibly due to blocking *notch1b* in *notch3* mutant background, that is expected to be more efficient than our injection of *notch1b* and *notch3* morpholinos, and there is also a possibility of injecting slightly different dosages of the combined *notch1a/notch1b* morpholinos in the Quillien et al. (2014) work.

Together our findings provide a possible explanation to one of the fundamental questions in the field about how Notch signalling pathway differently affects arterial specification and haematopoietic stem cells development. In the mouse animal model, it was hypothesised that specific Notch receptors and ligands are required for HSCs development. This hypothesis was mainly based on the *jagged1* loss of function experiment reported by Robert-Moreno et al. (2008). In this experiment, the authors showed a complete or severe reduction *gata2* and *runx1* expression following deletion of *jagged1* ligands, without affecting the arterial program. They also found that this loss can be rescued by co-culturing these cells with *jagged1* expressing stromal cells.

A similar loss of function experiment was also recently reproduced in zebrafish by the Traver Lab (Espin-Palazon et al., 2014). In this

study, it was also shown that loss of *jag1a* leads to decrease in HSC numbers as determined by the reduction in the *runx1* expressing cells in the DA. The other interpretation of the data provided by Robert-Moreno et al. (2008) and Espin-Palazon et al. (2014) in light of our work is that the residual Notch signalling provided by the remaining Notch components after deleting *jagged1* in the mouse or *jag1a* in the zebrafish was sufficient to support arterial specification. However, this low remaining signalling was below the level required for initiating the definitive haematopoietic program in the embryo. Furthermore, to our knowledge there are no published studies demonstrating that Jagged1 is an obligate ligand for any of the Notch receptors. Conversely, in mammalian cell culture, it was shown that Delta and Jagged ligands can bind Notch1 and Notch3 receptors interchangeably, and thus suggesting that binding between Notch receptors and ligands is promiscuous (Shimizu et al., 2000).

8.3 Studying the cell autonomous requirements for Notch in zebrafish definitive haematopoiesis

Notch signalling was demonstrated to be absolutely required for HSC formation in all studied vertebrates (Burns et al., 2005, Hadland et al., 2004, Krebs et al., 2000, Kumano et al., 2003, Robert-Moreno et al., 2008, Robert-Moreno et al., 2005, Yoon et al., 2008), but whether this requirement was cell autonomous or non-cell-autonomous

initially remained unclear. To determine the source of this Notch signal Hadland et al. (2004) generated mouse chimera with notch1 $^{-/-}$ cells and found that notch deficient cells lack the ability to contribute to HSCs. Based on these findings, it was presumed that the requirements for Notch are solely cell autonomous. Because this study did not show at which developmental stage Notch is required, or whether signalling from other tissues are also involved in the process. For this, several other endothelial specific Notch loss/gain of function studies were carried out to further confirm the findings of Hadland et al. (2004) and to determine when Notch is required in this tissues.

Nonetheless, these studies were hampered by the severe complications on blood circulation after mis-expressing Notch pathway in the endothelium. Unlike in mouse, zebrafish embryos can survive for days with non-functioning blood circulation, which makes them an attractive complement animal model to study HSCs development. However, several molecular tools available in the mouse model were still not established for zebrafish. One of the issues with the zebrafish model is the lack of a ubiquitous promoter comparable to the mouse *rosa26* (Mosimann et al., 2011).

In Chapter 5, we tried to optimise the currently available molecular tools to enable efficient and reliable endothelial specific over-activation/blocking of Notch signalling in stable transgenic lines. The

main obstacles faced in developing these tools were firstly, the complications associated with the *polyA* transcription termination signal read-through, and consequently the early death of embryos in which the constructs were integrated in supportive genomic regions. Read-through the *polyA* transcription termination signal has been previously reported (Maxwell et al., 1989). One strategy to overcome the previously reported read-trough the *pA* problem is to add multiple SV40 *polyA* repeats at the 3′ end of the floxed cassettes. This provided tighter spatial and temporal controls, and enabled generating transgenic lines with incorporated toxic or oncogenes. Utilising this approach Jackson et al. (2001) generated a floxed super-stop cassette made of four SV40 *polyA* signals, and were able to study involvement of the oncogene *k-ras* in lung tumour initiation and progression. We utilised the Jackson et al. (2001) cassette to over-come the read-through and generated effector transgenic lines floxed super-stop cassettes.

The other complication we faced was the weak activity of the *ef1α* promoter in driving the *nicd* or the *dnRbpj* expression in the endothelium after recombination. Mosimann et al. (2011) reported isolation and characterisation of the zebrafish ubiquitin promoter (*ubi*), which they showed to be constitutively expressed in all developmental stages, including all blood lineages. To further enhance our effector lines, we also replaced the *ef1α* promoters in our constructs with the *ubi* promoter then generated new effector

lines with these modified constructs. Our data suggests that even with the *ubi* promoter the expression of *nicd* or *dnRbpj* were still tolerated by the embryos, as the embryos appeared completely normal and in distinguishable from their WT siblings.

Mosimann et al. (2013) showed that *ubi* promoter driven expression pattern can vary significantly due to the location in which it is inserted in the genome. They even showed that in two lines generated by the same construct, a complete silencing for *gfp* expression in haematopoietic cells at adulthood in one line, while *gfp* expression was maintained in the haematopoietic cells in the other. We and others, have previously shown that implementing the binary Gal4-Uas system efficiently amplifys the amount of over-expressed *nicd* in the whole embryo to a level sufficient to expand the HSCs markers *runx1 and c-myb* (Rowlinson and Gering, 2010, Burns et al., 2005). In this thesis, we demonstrated that combining the Gal4-Uas system with the Cre/LoxP system provided a powerful tool to mis-express Notch signalling in targeted tissue.

In our generated quadruple transgenic embryos we showed that by expressing the *cre recombinase* gene under control of the *flk1* promoter, we were able to excise the floxed super stop cassette, and so limit activation of the Gal4-Uas system and accompanied Notch over-activation to the endothelium, which was confirmed by the significant up-regulation of the reporter fluorescent protein

expression. Consistent with Siekmann and Lawson (2007), we found that over-activating Notch in the endothelium does block tip cell formation, indicated by cell failure in forming the DLAV, and instead arterial endothelial cells were preferentially located in the dorsal aorta or the base cell of the developing arterial ISV. Unlike with whole embryo over-activation, previously shown to repress *flt4* expression in the CV (Lawson et al., 2001), *flt4* expression in the CV was not affected. This is likely due to the lower *flk1* activity in the endothelial cells forming the CV, compared to cells forming the DA (Sumoy et al., 1997, Kohli et al., 2013).

One of the issues we also reported in this work was the likely toxic effect resulting from the Gal4-vp16 accumulation in the endothelium, which we found to lead to late vascular defects and lack of blood circulation. It was previously proposed that accumulating high intercellular levels of the Gal4-vp16 can interfere with the cellular transcriptional machinery in yeast and mammalian cell culture (Gilbert and Glynias, 1993, Sadowski et al., 1988, Triezenberg et al., 1988). Consistent with that, we hypothesised that the observed late defect in blood circulation, and also lack of HSCs markers *runx1* and *c-myb,* were due to the accumulation of high levels of Gal4-vp16 in these cells. Our data also suggest that endothelial Notch over-activation partially rescues the hematopoietic defects in these embryos. Moreover, we found that truncating the last 20 amino acids of the VP16 activating domain as previously employed (Davison et

al., 2007, Inbal et al., 2006, Koster and Fraser, 2001, Sagasti et al., 2005, Scott et al., 2007)

Addition of temporal control, by replacing the *ubi* promoter with the heat shock promoter in the effector line, significantly delays the transcriptional interference resulting from Gal4-vp16 protein accumulation in the cells. This contributed to developing a strategy by which we over-activated Notch in the endothelium and moderately enhanced *runx1* and *c-myb* expression in the DA aorta and the CHT. The fact that *gfi1.1* expression persisted until day 2 in the DA also suggests that these cells failed to differentiate and leave the DA. In recent work done by the Jafferdo lab, it was shown in chicken embryo, that temporally restricted decrease in Notch signalling is critical for HSCs emergence from the haemogenic endothelium (Drevon and Jaffredo, 2014).

We also showed that transient gene expression under control of the minimal *flk1* or *fli1* promoters, due to the high copy number of injected plasmids led to a strong endothelial specific Notch induction, indicated by the strong expression of the fused *gfp*. This strong up-regulation appeared to be essential for the endothelial to haematopoietic transition, whereas the sharp decrease in later time points indicated by loss of the *gfp* expression, due to rapid cell division and foreign DNA degradation, allowed the fated HSCs to differentiate into mature HSCs that are able to leave the vDA and

seed the CHT. Together, we demonstrated for the first time in the zebrafish animal model that cell autonomous Notch induction is sufficient to expand HSCs markers expression in the DA and the CHT.

Collectively, our data demonstrate that endothelial specific Notch induction is sufficient to expand haematopoietic stem cell markers in the DA and the CHT. We also showed that a high transient Notch signal is required to initiate the HSCs fate, followed by a low Notch signal to enable HSC differentiation into mature cells that are able to leave the DA and seed the CHT. These data represent the first demonstration, to our knowledge, that cell autonomous Notch signalling in vivo is sufficient to expand HSC formation in vertebrates.

In the last four years, an intensive work was carried out in several labs to analyse the non-cell autonomous requirements for Notch in definitive haematopoiesis proposed by (Clements et al., 2011). These efforts have not only confirmed existence of such requirements, but also suggested several pathways and intermediate factors to transmit or facilitate transmission of these signals to the developing DA (reviewed in chapter 1). In our study, we showed that up-regulation of the cell autonomous Notch in the context of normal non-cell autonomous Notch signalling is sufficient to expand the zebrafish haematopoietic stem cells both in the DA and the CHT. What is still to be shown is whether up-regulation of the cell autonomous Notch

in absence of non-cell autonomous signalling is still sufficient to lead to the same expansion.

It is still not clear if up-regulation of the somatic Notch signalling will lead to similar expansion in absence of normal cell autonomous Notch signal. Several molecular tools are currently available to address these questions, like the phldb1 and pax3a promoters that were shown to drive expression of downstream genes, specifically in zebrafish somites (Kim et al., 2014, Nguyen et al., 2014). Somitic contribution to the zebrafish DA endothelium suggested by (Nguyen et al., 2014) and shown to be essential to HSCs development added another layer of non-cell autonomous requirement for Notch, in which Notch signalling contributes to maturation and specification of these migrating endothelial cells. Even though these cells do not directly contribute to formed HSCs, in light of our findings, it is still to be determined if the Notch activity in somite derived endothelial cells contributes to overall Notch level in the DA.

Fgf signalling was also recently shown to act upstream of the Bmp signalling in the mesenchyme beneath the DA and shown to be essential for polarizing HSCs formation (Wilkinson et al., 2009, Pouget et al., 2014). Fgf also mediates the signalling between the somitic Wnt16 and the Dlc to regulate HSCs specification in the non-cell autonomous Wnt16/Dlc;Dld pathway (Wilkinson et al., 2009, Pouget et al., 2014, Lee et al., 2014). Because proper somitic Fgf

signalling requires correctly differentiated somites, which are also Notch dependent, it is still not clear to what extent the Notch dependent somitic maturation affects HSCs specification. Putting our findings in the context of recently gained knowledge about the non-cell autonomous rules for Notch in definitive haematopoiesis, it is possible that proper somitic Notch signalling is a pre-requisite for the observed HSCs expansion in our study. More advanced experiments, utilizing currently available somite and endothelial specific promoters, may provide further insight into the degree of cooperation and coordination between the two signalling pathways to instruct HSCs program.

8.4 *tet1* and *tet3* deletion abolishes organogenesis and leads to decrease in global 5-hydroxymethylcytosine content in zebrafish

From previous work performed by the Ruzov lab with collaboration from our lab, we showed that the 5hmC enrichment of non-committed cells is not a universal feature in vertebrate development (Almeida et al., 2012). Unlike in mammals, 5hmC enrichment in chick and zebrafish only take place later in development in a stage coinciding with the onset of organogenesis. We also showed that whereas Tet genes are highly expressed in the mammalian zygotic stage, they are undetectable in in the zebrafish or chick zygotes. Interestingly, both Tet1/2/3 mRNAs and 5hmC peak during zebrafish

organogenesis at 24-48 hpf, which suggests that Tet-dependent 5mC oxidation may be important for cell lineage specification and differentiation occurring at these developmental time points.

Other indications of methylation mark involvement in zebrafish organogenesis came the fact that blocking the enzymes required for maintaining DNA methylation, such as the DNA methyltransferase Dnmt1 or Dnmt3, interferes with the normal organ specification of various tissues. This includes defects in eye development, intestinal development and brain development (Rai et al., 2006; Anderson et al., 2009; Tittle et al., 2011; Rai et al., 2010; Seritrakul et al., 2014). In consistence with the findings of the Ruzov lab, several other studies also reported a strong DNA demethylation taking place in the developmental window corresponding to organogenesis and Tet genes expression (Collas 1998, Rai et al., 2008). To test whether the Tet dependent DNA demethylation is essential for proper organogenesis, former student in our lab (Sabrina Boudon) blocked expression of the Tet genes during early development with anti-sense morpholinos.

Because the morpholinos were designed to target the catalytic C-terminal of the dioxygenase domain in the three tet genes, they are expected to lead to frame-shifts and premature termination of their transcripts. In consistence with this, we observed severe defects in organogenesis and developmental arrest after somitogenesis

initiation in *tet1* and *tet3* morphants, whereas Tet2 morphants appeared normal until day3. These phenotypes were associated with deletion of *tet* genes targeted exons, as demonstrated by the shift in PCR amplified fragments with primers targeting the sequences outside these exons. Sequencing results of these fragments also confirmed the complete deletion of targeted *tet1* and *tet3* exons and the introduction of frame shifts and premature translation terminations, as predicted. We also showed that targeting different exons in *tet1* and *tet3* transcripts also produced phenotypes identical to those observed in the preliminary data, and that these phenotypes persist even with *p53* morpholino co-injection. Together these findings strongly suggest that observed phenotypes were specific to morpholino injections and not were due to non-specific complication resulting from morpholino toxicity.

The immune-staining and mass spectrometry results also showed a dramatic decrease in global 5hmC levels in both *tet1* and *tet3* morphants compared to uninjected controls when examined at 24hpf, which strongly suggests that cell lineage fates determination during organogenesis were controlled by Tet dependent DNA demethylation. In mouse, it was reported that blocking *tet1* expression alters the normal neurogenesis (Zhang et al., 2013). This *tet1* induced alteration in neurogenesis was also found to be accompanied by failure in demethylating number of promoters involved in the proliferation of neural progenitor cells. Correspondingly, we observed

severe neurological abnormalities in *tet1* morphant embryos. These abnormalities include alteration in Notch signalling as reflected by alteration in Notch activity in these morphants. We also found that expression of the neural marker *elavl3* was significantly altered when examined at 23 hpf. Interestingly, these neurological alterations were found to coincide with the time point when *tet1* become highly active in WT, thus suggesting *tet1* dependent demethylation, and activation of these promoters, in similar manner to that reported in mouse.

In a recent methylome study of different human tissues, it was also suggested that DNA methylation may provide an additional layer of control on Notch signalling. The newly proposed Notch control is thought to be Tet dependent, and take place through alteration of the methylation marks within or near the Notch receptors and ligands promoters, which eventually alters the expression pattern of the targeted gene (Terragni et al., 2014, Tsumagari et al., 2013). To investigate the regulatory roles for the Tet genes on Notch activity during early development, we injected the *tet1* morpholinos to our in-house generated Notch reporter line *Tg(csl:venus)*^{qmc61}, and examined the expression pattern of the reporter gene and also the expression pattern of several Notch components and downstream targets at different time points in these injected morphants.

In agreement with our microscopic observations, in which we reported normal embryonic development until early somitogenesis, the expression pattern of the Notch reporter and examined Notch

components and downstream targets appeared indistinguishable from their uninjected siblings. However, we found significant changes in the expression pattern of these genes when examined at 23hpf, which strongly suggests a Tet1 depletion dependent mis-regulation of the Notch signalling pathway. Despite this, caution must be taken in interpreting these data, as it is still possible that observed alteration in Notch activity was a complication associated with failure in tissue formation in these embryos rather than being caused by an alteration in Notch activity downstream of Tet1. The low levels of 5fC/5caC in zebrafish embryos at 24 hpf relative to mouse ESC also suggests that unlike in mouse, the early zebrafish development may be mainly dependent on passive DNA demethylation, as Dnmt1 poorly recognise and bind 5hmC (Valinluck and Sowers, 2007). This in turn prohibits the maintenance of existing DNA methylation patterns in the zebrafish actively dividing cells at early stages of development.

Unlike in the mouse where a high degree of redundancy between the three Tet proteins was demonstrated (Dawlaty et al., 2013), in this study we reported a low redundancy between Tet1 and Tet3 in zebrafish. Interestingly, zebrafish Tet3 protein also lacks the CXXC domain present in mammalian and Xenopus Tet3 proteins, which was shown to play critical role in specific Tet3 targeting (Xu et al., 2012). It can therefore be assumed that the zebrafish Tet3 utilises a different targeting mechanism from those in frogs and mammals, which may

account for the absence of redundancy between Tet1 and Tet3 in zebrafish.

In a recent work from the Goll Lab, zebrafish mutants for the three tet genes were generated and examined in single, double and triple mutant genotypes. Unlike in our study, organogenesis appeared unaffected in individual or combined homozygous mutation of tet1, tet2, or tet3 (Li et al., 2015). The discrepancy between our tet1 and tet3 morpholino knock-down results and those of Li et al. (2015) is possibly due to the fact that the targeted loci in their mutants were at the ends of tet1 and tet3 genes, which leaves most of these genes unaffected. Even though the authors predicted that deletion of the Dioxygenase arginine c-terminal residue compromised their Dioxygenase activity, it is possible that the produced terminally truncated Tet1 and Tet3 proteins were still partially active. Moreover, it has been recently reported that zebrafish mutants generated by any of the currently available genome editing tools, such as TALENs and CRISPRs, can compensate for mutated genes, by fine-tuning their transcriptomes (Rossi et al., 2015).

To demonstrate this compensation and its contribution to the inconsistency between the egfl7 mutants and egfl7 morphants, Rossi et al. (2015) generated a mutant for egfl7 with the use of TALENs technology and also designed morpholinos for the same gene through. They then injected similar amounts of egfl7 morpholinos to

a batch of egfl7 mutants and a batch of WT embryos and found that while egfl7 has no effect on egfl7 mutants, a clear vascular phenotype was observed in WT embryos. Tracing possible mechanisms of compensation in these mutants, the authors identified a clear upregulation of several members of the emilin gene family, which shares an important functional domain with the egfl7, which may be responsible for this compensation.

On the other hand, the possibility of an off-target effect caused by the morpholinos used in our study cannot be excluded. Toxicity due to off-target effects can be resulting from morpholinos activation or blocking of other genes, such as those resulting from activation of the apoptotic p53 gene, induction of Interferon response, activation of Toll-like receptors and compromising the RNA interference machinery (Anon, 2006, Robu et al., 2007). In a study performed by the Lawson Lab that involved generating a megamind mutant that appeared normal despite of deletion of most of the megamind genomic sequence, including a target sequence of previously published morpholinos shown to lead to clearly distinct phenotypes when used to block the same gene (Ulitsky et al., 2011). Surprisingly, injecting same morpholino to the generated megamind mutant embryos was shown to produce the same phenotypes in the mutants, despite the absence of the morpholino target site in their genomic sequences (Kok et al., 2015).

In summary, gene knock-down by mutating targeted genes or silencing their expression with anti-sense morpholinos both have inherent limitations that sometimes lead to inconsistencies between the gene knock-down results obtained by the two strategies. Therefore, it is desirable to reproduce morpholinos results in mutants that lack the same morpholino targeted genes, whenever possible, before assigning specific functions for that gene.

8.5 Future perspectives

In this project we presented data suggesting that Notch activity initiates in the migrating hECs progenitors before their arrival to the midline to form the DA. Based on these data it would be of great value to confirm these findings at a single cell level by FACS sorting trunk endothelial cells of Notch reporter embryos at early somitogenesis, then quantifying the Notch reporter mRNA in these cells compared to their controls. We have also generated several transgenic lines and constructs to mis-express Notch signalling in the endothelium and showed expansion of HSCs markers in the DA and the CHT, yet it would be of great value to examine their ability to seed the kidney and the thymus, and also to see if they can reconstitute the zebrafish haematopoietic system.

Our *tet* morpholino studies showed an essential role for Tet1 and Tet3 in organogenesis. To confirm these morpholino data, Dr. Martin

Gering and the summer student working in our Lab designed CRISPRs guide RNA which targets the same exons we targeted in the morpholino injections. Deleting these exons in F0 embryos or in stable mutant lines and carefully analysing them and also comparing their phenotypes to the morpholino phenotypes will greatly expand our understanding of *tet* genes involvement in organogenesis.

APPENDICES

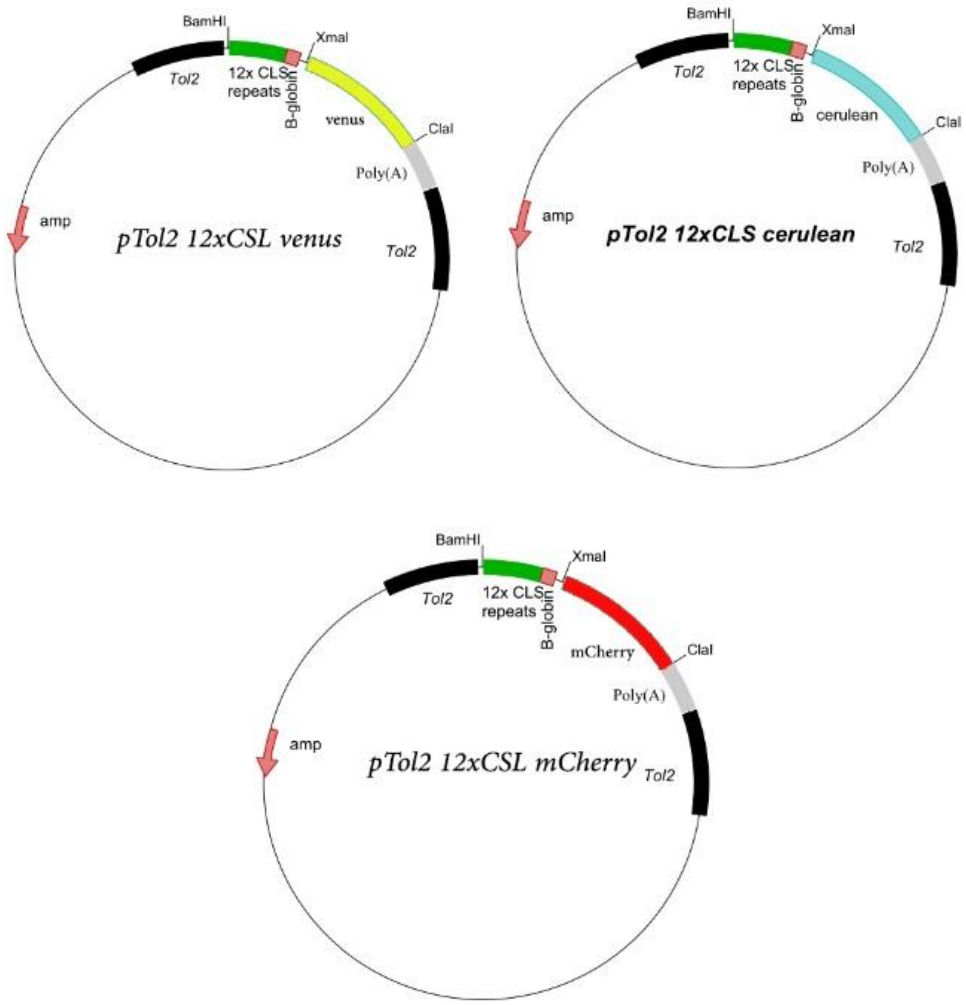

Appendix 1: Tol2 plasmids generated and injected to generate the Notch reporter lines.

Diagrams of the three plasmid constructs generated and injected to establish the three Notch reporter lines. The three constructs are identical in their tol2 back bone structure and regulatory elements but with different fluorescent protein gene downstream of the regulatory elements, with venus gene in the first, cerulean gene in the second and mCherry in the third.

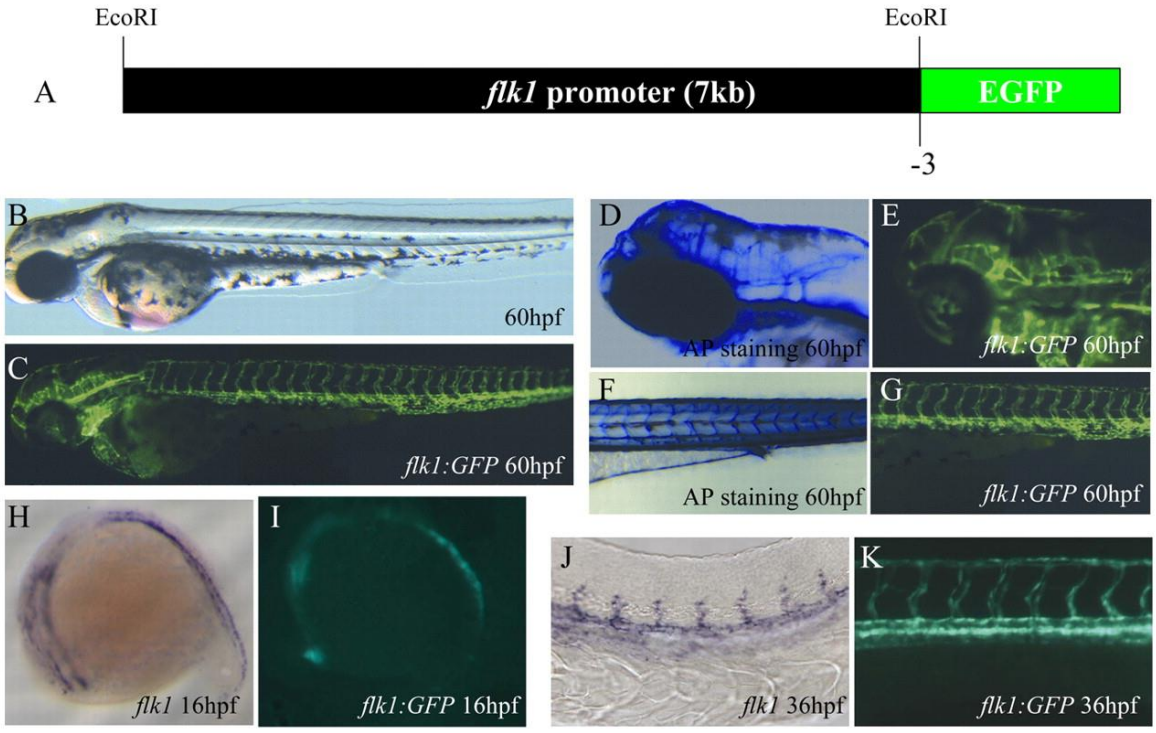

Appendix 2: GFP expression driven by the *flk1* promoter in *Tg(flk1:EGFP)s843* line recapitulates endogenous *flk1* expression.

(A) Diagram showing the injected construct in which the 6.5 kb upstream sequence of zebrafish *flk1* was used to drive GFP fluorescent protein expression in the *Tg(flk1:EGFP)s843* line. (B-C) Same embryo imaged at 60hpf under bright-field (B) and fluorescent microscopy, in which head and trunk vasculature were specifically highlighted by the GFP fluorescent protein (C). (D-G) Show head vasculature (D) and trunk vasculature (F) at 60 hpf embryos stained by endogenous alkaline phosphatase (AP) activity compared to fluorescently labelled head (E) and trunk (G) vasculature of similar areas in a *Tg(flk1:EGFP)s843* embryo. (H,J) endogenous *flk1* expression detected by In situ hybridization at 16hpf (H) and 36hpf (J) compared to GFP expression in *Tg(flk1:EGFP)s843* embryos at similar stages and similar areas (I,K) visualized by fluorescent microscopy. Source: adapted from Jin et al. (2005).

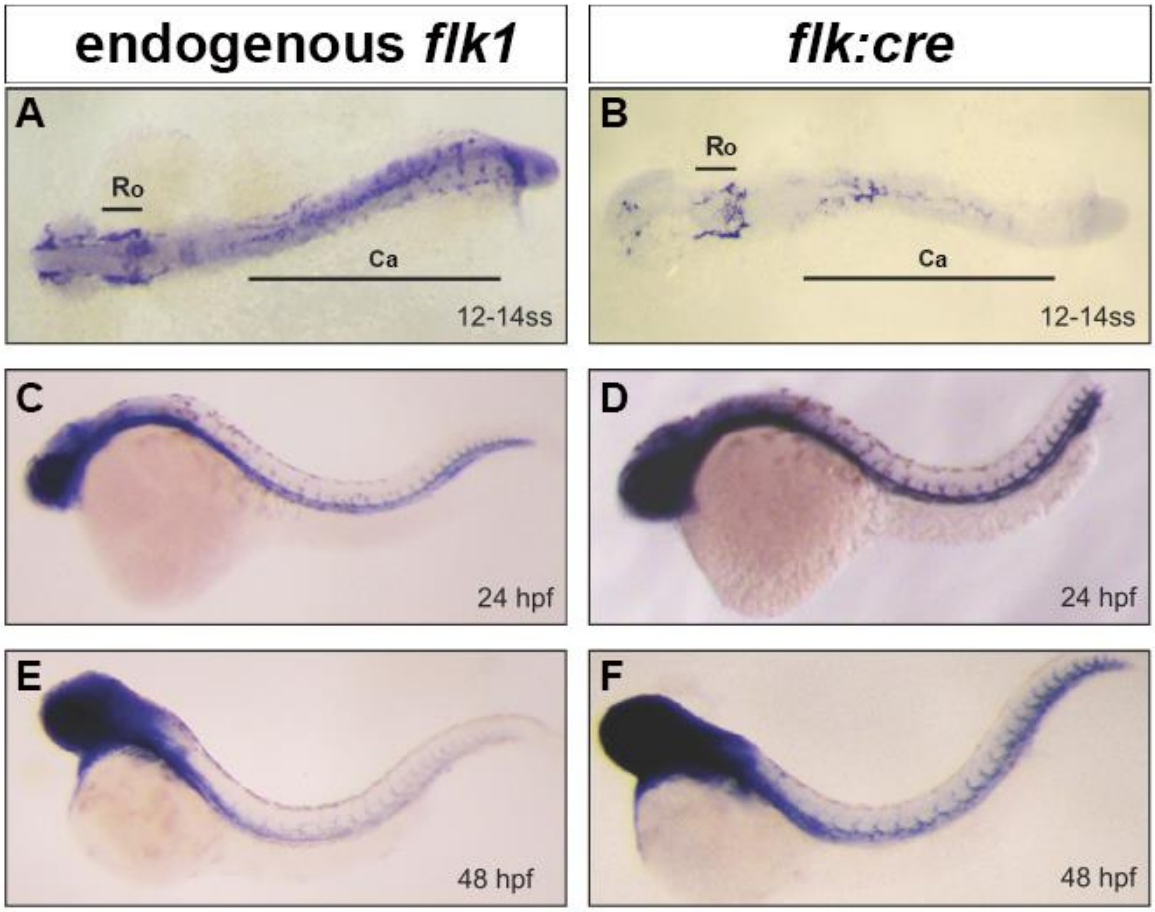

Appendix3: Cre expression driven by the *flk1* promoter in *Tg(flk1:cre) s898* line recapitulates endogenous *flk1* expression.

Whole mount in situ hybridization of endogenous flk1 expression (A,C,E)compared to cre recombinase expression in Tg(flk1:cre) s898 line (B,D,F). (A-B) Expression of both transcripts are visible in rostral tissues (Ro), in the area where primitive macrophages first appear in the embryo, and also in the caudal tissues (Ca), in the area where primitive erythrocytes, HSCs, and EMPs first appear in the embryo. (C-F) Both endogenous flk1 and flk1:cre are similar in their expression in cells of the developing vasculature. Source: (adapted from Bertrand et al., 2010).

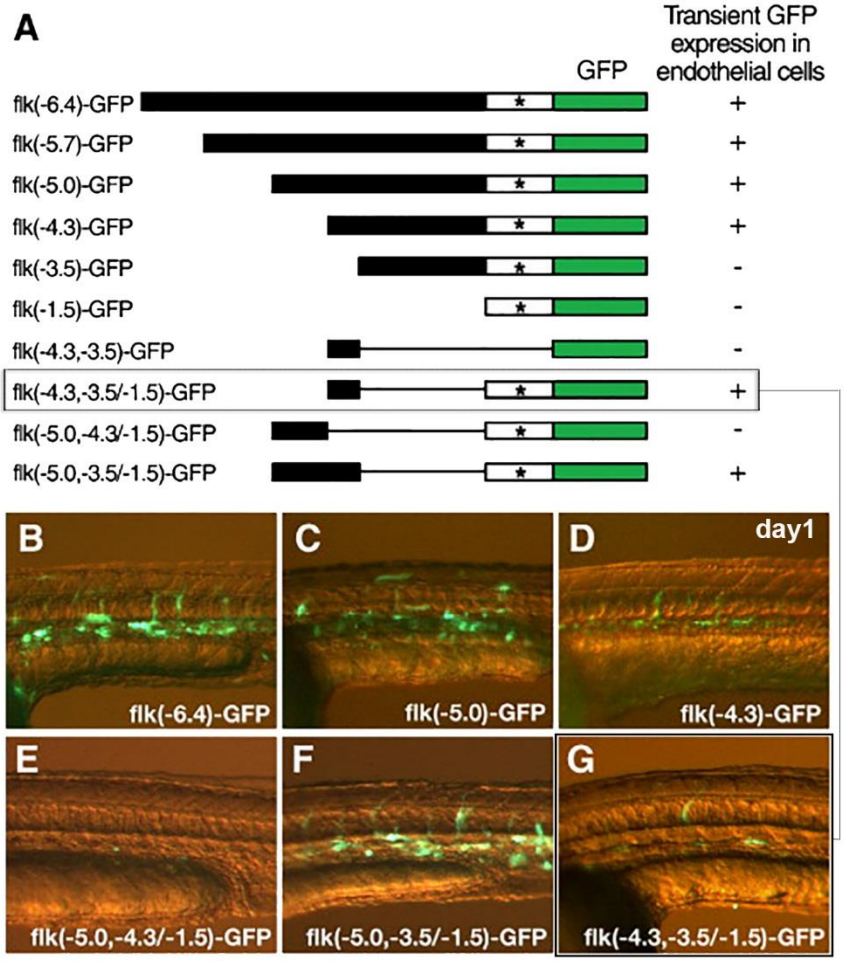

Appendix 4: Identification of the minimal *flk1* promoter.
(A) Diagram showing structures of generated deletion constructs of *flk1:GFP* and summary of their ability to drive endothelial specific GFP expression as indicated by the + and – signs (* marks the transcription initiation site of *flk1*). (B-G) fluorescent microscopy images of 1-day-old WT embryos injected with the linearized DNA of constructs as described in each image. A strong endothelial restricted *GFP* expression was observed with the full *flk1*(−6.5)-*GFP* (B), *flk1*(−5.0)-*GFP* (C) and *flk1*(−5.0,−3.5/−1.5)-*GFP* (F). A weaker but endothelial specific *GFP* expression was also observed with the construct *flk1*(−4.3)-*GFP* (D), and also with the *flk1*(−4.3,−3.5/−1.5)-*GFP* (G). While no *GFP* expression was observed with the *flk1*(−5.0,−4.3/−1.5)-*GFP* (E). The highlighted parts of the figure are the minimal *flk1* promoter construct and its expression pattern. Source: (adapted from Choi et al., 2007).

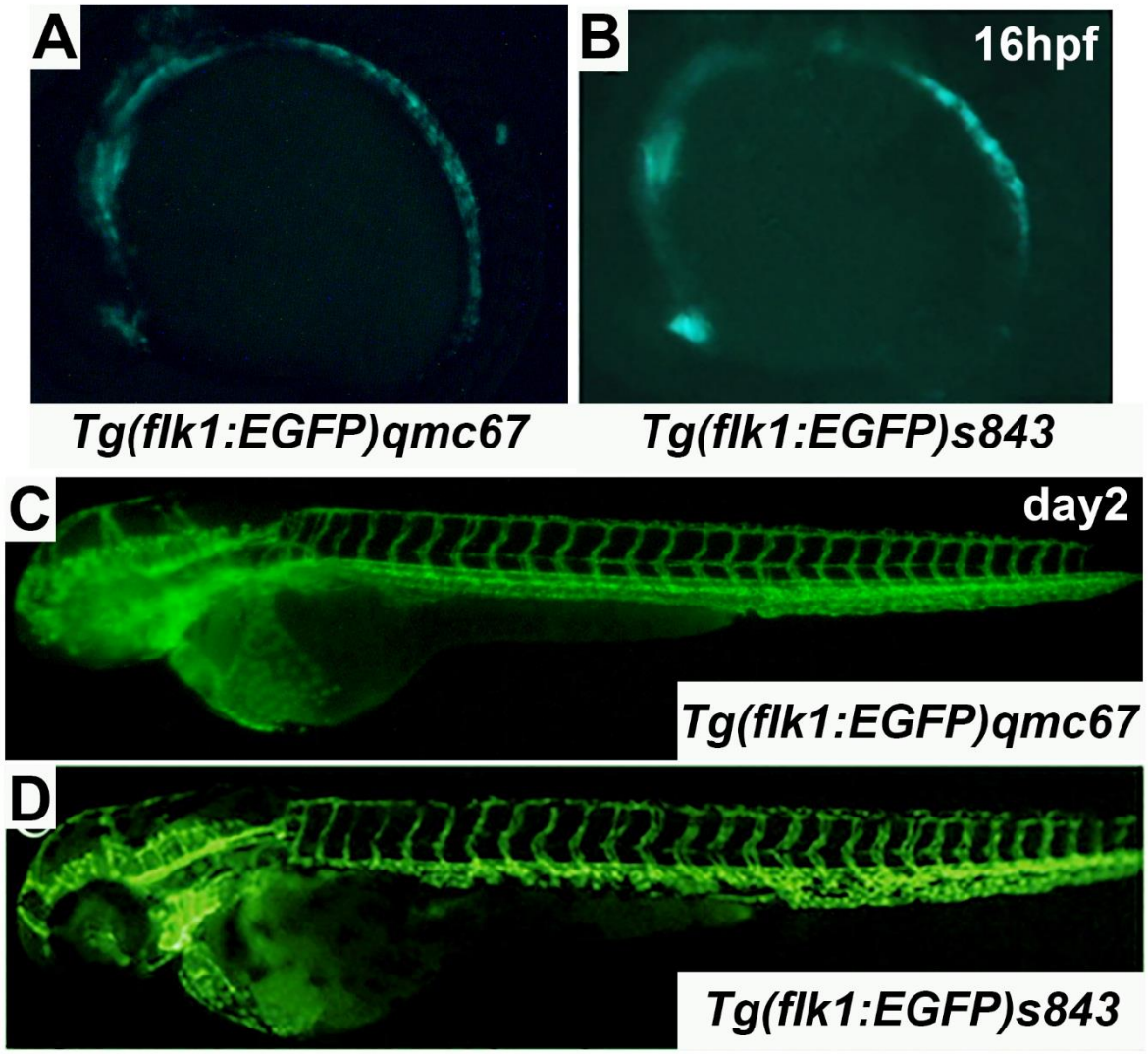

Appendix 5: Minimal and full *flk1* promoters drives identical expression pattern in stable reporter transgenic lines.
(A, C) *gfp* expression driven by the minimal *flk1* promoter in our in-house *Tg(flk:gfp)qmc67* is identical to expression driven by the full (6.5kb) flk1 promoter fragment in Jin et al. (2005) line, *Tg(flk1:gfp)s843 (B, D)*. (A-B) *gfp* expression become detectable in the migrating endothelial progenitors migrating to the mid-line to form the main axial vessels. (C-D) *gfp* expression persists in the endothelium of axial and ISVs till late developmental stages. Source (images (B,D) adapted from (Jin et al., 2005), images (A,C) from Gering lab, unpublished data).

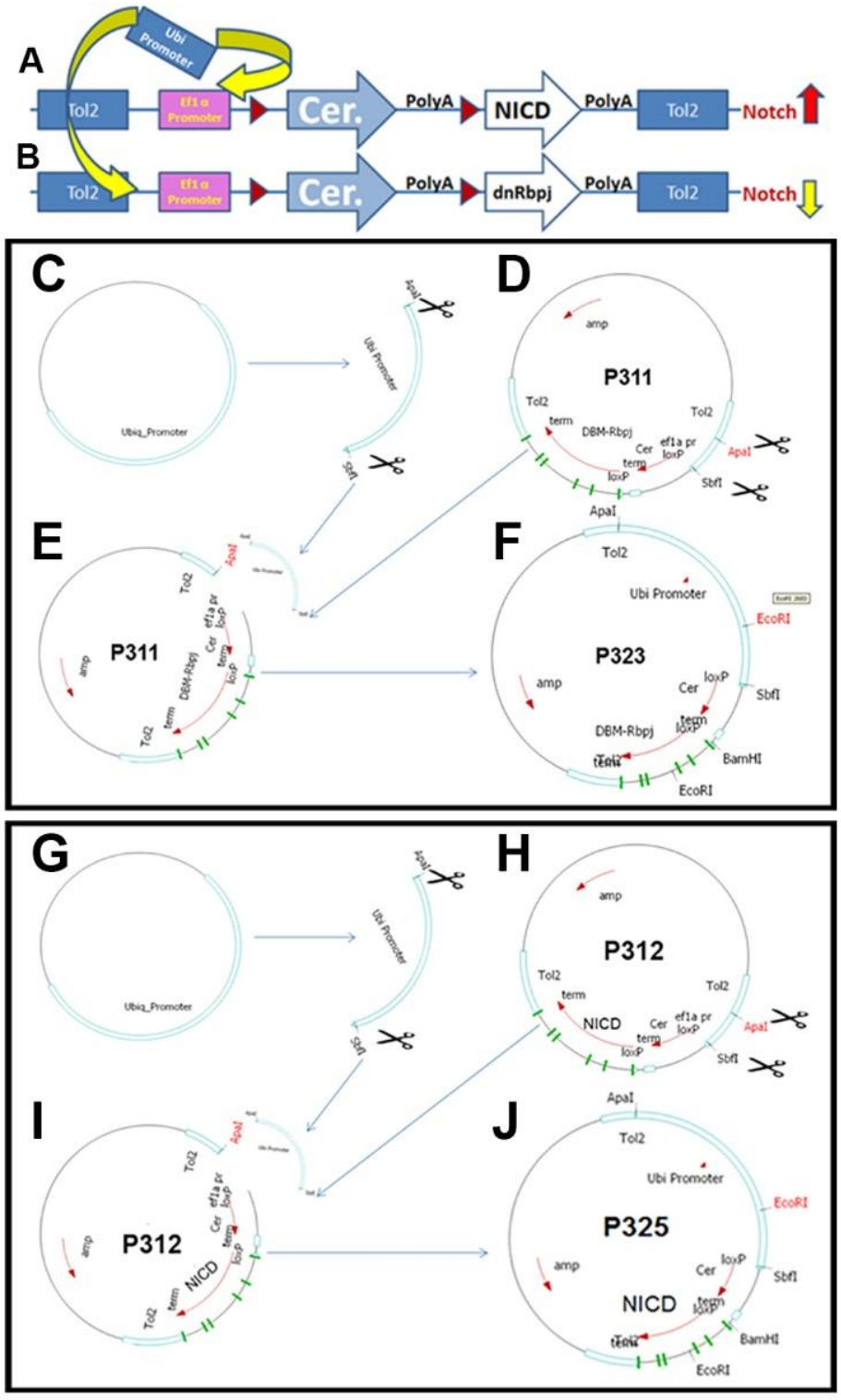
A
Ubi Promoter
Tol2
Ef1 α Promoter
Cer.
PolyA
NICD
PolyA
Tol2
Notch
B
Tol2
Ef1 α Promoter
Cer.
PolyA
dnRbpj
PolyA
Tol2
Notch
C
Ubiq_Promoter
ApaI
Ubi Promoter
SbfI
D
P311
amp
Tol2
term
DBM-Rbpj
Cer
ef1a pr
loxP
ApaI
SbfI
E
P311
F
P323
Ubi Promoter
EcoRI
amp
Cer
SbfI
DBM-Rbpj
BamHI
EcoRI
G
Ubiq_Promoter
ApaI
Ubi Promoter
SbfI
H
P312
NICD
I
P312
J
P325
NICD

Appendix 6: Cloning steps followed to replace *ef1α* promoter with the *ubi* promoter in the constructs P311 and P312.

(A-B) Schematics of the constructs P311 (A) and P312 (B) with the red arrows indicating where the promoter replacement step. (C-J) shows the cloning steps followed to replace the *ef1α* promoter with the *ubi* promoter in P311 and P312 plasmids. (C,G) we firstly amplified the *ubi* promoter from the containing plasmid with addition of ApaI and SbfI restriction sites, then cut and cleaned amplified fragments, preparing them for ligation. (D,H) P311 and P312 were also cut with the same enzymes ApaI and SbfI then cleaned. (E,I) amplified ApaI and SbfI cut ubi promoter was then ligated to the cut, cleaned P311 plasmid (E) and also ligated to the cut cleaned P312 plasmid (I). (F,J) show the final constructs P323 and P325 with the *ubi* promoter replacing the *ef1α* promoter.

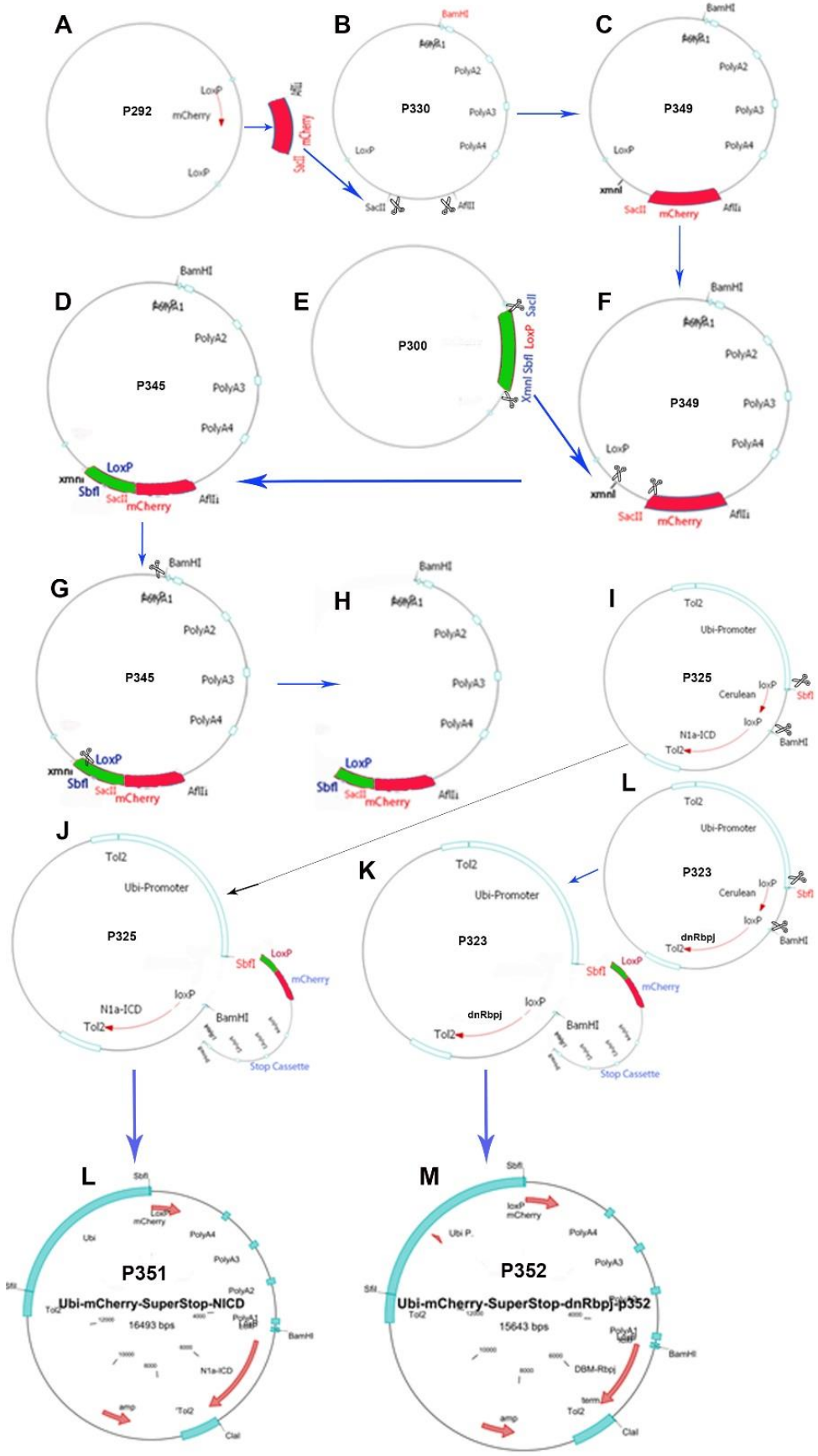
A
P292
LoxP
mCherry
LoxP
SacII
mCherry
B
BamHI
P330
PolyA2
PolyA3
PolyA4
LoxP
SacII
AflII
C
BamHI
P349
PolyA2
PolyA3
PolyA4
LoxP
XmnI
SacII
mCherry
AflII
D
BamHI
P345
PolyA2
PolyA3
PolyA4
XmnI
LoxP
SbfI
SacII
mCherry
AflII
E
P300
SacII
LoxP
XmnI
SbfI
F
BamHI
P349
PolyA2
PolyA3
PolyA4
LoxP
XmnI
SacII
mCherry
AflII
G
BamHI
P345
PolyA2
PolyA3
PolyA4
XmnI
LoxP
SbfI
SacII
mCherry
AflII
H
BamHI
PolyA2
PolyA3
PolyA4
LoxP
SbfI
SacII
mCherry
AflII
I
Tol2
Ubi-Promoter
P325
loxP
Cerulean
SbfI
loxP
N1a-ICD
BamHI
Tol2
L
Tol2
Ubi-Promoter
P323
loxP
Cerulean
SbfI
loxP
dnRbpj
BamHI
Tol2
J
Tol2
Ubi-Promoter
P325
SbfI
LoxP
mCherry
loxP
N1a-ICD
BamHI
Tol2
Stop Cassette
K
Tol2
Ubi-Promoter
P323
SbfI
LoxP
mCherry
loxP
dnRbpj
BamHI
Tol2
Stop Cassette
L
SbfI
LoxP
mCherry
Ubi
PolyA4
PolyA3
PolyA2
P351
Ubi-mCherry-SuperStop-NICD
16493 bps
BamHI
N1a-ICD
amp
Tol2
ClaI
M
SbfI
loxP
mCherry
Ubi P.
PolyA4
PolyA3
P352
Ubi-mCherry-SuperStop-dnRbpj-p352
15643 bps
BamHI
DBM-Rbpj
amp
Tol2
ClaI

Appendix 7: Cloning steps followed to replace the *cerulean pA* fragment in P323 and P325 with the *mCherry-s.stop* cassette fragment.

Schematic showing the cloning steps followed to generate the P351 and P352 plasmids. (A) *mCherry* gene was PCR amplified from P292 with the DB377 and DB378 that also add SacII and AflII at the mCherry 5' and the 3' sites respectively. (B) Both amplified fragment and the *s.stop* plasmid P330 were cut with the SacII and AflII enzymes, then the removed fragment upstream of the *s.stop* cassette was replaced with the *mCherry* fragment. This has led to generation of the *mCherry-s.stop* plasmid P349 (C). Both P349 (F) and P300 (E) were cut with SacII and XmnI to enable addition of the *loxP* site upstream of the *mCherry* and generation of the *loxP-mCherry-s.stop* cassette P345 (D). P345 and the backbone plasmids P323 and P325 were then cut with BamHI and SbfI (G,H,I,L) to remove the *cerulean-pA* fragment and replace it with the *loxP-mCherry-s.stop* fragment (J-K). This led to generation of the plasmids P351 and P352.

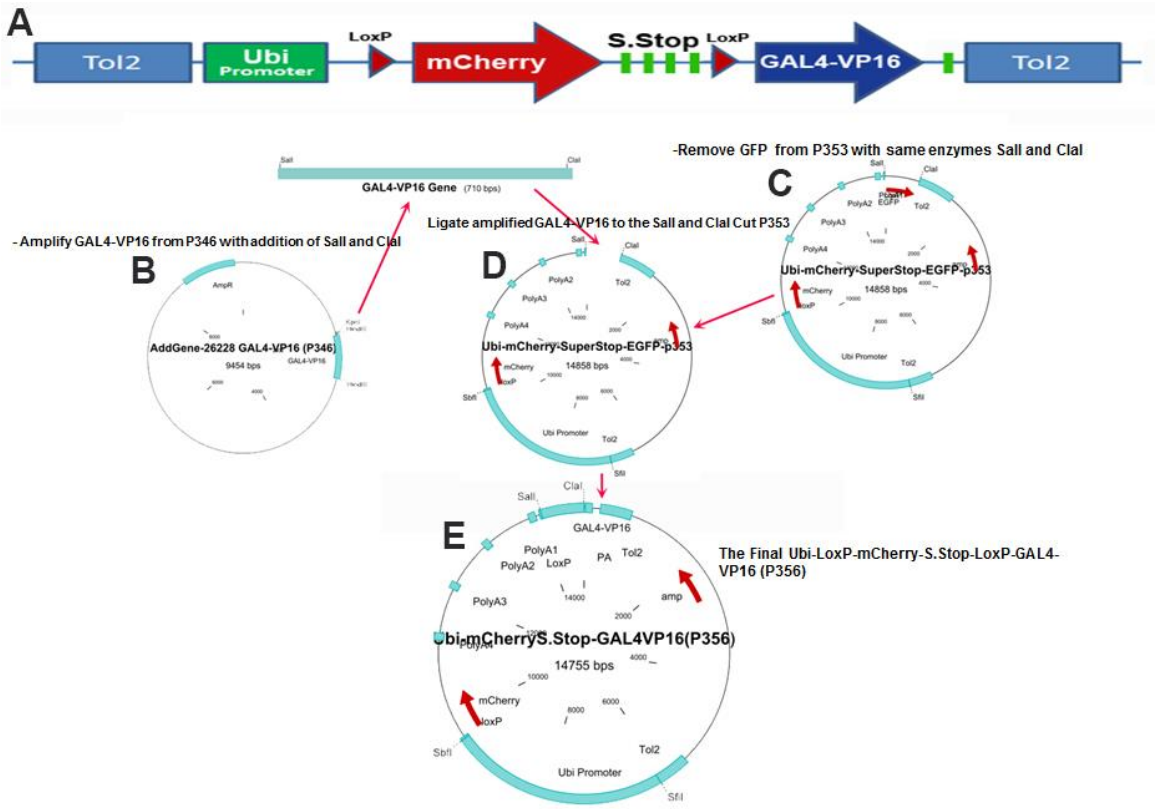

Appendix 8: Cloning steps followed to generate the *Tol2-ubi-loxP-mCherry-s.stop-loxP-gal4-vp16* construct P356.
(A) Diagram showing the main components of the P356 construct. (B-E) construction steps followed to generate the P356 plasmid in which the *gal4-vp16* gene was PCR amplified from the plasmid P346 with the primers DB414 and DB415 that add the restriction site SalI followed by the *kozak* sequence (GCCACC) at the 5′ and ClaI at the 3′ end (B). The plasmid P353 (C) was cut with the same enzymes (SalI and ClaI) to replace the *EGFP* gene with the *gal4-vp16* gene (D), thus generating the final *Tol2-ubi-loxP-mCherry-s.stop-loxP-gal4-vp16* plasmid (P356).

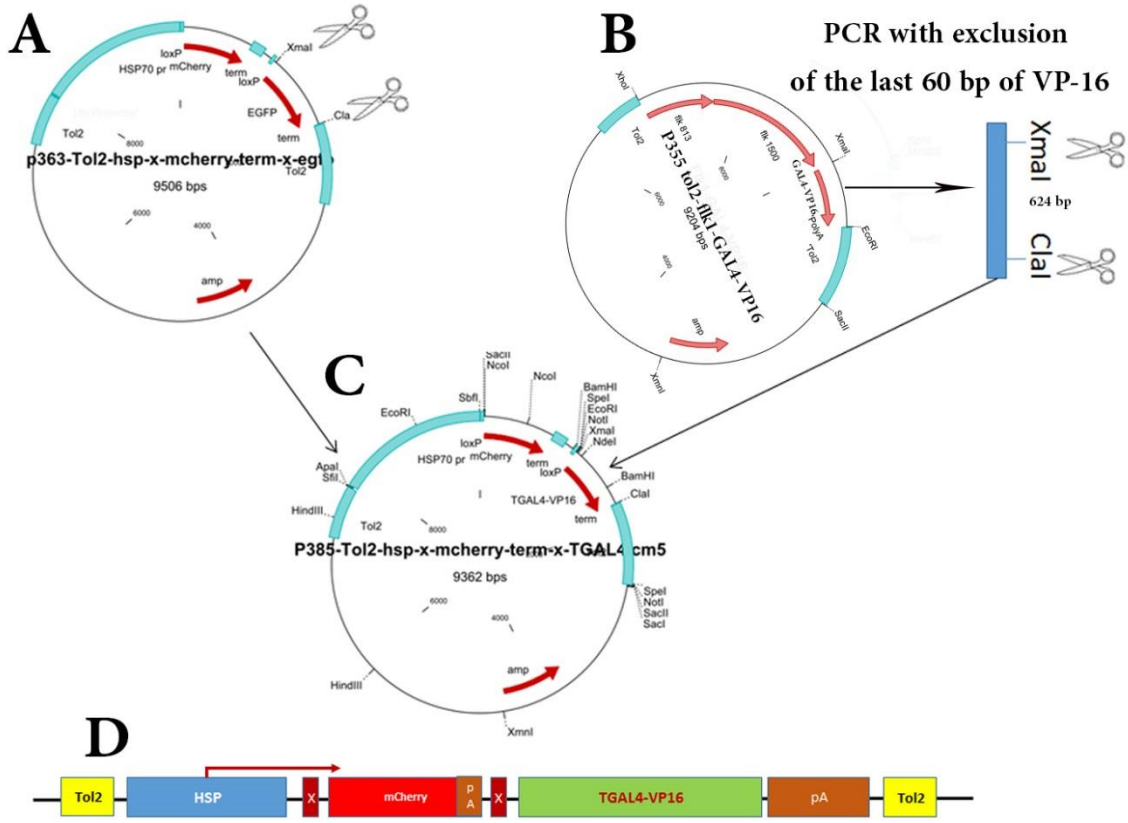

Appendix 9: Cloning steps followed to generate the P385 construct *HSP-loxP-mCherry-pA-loxP-Tgal4-vp16*.
(A) Restriction map of plasmid P363 that was modified to generate P385 by firstly removing the *GFP* gene with the restriction enzymes XmaI and ClaI. (B) PCR amplification of the 624bp truncated *gal4-vp16* (*tgal4-vp16*) with the primers DB542 and DB543 from plasmid P355. DB542 is a forward primer that includes the XmaI and the *kozak* sequence whereas DB543 is a reverse primer that exclude the last 60 bp of the *VP16* and add a stop codon followed by the restriction site ClaI. (C) The final P385 map after cloning the amplified, XmaI and ClaI cut fragment to the prepared *HSP-loxP-mCherry-pA* backbone thus generating the final construct *HSP-loxP-mCherry-pA-loxP-tgal4-vp16* (P385). (D) The main components of the generated plasmid.

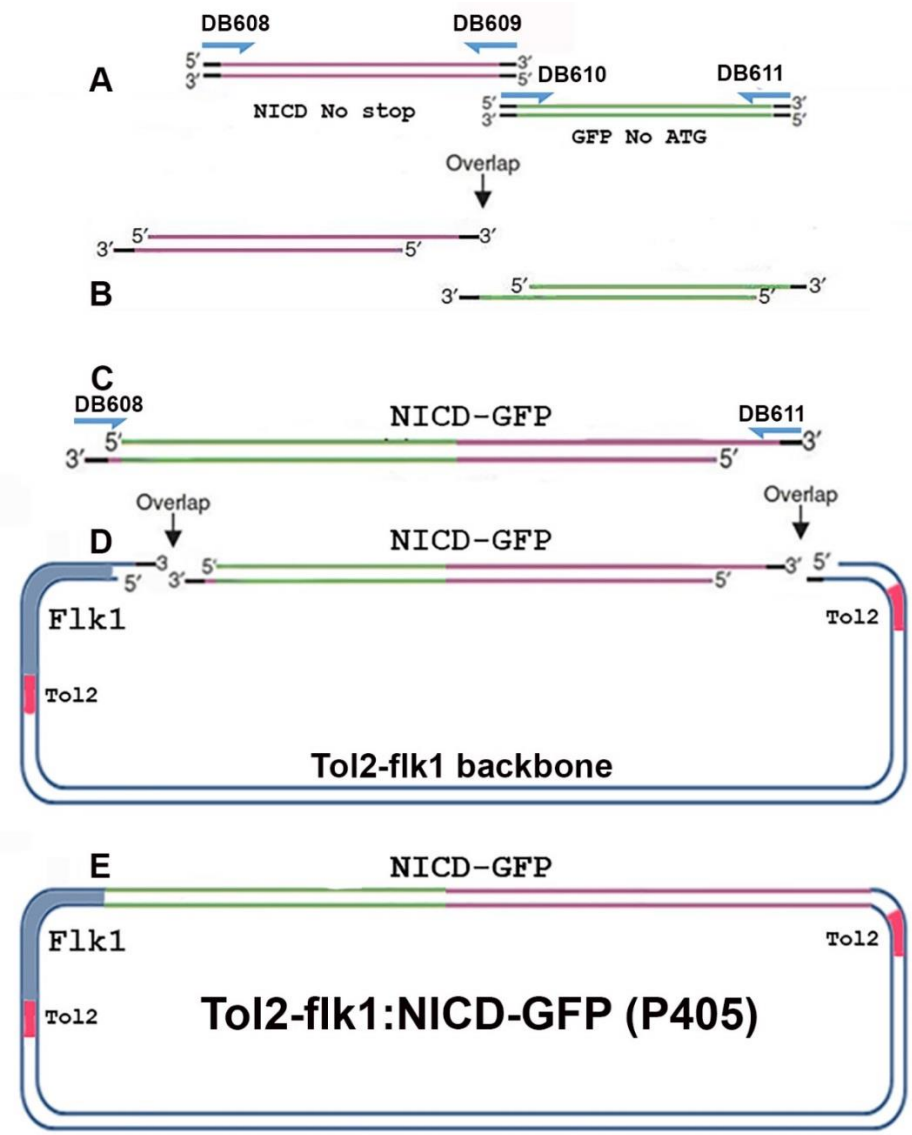

Appendix 10: Diagram showing GIBSON assembly steps followed to generate the *tol2-m.flk1:NICD-GFP* plasmid P405. (A) *NICD* gene was firstly amplified from P312 with the primers DB608 and DB609 which add a *kozak* sequence preceded by an overlap sequence to the linearized *tol2-m.flk1* plasmid at the 5' end and exclude the *NICD* stop codon and also add an overlap to the no-start *GFP* in-frame with the *NICD* at the 3' end. No-ATG *GFP* was also amplified with DB610 and DB611 from P252 with exclusion of the ATG and addition of an overlap sequence to *NICD* at the 5' end and overlap sequence to the backbone plasmid at the 3' end. (B) The two amplified fragments were firstly fused with GIBSON assembly method then PCR amplified as one fragment with DB 608 and DB610 (C). A second GIBSON assembly was then done to ligate the *NICD-GFP* fusion gene to the *tol2-m.flk1* backbone plasmid (D). This led to generation of the final plasmid *tol2-m.flk1:NICD-GFP* plasmid P405 (E).

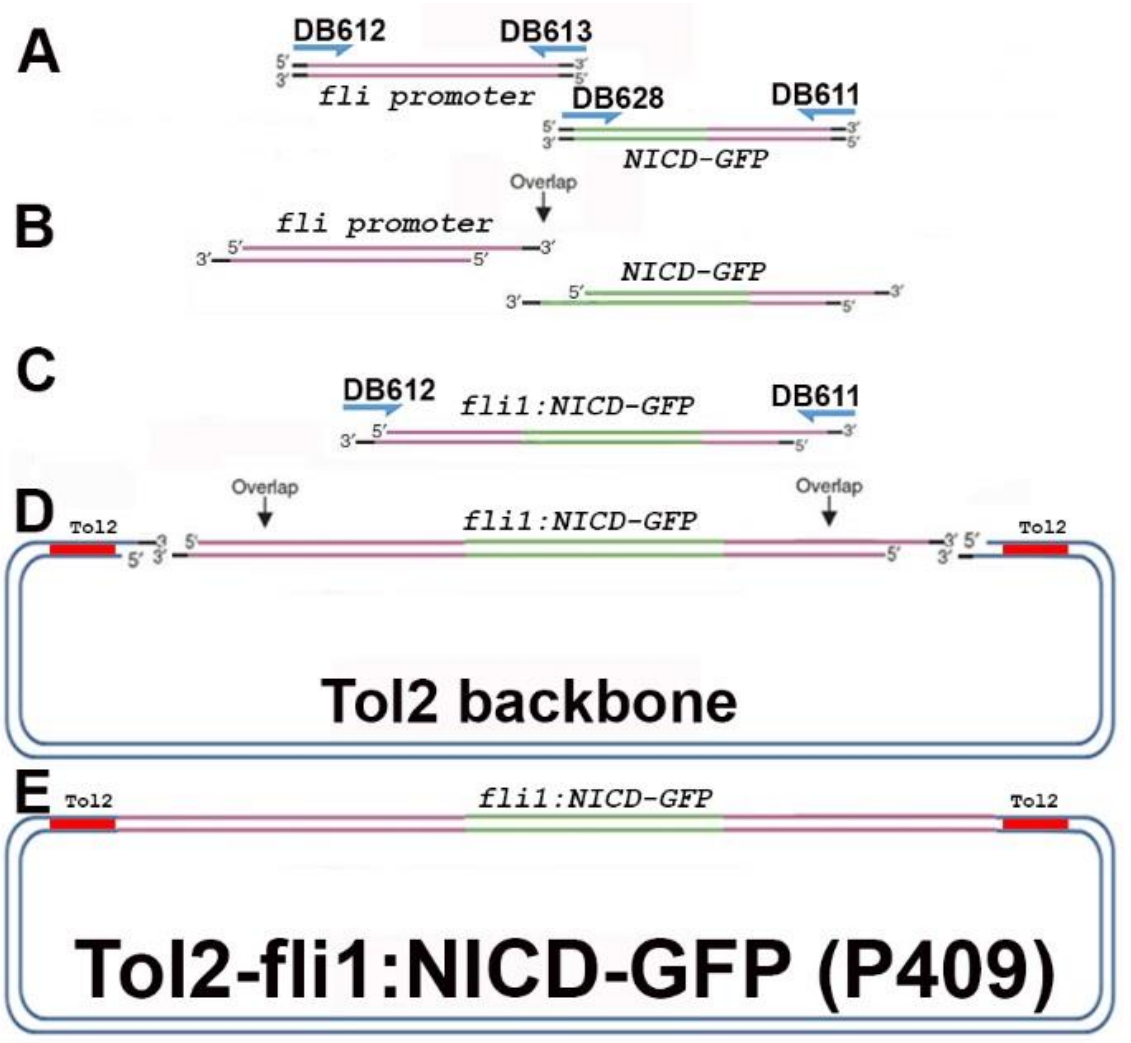

Appendix 11: Diagram showing GIBSON assembly steps followed to generate the tol2-fli1:NICD-GFP plasmid P409.
(A) *fli1* promoter was firstly amplified from P377 with the primers DB612 and DB613 that add an overlap sequence to the linearized *tol2* plasmid at the 5' end *NICD-GFP* fusion at the 3' end. *NICD-GFP* fusion was also amplified with the primers DB628 and DB611 from P405. The two amplified fragments were then firstly ligated together with GIBSON assembly method then PCR amplified as one fragment with DB 612 and DB611 (C). A second GIBSON assembly was then done to ligate the *fli1-NICD-GFP* fragment to the *tol2* backbone plasmid (D). This led to generation of the final plasmid *tol2-fli:NICD-GFP* plasmid (P409;E).

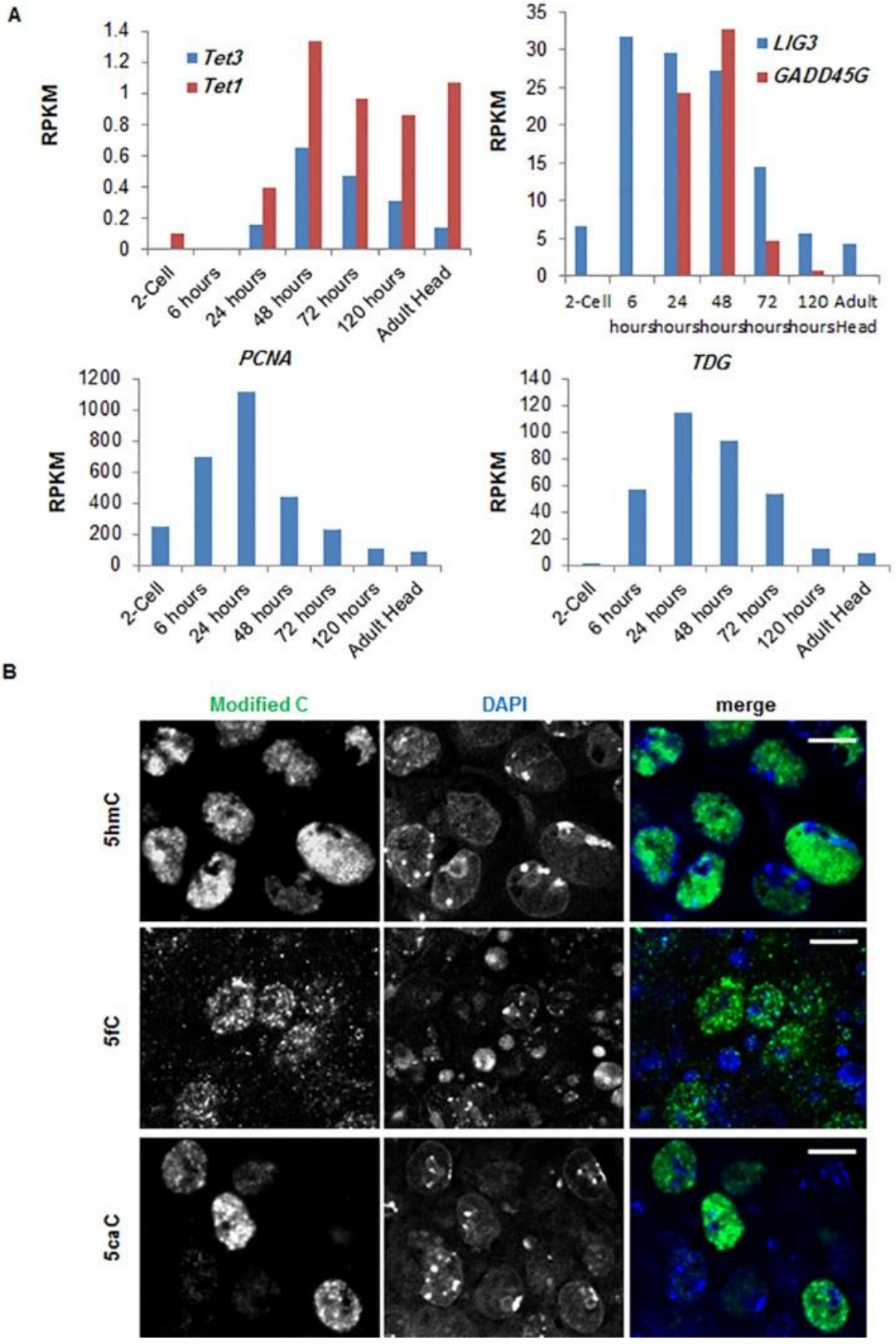
A
RPKM
Tet3
Tet1
2-Cell
6 hours
24 hours
48 hours
72 hours
120 hours
Adult Head
LIG3
GADD45G
2-Cell 6 hours 24 hours 48 hours 72 hours 120 hours Adult Head
PCNA
TDG
B
Modified C
DAPI
merge
5hmC
5fC
5caC

Appendix 12: 5fC and 5caC are detectable by immunochemistry in mESCs.

(A) The expression of Tet1, Tet3 and BER-related genes (GADD45G, LIG3, PCNA and TDG) at indicated zebrafish developmental stages. The Y axes show RPKM (Reads Per Kilobase of exon model per Million mapped reads) values. The analysis was performed using zebrafish time course data set provided by the zebrafish genome sequencing group at the Wellcome Trust Sanger Institute. (B) The results of 5hmC, 5fC and 5caC immunostaining of mESCs colonies. 5hmC/5fC/5caC, DAPI and merged views are shown. Scale bars are 10 μm (The figure was courtesy of Dr. Alexey Ruzov).

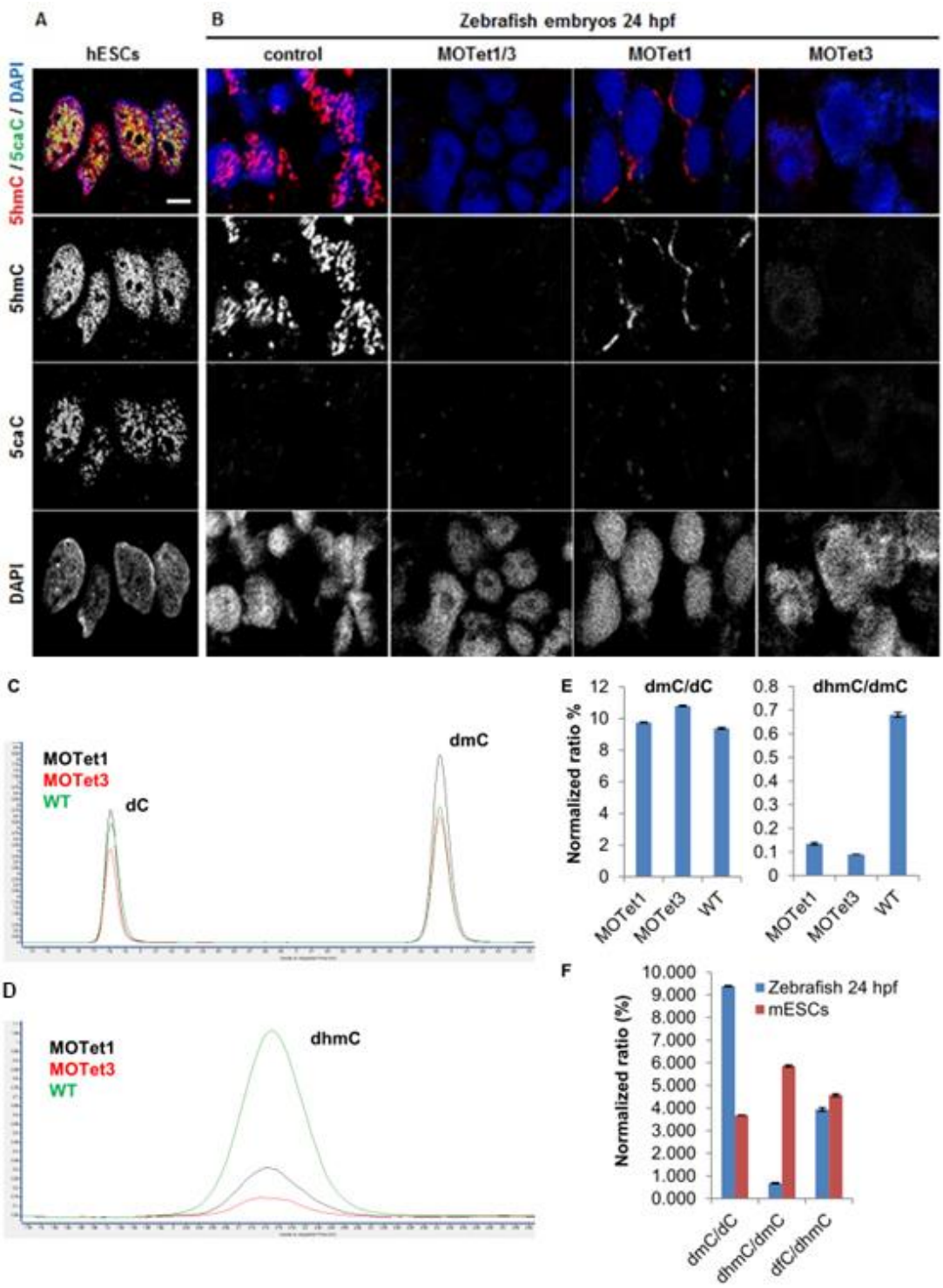
A
B
Zebrafish embryos 24 hpf
hESCs
control
MOTet1/3
MOTet1
MOTet3
5hmC / 5caC / DAPI
5hmC
5caC
DAPI
C
MOTet1
MOTet3
WT
dC
dmC
D
MOTet1
MOTet3
WT
dhmC
E
dmC/dC
dhmC/dmC
Normalized ratio %
MOTet1
MOTet3
WT
F
Zebrafish 24 hpf
mESCs
Normalized ratio (%)
dmC/dC
dhmC/dmC
dfC/dhmC

Appendix 13: Global 5hmC levels are dramatically decreased in both Tet1 and Tet3 morphants.
(A) 5hmC co-localization with 5caC in hESCs. Scale bars are 10 μm. (B) Immunostaining of uninjected control, MOTet1/3, MOTet1 and MOTet3 embryos for 5hmC and 5caC. Representative views of sections through the axial embryonic tissues are shown. The slides were processed in parallel and imaged using identical settings. Identical dilutions of the antibodies and times of incubation with amplification reagent were used in (A) and in (B). 5hmC, 5caC, DAPI and merged views are shown. (C, D) Overlays of total ion chromatograms of global dC, dmC, (C) and dhmC (D) content recorded in Dynamic Multiple Reaction Monitoring (DMRM) mode in the DNA derived from MOTet1, MOTet3 and wild type (WT) zebrafish embryos at 24 hpf. (E) dmC/dC and dhmC/dmC ratios obtained from the quantification of mass spec peaks in the DNA derived from MOTet1, MOTet3 and wild type embryos at 24 hpf. (F) dmC/dC, dhmC/dmC and dfC/dhmC ratios obtained from the quantification of mass spec peaks in the DNA samples derived from 24 hpf zebrafish embryos and mESCs. (The figure was courtesy of Dr. Alexey Ruzov).

REFERENCES

Al-Adhami, M. A. & Kunz, Y. W. 1977. Ontogenesis of Haematopoietic Sites in Brachydanio rerio (Hamilton-Buchanan) (Teleostei)*. *Development, Growth & Differentiation,* 19**,** 171-179.

Almeida, R. D., Loose, M., Sottile, V., Matsa, E., Denning, C., Young, L., Johnson, A. D., Gering, M. & Ruzov, A. 2012. 5-hydroxymethyl-cytosine enrichment of non-committed cells is not a universal feature of vertebrate development. *Epigenetics,* 7**,** 383-9.

Alvarez-Silva, M., Belo-Diabangouaya, P., Salaun, J. & Dieterlen-Lievre, F. 2003. Mouse placenta is a major hematopoietic organ. *Development,* 130**,** 5437-44.

Amatruda, J. F. & Zon, L. I. 1999. Dissecting hematopoiesis and disease using the zebrafish. *Dev Biol,* 216**,** 1-15.

Anderson, R. M., Bosch, J. A., Goll, M. G., Hesselson, D., Dong, P. D., Shin, D., Chi, N. C., Shin, C. H., Schlegel, A., Halpern, M. & Stainier, D. Y. 2009. Loss of Dnmt1 catalytic activity reveals multiple roles for DNA methylation during pancreas development and regeneration. *Dev Biol,* 334**,** 213-23.

Anon 2006. RNA interference on target. *Nat Meth,* 3**,** 659-659.

Bahary, N., Goishi, K., Stuckenholz, C., Weber, G., Leblanc, J., Schafer, C. A., Berman, S. S., Klagsbrun, M. & Zon, L. I. 2007. Duplicate VegfA genes and orthologues of the KDR receptor tyrosine kinase family mediate vascular development in the zebrafish. *Blood,* 110**,** 3627-36.

Baron, M. H., Isern, J. & Fraser, S. T. 2012. The embryonic origins of erythropoiesis in mammals. *Blood,* 119**,** 4828-37.

Bedell, V. M., Westcot, S. E. & Ekker, S. C. 2011. Lessons from morpholino-based screening in zebrafish. *Brief Funct Genomics,* 10**,** 181-8.

Beis, D., Bartman, T., Jin, S. W., Scott, I. C., D'amico, L. A., Ober, E. A., Verkade, H., Frantsve, J., Field, H. A., Wehman, A., Baier, H., Tallafuss, A., Bally-Cuif, L., Chen, J. N., Stainier, D. Y. & Jungblut, B. 2005. Genetic and cellular analyses of zebrafish atrioventricular cushion and valve development. *Development,* 132**,** 4193-204.

Bertrand, J. Y., Chi, N. C., Santoso, B., Teng, S., Stainier, D. Y. R. & Traver, D. 2010a. Hematopoietic stem cells derive directly from aortic endothelium during development. *Nature,* 464**,** 108-11.

Bertrand, J. Y., Chi, N. C., Santoso, B. & Traver, D. 2009. primitive and definitive hematopoiesis arise from hemogenic endothelial cells in the zebrafish embryo. *Poster presented at 6 th European Zebrafish Genetics and Development Meeting*.

Bertrand, J. Y., Cisson, J. L., Stachura, D. L. & Traver, D. 2010b. Notch signaling distinguishes 2 waves of definitive hematopoiesis in the zebrafish embryo. *Blood,* 115**,** 2777-83.

Bertrand, J. Y., Kim, A. D., Violette, E. P., Stachura, D. L., Cisson, J. L. & Traver, D. 2007. Definitive hematopoiesis initiates through a committed erythromyeloid progenitor in the zebrafish embryo. *Development,* 134**,** 4147-56.

Bierkamp, C. & Campos-Ortega, J. A. 1993. A zebrafish homologue of the Drosophila neurogenic gene Notch and its pattern of transcription during early embryogenesis. *Mech Dev,* 43**,** 87-100.

Bigas, A., Guiu, J. & Gama-Norton, L. 2013. Notch and Wnt signaling in the emergence of hematopoietic stem cells. *Blood Cells Mol Dis,* 51**,** 264-70.

Burns, C. E., Traver, D., Mayhall, E., Shepard, J. L. & Zon, L. I. 2005. Hematopoietic stem cell fate is established by the Notch-Runx pathway. *Genes Dev,* 19**,** 2331-42.

Bussmann, J., Lawson, N., Zon, L. & Schulte-Merker, S. 2008. Zebrafish VEGF receptors: a guideline to nomenclature. *PLoS Genet,* 4**,** e1000064.

Butko, E., Distel, M., Pouget, C., Weijts, B., Kobayashi, I., Ng, K., Mosimann, C., Poulain, F. E., Mcpherson, A., Ni, C. W., Stachura, D. L., Del Cid, N., Espin-Palazon, R., Lawson, N. D.,

Dorsky, R., Clements, W. K. & Traver, D. 2015. Gata2b is a restricted early regulator of hemogenic endothelium in the zebrafish embryo. *Development,* 142**,** 1050-61.

Cambier, T., Honegger, T., Vanneaux, V., Berthier, J., Peyrade, D., Blanchoin, L., Larghero, J. & Thery, M. 2015. Design of a 2D no-flow chamber to monitor hematopoietic stem cells. *Lab Chip,* 15**,** 77-85.

Chen, M. J., Yokomizo, T., Zeigler, B. M., Dzierzak, E. & Speck, N. A. 2009. Runx1 is required for the endothelial to haematopoietic cell transition but not thereafter. *Nature,* 457**,** 887-91.

Choi, J., Dong, L., Ahn, J., Dao, D., Hammerschmidt, M. & Chen, J. N. 2007. FoxH1 negatively modulates flk1 gene expression and vascular formation in zebrafish. *Dev Biol,* 304**,** 735-44.

Clements, W. K., Kim, A. D., Ong, K. G., Moore, J. C., Lawson, N. D. & Traver, D. 2011. A somitic Wnt16/Notch pathway specifies haematopoietic stem cells. *Nature,* 474**,** 220-4.

Clements, W. K. & Traver, D. 2013. Signalling pathways that control vertebrate haematopoietic stem cell specification. *Nat Rev Immunol,* 13**,** 336-48.

Collas, P. 1998. Modulation of plasmid DNA methylation and expression in zebrafish embryos. *Nucleic Acids Res,* 26**,** 4454-61.

Coultas, L., Chawengsaksophak, K. & Rossant, J. 2005. Endothelial cells and VEGF in vascular development. *Nature,* 438**,** 937-45.

Covassin, L. D., Villefranc, J. A., Kacergis, M. C., Weinstein, B. M. & Lawson, N. D. 2006. Distinct genetic interactions between multiple Vegf receptors are required for development of different blood vessel types in zebrafish. *Proc Natl Acad Sci U S A,* 103**,** 6554-9.

Cross, L. M., Cook, M. A., Lin, S., Chen, J. N. & Rubinstein, A. L. 2003. Rapid analysis of angiogenesis drugs in a live fluorescent zebrafish assay. *Arterioscler Thromb Vasc Biol,* 23**,** 911-2.

Davison, J. M., Akitake, C. M., Goll, M. G., Rhee, J. M., Gosse, N., Baier, H., Halpern, M. E., Leach, S. D. & Parsons, M. J. 2007. Transactivation from Gal4-VP16 transgenic insertions for tissue-specific cell labeling and ablation in zebrafish. *Dev Biol,* 304**,** 811-24.

Dawlaty, M. M., Breiling, A., Le, T., Barrasa, M. I., Raddatz, G., Gao, Q., Powell, B. E., Cheng, A. W., Faull, K. F., Lyko, F. & Jaenisch, R. 2014. Loss of Tet enzymes compromises proper differentiation of embryonic stem cells. *Dev Cell,* 29**,** 102-11.

Dawlaty, M. M., Breiling, A., Le, T., Raddatz, G., Barrasa, M. I., Cheng, A. W., Gao, Q., Powell, B. E., Li, Z., Xu, M., Faull, K. F., Lyko, F. & Jaenisch, R. 2013. Combined deficiency of Tet1 and Tet2 causes epigenetic abnormalities but is compatible with postnatal development. *Dev Cell,* 24**,** 310-23.

De Bruijn, M. F., Ma, X., Robin, C., Ottersbach, K., Sanchez, M. J. & Dzierzak, E. 2002. Hematopoietic stem cells localize to the endothelial cell layer in the midgestation mouse aorta. *Immunity,* 16**,** 673-83.

Deaton, A. M. & Bird, A. 2011. CpG islands and the regulation of transcription. *Genes Dev,* 25**,** 1010-22.

Detrich, H. W., 3rd, Kieran, M. W., Chan, F. Y., Barone, L. M., Yee, K., Rundstadler, J. A., Pratt, S., Ransom, D. & Zon, L. I. 1995. Intraembryonic hematopoietic cell migration during vertebrate development. *Proc Natl Acad Sci U S A,* 92**,** 10713-7.

Detrich, H. W., Westerfield, M. & Zon, L. I. 2011. *The zebrafish: disease models and chemical screens*, Academic Press.

Dieterlen-Lievre, F. 1975. On the origin of haemopoietic stem cells in the avian embryo: an experimental approach. *J Embryol Exp Morphol,* 33**,** 607-19.

Drevon, C. & Jaffredo, T. 2014. Cell interactions and cell signaling during hematopoietic development. *Exp Cell Res,* 329**,** 200-6.

Drew, E. 2010. *The Role of the PI3K/AKT Pathway in HSC Formation in the Zebrafish Embryo.* Master, University of Nottingham.

Eilken, H. M., Nishikawa, S. & Schroeder, T. 2009. Continuous single-cell imaging of blood generation from haemogenic endothelium. *Nature,* 457**,** 896-900.

Eisen, J. S. & Smith, J. C. 2008. Controlling morpholino experiments: don't stop making antisense. *Development,* 135**,** 1735-43.

Ellisen, L. W., Bird, J., West, D. C., Soreng, A. L., Reynolds, T. C., Smith, S. D. & Sklar, J. 1991. TAN-1, the human homolog of the Drosophila notch gene, is broken by chromosomal translocations in T lymphoblastic neoplasms. *Cell,* 66**,** 649-61.

Espin-Palazon, R., Stachura, D. L., Campbell, C. A., Garcia-Moreno, D., Del Cid, N., Kim, A. D., Candel, S., Meseguer, J., Mulero, V. & Traver, D. 2014. Proinflammatory signaling regulates hematopoietic stem cell emergence. *Cell,* 159**,** 1070-85.

Ford, C. E., Hamerton, J. L., Barnes, D. W. & Loutit, J. F. 1956. Cytological identification of radiation-chimaeras. *Nature,* 177**,** 452-4.

Fouquet, B., Weinstein, B. M., Serluca, F. C. & Fishman, M. C. 1997. Vessel patterning in the embryo of the zebrafish: guidance by notochord. *Dev Biol,* 183**,** 37-48.

Gekas, C., Dieterlen-Lievre, F., Orkin, S. H. & Mikkola, H. K. 2005. The placenta is a niche for hematopoietic stem cells. *Dev Cell,* 8**,** 365-75.

Gering, M. & Patient, R. 2005. Hedgehog signaling is required for adult blood stem cell formation in zebrafish embryos. *Dev Cell,* 8**,** 389-400.

Gering, M., Rodaway, A. R., Gottgens, B., Patient, R. K. & Green, A. R. 1998. The SCL gene specifies haemangioblast development from early mesoderm. *Embo j,* 17**,** 4029-45.

Gibson, D. G., Glass, J. I., Lartigue, C., Noskov, V. N., Chuang, R. Y., Algire, M. A., Benders, G. A., Montague, M. G., Ma, L., Moodie, M. M., Merryman, C., Vashee, S., Krishnakumar, R., Assad-Garcia, N., Andrews-Pfannkoch, C., Denisova, E. A., Young, L., Qi, Z. Q., Segall-Shapiro, T. H., Calvey, C. H., Parmar, P. P., Hutchison, C. A., 3rd, Smith, H. O. & Venter, J. C. 2010. Creation of a bacterial cell controlled by a chemically synthesized genome. *Science,* 329**,** 52-6.

Gibson, D. G., Young, L., Chuang, R. Y., Venter, J. C., Hutchison, C. A., 3rd & Smith, H. O. 2009. Enzymatic assembly of DNA molecules up to several hundred kilobases. *Nat Methods,* 6**,** 343-5.

Gilbert, W. & Glynias, M. 1993. On the ancient nature of introns. *Gene,* 135**,** 137-44.

Goll, M. G., Anderson, R., Stainier, D. Y., Spradling, A. C. & Halpern, M. E. 2009. Transcriptional silencing and reactivation in transgenic zebrafish. *Genetics,* 182**,** 747-55.

Golub, R. & Cumano, A. 2013. Embryonic hematopoiesis. *Blood Cells Mol Dis,* 51**,** 226-31.

Gross, J. B., Hanken, J., Oglesby, E. & Marsh-Armstrong, N. 2006. Use of a ROSA26:GFP transgenic line for long-term Xenopus fate-mapping studies. *J Anat,* 209**,** 401-13.

Gu, T. P., Guo, F., Yang, H., Wu, H. P., Xu, G. F., Liu, W., Xie, Z. G., Shi, L., He, X., Jin, S. G., Iqbal, K., Shi, Y. G., Deng, Z., Szabo, P. E., Pfeifer, G. P., Li, J. & Xu, G. L. 2011. The role of Tet3 DNA dioxygenase in epigenetic reprogramming by oocytes. *Nature,* 477**,** 606-10.

Gupta-Rossi, N., Le Bail, O., Gonen, H., Brou, C., Logeat, F., Six, E., Ciechanover, A. & Israel, A. 2001. Functional interaction between SEL-10, an F-box protein, and the nuclear form of activated Notch1 receptor. *J Biol Chem,* 276**,** 34371-8.

Habeck, H., Odenthal, J., Walderich, B., Maischein, H. & Schulte-Merker, S. 2002. Analysis of a zebrafish VEGF receptor mutant reveals specific disruption of angiogenesis. *Curr Biol,* 12**,** 1405-12.

Haddon, C., Jiang, Y. J., Smithers, L. & Lewis, J. 1998. Delta-Notch signalling and the patterning of sensory cell differentiation in the zebrafish ear: evidence from the mind bomb mutant. *Development,* 125**,** 4637-44.

Hadland, B. K., Huppert, S. S., Kanungo, J., Xue, Y., Jiang, R., Gridley, T., Conlon, R. A., Cheng, A. M., Kopan, R. & Longmore, G. D. 2004. A requirement for Notch1 distinguishes 2 phases of definitive hematopoiesis during development. *Blood,* 104**,** 3097-105.

Haffter, P., Granato, M., Brand, M., Mullins, M. C., Hammerschmidt, M., Kane, D. A., Odenthal, J., Van Eeden, F. J., Jiang, Y. J., Heisenberg, C. P., Kelsh, R. N., Furutani-Seiki, M., Vogelsang, E., Beuchle, D., Schach, U., Fabian, C. & Nusslein-Volhard, C. 1996. The identification of genes with unique and essential functions in the development of the zebrafish, Danio rerio. *Development,* 123**,** 1-36.

Hans, S., Kaslin, J., Freudenreich, D. & Brand, M. 2009. Temporally-controlled site-specific recombination in zebrafish. *PLoS One,* 4**,** e4640.

He, Y. F., Li, B. Z., Li, Z., Liu, P., Wang, Y., Tang, Q., Ding, J., Jia, Y., Chen, Z., Li, L., Sun, Y., Li, X., Dai, Q., Song, C. X., Zhang, K., He, C. & Xu, G. L. 2011. Tet-mediated formation of 5-carboxylcytosine and its excision by TDG in mammalian DNA. *Science,* 333**,** 1303-7.

Henkel, T., Ling, P. D., Hayward, S. D. & Peterson, M. G. 1994. Mediation of Epstein-Barr virus EBNA2 transactivation by recombination signal-binding protein J kappa. *Science,* 265**,** 92-5.

Herbert, S. P., Huisken, J., Kim, T. N., Feldman, M. E., Houseman, B. T., Wang, R. A., Shokat, K. M. & Stainier, D. Y. 2009. Arterial-venous segregation by selective cell sprouting: an alternative mode of blood vessel formation. *Science,* 326**,** 294-8.

Hirai, H., Samokhvalov, I. M., Fujimoto, T., Nishikawa, S., Imanishi, J. & Nishikawa, S. 2005. Involvement of Runx1 in the down-regulation of fetal liver kinase-1 expression during transition of endothelial cells to hematopoietic cells. *Blood,* 106**,** 1948-55.

Hsieh, J. J., Henkel, T., Salmon, P., Robey, E., Peterson, M. G. & Hayward, S. D. 1996. Truncated mammalian Notch1 activates CBF1/RBPJk-repressed genes by a mechanism resembling that of Epstein-Barr virus EBNA2. *Molecular and Cellular Biology,* 16**,** 952-959.

Inbal, A., Topczewski, J. & Solnica-Krezel, L. 2006. Targeted gene expression in the zebrafish prechordal plate. *Genesis,* 44**,** 584-8.

Ishitobi, H., Matsumoto, K., Azami, T., Itoh, F., Itoh, S., Takahashi, S. & Ema, M. 2010. Flk1-GFP BAC Tg mice: an animal model for the study of blood vessel development. *Exp Anim,* 59**,** 615-22.

Isogai, S., Lawson, N. D., Torrealday, S., Horiguchi, M. & Weinstein, B. M. 2003. Angiogenic network formation in the developing vertebrate trunk. *Development,* 130**,** 5281-5290.

Ito, S., D'alessio, A. C., Taranova, O. V., Hong, K., Sowers, L. C. & Zhang, Y. 2010. Role of Tet proteins in 5mC to 5hmC conversion, ES-cell self-renewal and inner cell mass specification. *Nature,* 466**,** 1129-33.

Itoh, M., Kim, C. H., Palardy, G., Oda, T., Jiang, Y. J., Maust, D., Yeo, S. Y., Lorick, K., Wright, G. J., Ariza-Mcnaughton, L., Weissman, A. M., Lewis, J., Chandrasekharappa, S. C. & Chitnis, A. B. 2003. Mind bomb is a ubiquitin ligase that is essential for efficient activation of Notch signaling by Delta. *Dev Cell,* 4**,** 67-82.

Jackson, E. L., Willis, N., Mercer, K., Bronson, R. T., Crowley, D., Montoya, R., Jacks, T. & Tuveson, D. A. 2001. Analysis of lung tumor initiation and progression using conditional expression of oncogenic K-ras. *Genes Dev,* 15**,** 3243-8.

Jaffredo, T., Gautier, R., Eichmann, A. & Dieterlen-Lievre, F. 1998. Intraaortic hemopoietic cells are derived from endothelial cells during ontogeny. *Development,* 125**,** 4575-83.

Jalali, M. 2012. *Using the Cre/LoxP recombination system to study the role of the PI3K/AKT signalling transduction pathway and the embryonic cellular origin of adult haematopoietic stem cells in the zebrafish.* Master, University of Nottingham.

Janicke, M., Carney, T. J. & Hammerschmidt, M. 2007. Foxi3 transcription factors and Notch signaling control the formation of skin ionocytes from epidermal precursors of the zebrafish embryo. *Dev Biol,* 307**,** 258-71.

Jiang, Y. J., Brand, M., Heisenberg, C. P., Beuchle, D., Furutani-Seiki, M., Kelsh, R. N., Warga, R. M., Granato, M., Haffter, P., Hammerschmidt, M., Kane, D. A., Mullins, M. C., Odenthal, J., Van Eeden, F. J. & Nusslein-Volhard, C. 1996. Mutations affecting neurogenesis and brain morphology in the zebrafish, Danio rerio. *Development,* 123**,** 205-16.

Jin, H., Sood, R., Xu, J., Zhen, F., English, M. A., Liu, P. P. & Wen, Z. 2009. Definitive hematopoietic stem/progenitor cells manifest distinct differentiation output in the zebrafish VDA and PBI. *Development,* 136**,** 647-54.

Jin, H., Xu, J. & Wen, Z. 2007. Migratory path of definitive hematopoietic stem/progenitor cells during zebrafish development. *Blood,* 109**,** 5208-14.

Jin, S. W., Beis, D., Mitchell, T., Chen, J. N. & Stainier, D. Y. 2005. Cellular and molecular analyses of vascular tube and lumen formation in zebrafish. *Development,* 132**,** 5199-209.

Jones, R. J., Celano, P., Sharkis, S. J. & Sensenbrenner, L. L. 1989. Two phases of engraftment established by serial bone marrow transplantation in mice. *Blood,* 73**,** 397-401.

Joutel, A., Monet, M., Domenga, V., Riant, F. & Tournier-Lasserve, E. 2004. Pathogenic mutations associated with cerebral autosomal dominant arteriopathy with subcortical infarcts and leukoencephalopathy differently affect Jagged1 binding and Notch3 activity via the RBP/JK signaling Pathway. *Am J Hum Genet,* 74**,** 338-47.

Kataoka, H., Takakura, N., Nishikawa, S., Tsuchida, K., Kodama, H., Kunisada, T., Risau, W., Kita, T. & Nishikawa, S. I. 1997. Expressions of PDGF receptor alpha, c-Kit and Flk1 genes clustering in mouse chromosome 5 define distinct subsets of nascent mesodermal cells. *Dev Growth Differ,* 39**,** 729-40.

Kato, H., Taniguchi, Y., Kurooka, H., Minoguchi, S., Sakai, T., Nomura-Okazaki, S., Tamura, K. & Honjo, T. 1997. Involvement of RBP-J in biological functions of mouse Notch1 and its derivatives. *Development,* 124**,** 4133-41.

Kawakami, K., Takeda, H., Kawakami, N., Kobayashi, M., Matsuda, N. & Mishina, M. 2004. A transposon-mediated gene trap approach identifies developmentally regulated genes in zebrafish. *Dev Cell,* 7**,** 133-44.

Kawamata, S., Du, C., Li, K. & Lavau, C. 2002. Overexpression of the Notch target genes Hes in vivo induces lymphoid and myeloid alterations. *Oncogene,* 21**,** 3855-63.

Kim, A. D., Melick, C. H., Clements, W. K., Stachura, D. L., Distel, M., Panakova, D., Macrae, C., Mork, L. A., Crump, J. G. & Traver, D. 2014. Discrete Notch signaling requirements in the specification of hematopoietic stem cells. *Embo j,* 33**,** 2363-73.

Kim, Y. H., Hu, H., Guevara-Gallardo, S., Lam, M. T., Fong, S. Y. & Wang, R. A. 2008. Artery and vein size is balanced by Notch and ephrin B2/EphB4 during angiogenesis. *Development,* 135**,** 3755-64.

Kimmel, C. B., Ballard, W. W., Kimmel, S. R., Ullmann, B. & Schilling, T. F. 1995. Stages of embryonic development of the zebrafish. *Dev. Dyn. Developmental Dynamics,* 203**,** 253-310.

Kissa, K. & Herbomel, P. 2010. Blood stem cells emerge from aortic endothelium by a novel type of cell transition. *Nature,* 464**,** 112-5.

Kissa, K., Murayama, E., Zapata, A., Cortes, A., Perret, E., Machu, C. & Herbomel, P. 2008. Live imaging of emerging hematopoietic stem cells and early thymus colonization. *Blood,* 111**,** 1147-56.

Kobayashi, I., Kobayashi-Sun, J., Kim, A. D., Pouget, C., Fujita, N., Suda, T. & Traver, D. 2014. Jam1a-Jam2a interactions regulate haematopoietic stem cell fate through Notch signalling. *Nature,* 512**,** 319-23.

Koch, U., Lehal, R. & Radtke, F. 2013. Stem cells living with a Notch. *Development,* 140**,** 689-704.

Koh, K. P., Yabuuchi, A., Rao, S., Huang, Y., Cunniff, K., Nardone, J., Laiho, A., Tahiliani, M., Sommer, C. A., Mostoslavsky, G., Lahesmaa, R., Orkin, S. H., Rodig, S. J., Daley, G. Q. & Rao, A. 2011. Tet1 and Tet2 Regulate 5-Hydroxymethylcytosine Production and Cell Lineage Specification in Mouse Embryonic Stem Cells. *Cell Stem Cell,* 8**,** 200-213.

Kohli, V., Schumacher, J. A., Desai, S. P., Rehn, K. & Sumanas, S. 2013. Arterial and venous progenitors of the major axial vessels originate at distinct locations. *Dev Cell,* 25**,** 196-206.

Kohyama, J., Tokunaga, A., Fujita, Y., Miyoshi, H., Nagai, T., Miyawaki, A., Nakao, K., Matsuzaki, Y. & Okano, H. 2005. Visualization of spatiotemporal activation of Notch signaling: live monitoring and significance in neural development. *Dev Biol,* 286**,** 311-25.

Kok, F. O., Shin, M., Ni, C. W., Gupta, A., Grosse, A. S., Van Impel, A., Kirchmaier, B. C., Peterson-Maduro, J., Kourkoulis, G., Male, I., Desantis, D. F., Sheppard-Tindell, S., Ebarasi, L., Betsholtz, C., Schulte-Merker, S., Wolfe, S. A. & Lawson, N. D. 2015. Reverse genetic screening reveals poor correlation between morpholino-induced and mutant phenotypes in zebrafish. *Dev Cell,* 32**,** 97-108.

Kopan, R. & Ilagan, M. X. 2009. The canonical Notch signaling pathway: unfolding the activation mechanism. *Cell,* 137**,** 216-33.

Koster, R. W. & Fraser, S. E. 2001. Tracing transgene expression in living zebrafish embryos. *Dev Biol,* 233**,** 329-46.

Krebs, L. T., Shutter, J. R., Tanigaki, K., Honjo, T., Stark, K. L. & Gridley, T. 2004. Haploinsufficient lethality and formation of arteriovenous malformations in Notch pathway mutants. *Genes Dev,* 18**,** 2469-73.

Krebs, L. T., Xue, Y., Norton, C. R., Shutter, J. R., Maguire, M., Sundberg, J. P., Gallahan, D., Closson, V., Kitajewski, J., Callahan, R., Smith, G. H., Stark, K. L. & Gridley, T. 2000. Notch signaling is essential for vascular morphogenesis in mice. *Genes Dev,* 14**,** 1343-52.

Kriaucionis, S. & Heintz, N. 2009. The nuclear DNA base 5-hydroxymethylcytosine is present in Purkinje neurons and the brain. *Science,* 324**,** 929-30.

Kumano, K., Chiba, S., Kunisato, A., Sata, M., Saito, T., Nakagami-Yamaguchi, E., Yamaguchi, T., Masuda, S., Shimizu, K., Takahashi, T., Ogawa, S., Hamada, Y. & Hirai, H. 2003. Notch1 but not Notch2 is essential for generating hematopoietic stem cells from endothelial cells. *Immunity,* 18**,** 699-711.

Kumaravelu, P., Hook, L., Morrison, A. M., Ure, J., Zhao, S., Zuyev, S., Ansell, J. & Medvinsky, A. 2002. Quantitative developmental anatomy of definitive haematopoietic stem cells/long-term repopulating units (HSC/RUs): role of the aorta-gonad-mesonephros (AGM) region and the yolk sac in colonisation of the mouse embryonic liver. *Development,* 129**,** 4891-9.

Lam, E. Y., Hall, C. J., Crosier, P. S., Crosier, K. E. & Flores, M. V. 2010. Live imaging of Runx1 expression in the dorsal aorta tracks the emergence of blood progenitors from endothelial cells. *Blood,* 116**,** 909-14.

Lancrin, C., Sroczynska, P., Stephenson, C., Allen, T., Kouskoff, V. & Lacaud, G. 2009. The haemangioblast generates haematopoietic cells through a haemogenic endothelium stage. *Nature,* 457**,** 892-5.

Latimer, A. J., Dong, X., Markov, Y. & Appel, B. 2002. Delta-Notch signaling induces hypochord development in zebrafish. *Development,* 129**,** 2555-63.

Lawson, N. D., Mugford, J. W., Diamond, B. A. & Weinstein, B. M. 2003. phospholipase C gamma-1 is required downstream of vascular endothelial growth factor during arterial development. *Genes Dev,* 17**,** 1346-51.

Lawson, N. D., Scheer, N., Pham, V. N., Kim, C. H., Chitnis, A. B., Campos-Ortega, J. A. & Weinstein, B. M. 2001. Notch signaling is required for arterial-venous differentiation during embryonic vascular development. *Development,* 128**,** 3675-83.

Lawson, N. D., Vogel, A. M. & Weinstein, B. M. 2002. sonic hedgehog and vascular endothelial growth factor act upstream of the Notch pathway during arterial endothelial differentiation. *Dev Cell,* 3**,** 127-36.

Lee, Y., Manegold, J. E., Kim, A. D., Pouget, C., Stachura, D. L., Clements, W. K. & Traver, D. 2014. FGF signalling specifies haematopoietic stem cells through its regulation of somitic Notch signalling. *Nat Commun,* 5**,** 5583.

Leslie, J. D., Ariza-Mcnaughton, L., Bermange, A. L., Mcadow, R., Johnson, S. L. & Lewis, J. 2007. Endothelial signalling by the Notch ligand Delta-like 4 restricts angiogenesis. *Development,* 134**,** 839-44.

Li, C., Lan, Y., Schwartz-Orbach, L., Korol, E., Tahiliani, M., Evans, T. & Goll, M. G. 2015. Overlapping Requirements for Tet2 and Tet3 in Normal Development and Hematopoietic Stem Cell Emergence. *Cell Rep,* 12**,** 1133-43.

Li, Z., Cai, X., Cai, C. L., Wang, J., Zhang, W., Petersen, B. E., Yang, F. C. & Xu, M. 2011. Deletion of Tet2 in mice leads to dysregulated hematopoietic stem cells and subsequent development of myeloid malignancies. *Blood,* 118**,** 4509-18.

Liao, W., Bisgrove, B. W., Sawyer, H., Hug, B., Bell, B., Peters, K., Grunwald, D. J. & Stainier, D. Y. 1997. The zebrafish gene cloche acts upstream of a flk-1 homologue to regulate endothelial cell differentiation. *Development,* 124**,** 381-9.

Lichanska, A. M. & Hume, D. A. 2000. Origins and functions of phagocytes in the embryo. *Exp Hematol,* 28**,** 601-11.

Lorenz, E., Uphoff, D., Reid, T. R. & Shelton, E. 1951. Modification of irradiation injury in mice and guinea pigs by bone marrow injections. *J Natl Cancer Inst,* 12**,** 197-201.

Makinodan, T. 1956. Circulating rat cells in lethally irradiated mice protected with rat bone marrow. *Proc Soc Exp Biol Med,* 92**,** 174-9.

Maximow, A. 1908. Untersuchungen über Blut und Bindegewebe. *Archiv für mikroskopische Anatomie,* 73**,** 444-561.

Maxwell, I. H., Harrison, G. S., Wood, W. M. & Maxwell, F. 1989. A DNA cassette containing a trimerized SV40 polyadenylation signal which efficiently blocks spurious plasmid-initiated transcription. *Biotechniques,* 7**,** 276-80.

Medvinsky, A. & Dzierzak, E. 1996. Definitive hematopoiesis is autonomously initiated by the AGM region. *Cell,* 86**,** 897-906.

Medvinsky, A., Rybtsov, S. & Taoudi, S. 2011. Embryonic origin of the adult hematopoietic system: advances and questions. *Development,* 138**,** 1017-31.

Modhara, S. 2014. *Mathematical modelling of vascular development in zebrafish.* PhD, University of Nottingham.

Moore, M. A. & Metcalf, D. 1970. Ontogeny of the haemopoietic system: yolk sac origin of in vivo and in vitro colony forming cells in the developing mouse embryo. *Br J Haematol,* 18**,** 279-96.

Morgan, T. H. 1917. The Theory of the Gene. *The American Naturalist,* 51**,** 513-544.

Mosimann, C., Kaufman, C. K., Li, P., Pugach, E. K., Tamplin, O. J. & Zon, L. I. 2011. Ubiquitous transgene expression and Cre-based recombination driven by the ubiquitin promoter in zebrafish. *Development,* 138**,** 169-77.

Mosimann, C., Puller, A. C., Lawson, K. L., Tschopp, P., Amsterdam, A. & Zon, L. I. 2013. Site-directed zebrafish transgenesis into single landing sites with the phiC31 integrase system. *Dev Dyn,* 242**,** 949-63.

Motoike, T., Markham, D. W., Rossant, J. & Sato, T. N. 2003. Evidence for novel fate of Flk1+ progenitor: contribution to muscle lineage. *Genesis,* 35**,** 153-9.

Murayama, E., Kissa, K., Zapata, A., Mordelet, E., Briolat, V., Lin, H. F., Handin, R. I. & Herbomel, P. 2006. Tracing hematopoietic precursor migration to successive hematopoietic organs during zebrafish development. *Immunity,* 25**,** 963-75.

Nasevicius, A. & Ekker, S. C. 2000. Effective targeted gene 'knockdown' in zebrafish. *Nat Genet,* 26**,** 216-20.

Nguyen, P. D., Hollway, G. E., Sonntag, C., Miles, L. B., Hall, T. E., Berger, S., Fernandez, K. J., Gurevich, D. B., Cole, N. J., Alaei, S., Ramialison, M., Sutherland, R. L., Polo, J. M., Lieschke, G. J. & Currie, P. D. 2014. Haematopoietic stem cell induction by somite-derived endothelial cells controlled by meox1. *Nature,* 512**,** 314-8.

North, T. E., De Bruijn, M. F., Stacy, T., Talebian, L., Lind, E., Robin, C., Binder, M., Dzierzak, E. & Speck, N. A. 2002. Runx1 expression marks long-term repopulating hematopoietic stem cells in the midgestation mouse embryo. *Immunity,* 16**,** 661-72.

Nowell, P. C., Cole, L. J., Habermeyer, J. G. & Roan, P. L. 1956. Growth and continued function of rat marrow cells in x-radiated mice. *Cancer Res,* 16**,** 258-61.

Nowotschin, S., Xenopoulos, P., Schrode, N. & Hadjantonakis, A. K. 2013. A bright single-cell resolution live imaging reporter of Notch signaling in the mouse. *BMC Dev Biol,* 13**,** 15.

Oberlin, E., Tavian, M., Blazsek, I. & Peault, B. 2002. Blood-forming potential of vascular endothelium in the human embryo. *Development,* 129**,** 4147-57.

Orkin, S. H. & Zon, L. I. 2008. Hematopoiesis: an evolving paradigm for stem cell biology. *Cell,* 132**,** 631-44.

Ottersbach, K. & Dzierzak, E. 2005. The murine placenta contains hematopoietic stem cells within the vascular labyrinth region. *Dev Cell,* 8**,** 377-87.

Palis, J. & Yoder, M. C. 2001. Yolk-sac hematopoiesis: the first blood cells of mouse and man. *Exp Hematol,* 29**,** 927-36.

Paranjpe, S. S. & Veenstra, G. J. 2015. Establishing pluripotency in early development. *Biochim Biophys Acta,* 1849**,** 626-36.

Pardanaud, L., Luton, D., Prigent, M., Bourcheix, L. M., Catala, M. & Dieterlen-Lievre, F. 1996. Two distinct endothelial lineages in ontogeny, one of them related to hemopoiesis. *Development,* 122**,** 1363-71.

Parsons, M. J., Pisharath, H., Yusuff, S., Moore, J. C., Siekmann, A. F., Lawson, N. & Leach, S. D. 2009. Notch-responsive cells initiate the secondary transition in larval zebrafish pancreas. *Mech Dev,* 126**,** 898-912.

Pastor, W. A., Aravind, L. & Rao, A. 2013. TETonic shift: biological roles of TET proteins in DNA demethylation and transcription. *Nat Rev Mol Cell Biol,* 14**,** 341-56.

Paw, B. H. & Zon, L. I. 2000. Zebrafish: a genetic approach in studying hematopoiesis. *Curr Opin Hematol,* 7**,** 79-84.

Pelster, B. & Burggren, W. W. 1996. Disruption of hemoglobin oxygen transport does not impact oxygen-dependent physiological processes in developing embryos of zebra fish (Danio rerio). *Circ Res,* 79**,** 358-62.

Penton, A. L., Leonard, L. D. & Spinner, N. B. 2012. Notch signaling in human development and disease. *Semin Cell Dev Biol,* 23**,** 450-7.

Pouget, C., Gautier, R., Teillet, M. A. & Jaffredo, T. 2006. Somite-derived cells replace ventral aortic hemangioblasts and provide aortic smooth muscle cells of the trunk. *Development,* 133**,** 1013-22.

Pouget, C., Peterkin, T., Simoes, F. C., Lee, Y., Traver, D. & Patient, R. 2014. FGF signalling restricts haematopoietic stem cell specification via modulation of the BMP pathway. *Nat Commun,* 5**,** 5588.

Quillien, A., Moore, J. C., Shin, M., Siekmann, A. F., Smith, T., Pan, L., Moens, C. B., Parsons, M. J. & Lawson, N. D. 2014. Distinct Notch signaling outputs pattern the developing arterial system. *Development,* 141**,** 1544-52.

Rai, K., Huggins, I. J., James, S. R., Karpf, A. R., Jones, D. A. & Cairns, B. R. 2008. DNA demethylation in zebrafish involves the coupling of a deaminase, a glycosylase, and gadd45. *Cell,* 135**,** 1201-12.

Rai, K., Jafri, I. F., Chidester, S., James, S. R., Karpf, A. R., Cairns, B. R. & Jones, D. A. 2010. Dnmt3 and G9a cooperate for tissue-specific development in zebrafish. *J Biol Chem,* 285**,** 4110-21.

Rai, K., Nadauld, L. D., Chidester, S., Manos, E. J., James, S. R., Karpf, A. R., Cairns, B. R. & Jones, D. A. 2006. Zebra fish Dnmt1 and Suv39h1 regulate organ-specific terminal differentiation during development. *Mol Cell Biol,* 26**,** 7077-85.

Robert-Moreno, A., Espinosa, L., De La Pompa, J. L. & Bigas, A. 2005. RBPjkappa-dependent Notch function regulates Gata2 and is essential for the formation of intra-embryonic hematopoietic cells. *Development,* 132**,** 1117-26.

Robert-Moreno, A., Guiu, J., Ruiz-Herguido, C., Lopez, M. E., Ingles-Esteve, J., Riera, L., Tipping, A., Enver, T., Dzierzak, E., Gridley, T., Espinosa, L. & Bigas, A. 2008. Impaired embryonic haematopoiesis yet normal arterial development in the absence of the Notch ligand Jagged1. *Embo j,* 27**,** 1886-95.

Robu, M. E., Larson, J. D., Nasevicius, A., Beiraghi, S., Brenner, C., Farber, S. A. & Ekker, S. C. 2007. p53 activation by knockdown technologies. *PLoS Genet,* 3**,** e78.

Rossi, A., Kontarakis, Z., Gerri, C., Nolte, H., Holper, S., Kruger, M. & Stainier, D. Y. R. 2015. Genetic compensation induced by deleterious mutations but not gene knockdowns. *Nature,* 524**,** 230-233.

Rowlinson, J. 2010. *defining the role of Notch in Definitive Hematopoiesis.* PhD, University of Nottingham.

Rowlinson, J. M. & Gering, M. 2010. Hey2 acts upstream of Notch in hematopoietic stem cell specification in zebrafish embryos. *Blood,* 116**,** 2046-56.

Rudenko, A., Dawlaty, M. M., Seo, J., Cheng, A. W., Meng, J., Le, T., Faull, K. F., Jaenisch, R. & Tsai, L. H. 2013. Tet1 is critical for neuronal activity-regulated gene expression and memory extinction. *Neuron,* 79**,** 1109-22.

Ruzov, A., Tsenkina, Y., Serio, A., Dudnakova, T., Fletcher, J., Bai, Y., Chebotareva, T., Pells, S., Hannoun, Z., Sullivan, G., Chandran, S., Hay, D. C., Bradley, M., Wilmut, I. & De Sousa, P. 2011. Lineage-specific distribution of high levels of genomic 5-hydroxymethylcytosine in mammalian development. *Cell Res,* 21**,** 1332-42.

Sadowski, I., Ma, J., Triezenberg, S. & Ptashne, M. 1988. GAL4-VP16 is an unusually potent transcriptional activator. *Nature,* 335**,** 563-4.

Sagasti, A., Guido, M. R., Raible, D. W. & Schier, A. F. 2005. Repulsive interactions shape the morphologies and functional arrangement of zebrafish peripheral sensory arbors. *Curr Biol,* 15**,** 804-14.

Scheer, N. & Campos-Ortega, J. A. 1999. Use of the Gal4-UAS technique for targeted gene expression in the zebrafish. *Mech Dev,* 80**,** 153-8.

Scheer, N., Groth, A., Hans, S. & Campos-Ortega, J. A. 2001. An instructive function for Notch in promoting gliogenesis in the zebrafish retina. *Development,* 128**,** 1099-107.

Schier, A. F., Neuhauss, S. C., Harvey, M., Malicki, J., Solnica-Krezel, L., Stainier, D. Y., Zwartkruis, F., Abdelilah, S., Stemple, D. L., Rangini, Z., Yang, H. & Driever, W. 1996. Mutations affecting the development of the embryonic zebrafish brain. *Development,* 123**,** 165-78.

Scott, E. K., Mason, L., Arrenberg, A. B., Ziv, L., Gosse, N. J., Xiao, T., Chi, N. C., Asakawa, K., Kawakami, K. & Baier, H. 2007. Targeting neural circuitry in zebrafish using GAL4 enhancer trapping. *Nat Methods,* 4**,** 323-6.

Seritrakul, P. & Gross, J. M. 2014. Expression of the de novo DNA methyltransferases (dnmt3 - dnmt8) during zebrafish lens development. *Dev Dyn,* 243**,** 350-6.

Shalaby, F., Rossant, J., Yamaguchi, T. P., Gertsenstein, M., Wu, X. F., Breitman, M. L. & Schuh, A. C. 1995. Failure of blood-island formation and vasculogenesis in Flk-1-deficient mice. *Nature,* 376**,** 62-6.

Shen, L., Wu, H., Diep, D., Yamaguchi, S., D'alessio, A. C., Fung, H. L., Zhang, K. & Zhang, Y. 2013. Genome-wide analysis reveals TET- and TDG-dependent 5-methylcytosine oxidation dynamics. *Cell,* 153**,** 692-706.

Shimizu, K., Chiba, S., Hosoya, N., Kumano, K., Saito, T., Kurokawa, M., Kanda, Y., Hamada, Y. & Hirai, H. 2000. Binding of Delta1, Jagged1, and Jagged2 to Notch2 rapidly induces cleavage, nuclear translocation, and hyperphosphorylation of Notch2. *Mol Cell Biol,* 20**,** 6913-22.

Sieger, D., Tautz, D. & Gajewski, M. 2003. The role of Suppressor of Hairless in Notch mediated signalling during zebrafish somitogenesis. *Mech Dev,* 120**,** 1083-94.

Siekmann, A. F. & Lawson, N. D. 2007. Notch signalling limits angiogenic cell behaviour in developing zebrafish arteries. *Nature,* 445**,** 781-4.

Sinha, D. K., Neveu, P., Gagey, N., Aujard, I., Benbrahim-Bouzidi, C., Le Saux, T., Rampon, C., Gauron, C., Goetz, B., Dubruille, S., Baaden, M., Volovitch, M., Bensimon, D., Vriz, S. & Jullien, L. 2010. Photocontrol of protein activity in cultured cells and zebrafish with one- and two-photon illumination. *Chembiochem,* 11**,** 653-63.

Siridechadilok, B., Gomutsukhavadee, M., Sawaengpol, T., Sangiambut, S., Puttikhunt, C., Chin-Inmanu, K., Suriyaphol, P., Malasit, P., Screaton, G. & Mongkolsapaya, J. 2013. A simplified positive-sense-RNA virus construction approach that enhances analysis throughput. *J Virol,* 87**,** 12667-74.

Slukvin, Ii 2013. Hematopoietic specification from human pluripotent stem cells: current advances and challenges toward de novo generation of hematopoietic stem cells. *Blood,* 122**,** 4035-46.

Smithers, L., Haddon, C., Jiang, Y. J. & Lewis, J. 2000. Sequence and embryonic expression of deltaC in the zebrafish. *Mech Dev,* 90**,** 119-23.

Sniegowski, J. A., Lappe, J. W., Patel, H. N., Huffman, H. A. & Wachter, R. M. 2005. Base catalysis of chromophore formation in Arg96 and Glu222 variants of green fluorescent protein. *J Biol Chem,* 280**,** 26248-55.

Souilhol, C., Cormier, S., Monet, M., Vandormael-Pournin, S., Joutel, A., Babinet, C. & Cohen-Tannoudji, M. 2006. Nas transgenic mouse line allows visualization of Notch pathway activity in vivo. *Genesis,* 44**,** 277-86.

Stone, H. 2010. *How Notch signalling varies to differentially regulate arterial endothelial gene expression and Haematopoietic Stem cell emergence in Danio rerio* Master, University of Nottingham.

Sumoy, L., Keasey, J. B., Dittman, T. D. & Kimelman, D. 1997. A role for notochord in axial vascular development revealed by analysis of phenotype and the expression of VEGR-2 in zebrafish flh and ntl mutant embryos. *Mech Dev,* 63**,** 15-27.

Tahiliani, M., Koh, K. P., Shen, Y., Pastor, W. A., Bandukwala, H., Brudno, Y., Agarwal, S., Iyer, L. M., Liu, D. R., Aravind, L. & Rao, A. 2009. Conversion of 5-methylcytosine to 5-hydroxymethylcytosine in mammalian DNA by MLL partner TET1. *Science,* 324**,** 930-5.

Takke, C. & Campos-Ortega, J. A. 1999. her1, a zebrafish pair-rule like gene, acts downstream of notch signalling to control somite development. *Development,* 126**,** 3005-14.

Takke, C., Dornseifer, P., V Weizsacker, E. & Campos-Ortega, J. A. 1999. her4, a zebrafish homologue of the Drosophila neurogenic gene E(spl), is a target of NOTCH signalling. *Development,* 126**,** 1811-21.

Terragni, J., Zhang, G., Sun, Z., Pradhan, S., Song, L., Crawford, G. E., Lacey, M. & Ehrlich, M. 2014. Notch signaling genes: myogenic DNA hypomethylation and 5-hydroxymethylcytosine. *Epigenetics,* 9**,** 842-50.

Thompson, M. A., Ransom, D. G., Pratt, S. J., Maclennan, H., Kieran, M. W., Detrich, H. W., 3rd, Vail, B., Huber, T. L., Paw, B., Brownlie, A. J., Oates, A. C., Fritz, A., Gates, M. A., Amores, A., Bahary, N., Talbot, W. S., Her, H., Beier, D. R., Postlethwait, J. H. & Zon, L.

I. 1998. The cloche and spadetail genes differentially affect hematopoiesis and vasculogenesis. *Dev Biol,* 197**,** 248-69.

Thummel, R., Bai, S., Sarras, M. P., Jr., Song, P., Mcdermott, J., Brewer, J., Perry, M., Zhang, X., Hyde, D. R. & Godwin, A. R. 2006. Inhibition of zebrafish fin regeneration using in vivo electroporation of morpholinos against fgfr1 and msxb. *Dev Dyn,* 235**,** 336-46.

Till, J. E. & Mcculloch, E. A. 1961. A Direct Measurement of the Radiation Sensitivity of Normal Mouse Bone Marrow Cells. *Radiation Research,* 14**,** 213-222.

Tittle, R. K., Sze, R., Ng, A., Nuckels, R. J., Swartz, M. E., Anderson, R. M., Bosch, J., Stainier, D. Y., Eberhart, J. K. & Gross, J. M. 2011. Uhrf1 and Dnmt1 are required for development and maintenance of the zebrafish lens. *Dev Biol,* 350**,** 50-63.

Triezenberg, S. J., Lamarco, K. L. & Mcknight, S. L. 1988. Evidence of DNA: protein interactions that mediate HSV-1 immediate early gene activation by VP16. *Genes Dev,* 2**,** 730-42.

Tsumagari, K., Baribault, C., Terragni, J., Varley, K. E., Gertz, J., Pradhan, S., Badoo, M., Crain, C. M., Song, L., Crawford, G. E., Myers, R. M., Lacey, M. & Ehrlich, M. 2013. Early de novo DNA methylation and prolonged demethylation in the muscle lineage. *Epigenetics,* 8**,** 317-32.

Ulitsky, I., Shkumatava, A., Jan, C. H., Sive, H. & Bartel, D. P. 2011. Conserved function of lincRNAs in vertebrate embryonic development despite rapid sequence evolution. *Cell,* 147**,** 1537-50.

Uyttendaele, H., Ho, J., Rossant, J. & Kitajewski, J. 2001. Vascular patterning defects associated with expression of activated Notch4 in embryonic endothelium. *Proc Natl Acad Sci U S A,* 98**,** 5643-8.

Valinluck, V. & Sowers, L. C. 2007. Endogenous cytosine damage products alter the site selectivity of human DNA maintenance methyltransferase DNMT1. *Cancer Res,* 67**,** 946-50.

Varnum-Finney, B., Xu, L., Brashem-Stein, C., Nourigat, C., Flowers, D., Bakkour, S., Pear, W. S. & Bernstein, I. D. 2000. Pluripotent, cytokine-dependent, hematopoietic stem cells are immortalized by constitutive Notch1 signaling. *Nat Med,* 6**,** 1278-81.

Venkatesh, D. A., Park, K. S., Harrington, A., Miceli-Libby, L., Yoon, J. K. & Liaw, L. 2008. Cardiovascular and hematopoietic defects associated with Notch1 activation in embryonic Tie2-expressing populations. *Circ Res,* 103**,** 423-31.

Walls, J. R., Coultas, L., Rossant, J. & Henkelman, R. M. 2008. Three-dimensional analysis of vascular development in the mouse embryo. *PLoS One,* 3**,** e2853.

Weber, J. M. & Calvi, L. M. 2010. Notch signaling and the bone marrow hematopoietic stem cell niche. *Bone,* 46**,** 281-5.

Westerfield, M. & Zfin. 2000. *The zebrafish book a guide for the laboratory use of zebrafish Danio (Brachydanio) rerio* [Online]. [Eugene, Or.]: ZFIN. Available: http://zfin.org/zf_info/zfbook/zfbk.html.

Westin, J. & Lardelli, M. 1997. Three novel Notch genes in zebrafish: implications for vertebrate Notch gene evolution and function. *Dev Genes Evol,* 207**,** 51-63.

Wilkinson, R. N., Pouget, C., Gering, M., Russell, A. J., Davies, S. G., Kimelman, D. & Patient, R. 2009. Hedgehog and Bmp polarize hematopoietic stem cell emergence in the zebrafish dorsal aorta. *Dev Cell,* 16**,** 909-16.

Wu, H. & Zhang, Y. 2011. Mechanisms and functions of Tet protein-mediated 5-methylcytosine oxidation. *Genes Dev,* 25**,** 2436-52.

Xu, M. J., Matsuoka, S., Yang, F. C., Ebihara, Y., Manabe, A., Tanaka, R., Eguchi, M., Asano, S., Nakahata, T. & Tsuji, K. 2001. Evidence for the presence of murine primitive megakaryocytopoiesis in the early yolk sac. *Blood,* 97**,** 2016-22.

Xu, Y., Xu, C., Kato, A., Tempel, W., Abreu, J. G., Bian, C., Hu, Y., Hu, D., Zhao, B., Cerovina, T., Diao, J., Wu, F., He, H. H., Cui, Q., Clark, E., Ma, C., Barbara, A., Veenstra, G. J. C., Xu, G., Kaiser, U. B., Liu, X. S., Sugrue, S. P., He, X., Min, J., Kato, Y. & Shi, Y. G. 2012. Tet3

CXXC Domain and Dioxygenase Activity Cooperatively Regulate Key Genes for Xenopus Eye and Neural Development. *Cell,* 151**,** 1200-13.

Yamaguchi, T. P., Dumont, D. J., Conlon, R. A., Breitman, M. L. & Rossant, J. 1993. flk-1, an flt-related receptor tyrosine kinase is an early marker for endothelial cell precursors. *Development,* 118**,** 489-98.

Yoon, K. J., Koo, B. K., Im, S. K., Jeong, H. W., Ghim, J., Kwon, M. C., Moon, J. S., Miyata, T. & Kong, Y. Y. 2008. Mind bomb 1-expressing intermediate progenitors generate notch signaling to maintain radial glial cells. *Neuron,* 58**,** 519-31.

Zecchin, E., Conigliaro, A., Tiso, N., Argenton, F. & Bortolussi, M. 2005. Expression analysis of jagged genes in zebrafish embryos. *Developmental Dynamics,* 233**,** 638-645.

Zhang, R. R., Cui, Q. Y., Murai, K., Lim, Y. C., Smith, Z. D., Jin, S., Ye, P., Rosa, L., Lee, Y. K., Wu, H. P., Liu, W., Xu, Z. M., Yang, L., Ding, Y. Q., Tang, F., Meissner, A., Ding, C., Shi, Y. & Xu, G. L. 2013. Tet1 regulates adult hippocampal neurogenesis and cognition. *Cell Stem Cell,* 13**,** 237-45.

Zovein, A. C., Hofmann, J. J., Lynch, M., French, W. J., Turlo, K. A., Yang, Y., Becker, M. S., Zanetta, L., Dejana, E., Gasson, J. C., Tallquist, M. D. & Iruela-Arispe, M. L. 2008. Fate tracing reveals the endothelial origin of hematopoietic stem cells. *Cell Stem Cell,* 3**,** 625-36.